Surface energy balance of shrub vegetation in the Sahel

Promotor	:	Dr. J. Wieringa Hoogleraar in de meteorologie
Co-promotor	:	Dr. H.A.R. de Bruin Universitair hoofddocent meteorologie

NN08201, 2017

Anne Verhoef

Surface energy balance of shrub vegetation in the Sahel

Proefschrift
ter verkrijging van de graad van doctor
in de landbouw- en milieuwetenschappen
op gezag van de rector magnificus,
dr. C.M. Karssen,
in het openbaar te verdedigen
op woensdag 6 december 1995
des namiddags te half twee in de Aula
van de Landbouwuniversiteit te Wageningen

CIP-DATA KONINKLIJKE BIBLIOTHEEK, DEN HAAG

Verhoef, Anne.

Surface energy balance of shrub vegetation in the Sahel /
Anne Verhoef.- [S.l.: s.n.]
Thesis Landbouwuniversiteit Wageningen . - With ref. - With
summary in Dutch.
ISBN 90-5485-458-8
Subject headings: micrometeorology / shrubs ; surface energy
balance ; Sahel / soil heat flux.

This study was carried out at the Department of Meteorology, Wageningen
Agricultural University, the Netherlands, with financial support of the Nederlandse
Organisatie voor Wetenschappelijk Onderzoek (NWO).

Stellingen

1. Voor de berekening van kB^{-1}-waarden zijn geen eenvoudige en algemene vuistregels te geven, zodat de toepasbaarheid van eenvoudige uitwisselingsformules in bijv. 'remote sensing' beperkt is.

   - *Dit proefschrift*

2. De vaak onzorgvuldige opstelling van stralingsmeters boven spaarzaam begroeide oppervlakken leidt tot foutieve waarden van netto straling.

   - *Dit proefschrift*

3. Voor het bepalen van de bodemwarmtestroomdichtheid met bodemwarmtestroomplaatjes worden correcties betrekking hebbend op warmteopslag en latente warmteprocessen niet of onzorgvuldig toegepast, wat met name in semi-aride gebieden een slecht sluitende energiebalans oplevert.

   - *Dit proefschrift*
   - *Zie ook: Mayocchi, C.L., and Bristow, K.L., 1995. Soil surface heat flux: some general questions and comments on measurements. Agric. For. Meteorol. 75: 43-50*

4. Voor de berekening van de ruwheidslengte en verplaatsingshoogte van spaarzaam begroeide oppervlakken zijn naast informatie omtrent de gewashoogte ook gegevens van de obstakeldistributie benodigd.

   - *Dit proefschrift*
   - *Zie ook: Raupach, M.R., 1992. Drag and drag partition on rough surfaces. Boundary-Layer Meteorology 60: 375-395*

5. Omdat in het geval van een niet gesloten vegetatiedek de aerodynamische weerstand in de gewaslaag van grote invloed is op de oppervlaktetemperatuur, werkt deze weerstand ook door op de bodemwarmtestroomdichtheid en de verdamping.

   - *Van den Hurk, B.J.J.M., 1995. Sparse canopy parameterization for meteorological models. Proefschrift vakgroep Meteorologie, Landbouwuniversiteit Wageningen*
   - *Dit proefschrift*

6. Advective effects cause the total surface flux of heat and moisture to depend on the length scale of the heterogeneity. This dependence can be quantified by calculating the fluxes from atmospheric conditions at the blending height.

   - *Zie bijv. Blyth, E.M., 1994. The effect of small-scale heterogeneity on surface fluxes of heat and moisture. PhD-thesis, University of Reading, England*

7. Sterke aanwijzingen voor een positief verband tussen plasma homocysteïne en het risico op hart- en vaatziekten enerzijds, en het feit dat met foliumzuur (vitamine B-11) het plasma homocysteine effectief kan worden verlaagd, geven mogelijk een eenvoudig middel in handen om het aantal gevallen van hart- en vaatziekten terug te dringen.

   - Verhoef, P., 1995. Homocysteine and cardiovascular disease: epidemiologic studies. Proefschrift vakgroep Humane Epidemiologie en Gezondheidsleer, Landbouw-universiteit Wageningen.

8. Het voortdurend aanpassen van de theorie aan de observaties kan de gerenommeerde wetenschapper in een onhoudbare positie brengen.

   - Zie bijv. "Round in circles" van Jim Schnabel, dat de achtergronden van het onderzoek naar het fenomeen graancirkels beschrijft)

9. In de studie medicijnen zou meer aandacht besteed moeten worden aan erkende fytotherapeutische en homeopathische geneesmiddelen, zodat alle huisartsen deze middelen als vanzelfsprekend zouden voorschrijven ter bestrijding van eenvoudige kwalen.

10. Wetenschappelijk onderzoek van Westerse universiteiten verricht in de Derde Wereld hoeft zich niet te beperken tot dat wat uitgaat van direkte toepasbaarheid in het kader van ontwikkelingssamenwerking.

    - Zie bijv. "Wageningse Desert Storm in de Sahel", WUB 35, 1992

11. Naast onderwijs in vakken zoals 'techniek' en 'verzorging', die gericht zijn op het gelijk trekken der seksen, dienen jonge mensen al vroeg vertrouwd gemaakt te worden met de *verschillen* tussen man en vrouw. Dit zou het kunnen vergemakkelijken om te gaan met maatschappelijke problemen, zoals ongewenste intimiteiten op het werk.

12. Stotteren bemoeilijkt niet alleen de uitgaande informatiestroom maar tevens de binnenkomende.

13. Als het aan de samenzwerende producenten van hygiënische produkten en van reclameprogrammas ligt, blijft de moderne vrouw van de wieg tot het graf in de luiers.

Stellingen behorende bij het proefschrift van Anne Verhoef
"Surface energy balance of shrub vegetation in the Sahel"
Wageningen, 6 december 1995

Abstract

Recently, the development and use of Global Circulation Models, employed for climate change prediction, has taken off. These models provide us with the current and future status of the surface, expressed by the surface energy and water balances. In order to obtain reliable climate-predictions there is an urgent need for reliable input data from all major biomes covering our Globe. The Sahel has been one of the most important areas of application for GCMs, in order to understand the reasons for its declining rainfall, a process that started in the early seventies. It is therefore of paramount importance to monitor the surface conditions of this vulnerable area, where drought and land use interact to create surface conditions able of altering the regional climate.

This thesis describes the surface energy balance of Sahelian shrub vegetation (fallow savannah and tiger-bush) by using micrometeorological data obtained in the framework of the HAPEX-Sahel and SEBEX project. The surface energy balance defines how net radiation is partitioned over the atmospheric fluxes (sensible and latent heat flux) and the soil heat flux. The energy balance is studied on a diurnal, seasonal and interannual scale. In addition the CO_2 flux of savannah is described. The fallow savannah is part of a rotation scheme (usually millet) and consists of scattered shrubs (*Guiera senegalensis*) interspersed by a sparse undergrowth of grasses and herb species. The tiger-bush takes its name, when viewed from the sky, from the resemblance to a tiger skin. It is composed of elongated vegetation patches, mainly consisting of *Guiera senegalensis* with an occasional tree, growing on bare, crusted, practically impenetrable soil.

To study the exchange between the (Sahelian) land surface and the atmosphere, various surface parameterizations have been developed. These soil-vegetation-atmosphere-transfer schemes (SVATs, in their simplified form being the basis of the large-scale models) require detailed input of surface parameters (e.g. albedo, roughness length for momentum, or soil thermal conductivity) and the resistances encountered by the fluxes. This thesis provides the various input parameters and surface and aerodynamic resistances of the savannah and tiger-bush and their possible temporal variability. Various SVATs have been tested and it can be concluded that simple parameterizations of soil heat flux give results comparable to elaborate soil models. Of major importance are the surface resistances and the aerodynamic resistance describing the transport within the understorey. Simple relationships, in which the roughness length and the displacement height are characterized by canopy height only, do not work satisfactorily for these sparse canopies. They require a relatively detailed drag partition model, applying roughness density.

If simple, one-layer, bulk transfer models are used (e.g. for remote sensing) the excess resistance has to be taken into account. It appears that the resistance for this shrub-dominated vegetation is much larger than the usually applied value.

Keywords: surface energy balance, evaporation, radiation, soil heat flux, CO_2, resistance parameterization, SVAT

Bombus terrestris:

....

Als de lucht ligt liggen ook de meren.
Maar op allergeringste hoogte, een handbreed boven de grond.
verandert merkbaar de temperatuur: twee graden warmer

en wat doffe bruine geluiden.
De hele leer der natuur gaat over warmte

en lage verduisterende wolken.

Uit : De stilte van de wereld voor Bach, Gedichten van Lars Gustafsson. Keuze, vertaling, nawoord J. Bernlef, Uitgeverij De Bezige Bij.

Voor mijn ouders

Voorwoord

De weg is beter dan de herberg (?). Na ruim vier jaar met onzettend veel plezier gewerkt te hebben aan de vakgroep Meteorologie, wordt het ook nu weer tijd om verder te gaan. Het resultaat van mijn OIO-onderzoek vindt u in dit groengevlekte boekje, dat nooit geschreven had kunnen worden zonder de bijdragen en steun van de volgende personen of instanties.

Allereerst wil ik mijn promotor Jon Wieringa noemen. Hoewel pas later aan boord gekomen is hij met name het laatste half jaar van groot belang geweest. Ik wil hem hierbij hartelijk bedanken voor zijn wetenschappelijke bijdragen en belangstelling.

Mijn co-promotor Henk de Bruin ben ik dankbaar voor zijn gedreven begeleiding en leerzame kritiek. In 1988 begon ik bij jou een afstudeervak micrometeorologie, zij het geworteld in de bodem, waarna in 1991 deze OIO-baan volgde. Hoewel we heel af en toe last hadden van het Ajax-Feyenoord effect, hebben we samen menig succesvol partijtje (paniek)voetbal gespeeld als er op de valreep weer eens een rapport, voorstel of artikel de deur uit moest. Bedankt ook voor het vertrouwen dat je in me gesteld hebt gedurende de voorbereiding en de afwikkeling van 'Niger'. Daarnaast ben ik blij dat je me naar Wallingford hebt 'gestuurd': het onderzoek daar is zeer nuttig gebleken en heeft bovendien geleid tot een twee-jarige post-doc plaats. Ik hoop dat we dan ook in de toekomst kunnen blijven samenwerken.

De meeste gegevens gebruikt in dit proefschrift zijn verzameld in het kader van het HAPEX-Sahel experiment (Niger, 1992). Dit project maakt deel uit van twee internationale programmas, te weten het 'World Climate Research Programme' (WRCP), opgestart door de 'International Council of Scientific Unions' en de 'World Meteorological Organization' (WMO) en één van de kernprojecten van het 'International Geosphere-Biosphere Programme' (IGBP), namelijk 'Biospheric Aspects of the Hydrological Cycle' (BAHC). Het HAPEX-Sahel project en een groot deel van de uitwerkingsfase nadien werden gefinancierd door nationale en internationale instanties. De vakgroep Meteorologie van de LUW kreeg ondersteuning van de Europese Unie (EPOCH programme, contract nr. EPOC-0024-C(CD)), NOP, BCRS en NWO-MFO (project nr. 750.650.37).

Mensen van Duivendaal 2, bedankt ! Deze tijd komt nooit meer terug (snif). Adrie Jacobs bedankt voor je bijdragen aan HAPEX-Sahel en EFEDA en je relativerende kijk op de dingen. Cor Jacobs bedankt voor je hulp bij het CO_2-model en alle nuttige tips in de afgelopen maanden; Ad van den Berg voor het beeldschoon programmeren van Cindy en Claudia en hun voorgangers; Rolf Krikke voor het ontwikkelen van het databestand en andere klussen. Kees van den Dries, bedankt voor je eindeloze geduld als ik weer eens overhoop lag met mijn altijd Mackerende pc, fonts, software, printer, figuren, back-ups en wat er verder allemaal nog mis kan gaan. (Rush)di El Kilani voor de ontelbare " How is it going ?"s. Een veilig gevoel zo 'n brede vent in de buurt tijdens de stille avonduren. De secretaresses (in het bijzonder Gerrie van den Brink) voor alle bijdragen achter de schermen. Verder wil ik de mensen bedanken die zowel ons HAPEX-Sahel als het EFEDA-avontuur tot een succes hebben gemaakt. Zonder de technische assistentie van Frits Antonysen, Johan Birnie, Anton Jansen, Teun Jansen, Willy Hillen, en Dick Welgraven zou er van beide veldexperimenten niet veel terecht gekomen zijn.

En dan mijn paranimfen.... Bert Heusinkveld en Bart van den Hurk. Bert, jouw nimmer aflatend elektro-technisch enthousiasme en doorzettingsvermogen hebben geleid tot meet-gegevens van hoge kwaliteit. Nooit heb ik ook maar één moment paniek gevoeld als zich weer eens een instrumentele ramp voltrok: Bert weet het wel te fixen (zolang je hem maar genoeg te eten geeft). Bart, bedankt voor de gezellige jaren samen in de nok van onze vakgroep. Je was altijd een gewillig oor als mijn vragend " Bahart (je) ?" weer een Kabééminéén-discussie of een SI-black-out inluidde. Ook denk ik graag terug aan de goeie tijd in Tomelloso, waar we heel wat tapas ("doet u mij een broodje zeep") verorberd hebben en waar je al het geregelneef voor je rekening hebt genomen.

De studenten van de vakgroep meteorologie ben ik dankbaar voor hun inzet in het veld tijdens de HAPEX-Sahel campagne en de verwerking van een deel van de gegevens na thuiskomst. Miranda van den Broek, Esther van Eersel, Ben Habets, Wilco Hazeleger, Marco Nell en Paul Smeets. Fijn dat jullie wel de 10-meter mast in durfden... Het gepiep van de porometer om 6 uur 's morgens zullen jullie niet gauw vergeten. Ook Cor Hofstee ben ik dank verschuldigd voor zijn assistentie in Niger.

Keith McNaughton: even though you modestly described yourself as a scientific tourist, you have been of great scientific help and support before, during and after the HAPEX-Sahel experiment. I hope your limerick (a tiger in Niger) works out one day !

Dan zijn er de mensen van de 'HAPEX-familie' die zeer broederlijk/zusterlijk hun gegevens met ons gedeeld hebben. Allereerst de medewerkers van het Staring Centrum en dan met name Jan Elbers die als een wervelwind de instrumenten in de savanne en het tijgerbos aan het draaien wist te houden. Ook na thuiskomst in Wageningen is er nog menig megabytje over het Net gegaan. De vakgroep Waterhuishouding (vooral Peter Droogers, René Kim, Margje Soet en Han Stricker) wil ik bedanken voor het afstaan van hun bodemfysische gegevens: zonder jullie was de bodemwarmteflux niet van de grond gekomen. Verder wil ik nog een aantal andere HAPEX-wetenschappers noemen. Bhaskar Choudhury is acknowledged for his assistance with the set-up of our surface temperature transect and helping us break the record of fitting atmospheric scientists in a Niamey taxi. Furthermore, I am indepted to Nial Hanan, Agnes Bègue, Shelley Thawley and their colleages, and to Peter Levy for putting some of their (vegetation) data at my disposal. De 'site-captains' Pavel Kabat en Steve Prince wil ik bedanken voor het vakkundig besturen van de Central West super-site. Thierry Lebel is acknowledged for providing rainfall data. I want to thank Henrik Søgaard and his team for the brave management of the Northern super-site. Jean-Paul Goutorbe (père-HAPEX) is acknowledged for all his efforts and Meteo France/CNRM for giving the HAPEX-Sahel scientists (including me) the opportunity to exchange data and viewpoints during two meetings in Toulouse.

From May until August 1994, I stayed at the Institute of Hydrology to work on their SEBEX data. This visit has been very useful and pleasant and I want to thank everybody for the offered facilities and scientific input. I want to give special thanks to Simon Allen for his guidance and contributions. Furthermore I want to thank Eleanor Blyth, Alistair Culf, Steve Gaze, Cathy Holwill, Nick Jackson, Chris Huntingford, John Roberts, John Stewart, Chris Taylor and Jim Wallace. I am looking forward to my 2-years post-doc job at the Institute. David Macdonald: thanks for your support and patience during the past one and a half years. Thanks also for your help while designing the cover.

Dr. M.V.K. Sivakumar is acknowledged for letting me use the meteorological data of the ICRISAT Sahelian Centre, Sadoré, Niger.

I want to thank all participants of the Wallingford HAPEX-Sahel Workshop and especially IH for organizing it. Furthermore, I want to give credit to the pioneer authors/editors of the papers resulting from this workshop: Pierre Bessemoulin, Han Dolman, John Gash, Pavel Kabat, Colin Lloyd, and especially John Moncrieff and Bruno Monteny.

Hein ten Berge bedankt voor je steun, inspiratie en gezelligheid tijdens mijn studie en deze zware promotie-jaren.

Tot slot wil ik mijn ouders, mijn zus Petra, tante Ulla en oom Cor en mijn vrienden bedanken voor de belangstelling en mentale ondersteuning gedurende de afgelopen vier jaren (en zovele jaren daarvoor).

CONTENTS

Abbreviatons and acronyms

CM	SVAT-parameterization predominantly based on Choudhury and Monteith (1988)
C_3	With C_3 mechanism for photosynthesis
C_4	With C_4 mechanism for photosynthesis
BREB	Bowen ratio energy balance
CES	Central east super-site
CWS	Central west super-site
DCM	Dual component model
DD	SVAT-parameterization predominantly based on Deardorff (1978)
DG	Danguey Gourou super-site (northern super-site)
EC	Eddy covariance
ECHIVAL	European international project on Climatic and Hydrological Interactions between Vegetation, the Atmosphere and the Land surface
EFEDA	ECHIVAL Field Experiment in Desertification-threatened Areas
FIVE	First ISLSCP Field Experiment
HAPEX-Mobilhy	Hydrological Atmospheric Pilot EXperiment - MOdélisation du BILan HYdrique
HAPEX-Sahel	Hydrological Atmospheric Pilot EXperiment in the Sahel
HP96	Hanan and Prince, 1996
IH	Institute of Hydrology
IOP	Intensive observation period (of the HAPEX-Sahel campaign)
IRGA	Infra-red gas analyzer
IRT	Infra-red thermometer
ISC	ICRISAT Sahelian Centre
JS	Jarvis (1986), Stewart (1988)
LAI	Leaf area index
NDVI	Normalized difference vegetation index
PAR	Photosynthetically active radiation
PET	Potential evapotranspiration
SC-DLO	Winand Staring Centre, DLO
SEB	Surface energy balance
SEBEX	Sahelian Energy Balance EXperiment
SSS	Southern super-site
SSZ	Sudano-Sahelian zone
SVAT	Soil-vegetation-atmosphere-transfer-scheme
SW	SVAT-parameterization predominantly based on Shuttleworth & Wallace (1985)
TCM	Triple component model
TL	Two layer model (as proposed by Huntingford et al., 1995)
WAUMET	Wageningen Agricultural University, Dept. of METeorology

Symbols

a	surface albedo [-] with additional subscripts x (i.e. a_x)	
	b	bushes
	c	canopy (upperstorey), used in SVATs
	s	soil
	t	total
	u	understorey (herbs/grass/soil) layer or undergrowth (SVATs)
$a_1..a_5$	fitting parameters in JS-type g_l-parameterization	
A	particular atmospheric quantity, e.g. temperature, wind speed	
A_x	available energy (R_n - G) [W m^{-2}] with additional subscripts x	
	b	bushes
	c	canopy (upperstorey), used in SVATs

	s soil
	t total
	u understorey (herbs/grass/soil) layer or undergrowth (SVATs)
A_n	cosine-related amplitude of the n th harmonic in a Fourier series
A_m	photosynthetic rate at saturating light intensity [mg m^{-2} s^{-1}]
$A_{m,max}$	leaf photosynthetic capacity [mg m^{-2} s^{-1}]
A_n	photosynthetic rate [mg m^{-2} s^{-1}]
A_1 or A_2	soil temperature amplitudes at depths z_1 and z_2 [°C], see Eq. A2.3
A_{0n}	the amplitude of the n^{th} soil temperature harmonic for the upper boundary
b	Clapp and Hornberger exponent
b	breadth of isolated surface elements [m]
B	Stanton number [-]
B_n	sine-related amplitude of the n th harmonic in a Fourier series
c_c	a quantity defined by ρ_c/ρ [-]
c_d	constant (0.3, 0.6 or 1.2) in drag partition model [-]
c_s	soil specific heat [J kg^{-1} K^{-1}]
c_w	constant (4.6) in drag partition model [-]
c_1	constant (0.37 or 0.5) in drag partition model [-]
C	drag coefficient in DD [-]
$\mathrm{C_c}$	help coefficients in SW (functions of resistances) [-]
C_i	intercellular CO_2 concentration [mg m^{-3}]
C_h	bulk volumetric soil heat capacity [J m^{-3} K^{-1}]
$C_{h,l}$	volumetric heat capacity of water (4.2 x 10^6) [J m^{-3} K^{-1}]
$C_{h,s}$	volumetric heat capacity of the solid soil particles (2.0 x 10^6) [J m^{-3} K^{-1}]
C_p	heat capacity of air at constant pressure (1005) [J kg^{-1} K^{-1}]
C_R	drag coefficient (0.25, 0.3 or 0.4) for an isolated roughness element [-]
C_s	CO_2-concentration at leaf surface [mg m^{-3}]
C_s	help coefficients in SW (functions of resistances) [-]
C_S	drag coefficient for the substrate surface [-]
C_1 and C_2	constants being dependent on soil moisture and texture (see DD) [-]
d	displacement height for momentum [m]
d_1	depth reached by the diurnal temperature wave (see DD) [m]
d_{1,H_2O}	arbitrary normalization depth (see DD) [m]
d_2	depth reached by the annual temperature wave (see DD) [m]
d_{1,H_2O}	depth over which the soil water budget extends (see DD) [m]
D	atmospheric vapour pressure deficit (at reference height) [kPa]
D	element spacing [m]
D_0	atmospheric in-canopy vapour pressure deficit [Pa *or* mb]
D_h	advection term in Eq. 1.1 [W m^{-2}]
Dir	wind direction
D_v	molecular diffusivity of water vapour [m^2 s^{-1}]
D_s	specific humidity deficit at the leaf surface [g kg^{-1}]
e_a	atmospheric vapour pressure at screen height with extra superscript *sat* to denote saturated conditions [mb or Pa]
e_0	in-canopy atmospheric vapour pressure [Pa]
e^*	evaporativity (see evapoclimatonomy model) [-]
E	evaporation [kg m^{-2} s^{-1}] with additional subscripts b, c, tr and s referring to bush, partly wet canopy (upperstorey), transpiration from dry leaf surfaces only and soil. DD, DCM and TCM
E	daily evaporation [mm] with additional subscripts b, u, and s referring to bush, undergrowth and soil (see Chapter 5).

E_c^{pot}	maximum possible evaporation of the vegetation (DD) [kg m^{-2} s^{-1}]
E_p	Penman potential evaporation
f_p	normalized frequencies being a function of wind speed and of sensor path length [-]
f_s	normalized frequencies being a function of wind speed and sensor separation distance [-]
f	factors in calculation of empirical (JS-approach) g_l (or $\overline{r_s^c}$) values [-] with additional subscripts *1, 2, 3, 4*
f	parameter in A-g_s-model [-]
F_c	CO_2 flux [μmol m^{-2} s^{-1}] in Chapter 7 or [kg m^{-2} s^{-1}] in Eq. 2.16
F_i	sap flow in stem i [kg s^{-1}]
g	acceleration due to gravity [m s^{-2}]
g_c	'bottom-up' canopy conductance
g_m	mesophyll conductance at leaf scale [mm s^{-1}]
g_{cs}	'top-down' canopy surface conductance
g_l	leaf stomatal conductance with extra subscript *max* to denote maximum [m s^{-1}]
g_0	cuticular conductance [m s^{-1}]
G	soil heat flux [W m^{-2}] with additional subscripts x (i.e. G_x) *b* bushes *c* canopy (upperstorey), used in SVATs *s* soil *t* total *u* understorey (herbs/grass/soil) layer
G_0	heat flux into the dry soil layer (see CM) [W m^{-2}]
h	canopy (upperstorey) height [m]
h	parameter (8 z_{0m}) in Eq. A4.3 (see Owen and Thomson, 1963; Brutsaert, 1982)
h and h_s	soil water potential head with subscript s to refer to saturation [m]
H	sensible heat flux [W m^{-2} or mm] with additional subscripts (i.e. H_x) *b* bushes *c* canopy (upperstorey), used in SVATs *s* soil *t* total *u* understorey (herbs/grass/soil)
k	Von Kármán constant (0.4) [-]
I_a	absorbed PAR [W m^{-2}]
k	parameter in A-g_s-model = C_i/C_s [-]
K	eddy diffusivities or turbulent exchange coefficients, with subscripts *h*, *e*, and *m* for heat, water vapour or momentum, respectively.
K_s	soil hydraulic conductivity with extra superscript *sat* to indicate saturation [m s^{-1}]
$K(h)$	eddy diffusivity at canopy height [m^2 s^{-1}]
l	lower depth of upper soil layer (see CM) [m]
l_m	lower depth of lower soil layer (see CM) [m]
l_0	limit value of depth of upper soil layer (see CM) [m]
L	Monin-Obukhov length [m]
LAI_b	leaf area index of bush (used for vegetation description)[m^2 m^{-2}]
LAI_c	leaf area index of upper canopy (used in SVATs) [m^2 m^{-2}]
LAI_u	leaf area index of undergrowth/understorey [m^2 m^{-2}]
L_i	leaf area in stem i [m^2]
L_v	latent heat of vaporization (2.45 x 10^6) [J kg^{-1}]

L_vE	Evaporation [W m-2] with additional subscripts (i.e. L_vE_x) b bushes c canopy (upperstorey), used in SVATs s soil t total u understorey (herbs/grass/soil)
M	total number of harmonics used in Fourier series representation of soil temperature.
N	runoff (see evapoclimatonomy-model) [mm]
m	constant (0.45) in Eq. A4.3 (see Owen and Thomson, 1963)
n	counter in Fourier series
n	constant (0.8) in Eq. A4.3 (see Owen and Thomson, 1963)
n	attenuation coefficient of eddy diffusivity within the vegetation [-]
n'	attenuation coefficient of wind speed within the vegetation [-]
p	power in the Stefan-Boltzmann law valid for the entire longwave spectrum (4.0) [-]
$p^{8\text{-}14}$	power in the Stefan-Boltzmann law valid for 8-14 μm only (4.49) [-]
pF	$^{10}\log(h)$ with h (soil water potential head) in cm
P	precipitation [mm or kg m^{-2} s^{-1}] with subscript s for soil
P	period of the fundamental cycle (24 x 3600) [s]
PM_c and PM_s	help functions in SW [W m^{-2}]
Pr	Prandtl number [-]
q	specific humidity [g/kg] with additional subscripts a reference level c canopy (upperstorey) level s soil surface level with superscript *sat* for saturated u understorey level 0 mean vegetation air stream level
Q_p	Photosynthetically active radiation [μmol m^{-2} s^{-1}]
r_h	total resistance for heat in a bulk transfer equation [s m^{-1}]
r_{ah}	aerodynamic resistance between T_a and T_{z0m} for heat in a bulk transfer equation [s m^{-1}]
r_r	excess resistance for heat in a bulk transfer equation [s m^{-1}]
$r_a{}^a$	aerodynamic resistance (SVATs) between mean canopy air stream and reference level [s m^{-1}]
$r_a{}^a(0)$	aerodynamic resistance (SVATs) between mean canopy air stream and reference level in the extreme case of bare soil [s m^{-1}]
$r_a{}^a(4)$	aerodynamic resistance (SVATs) between mean canopy air stream and reference level in the extreme case of a complete canopy cover (see SW) [s m^{-1}]
$r_a{}^s$	aerodynamic resistance (SVATs) between the soil source and the mean canopy air stream [s m^{-1}]
$r_a{}^u(0)$	aerodynamic resistance (SVATs) between the understorey source and the mean canopy air stream in the extreme case of understorey [s m^{-1}]
$r_a{}^u(4)$	aerodynamic resistance (SVATs) between the understorey source and the mean canopy air stream in the extreme case of complete canopy cover (see SW) [s m^{-1}]
$r_a{}^u$	aerodynamic resistance (SVATs) between the understorey source and the mean canopy air stream [s m^{-1}]
$r_b{}^c$	canopy (upperstorey) bulk boundary layer resistance (per unit ground area) [s m^{-1}]

$\overline{r_b^c}$	mean canopy (upperstorey) boundary layer resistance (per unit leaf area) [s m^{-1}]
$r_b{}^u$	undergrowth bulk boundary layer resistance [s m^{-1}]
$r_s{}^c$	canopy bulk stomatal surface resistance (per unit ground area) [s m^{-1}]
$r_s{}^u$	undergrowth stomatal surface resistance [s m^{-1}]
$r_s{}^s$	soil surface resistance [s m^{-1}]
$r_l{}^s$	soil resistance to water vapour transfer of the dry soil layer (see CM) [s m^{-1}]
$r_h{}^{s},_{dry}$	resistance of upper soil layer (see CM) [s m^{-1}]
$r_h{}^{s},_{wet}$	resistance of lower soil layer (see CM) [s m^{-1}]
R	gas constant [J mol^{-1} K^{-1}]
R_{dk}	dark respiration [mg m^{-2} s^{-1}]
R_d	diffuse radiation flux density [W m^{-2}]
$Re*$	Reynolds number [-]
Ri_B	Bulk Richardson number [-]
$R_{l,\downarrow}$	longwave incoming radiation [W m^{-2}]
$R_{8-14,\downarrow}$	longwave incoming radiation between 8 and 14 μm [W m^{-2}]
$R_{l,\uparrow}$	longwave outgoing radiation [W m^{-2}] with additional subscript *b* bushes *s* soil *t* total *u* understorey (herbs/grass/soil)
R_n	net radiation [W m^{-2}] with additional subscripts *b* bushes *c* canopy (upperstorey), used in SVATs *s* soil *t* total *u* understorey (herbs/grass/soil) or undergrowth (SVATs)
R_p	intercepted PAR (sometimes per unit leaf area) [W m^{-2}]
R_s	total downward solar radiation flux density [W m^{-2}] with occasional subscript *max* to denote a maximum value (TL g_l-parameterization)
t	time [s], in Appendix 2 used with subscripts *1* and *2*
$t*$	residence time (see evapoclimatonomy model) [months]
T	general temperature [°C *or* K], often soil temperature
T_a	air temperature at screen or reference height [°C *or* K]
T_c	temperature at canopy (or upperstorey) surface level (SVATs) [°C *or* K]
T_l	temperature of the upper (dry) soil layer in CM [K]
T_i	soil temperature at six hour intervals (subscripts i =1, 4) at depths z_1 [°C]. See Eq. A2.5
T_i'	soil temperature at six hour intervals (subscripts i =1, 4) at depths z_2 [°C]. See Eq. A2.5
$T_{i,z}$ and $T_{i+1,z}$	temperatures at times t_i and t_{i+1}, respectively, at several depths z.
T_L	lower temperature limit in JS g_l-parameterization
T_m	maximum air temperature[°C]
T_m	temperature of the lower boundary of the lower (wet) soil layer in CM [K]
T_n	minimum air temperature[°C]
T_s	surface temperature in a general sense [°C *or* K]
T_s	soil surface temperature in SVATs [K]

$T_{s,x}$	measured surface temperature [K] with additional subscripts x
	b bushes
	s soil
	t total
	u understorey (herbs/grass/soil) layer or undergrowth
	1 soil in DD Force-Restore equation (see DD)
$T_{s,1}$	upper soil temperature in DD [K]
$T_{s,2}$	deep soil temperature in DD [K]
T_U	upper temperature limit in JS g_l-parameterization
T_0	temperature at mean canopy air stream
u	wind speed [m s^{-1}]
u	wind speed in the x direction [m s^{-1}]
u_h	wind speed at canopy top [m s^{-1}]
u_*	friction velocity [m s^{-1}]
v	wind speed in the y direction [m s^{-1}]
w	vertical wind speed [m s^{-1}]
w	mass of water retained on the vegetation surface per unit ground area with extra subscript *max* to denote its maximum value [kg m^{-2}]
w_c	canopy (upperstorey) leaf width [m]
w_u	undergrowth leaf width [m]
X_i	surface variable or flux with subscripts i:
	t total
	s soil
	b bushes
	u understorey (herb/grass) layer
z	depth in soil or height in atmosphere [m] with various subscripts
z_{0h}	roughness length for heat [m]
z_{0m}	roughness length for momentum [m]
$z_{0m,s}$	soil roughness length for momentum in SVATs
$z_{0m,u}$	understorey roughness length for momentum in SVATs

Greek

α	a factor (0.52) in formula A4.3, depending to some extent on the shape of the roughness elements
α	proportional coverage of understorey or soil in case of savannah (0.80-0.90) or tiger-bush (0.66) [-]
α_i	proportional coverage of surface i [-]
β	Bowen ratio [-]
β	radiation extinction coefficient [-]
γ	psychrometer constant, C_p/L_v (4 x 10^{-4}) [K^{-1}]
γ	psychrometric constant [Pa K^{-1}]
γ	$= u_h/u_*$ in drag partition model [-]
γ_1 or γ_2	function of psychrometric constant and resistances (see CM) [Pa K^{-1}]
Γ	correction factor in DD [-]
Γ	CO_2 compensation concentration [mg m^{-3}]
δ	step function in DD [-]
Δ	change of saturation vapour pressure with temperature [kPa/°C or Pa K^{-1}] with extra subscripts *1* (canopy level), *2* (soil level) and *3*

	(reference level)
ΔS	lump storage term in Eq. 1.1
ε and ε_0	initial and maximum initial quantum use efficiency [mg J^{-1} PAR]
ε_a	atmospheric emissivity after correction for clouds [-]
$\varepsilon_a (0)$	atmospheric emissivity without correction for clouds [-]
ε_c	canopy (upperstorey) emissivity (see DD) [-]
ε_s	soil emissivity (see DD) [-]
$\varepsilon_{s,\,x}$	surface emissivity [-] with additional subscripts x *b* bushes *s* soil *t* total *u* understorey (herb/grass) layer
η	help function in CM (-)
ζ	help function in CM (-)
θ	volumetric soil moisture content [m^3 m^{-3}]
θ_{equ}	equilibrium volumetric soil moisture content [m^3 m^{-3}]
$\theta_{s,1}$ or $\theta_{s,2}$	θ of the upper and lower soil layer, respectively [m^3 m^{-3}]
θ_s^{crt}	critical θ [m^3 m^{-3}]
θ_s	saturated θ [m^3 m^{-3}]
Θ	integrated volumetric soil moisture content [mm]
κ	soil thermal diffusivity [m^2 s^{-1}]
κ_θ	molecular thermal diffusivity (2.06 x 10^{-5}) [m^2 s^{-1}]
λ	soil thermal conductivity [W m^{-1} K^{-1}] with occasional subscript *sat* to denote the saturated lower soil layer (see CM)
λ	constant (11.6) in Eq. A4.10, see Kondo (1975)
λ	roughness density [-]
μ	spectral wavelength [μm]
ν	kinematic molecular viscosity (1.461 x 10^{-5}) [m^2 s^{-1}]
ξ	fraction of potential evaporation [-]
Ξ	relative saturation [-]
ρ	density of air [kg m^{-3}]
ρ_c	CO_2 density (kg m^{-3})
ρ_l	density of water (kg m^{-3})
ρ_s	density of the soil solid phase (kg m^{-3})
ρ_v	density of water vapour [kg m^{-3}]
$^b\rho_d$	dry bulk density (kg m^{-3})
σ	Stefan-Boltzmann constant (5.67 x 10^{-8}) [W m^{-2} K^{-1}]
σ_c	vegetation area average shielding factor
σ_{8-14}	Stefan-Boltzmann constant for the longwave window (1.25 x 10^{-9}) [W m^{-2} K^{-1}]
τ	momentum flux density or surface Reynold's stress [N]
τ	tortuosity factor of the dry soil layer (see CM) [-]

τ_l	period of one day (see DD) [s]
τ_a	atmospheric transmissivity [-]
φ_i	volume fraction of soil component i [-] with subscripts l liquid component s solid particles
φ_{0n}	phase angle of the n^{th} soil temperature harmonic for the upper boundary (see Eq. A2.7)
φ_x	atmospheric stability function [-] with subscript $x = h, e, m$ for heat , water vapour or momentum, respectively.
Ψ	ratio between $\overline{r_s^c}$ and $\overline{r_b^c} + \overline{r_s^c}$ (see DD) [-]
Ψ	profile influence function in drag partition model, Ψ_h is Ψ at $z=h$ [-]
$\Psi_{r,max}$ and Ψ_r	(maximum) root-weighted soil water potential [cm] in HP96
Ψ_x	integrated stability function, needed in resistance analogue of flux-profile relationship with subscript $x = h, e, m$ for heat , water vapour or momentum, respectively.
ω	radial frequency in Fourier series representation ($=2\pi/P$) [s^{-1}]

1 INTRODUCTION

1.1 The surface energy balance in semi-arid regions

1.1.1 General

A continuous exchange of energy takes place between the Earth's surface and the atmosphere. According to the basic law of energy conservation, stating that incoming energy balances outgoing energy, these land-surface-atmosphere interactions can be described by:

$$R_n = H + L_vE + G + \Delta S + D_h \tag{1.1}$$

(see De Bruin, 1982; Stull, 1988; Garratt, 1992). If it is assumed that horizontal flux divergence (D_h) and heat storage (ΔS) are insignificant (Brutsaert, 1982; Stannard et al., 1994), Eq. 1.1 states that the external forcing of land-atmosphere processes, the net radiation (R_n), is redistributed over sensible heat (H), evaporation (L_vE, the latent heat) and soil heat (G) fluxes. The surface energy balance (SEB) is an important boundary condition for the land surface, determining the partitioning of available energy (R_n-G) between H and L_vE. The energy balance is related to the hydrological cycle through the evaporation term. An accurate quantification of the surface energy balance components, in combination with the water budget, is important for solving practical questions relating to environmental sciences such as hydrology, meteorology and agronomy. For agronomists, understanding the SEB will enhance efficient and sustainable land use by better crop management (irrigation, pest management), soil management and erosion control (Feddes, 1971; Doorenbos and Pruitt, 1977; Hall et al., 1979; De Bruin, 1982; Jensen et al., 1990; Lövenstein et al., 1991; Stroosnijder, 1991; Stannard, 1993; Sivakumar et al., 1993; Atzema, 1994; Wallace, 1995).

In meteorology, knowledge of the SEB is of vital importance in advancing our understanding and ability to model land surface-atmosphere interactions, leading to more reliable weather forecasts (Perrier, 1982; Eagleson, 1986; Beljaars and Holtslag, 1991; Kustas and Goodrich, 1994). This will also assist us in forecasting local and larger-scale effects of climate changes on rainfall, for example, which influences desertification and agricultural yield amongst other things (Nicholson, 1981; Shukla and Mintz, 1982; Oliver and Sene, 1992; Xue and Shukla, 1993).

The relative portion of each flux depends on surface and atmospheric properties (Van Wijk, 1963; Brutsaert, 1982; Dickinson, 1983; Stull, 1988; Monteith and Unsworth, 1990; Shuttleworth, 1991). To illustrate this we can use the example of a dry desert surface: evaporation will be practically zero, and H and G will consume roughly equal amounts of energy (Menenti, 1984; Novak, 1990). For a wet rain forest, however, H and G are negligible and all captured energy will be converted into latent heat (Shuttleworth et al., 1984; Sellers et al., 1989).

The surface exerts its influence on the energy balance via several mechanisms (Monteith and Unsworth, 1990; Shuttleworth, 1991). Firstly, R_n is affected by the radiative properties albedo and emissivity (Van Wijk, 1963; Dickinson, 1983; Garratt, 1992). These properties are a function of surface type, that is soil or vegetation, and status, such as moisture content of soil or biomass. Given a certain amount of energy at the soil surface, G depends predominantly on thermal soil properties, which are a function of soil composition and soil moisture content (Van Wijk, 1963; Kimball and Jackson, 1975; Ten Berge, 1990).

H and L_vE are directly determined by available energy, the relevant potential difference (temperature or humidity) and the aerodynamic transfer coefficient (Shuttleworth, 1991). The latter is dependent primarily on the geometry of surface roughness elements (Shaw and Pereira, 1982; Raupach, 1992). These effects can be summarized by two parameters, determining the effectivity of exchange between the surface and the atmosphere, the roughness lengths for wind, z_{0m} , and temperature z_{0h} (Beljaars and Holtslag, 1991; Kohsiek et al., 1993). Furthermore, atmospheric stability also plays a role (Richardson, 1920; Mahrt and Ek, 1984).

Finally L_vE, and thus the SEB, is affected by surface processes, i.e. the exchange of water vapour between the surface cavities, either stomatal cavities or soil pores, and the atmosphere (Monteith, 1965; Jarvis, 1976; Van de Griend and Owe, 1994). The magnitude of this effect can be described through a surface-related resistance or its reciprocal, the conductance. It is mainly governed by environmental entities and surface status.

For the most part, this thesis will discuss the physical significance of the energy fluxes described above. Furthermore, the influence of aerodynamic and surface resistances on the apportionment of available energy over L_vE and H will be examined. These processes will be considered in a micrometeorological, theoretical framework.

Besides R_n, H, L_vE and G, this thesis will also study the CO_2 flux. Although we realize that its contribution to the SEB is negligible, its measured diurnal and seasonal course, together with measured values of L_vE and leaf conductance, has proven to be useful in understanding the behaviour of plant species under various conditions (Tenhuenen et al, 1987; Baldocchi, 1994; Jacobs, 1994).

1.1.2 Interdisciplinary experiments

For several decades, meteorologists have tried to capture the SEB by making direct ground measurements and computations. These efforts were mainly confined to the wetter and cooler parts of the world, and to 'commercial' vegetation such as agricultural crops (Penman and Long, 1960), pasture fields (Rider and Robinson, 1951; De Bruin, 1982) or forest areas (Stewart and Thom, 1973; McNaughton and Black, 1973). Recently, climatological interest has shifted to the more arid areas. Arid climates cover nearly 40 % of the world, of which 7.5 % are hyper-arid, 12.5 % arid and 17.5 % semi-arid (Hare and Ogallo, 1993). Nevertheless, comparatively little is known about the interrelationship between vegetation growing in these areas and the atmosphere. More insight is needed into the considerable influence of these areas on global circulation, triggered by growing concern about the greenhouse effect and desertification (ICIHI, 1986; Hare and Ogallo, 1993).

At the same time, two new tools came to our aid in the search for an understanding of the processes at work on the Earth's surface: remote sensing (Pinker, 1990) enabled us to monitor larger surface patches in one go and digital computers helped us to handle elaborated simulations. These developments resulted in various interdisciplinary campaigns aiming at aggregating single point ground measurements using remote sensing (Moran et al., 1994; Prince et al., 1996), in combination with regional soil-vegetation-atmosphere-transfer models and meso-scale models (Sellers et al., 1989; Jacquemin and Noilhan, 1990). Meteorological science made a leap forward and the demand for reliable data, serving as a ground truth for remote sensing and a lower boundary for the numerical weather-prediction models, of all biomes of the Earth increased considerably. Several experiments conducted in semi-arid regions can be mentioned in this context including FIVE (Sellers et al., 1988), WSEBRP

(Van de Griend et al., 1989), HAPEX-Mobilhy (André et al., 1986), SEBEX (Wallace et al., 1992), EFEDA (Bolle et al., 1991), MONSOON (Kustas and Goodrich, 1994) and HAPEX-Sahel (Goutorbe et al., 1994).

This thesis will consider micrometeorological, ground-based data as collected during the HAPEX-Sahel and SEBEX campaign. Occasionally, reference is made to results obtained during EFEDA.

1.1.3 Vegetation

Shortage of water in the semi-arid zones is not just a consequence of low annual rainfall. The problem for human settlement and particularly for agriculture is the seasonal distribution of rainfall, the rate at which it is lost because of evapotranspiration and the usually poor nutrient availability (see Monteith, 1991; Kessler and Breman, 1991; Sivakumar and Wallace, 1991). The processes mentioned above will predominantly result in sparse canopies because the limited amount of water and nutrients available cannot support full vegetative cover (see Wallace and Sivakumar, 1991; Breman, 1992). A considerable amount of these vegetation-types is natural and usually consist of drought-resistant shrub species, grasses and xerophytes with physiologically evolved adaptations to drought (see Cole, 1986; Vetaas, 1992). For this reason, several of the experiments mentioned in § 1.1.2 were carried out above natural, savannah-like vegetation (rangeland for FIVE and MONSOON, savannah and tiger-bush for SEBEX and HAPEX-Sahel).

Savannah can be described as a mixed formation of grasses and woody plants in any geographical area. This coexistence of grasses and shrubs, where the amount of soil moisture available controls the densities of the woodland and the grass, has been attributed to soil, climatological and anthropogenic factors (Eagleson and Segarra, 1985; Cole, 1986; Vetaas, 1992). The majority of the grasses are ascribed to the C_4-group whereas the trees exhibit the C_3 photosynthetic pathway. Tropical savannahs cover some 23 million km^2 between the equatorial rain forests and the mid-latitude deserts. They cover about 20 % of the Earth's surface, 65 % of Africa, 60 % of Australia, 45 % of South America and about 10 % of India and South-east Asia (Cole, 1986).

Grasses and woody species are believed to have developed a different response to the semi-arid environment. Grasses often transpire at their maximum rate (with almost no stomatal control), which causes them to senesce very rapidly and die off in the dry season. Therefore, most grasses have a very intensive, but shallow root system which usually does not extend deeper than 50 cm. The woody species regulate their transpiration via stomatal control, reducing it as moisture becomes scarce. Most species exercise leaf shedding in the dry season to limit water loss. Because of the perennial nature of the bushes, water needs to be transported to the upper plant parts throughout the year. This leads to a very extensive root system with long lateral and vertical roots with sometimes very deep pen roots.

One of the main features of the symbiosis of trees and grasses is the fact that the surface components influence each other. These interactions can be competitive, but recent studies have argued that small-scale facilitative interactions between woody perennials and the herbaceous understorey are also important. The woody perennials affect the sub-canopy grass or herb layer in several ways. There are processes influencing the water balance, the micro-climate and nutrient availability (Tolman, 1989; Von Maydell, 1990; Vetaas, 1992; Breman and Kessler, 1995)

Rainfall reaching the shrubs or trees will either be intercepted or fall through. Intercepted rain water may be returned to the atmosphere by direct evaporation from the leaves or reach the sub-canopy soil by stem flow. The relative importance of these processes depends on the intensity and duration of the rainstorm, on the size of the tree and on foliage density. Stem flow ensures a deep infiltration, usually causing increased moisture availability for the tree itself but not always for the interspace grass layer. Another moisture-affecting mechanism often mentioned is the so-called hydraulic lift (Vetaas, 1992). Some lateral tree roots may compete with the grass root system, thus exerting a negative influence on the water balance of the grass. However, it is usually assumed that most of the near-surface moisture is consumed by the grasses.

The sub-canopy micro-climate is for the most part influenced by the direct interception of solar radiation causing lower air and soil temperatures and higher air humidities. Furthermore, the presence of the canopy causes reduced wind speeds. This combination of factors will generally lead to lower evaporation and thus higher soil moisture content. Soil temperature affects germination whereas the shade plays a role in species composition (see Veenendaal, 1991).

In semi-arid climates it is more common to find higher fertility in the topsoil under tree canopies than in adjacent open land, as indicated by the availability of nutrients and organic matter. One has to question, however, whether a real increase of the nutrient availability for the ecosystem as a whole has occurred, or only a redistribution within the agro-ecosystem (Kessler and Breman, 1991).

This study is concerned with estimating the SEB of two sparsely vegetated, savannah-like Sahelian surface types called fallow savannah (or fallow bush) and tiger-bush. During the twentieth century the Sahel has experienced at least seven severe droughts and several of these have led to famines (Wessels, 1993). Due to the steady growth in population, the introduction of export crops such as groundnut and cotton and the increasing numbers of livestock, the amount of agricultural land has grown constantly. This continuing pressure on land has resulted in the utilization of marginal areas, too short a fallow period and finally to a decrease in soil fertility and environmental degradation. Wind and water erosion have taken their toll and the desertification process began. To understand and fight desertification, we must continue to monitor the Sahelian surface. There have been meteorological campaigns to observe the Sahel for at least ten years (Druilhet and Tinga, 1982; Pagès et al, 1988; Wallace et al., 1992; Goutorbe et al., 1994). In combination with this, remote sensing (Kerr et al., 1987; Tucker et al., 1991; Prince et al., 1996) and modelling (Charney, 1975; Shukla and Mintz, 1982; Sud and Smith, 1985; Novak, 1990; Nicholson and Lare, 1992; Huntingford et al., 1995; Blyth and Harding, 1995) appeared to be very useful.

1.1.4 CO_2 exchange

The amount of CO_2 exchanged by a canopy is important from an agricultural point of view - it largely determines its growth rate and therefore its yield (see Penning de Vries and Van Laar, 1982; Penning de Vries et al., 1989). Because water vapour and CO_2 pass through the same stomatal pores, transpiration and assimilation are closely linked to each other (Goudriaan, 1982). The amount of water 'lost' compared to the amount of CO_2 taken up determines the water use efficiency (see e.g. Lof, 1976; Baldocchi, 1994) governing the plant's water economy which is especially important in arid environments.

On a global scale, we are also interested in the effect of CO_2 enrichment (the 'greenhouse effect') on transpiration (see Jacobs, 1994). Increasing atmospheric CO_2 is likely to have both direct and indirect effects on the behaviour of vegetation (see Vugts, 1993; Jacobs, 1994). The indirect effects are those caused by changes in climate, resulting from the effect of increased CO_2 on the radiative balance of the atmosphere. The direct effects are caused by the response of plant physiological processes to ambient CO_2. Evidence from laboratory and greenhouse experiments (Kimball et al., 1993) shows that stomatal conductances tend to decrease as ambient CO_2 rises, therefore tending to reduce the evaporation from vegetated land surfaces. To properly assess the effect of this vegetation response on the global climate, it will be necessary to incorporate combined energy-water-carbon models into the land surface schemes used in General Circulation Models (GCMs) (Friend and Cox, 1995). Measurements of CO_2 and water fluxes are needed to develop suitable models, and calibrate them for the world's major biomes.

Hence, there is an increasing interest in quantifying the global carbon budget, to allow better prediction of trends in atmospheric carbon dioxide concentrations and global climate change. Gifford (1994) has estimated the missing sink in the global carbon budget as being about 0.4-4 Gt C yr^{-1}, and has suggested that this could be accounted for by an increase in carbon sequestration by terrestrial vegetation in response to increasing atmospheric CO_2 concentration. Recently it has been suggested that deep-rooted savannah grasses of African origin, introduced into the South American savannahs to improve grazing, could be storing enough carbon in their root systems to account for a substantial part of the missing carbon sink (Fisher et al., 1994). Clearly there is a need for a better quantification of the carbon balance of savannahs: this is especially true for the arid deciduous savannahs, such as those that occur in the Sahel, which have been studied less than more humid, evergreen savannahs (Medina, 1986).

This thesis will describe results of atmospheric CO_2 flux, F_c , from a shrub savannah by applying the eddy covariance technique. The measurements will make available some of the first data to be obtained on CO_2 and H_2O-exchange for a semi-natural, mixed plant community, growing in the semi-arid tropics. Such data are necessary for the development of improved soil-vegetation-atmosphere models, able to describe the complex interplay between atmospheric CO_2, vegetation conductance and the SEB in global climate models.

1.1.5 Monitoring the energy balance in semi-arid regions

The determination of the individual terms of Eq. 1.1 is relatively straightforward for a closed canopy. However, the estimation for sparse canopies may give rise to some problems, resulting from the intrinsic properties of semi-arid vegetation as described in § 1.1.3. To start with, any (micrometeorological) measurement in an arid climate is hampered by harsh environmental conditions and the remoteness of these areas. Furthermore, reliable micrometeorological or plant physiological measurements of L_vE, H or F_c require a considerable degree of maintenance, expertise, and financial and human resources.

Small-scale inhomogeneity causes a problem, that is the total surface consisting of a variety of sub-surfaces ranging from vegetation to bare soil with their typical energy flux values (see Allen and Grime, 1995; Wallace and Holwill, 1996; Jacobs and Verhoef, 1996). This introduces a sampling problem for measurement of R_n and G, because we have to find an average flux value for the entire surface (Blyth and Harding, 1995). Even if proper measurements of the several sub-systems are available, the assemblage of those two terms is still quite uncertain (Lhomme, 1992; Braden, 1995; Raupach, 1995). Furthermore, the available energy (R_n-G) must correspond to the upwind area where the latent and sensible heat flux originate, and this will only happen if the controlling upwind surface and atmospheric properties are representative (see Culf et al., 1993; Lloyd, 1995)

Related to this is the fact that semi-arid biomes often have a distinct upper (usually shrubs or bushes) and understorey (a mixture of herbs, grasses and bare soil) with totally different properties and heights. This fact causes complicated source/sink distributions (Lhomme, 1988; Paw U and Meyers, 1989; McNaughton and Van den Hurk, 1995).

Furthermore, the pronounced difference between the surface components may lead to a lateral flux exchange (Graser et al., 1987; Blyth and Harding, 1995; Lloyd, 1995), i.e. of sensible heat between the dry, hot substrate patches and the transpiring vegetation. This effect may sometimes lead to a unsatisfactory energy closure. Another point of consideration are sampling problems caused by the wakes generated by the individual surface elements (Raupach et al., 1980).

The above described demand that the experiment be carefully planned, taking into consideration the site, the instrument location and any averaging procedure used to translate component measurements into effective parameter values. Furthermore, the specific vegetation geometry and behaviour do challenge soil-vegetation-atmosphere models used to calculate the energy balance components (see § 1.2.1).

1.2 Evaporation models

1.2.1 General

The various physical and physiological aspects governing evaporation can be described by evaporation formulae or models. Relatively simple models are applied for practical purposes such as the management of scarce water resources (hydrology), or yield forecasting (Frère and Popov, 1979; Wallace, 1995) More complicated models provide a tool that can be used to gain a better understanding of the relative importance of the various atmospheric, soil and vegetation aspects influencing evaporation (See Goudriaan, 1977). By changing the magnitude of the model parameters, a sensitivity analysis can be carried out. Secondly, they can be used in large-scale climate models, thereby enabling us to estimate the effect of vegetation removal on climate change, for example (Shukla and Mintz, 1982; Dickinson and Henderson-Sellers, 1988; Xue et al., 1990).

Four types of evaporation models can be distinguished: those based on simple, empirical formulae (although physically based), those using diffusion theory (Waggoner and Reifsnyder, 1968), higher-order closure theory (Wilson and Shaw; 1977; Meyers and Paw U, 1987) or Lagrangian theory (Raupach, 1987). The first group employs the concept of potential evaporation (Penman, 1948) or reference crop evapotranspiration which, after using an empirical crop factor, yields actual evaporation (Doorenbos and Pruitt, 1977; Shuttleworth, 1991; Wallace, 1995). The lumping of complex factors like vegetation structure, stomatal behaviour and meteorological parameters into one parameter is very difficult and means that the evaporation estimates have to be treated with a great deal of care (Shuttleworth, 1991; Wallace, 1995).

The diffusion, or first order, or K-theory models assume that the rate of flow of an atmospheric entity can be described by a multiplication of a concentration (water vapour, heat, wind speed) gradient and a diffusion coefficient (Goudriaan, 1977; Norman, 1979). Although this approach works well for molecular flow, requiring molecular diffusivities, the transfer of this concept to turbulent flow often yields imprecise or even incorrect results. This is especially the case for high canopies like forests, where so-called counter-gradient fluxes occur which cannot be described well by diffusion theory (Denmead and Bradley, 1985; Baldocchi and Meyers, 1988). Integration of the differential diffusion equations for heat and energy allows the fluxes to be described by Ohm-type resistance laws.

Many models have been built using the resistance concept. This involves a partition of available energy into sensible heat and evaporation by mimicking the complex exchange process of real vegetation stands. Such models involve simultaneous, interactive solution of energy balance equations at several heights in the canopy, and require estimates of the resistances operating at each level (Shuttleworth, 1991). These resistances involve the aerodynamic and surface-related resistances already mentioned. If the array of in-canopy resistances are taken together, on our assumption that they have a parallel action at an effective source-sink height, single source models can be derived from the multi-level approach. By far the simplest approach is the Penman-Monteith equation, which requires no information on canopy structure and assumes that the air within the canopy is well-mixed with all the leaves of the canopy being exposed to exactly the same atmospheric properties. Moving in the direction of increasing complexity we find the two-layer models such as Deardorff (1978), Shuttleworth and Wallace (1985), Choudhury and Monteith (1988), Kustas (1990), or Dolman (1993). These have proven useful in describing sparse canopies (Smith and Barss, 1988; Lafleur and Rouse, 1990; Wallace et al., 1990; Nichols, 1992; Blyth, 1995; Blyth and Harding; 1995, Huntingford et al., 1995; Van den Hurk et al., 1995). These models allow for the separate behaviour of canopy and understorey, which may be useful because the evaporation from soil or shallow-rooted ground vegetation behaves quite differently to evaporation from deeper-rooted overstorey vegetation (Huntingford et al., 1995).

Higher order closure models introduce budget equations for the second-order moments; second-order moments include the turbulent covariances for mass and momentum transfer and velocity variance terms, and the variance terms represent components of turbulent kinetic energy (Baldocchi et al., 1991).

Yet another group of models is based on Lagrangian theory (Raupach, 1989; Raupach, 1991; Dolman and Wallace, 1991). Originally, these models computed concentration and scalar flux density profiles by repeated simulations of a large number of particle trajectories. A recent analytical representation of this approach (Raupach, 1991; Van den Hurk and McNaughton, 1995) constructed the canopy concentration profile as the sum of a diffusive (far-field) and a non-diffusive (near-field) component. This approach required much less computation time than the original trajectory models. From here, McNaughton and Van den Hurk (1995) combined this Lagrangian approach with a relatively simple two-layer resistance model. However, the lack of suitable energy balance data hampered them when it came to evaluating the usefulness of this method.

This thesis will only deal with diffusion type, resistance-based models. They will generally be referred to as soil-vegetation-atmosphere-transfer schemes (SVATs), a term often used in the literature to denote the land surface parameterization in GCMs. Although recognizing the importance of combined energy-water-carbon models, this thesis will limit itself to SVATs describing energy and water transfer only.

1.2.2 The resistance network

a) Terminology

In the literature, the terms resistance and conductance, the latter being the reciprocal of resistance, are often used alternately. To be consistent with the majority of the literature, the leaf- and canopy related entities, predominantly based on physiological measurements, will be called conductances in this thesis. Any other exchange based on diffusion-analogy, as well as all transfer processes in the evaporation models, will be described by resistances in order to follow the general terminology in present-day SVATs.

b) Leaf and canopy conductances

In plant physiological research the average stomatal opening of a multiple of leaves is often referred to as leaf or bulk stomatal conductance, here called g_l. Scaling this conductance, with knowledge of the leaf area, from the leaf to the canopy level yields the canopy stomatal conductance, g_c (Szeicz and Long, 1969; Whitehead et al., 1981; Wallace et al., 1990; Baldocchi et al., 1991; Rochette et al., 1991b; Kim and Verma, 1991; Norman, 1993; Raupach, 1995). This is called the 'bottom-up' approach and it can either be used with directly measured leaf conductances (porometry) as input or with estimates of g_l. The latter are obtained from a parameterization describing the response of the individual leaves to controlling environmental properties. This entails fitting a suitable model to the measured leaf conductances, thus yielding a set of parameter constants representative for the specific canopy. Until now, the empirical multiplicative model of Jarvis (1976), later modified by Stewart (1988) and thereafter referred to as the JS-approach, is widely used. Recent developments however, employ plant physiological formulae (Jacobs, 1994; Friend and Cox, 1995).

For the 'top-down' determination of canopy stomatal conductance, a stand-level or 'big-leaf' type exchange model is inverted to find g_c from water vapour or trace gas measurements (Baldocchi et al., 1991). If in this top-down scaling-technique the Penman-Monteith equation is applied, we obtain the canopy *surface* conductance, in this thesis denoted as g_{cs} (Kim and Verma, 1991; Baldocchi et al, 1991). In some cases, this single-layer PM-equation has been extended to a multi-layer approach (Lhomme, 1991; Huntingford et al., 1995).

Values of g_c and g_{cs} are often assumed to be identical, although it is shown both theoretically and experimentally that these two measures of canopy conductance are not the same (Finnigan and Raupach, 1987). The parameter g_{cs} contains additional information relating to the net radiation balance, the aerodynamic resistances inside the canopy and the fact that soil evaporation is usually non-zero (Finnigan and Raupach, 1987; Baldocchi et al, 1991). Some scientists (for example, Paw U and Meyers, 1989) incorporated soil surface conductance in g_{cs} by considering the soil as another big leaf with a *LAI* of 1.0. Finding g_c, both from a top-down or bottom-up approach, is severely hampered under the non-ideal conditions characteristic of semi-arid vegetation: a sparse canopy cover and a separate understorey canopy.

c) Soil surface resistance

Evapotranspiration studies of sparsely vegetated areas are particularly difficult because the relative contributions to the total evaporation from the soil and the plant components will vary throughout a day and throughout a season (Massman, 1992; Wallace and Holwill, 1996; Jacobs and Verhoef, 1996). Therefore the well-known single-source approach has been extended to allow for the partition between bare soil and vegetation (Shuttleworth and Wallace, 1985). Besides canopy conductance, these models require knowledge of the soil surface resistance. The soil surface resistance describes the resistance for water vapour to diffuse from the evaporation front, where the phase change from liquid to vapour takes place, to the soil surface. The evaporation front will be at or close to the surface for a wet soil. For a dry soil, evaporation will occur from wet soil below a progressively deepening dry layer (Monteith, 1981; Van de Griend and Owe, 1994) . The formulation of surface resistance to soil evaporation therefore plays an important role in the present-day SVATs.

Soil surface resistance can be measured directly with a so-called fast air circulation chamber (Kohsiek, 1981), or by applying a top-down approach similar to the one described above (Massman, 1992). These values are usually related to top soil moisture content (Katerji and Perrier, 1985; Camillo and Guerney, 1986; Van de Griend and Owe, 1994) or sometimes to wind speed (Kondo et al., 1990). For modelling purposes a rather arbitrary and constant value during the day is often chosen (Shuttleworth and Wallace, 1985).

d) Aerodynamic resistances

In the description of sensible or latent heat flux, the aerodynamic transfer resistance of a vegetation can be visualized as having two components. The first one is associated with the leaf boundary layer, whereas the other describes the resistance of the air between the mean canopy source height and reference (measurement) height. Estimates of the latter aerodynamic resistance, demand values of momentum roughness length, z_{0m} , and displacement height, d. In a one-layer or bulk transfer model an extra roughness length for heat or water vapour (z_{0h}) is used to describe the transfer through the leaf boundary layer. The multi-layer SVATs do not require an estimate of z_{0h} - the difference between scalar and momentum transfer is parameterized through the direct use of leaf boundary layer resistances that represent the interfacial sub-layer close to the surface (McNaughton and Van den Hurk, 1995; Blyth and Dolman, 1995).

e) Momentum roughness parameters, z_{0m} and d

Besides problems concerning the sampling strategy and the techniques for measurement of mass/energy fluxes, another complication of the semi-arid, sparsely vegetated areas is the fact that their roughness characteristics, along with other surface characteristics, are difficult to determine and to interpret. The scattered elements influence the wind profile by the wakes they generate and by possible lee effects.

Many articles about the determination and evaluation of z_{0m} and d for closed canopies can be found in the literature. Early results were summarized by the relations $d = 0.66h$ and $z_{0m} = 0.13h$ (Monteith, 1973). Note that only the height of the vegetation is considered in these old formulas, while many other characteristics contribute to z_{0m} and d, particularly for sparse vegetation. So far as the roughness parameters for vegetation under incomplete canopy cover are concerned, fewer experiments have been conducted and their z_{0m}/h and d/h-ratios seem to vary widely (Hicks, 1973; Garratt, 1978; Riou et al., 1987; Hatfield, 1989; Kustas et al., 1989a; Dolman et al., 1992). See Wieringa (1993) for an extensive review of this literature. Most authors agreed that a change in canopy height and branching effects cause the values of z_{0m} and d to vary throughout the season. For sparse canopies they claim that, besides plant height, density as well as plant shape become important. The estimates of z_{0m} and d might even be plant specific (Kustas et al., 1989a). Hatfield (1989) recognized that z_{0m} had to be a function of the height/width ratio for row crops (Verma and Barfield, 1979) or of the ratio silhouette area to the total area of an object (Lettau, 1969). Order in this apparent arbitrary range of z_{0m}/h and d/h-ratios may be obtained by applying drag partition theory (see Schlichting, 1936; Lettau, 1969; Wooding et al., 1973; Seginer, 1974; Arya, 1975; Shaw and Pereira, 1982; Raupach, 1992).

f) Roughness length for heat transfer

In most larger-scale (for example, GCMs) models the vertical heat flux in the surface layer is described as a function of $T_a - T_s$, with T_a the air temperature at reference level and T_s the surface temperature at z_{0h}, which is the roughness length for sensible heat transfer. In comparison to z_{0m}, the parameter z_{0h} is very poorly understood beyond empirical measurements and there have been fewer attempts at understanding the physics that determine its magnitude and behaviour (Malhi, 1993). Various studies have revealed that z_{0h} differs significantly from the roughness length for momentum that appears in the theoretical logarithmic wind profile (Tennekes, 1973). This implies that the parameter $kB^{-1} = \ln(z_{0m}/z_{0h})$ differs from 0 (Thom, 1972; Garratt and Hicks, 1973).

The topic of kB^{-1} has been investigated for all kinds of natural and artificial surfaces ranging from the aerodynamically smooth to the rough, involving the derivation of empirical formulae or deriving kB^{-1} inversely from experimentally obtained flux values and gradients (Sverdrup, 1937; Sheppard, 1958; Owen and Thomson, 1963; Thom, 1972; Garratt and Hicks, 1973; Brutsaert, 1982; Kohsiek et al., 1993). Originally, kB^{-1} was given a value of 2, but recent investigations revealed that much higher values are possible especially for sparse canopies (see Verma and Barfield, 1979; Garratt, 1980; Hatfield et al., 1985; Kustas et al., 1989b; Malhi, 1993; Stewart et al., 1994; Blyth and Dolman, 1995), but even for grass (Rider and Robinson; 1951; Beljaars and Holtslag, 1991; Duynkerke, 1992).

The above mentioned resistance-related topics (b, c, d, e, and f), and possible deviations from literature, will be studied in detail in this thesis.

1.3. Research objectives of the present study

The main objective of this study is to gain a better understanding of the behaviour of the exchange of mass and energy between sparsely vegetated surfaces and the atmosphere under the environmental conditions typical for a semi-arid climate, in particular the climate of the African Sahel region. The study will be confined to two Sahelian shrub-dominated vegetation-types. The first (tiger-bush) can be considered natural, whereas the second (fallow savannah, forming part of a rotation cycle) is semi-natural. SEB was studied both on a diurnal as well as on a seasonal scale, because of the large temporal (and spatial) gradients encountered under semi-arid conditions (Kowal and Kassam, 1978; Kustas and Goodrich, 1994).

To accomplish this main objective, an extensive micrometeorological data set, including soil and plant physiological studies, concerning the SEB and its controlling parameters has been gathered for both vegetation types. These data were collected during the HAPEX-Sahel Intensive Observation Period (August-October, 1992) by the Department of Meteorology, Wageningen Agricultural University (WAUMET), and the Winand Staring Centre, referred to in this thesis by the acronym SC-DLO. In addition, data obtained during the SEBEX campaign by the Institute of Hydrology (Wallingford, UK) were used to capture the seasonal course of the energy balance.

With these data, questions can be answered with respect to the magnitude of the separate terms in the energy balance and the way the relative importance of these terms varies with changes in environment (weather, soil status) or the physiological phase of the vegetation. For example: what percentage of the total incoming energy is accounted for by the soil heat flux? Or: how does the evaporation vary through the seasons? And also: is this pattern significantly different from those observed for more humid climates? With the joint measurement of leaf conductances and CO_2 flux more insight can be obtained into the physiological behaviour of the vegetation as expressed by entities such as water use efficiency, for example.

A second research objective is to test how well the energy balance can be predicted by existing SVATs. Furthermore, if there are major and consistent deviations between measurements and model, which parameterization (of net radiation, aerodynamic resistance, soil heat flux etceteras) used in these SVATs needs improvement. With sensitivity analyses we can address issues such as: is the difference in evaporation observed between both vegetation types predominantly caused by differences in available energy, or by distinctive surface and aerodynamic resistances ?

1.4 Organization of the thesis

The thesis is composed of eight chapters. These sometimes contain (parts of) papers published in or submitted to international scientific journals. Chapter 2, 3 and 4 provide tools for handling the experimental results and the model runs. Chapter 5, 6, 7, and 8 discuss the results of measurements (5,7) and modelling (8) or a combination of both (6).

Chapter 2 is concerned with explaining the theory behind the various terms of the energy balance. Attention is paid to the nature of net radiation and how it is composed of several gain and loss terms. Moreover, the theory behind the measurement of the soil, sensible and latent heat flux is described. Detailed formulae are to be found in the appendices. Any simplifications or limitations which are necessary to avoid complicated, time-consuming and error-prone calculation procedures in the rest of the thesis will be mentioned.

In Chapter 3 the experimental setting is illustrated and it includes information on climate and vegetation. Subsequently, the experimental set-up of the field campaigns is described and instrument types, locations and measurement procedures are summarized.

Chapter 4 contains a summary of the used SVATs (Deardorff, 1978; Shuttleworth and Wallace, 1985; Choudhury and Monteith, 1987; Huntingford et al., 1995; Van den Berg, 1995 a, b) and their governing equations. In addition, an outline of several models which have been applied to fit the average leaf conductance as a function of environmental conditions will be given (Jacobs, 1994; Huntingford et al., 1995; Hanan and Prince, 1996). Finally, the evapoclimatononomy model (Nicholson and Lare, 1990) and a drag partition model (Raupach, 1992), used to calculate z_{0m} and d, will be explained.

The contents of Chapter 5 concern the measurement results of R_n, G, H and L_vE. The information on R_n has been decomposed into sections describing its individual terms; shortwave incoming, shortwave outgoing, longwave incoming and longwave outgoing radiation. Special attention will be given to the topic of surface temperature, as this is a key parameter in the SEB. All fluxes and other governing surface parameters will be presented in a diurnal and seasonal fashion. For diurnal presentations half-hourly averages will be used, whereas the seasonal course is emphasized by applying daily averages. The diurnal course will be primarily depicted with the HAPEX-Sahel data, whereas the SEBEX data will be used to illustrate the seasonal changes monitored over fallow savannah and tiger-bush.

The results relating to the resistance network, largely determining the final magnitude of the fluxes, will be presented in Chapter 6. A considerable part of this chapter deals with the determination of z_{0m} and z_{0h} , or better their ratio, $kB^{-1}= \ln(z_{0m}/z_{0h})$. Hereafter, the results of the bulk stomatal conductance, the canopy conductance and the soil surface resistance will be discussed.

Chapter 7 mainly describes the measurements of the CO_2 flux as made for the CWS HAPEX-Sahel fallow savannah site. Links are made occasionally to CO_2 fluxes observed at other sites of the HAPEX-Sahel grid. Also, the ratio of the CO_2 flux and the evaporation, generally called the water use efficiency, will be studied and related to environmental variables.

Finally, Chapter 8 describes some preliminary results of the SVAT-modelling, combining the findings of the previous chapters to create a reliable set of input parameters and measured fluxes to verify the model output. The performance of the different SVATs to describe the SEB of both surfaces will be briefly tested. A sensitivity analysis will illustrate the theoretically possible difference between evaporation from savannah and tiger-bush. Finally, the interannual variation of the SEB will be studied using the Evapoclimatonomy model (Nicholson and Lare, 1990). Monthly averages of meteorological input and appropriate parameterizations for surface parameters such as albedo will be used.

2 THEORETICAL BACKGROUND

2.1 Introduction

The well-known energy budget is given by Equation 1.1 (all fluxes are in W m^{-2}). In this equation, R_n is the external forcing, while the other terms are response terms. If R_n is directed towards the surface, it is positive by definition. For the other fluxes, those cases where the fluxes are directed away from the surface are positive (i.e. under general daytime conditions). ΔS is a lump term that refers to processes such as radiation exchange between leaves or chemical storage by photosynthesis. For vegetation layers of a limited vertical extension and density, ΔS can be neglected. The advection term is also usually neglected, but it can be significant near the edges of crops or forests (Garratt, 1992). Without ΔS and D_h, the vegetation layer is considered as an infinitesimally thin layer and its energy balance is identical to that of a bare soil surface. In the rest of this thesis, this simplified version of the energy balance, i.e. without ΔS and D_h, will be applied.

As has been mentioned in Chapter 1, one of the major aims of this thesis is to assemble a proper set of data with which the energy balance of two Sahelian vegetation-types can be adequately quantified. In this chapter the theory behind the fluxes forming part of Eq. 1.1 and the measurement methods derived from it will be briefly described. Sections 2.2 to 2.4 will deal with net radiation and its incoming and outgoing components, soil heat flux and sensible and latent heat fluxes. Hereafter, in § 2.5, the procedure by which area-averaged entities will be derived from the sampled components will be described.

2.2 Radiation

2.2.1 Introduction

Eq. 1.1 showed that net radiation reaching the surface is the driving force of the atmospheric processes governing energy exchange. Together with G, it determines the energy available for sensible and latent heat transfer, and it is therefore needed to check the validity of those fluxes as directly measured by the eddy covariance (EC) method. Secondly, several indirect micrometeorological methods such as the Bowen ratio energy balance (BREB) method need an estimate of R_n and G, from which L_vE and H can be found in combination with humidity and temperature gradients. Net radiation is also the key input in the majority of the SVATs. It is therefore of paramount importance to establish this variable as accurately as possible. For sparse canopies, a challenge lies in the proper determination of the radiation flux densities upwelling from the inhomogeneous surfaces. This requires, among other things, reliable estimates of average surface properties such as albedo, a, and emissivity, ε_s.

2.2.2 Net radiation

The radiation exchanged at a surface consists of a variety of wavelengths, μ, ranging from very short wavelengths (i.e. ultraviolet radiation, $\mu = 0.01$-0.1 µm) to long wavelengths (infra-red radiation, μ = 1-100 µm). In micrometeorology, wavelengths between 0.1 and 50 µm are important. This radiation is split into two wavelength bands, short (0.1-0.3 µm) and longwave (3-50 µm). The reason for this is that the solar spectrum consists almost entirely of wavelengths that are shorter than 4 µm, while the earth/atmosphere system emits longwave (infra-red) radiation.

The net all-wave radiation flux density, R_n, is decomposed into the following combination of shortwave and longwave terms:

$$R_n = (1-a)R_s + R_{l,\downarrow} - R_{l,\uparrow} \tag{2.1}$$

where R_s is the total downward solar radiation flux density (W m^{-2}), a the surface albedo, and R_l the longwave radiation flux density (W m^{-2}). Upward and downward arrows represent upwelling and downwelling fluxes, respectively. All fluxes represent radiation through a horizontal plane. Net radiation is measured by a net radiometer. This instrument consists of a thermopile protected by two thin polyethylene domes, measuring net shortwave ($(1-a)R_s$) and net longwave radiation ($R_{l,\downarrow} - R_{l,\uparrow}$).

2.2.3 Shortwave incoming radiation

The intensity of incoming solar radiation at the top of the atmosphere is called the solar irradiance. Solar irradiance, although fairly constant, is subject to slight variations (± 3.5 % of the average annual value) owing to the variable distance between the earth and the sun. Changes in solar activity can also cause deviations of a few percent (Van Wijk, 1963). For general meteorological purposes an average value of 1370 W m^{-2} is used.

The actual solar radiation reaching the surface will be less due to attenuation caused by scattering, absorption, reflection from clouds and atmospheric turbidity (Van Wijk, 1963; Stull, 1988; Garratt, 1992). These factors together define the transmissivity of the atmosphere, τ_a, which is the fraction of shortwave radiation reaching the surface. The attenuation will be stronger for low sun angles, due to the longer path through the atmosphere on the way down to the surface. Typically, with the sun directly overhead, τ_a will be ≈ 0.8 in cloudless skies and τ_a will be ≈ 0.1 for a complete overcast of low, medium and high clouds (Garratt, 1992). Given the above it can be deduced that maximum values of R_s, observed for cloudless periods around noon, will be around 1000-1100 W m^{-2}.

Thus, total downward solar radiation flux density, R_s, consists of a direct-beam solar radiation flux density and of radiation that has been scattered in a downward direction by molecules (Raleigh scattering) and particles and of reflection from clouds. The scattered and reflected radiation together are referred to as downward diffuse solar radiation density, R_d. The fraction of incident radiation that is diffuse varies from about 0.1 for an overhead sun and cloudless sky to more than 0.9 below thick clouds.

R_s can be measured directly with a pyranometer (usually a Kipp solarimeter), where the wavelength range is delineated by the spectral transparency of the glass domes (generally 0.1-0.3 µm). Accurate measurement of R_s is important for the following reasons. First, together with the other incoming and outgoing radiative fluxes, it provides a check on directly measured net radiation. Furthermore, R_s is needed as an input parameter for some of the SVATs to be discussed in Chapter 4. Finally, by multiplying R_s with a simple factor (≈ 2.0, see Begue et al., 1995, for example), the photosynthetically active radiation, Q_p, can be calculated which is an essential parameter for CO_2 and stomatal resistance modelling.

2.2.4 Reflected shortwave radiation

A significant fraction of the incident shortwave radiation flux at the surface may be reflected back to the atmosphere. This is related to the albedo of the surface, a , defined as the ratio of reflected global shortwave flux to the incident flux. It represents an integral value of the surface reflectivity over the wavelength range 0.1-4 μm, and contrasts with the spectral albedo appropriate to a specific wavelength (Garratt, 1992).

The reflectivity of a certain surface is dependent on the wavelength and incidence angle of incoming solar radiation. Furthermore, its value depends on surface texture and structure as well as on composition (vegetation, soil, or water). A division between visible and near infra-red radiation can be made if surface reflectivity is considered. Plant canopies reflect a much larger fraction of the incident radiation in the near infra-red part of the solar spectrum than they do in the visible part. Soil surfaces typically reflect about twice as much near infra-red as visible radiation (Dickinson, 1983). Reflectivity as measured with an inverted or double-dome solarimeter, which yields the surface property called albedo, involves both types of radiation.

Measured canopy albedos are typically little more than half the albedos measured for individual leaves, due to light trapping. The following conditions determine the albedo of a *plant canopy.*

(1) Spectral composition of the incident solar radiation: albedo of a plant canopy decreases by about 0.02-0.03 from early morning to noon because of the increasing ratio of visible to near infra-red radiation.

(2) The zenith angle of the incident solar beam. As far as visible radiation is concerned this gives a decrease in albedo from sunrise to noon by a factor 3 and for near infra-red radiation by a factor of almost 2. Rougher surfaces have less diurnal variation due to increased shadowing by the vertical faces of roughness elements as the solar zenith angle increases. Noontime albedos of plant canopies are 0.10-0.15

(3) The optical properties of the individual leaves: leaf reflectances with overhead sun lie between 0.2 and 0.3, a few are as small as 0.15 or as large as 0.4. Albedos of homogeneous canopies at low sun are close to the albedos of individual leaf elements. Albedos of woody branches may be somewhat lower than those of green leaves.

(4) The structure of the canopy

The albedo of the soil surface is reported to depend on solar elevation, cloud cover, surface roughness, mineral composition and organic matter content (see Ten Berge, 1990). The greatest changes in soil albedo, however, are caused by changes in soil moisture content, θ. Most experiments yield a linear relationship between θ and a (Ten Berge, 1990). Values of soil albedo range between 0.10 and 0.40 (Stull, 1988; Ten Berge, 1990; Allen et al., 1994).

2.2.5 Longwave incoming radiation

Besides incoming shortwave solar radiation, natural surfaces also receive longwave radiation from the atmosphere. This is caused by the absorption and subsequent emission of radiation by the so-called 'greenhouse gases' (water vapour, CO_2, ozone) and by liquid water and ice in clouds. Because of the relatively low temperatures of the Earth's atmospheric system, this radiation is mainly confined to longwave radiation in the wavelength range 4-100 μm (the infra-red region). Absorption by greenhouse gases occurs in certain wavelength bands. For example, ozone absorbs primarily between 0.1 and 0.3 μm, whereas H_2O has its absorption bands in the near infra-red (0.74 -3 μm). The atmosphere can be considered as 'black' for these wavelengths. The only part of the radiation spectrum where absorption is almost negligible is between 8 and 14 μm, which is called the atmospheric window. Clouds also absorb and emit in this atmospheric window.

Absorption and emittance of thermal radiation takes place over the entire depth of the atmosphere, which makes it difficult to calculate longwave incoming radiation. To obtain reliable estimates, detailed knowledge of the vertical distribution of trace gas concentration, water and ice particles, temperature and water vapour content are required. With this information, and assuming that the troposphere contains several thin layers, the radiation received and emitted by each layer can be calculated. Besides theoretical complexity (Paltridge and Platt, 1976), a general lack of the above described input data inhibits this type of calculation. In many cases only standard meteorological observations at screen level are available and because of this a variety of empirical methods have been developed for calculation of longwave incoming radiation which need simple meteorological parameters as input.

For the radiation balance (Eq. 2.1) we need the flux density of atmospheric longwave radiation through a horizontal plane at the surface, $R_{l,\downarrow}$. If we assume that the atmosphere is a grey radiator at air temperature, the sky has an apparent emissivity, ε_a. The following formula can be derived for radiation reaching a horizontal surface:

$$R_{l,\downarrow} = \varepsilon_a \sigma T_a^4 \tag{2.2}$$

where ε_a is the mean apparent atmospheric emissivity, σ is the Stefan-Boltzmann constant and T_a the temperature of the atmosphere. This formula can be considered as a modified Stefan-Boltzmann law in which $\varepsilon \neq 1.0$.

Sky emissivity, ε_a, is usually found from a combination of a formula describing clear-sky emissivity, $\varepsilon_a(0)$, and a correction for the occurrence of clouds. Different parameterizations have been proposed to find a value of $\varepsilon_a(0)$, mainly depending on the atmospheric conditions under which they were developed (Wartena, 1973; Ten Berge, 1990). Most of them are a function of air temperature, T_a, and/or vapour pressure, e_a. Both variables are usually taken at screen height for convenience. The most used formula was proposed by Brunt in 1932 (Stroosnijder and Van Heemst, 1982; Ten Berge, 1990; Culf and Gash, 1993). Others were derived by Swinbank (1963), Idso and Jackson (1969) or Brutsaert (1975a). The equations are all empirical in nature, except for that of Brutsaert (1975a) which is derived from Schwarzschild's equation and an approximation to the U.S. Standard Atmosphere, 1976 (Culf and Gash, 1993). The formula of Brutsaert (1975a) will be applied in this thesis for calculations of $\varepsilon_a(0)$ in Chapters 5 and 8.

It is given by

$$\varepsilon_a(0) = 1.24(e_a / T_a)^{1/7} \tag{2.3}$$

with e_a given in mb and T_a in K. For dry season calculations, 1.24 will be replaced by 1.31 (see Culf and Gash, 1993).

Cloudiness is often taken into account by multiplication of the clear-sky atmospheric emissivity with a certain factor involving fractional cloudiness. For example, Sellers (1965) developed a correction for cloudy conditions described by

$$\varepsilon_a = \varepsilon_a(0)(1 + nc^2) \tag{2.4}$$

where c is the fraction of cloud cover, and n is a parameter ranging from 0.04 for high (cirrus) clouds, to 0.2 for low clouds (Monteith, 1973). Sometimes, an extra term is added to Eq. 2.2, involving cloudiness and sometimes cloud-base temperature (Paltridge and Platt, 1976). No correction for the occurrence of clouds will be employed in this thesis, because of a lack of continuous measurements of cloud cover. Formula 2.4 will be applied on the SEBEX data for back-calculation of cloud cover from measured $R_{l,\downarrow}$ and T_a.

Longwave downward radiation flux density, $R_{l,\downarrow}$, is an important term of the radiation balance, especially in warm climates. Values are usually around 300-500 W m^{-2}. This radiation flux density can be measured directly with a pyrgeometer (usually an Eppley) or it can be calculated according to the equations described above. Eppley pyrgeometers were installed at the HAPEX-Sahel (CWS) savannah site and at the SEBEX tiger-bush site. However, Eqs. 2.2-2.4 will be used to find values of $R_{l,\downarrow}$ for the HAPEX-Sahel radiation balance because of instrument failure.

2.2.6 Longwave upward radiation flux density

Surface temperature sets the boundary condition for latent and sensible heat transport through vegetation, soil and atmosphere. Therefore, it is an important parameter in the SEB. Together with surface emissivity, it determines the outgoing longwave radiation. This upward radiation is considered as originating from a plane. This makes complicated integration, which is essential theoretically in the case of $R_{l,\downarrow}$, unnecessary. Therefore, the modified ($\varepsilon_s < 1.0$) Stefan-Boltzmann law is a good and straightforward estimator of $R_{l,\uparrow}$.

The Earth, being a grey radiator, emits longwave radiation according to the following equation:

$$R_{l,\uparrow} = \varepsilon_s \sigma T_s^4 + (1 - \varepsilon_s) R_{l,\downarrow} \tag{2.5}$$

where ε_s is the surface emissivity, σ the Stefan-Boltzmann constant and T_s the surface temperature. The second term in Eq. 2.5 accounts for the fact that a part of the incoming longwave radiation is reflected by the surface.

The emissivity of a natural surface, ε_s, is dependent on the type of surface (soil, vegetation, water or rocks), moisture content (wet versus dry soil, green versus senesced biomass), composition (organic matter content of the soil) and the structure or roughness characteristics (smooth versus tilled soil, leaf angle distribution, density of canopy). Besides the influences coming from the surface itself, emissivity is also reported to be dependent on incidence angle: smooth surfaces such as individual leaves show a strong view-angle dependence, while this is not true for the emissivity of most natural soils (Ten Berge 1990; Van de Griend and Owe, 1993). Emissivity can be determined experimentally by the reflection method of Fuchs and Tanner (1966) to accuracies of about 0.01. No direct measurements have been executed for the experiments described in this thesis. Therefore, ε_s will be calculated from literature. Values between 0.92 and 0.95 are usually applied for vegetated surfaces (Stull, 1988). In the majority of cases, dry season or summer values will be different from wet season or winter values because of leaf shedding or agricultural practices (harvesting, fallow rotation) although this fact is usually not acknowledged in most of the large-scale models (see Stull, 1988). Bare soil emissivity exhibits a larger range - from 0.85 for a dry, sandy desert to 0.98 for wet, finer-textured soils (see Stull, 1988; Ten Berge, 1990). A dependence on soil moisture is often assumed (Ten Berge, 1990) which is, however, less clear than in the case of bare soil albedo.

Surface temperatures are usually obtained with infra-red thermometers (IRTs) and for this thesis they have also been obtained in this way. These instruments can be ground-based or mounted on remote sensing equipment (see Kustas et al., 1990, for example). General corrections have to be applied to directly measured radiation surface temperature to account for the incoming longwave radiation and the surface emissivity not being equal to unity (see Appendix 1), thus yielding 'true' T_S. For the ground-based measurements there is the additional question of a representative surface area. Sparsely vegetated surfaces present particular problems when it comes to the determination of an appropriate surface temperature. A representative area surface temperature is not easy to define and depends on the way of combining the surface temperatures of the various component surfaces (Malhi, 1993). However, the small viewing area of most radiometers makes ground-based verification of this composite temperature difficult, and airborne measurements may have too coarse a resolution. Moreover, they are highly influenced by the atmosphere between the actual surface and the sensor.

Surface temperature exhibits a large spatial variation, - values of well-watered, non-stressed vegetation are usually around air temperature, whereas values for dry soils can be higher than 60 ° C.

2.3 Soil heat flux

Heat is mainly by conduction transported within soils, i.e. the transfer of thermal energy on a molecular scale (Van Wijk and De Vries, 1963). Heat conduction is governed by the thermal soil properties, volumetric heat capacity and thermal conductivity, which are strongly dependent on soil moisture content. Soil heat flux can be described by Fourier's law for heat conduction in a homogeneous medium with uni-dimensional flow in a vertical direction:

$$G = -\lambda \frac{\delta T}{\delta z} \tag{2.6}$$

Hence, G depends on the thermal conductivity, λ (W m^{-1} K^{-1}), and the temperature difference over a layer of infinite thickness. Strictly speaking, Eq. 2.6 cannot be applied to soils as a soil is not a homogeneous medium but a composite one. However, for most purposes Eq. 2.6 holds when an appropriate average value of λ is introduced (Van Wijk and De Vries, 1963). The average λ can be defined on the basis of a discretization of Eq. 2.6, where δT and δz are replaced by ΔT and Δz, while Δz must be large in comparison with the dimensions of the soil particles. This discreticized version of Eq. 2.6 is also widely used for the calculation of G from two soil temperatures and an estimate of λ. It will also be used in this thesis, together with three other methods as explained below.

Another process by which soil heat can be transported is convection. Heat convection with accompanying phase changes can increase heat transfer substantially. This is especially true for water, which has very high values of latent heat of condensation/evaporation and freezing/melting (Koorevaar et al., 1983). In this thesis, the heat transport caused by mechanisms other than conduction will not be considered separately because some of them are still poorly understood (Ten Berge, 1990). Instead, field measurements are assumed to incorporate the heat transported by convection, so that λ represents an apparent thermal conductivity.

A combination of Eq. 2.6 with the principle of heat conservation stating that

$$\frac{\delta G}{\delta z} = -C_h \frac{\delta T}{\delta t} \tag{2.7}$$

leads to the equation describing conductive heat transfer in a one-dimensional isotropic medium:

$$\frac{\delta T}{\delta t} = \kappa \frac{\delta^2 T}{\delta z^2} \tag{2.8}$$

The soil thermal diffusivity, κ ($m^2\ s^{-1}$), is the ratio of thermal conductivity to the volumetric heat capacity:

$$\kappa = \lambda / C_h \tag{2.9}$$

The volumetric heat capacity, C_h, is defined as the change of heat content per soil volume and per change of temperature ($J\ m^{-3}\ K^{-1}$). In Eq. 2.9 κ is independent of depth and time.

Soil temperatures are determined by the heat transport within the soil and by the exchange of heat between the surface and the atmosphere. Thus, soil temperature fluctuates because of more or less cyclic variations of the surface temperature. Using the Fourier series representation, soil temperature near the soil surface can be described by a sum of sine and cosine terms according to the following equation

$$T(t) = \overline{T} + \sum_{n=1}^{M} \left[A_n \cos(n\omega t) + B_n \sin(n\omega t) \right] \tag{2.10}$$

where the overbar denotes an average in the time interval considered, M is the number of harmonics and A_n and B_n are the amplitudes. ω is the radial frequency ($= 2\pi\ /P$), with P representing the period of the fundamental cycle (generally diurnal or annual). This formula only applies to homogeneous soils where the thermal soil properties are independent of depth, time and temperature. The dependence on the temperature is only slight in the case of soils and can be ignored for most practical purposes (Van Wijk and De Vries, 1963). Independence on time means that the temperature returns to its initial value after the completion of a period. Many formulae, applying Equation 2.10 in its full or simplified form, have been used to calculate κ. Several of these methods, as described by Horton et al. (1983), were used to calculate κ for the soils encountered in the HAPEX-Sahel and SEBEX experiment. A summary of these methods is given in Appendix 2.

In the case of a closed (well-watered) canopy the soil heat flux is usually relatively small and parameterized as a fraction of R_n depending on the type of crop and soil moisture content (Idso et al., 1975). However, for sparse canopies under semi-arid or arid conditions G can account for a large part of the energy balance (up to 40 % of R_n, on a diurnal basis) and be equal to or even higher than L_vE. Under these circumstances accurate estimates of G have to be obtained.

As shown above, G is determined by the thermal soil properties (λ, C_h, κ) which are in turn dependent on soil moisture content, θ, and soil composition. Appendix 2 summarizes how the thermal properties for the HAPEX-Sahel and SEBEX data set were measured (HAPEX-Sahel, λ) or calculated (λ, C_h, κ).

Surface soil heat fluxes can be estimated using several methods. The most commonly used are the Calorimetric, Gradient, Harmonic and Plate method (see Tanner, 1963; Kimball and Jackson, 1975). These will also be used in this thesis and the theory behind them is described in Appendix 3.

2.4 Atmospheric fluxes

This section will concentrate on the two remaining fluxes of Eq. 1.1 - the sensible and latent heat fluxes. The continuous and considerable exchange of these fluxes is a result of the predominantly turbulent nature of the atmosphere. The turbulence is driven by two mechanisms - forced and free convection. The first term describes the fact that airflow experiences friction with the Earth's surface and its obstacles, so it is related to wind speed. The second process is caused by vertical density variations giving rise to vertical motions in the atmosphere. This effect is called buoyancy (Priestley, 1955).

The theory concerning these fluxes will mainly be confined to the methods by which they are measured. Two types of techniques can be considered: direct and indirect methods. If we restrict ourselves to meteorological methods and rule out methods such as lysimetry, the first category is based on turbulence theory, whereas the second group employs the flux-profile relationships. The latter links vertical flux densities with vertical profiles of quantities such as heat, water vapour, or wind velocity.

2.4.1 Total fluxes

a) Eddy covariance method

The eddy correlation method is based on the concept that the kinematic flux of any atmospheric quantity, A, such as temperature, moisture, wind speed, or a trace gas like CO_2 can be written as

$$F_A = \overline{w\rho c_A} + \overline{(w\rho)' c_A{}'} \qquad (2.11)$$

where F_A is the flux density of quantity A, w is the vertical wind speed and c_A is the temperature, specific humidity, concentration or horizontal wind speed. The overbar represents the mean, whereas the primes denote the fluctuation around the mean value.

If we assume that over a suitable interval of time there is no mass movement of air in the vertical, i.e. $\overline{w\rho}=0$ and thus $\overline{(w\rho)c_A'}$ = 0, this leaves us with $\overline{w\rho c_A}$. By using $(w\rho)=(\overline{w}+w')(\overline{\rho}+\rho')$ and the fact that $\overline{w'\rho' c_A'}$ is very small, we obtain from Eq. 2.11 the practical working equation for the eddy covariance method which is

$$F_A=\overline{\rho}\,\overline{w' c_A'} \quad + \text{ correction terms} \tag{2.12}$$

With this general formula the vertical eddy heat (H), moisture (L_vE), momentum and CO_2 fluxes can be found from

$$H=\overline{\rho}C_p\overline{w'T'} \qquad + \text{ correction terms} \tag{2.13}$$

$$L_vE=L_v\overline{\rho}\,\overline{w'q'} \qquad + \text{ correction terms} \tag{2.14}$$

$$\tau=\left(-\overline{\rho}\,\overline{u'w'}\right)^2+\left(-\overline{\rho}\,\overline{v'w'}\right)^2 \qquad + \text{ correction terms} \tag{2.15}$$

$$F_c=-\overline{\rho}\,\overline{w'c_c'} \qquad + \text{ correction terms} \tag{2.16}$$

where in this thesis the overbars denote 30-minute averages. T is the temperature, q the specific humidity, u the wind velocity in the direction of the mean wind, w the vertical wind velocity and c_c a quantity defined by ρ_c / ρ with ρ_c the CO_2 density. One consequence of this method is that it requires expensive equipment to sample the atmospheric air with a high frequency. If we want to measure the above described fluxes, the set-up for the eddy covariance system will consist of a device that is able to measure wind speed in three directions, temperature, water vapour density and CO_2 density. It is not possible to create an eddy covariance system which has no effect whatsoever on the fluxes it is designed to measure.

b) Corrections for the EC method

As a result of physical limitations in sensor size and response, experimental siting and data analysis techniques, eddy correlation systems will always lead to an underestimation of the turbulent fluxes, as shown in Eq. 2.12-2.16. To calculate the expected flux loss, correction factors will be calculated for each flux. Those correction factors concern frequency response loss (Moore, 1986) and co-ordinate rotation (McMillen, 1983). An additional correction is needed to account for the fact that, strictly speaking, $\overline{w\rho}\neq 0$ due to atmospheric buoyancy (Webb et al., 1980). This correction is relatively small for H, L_vE and τ, but can be considerable in the case of F_c. For the CO_2 flux, extra corrections have to be made for fluctuations occurring in ρ_v and T, for cross-sensitivity of the CO_2 analyser to water vapour and for losses caused by dampening of CO_2 fluctuations in the sampling tube (Leuning and King, 1992). The corrections procedures used in this thesis can be found in Moncrieff et al. (1996b) and Lloyd et al. (1996).

c) Flux-profile relationships

In the atmospheric surface layer

$$H = -\rho C_p K_h \frac{\delta \overline{T}}{\delta z} \tag{2.17}$$

$$L_v E = -\rho L_v K_e \frac{\delta \overline{q}}{\delta z} \tag{2.18}$$

$$\tau = \rho K_m \frac{\delta \overline{u}}{\delta z} \tag{2.19}$$

where H, L_vE and τ are the fluxes of heat, water vapour and momentum, and K_h, K_e and K_m are their respective eddy diffusivities or turbulent exchange coefficients. The turbulent K's are assumed to be related to wind shear (through $u*$) and buoyancy (via the stability function ϕ). Thus:

$$K_x = ku_*(z-d) / \phi_x \tag{2.20}$$

where x denotes one of the subscripts h, e or m, u_* the friction velocity (= $(\tau/\rho)^{-1/2}$), k the Von Kármán's constant (≈ 0.4) and d the zero-plane displacement (see Eq. 2.28). ϕ_x is a function of the Monin-Obukhov stability length L, where

$$L = \frac{-\overline{T}}{gk} \frac{u_*^3}{\overline{w'T'}} \tag{2.21}$$

g being the acceleration due to gravity. The stability functions have been empirically estimated for several field experiments (Dyer, 1974; Stull, 1988; Chen Fazu and Schwerdtfeger, 1989).

Because in practice the derivatives in Eqs. 2.17 -2.19 are difficult to measure, we work with discrete differences between levels z_1 and z_2. The heat flux equation, for example, will be written as

$$H = -\rho C_p \frac{\overline{T}(z_2) - \overline{T}(z_1)}{r_h} \tag{2.22}$$

$$\text{with} \quad r_h = \int_{z_1}^{z_2} \frac{dz}{K_h} \tag{2.23}$$

This equation is the resistance analogue of Eq. 2.17. Similar formula transformations can be executed for the latent heat and momentum flux. Eq. 2.23 indicates that K_x, and thus ϕ_x, has to be integrated from z_1 to z_2. The integrated stability functions read (Paulson, 1970):

a. Unstable:

$$\Psi_h = \Psi_e = 2\ln\left[\frac{1+x^2}{2}\right] \tag{2.24a}$$

$$\Psi_m = 2\ln\left[\frac{1+x}{2}\right] + \ln\left[\frac{1+x^2}{2}\right] - 2\arctan(x) + \frac{\pi}{2} \tag{2.24b}$$

$$\text{with } x = \left(1 - 16\frac{z-d}{L}\right) \tag{2.24c}$$

b. Stable

$$\Psi_h = \Psi_e = \Psi_m = -5\frac{z-d}{L} \tag{2.24d}$$

Eq. 2.24 has been used in most of the SVATs to be described in Chapter 4 to take care of stability effects.

Combining the discrete potential differences with the integrated stability functions will yield H, L_vE and τ. In practice, z_2 is taken as the reference level (usually at least two times the canopy height), whereas z_1 refers to the surface (i.e. $z \approx 0$). This leads to the bulk transfer equations, reading for example

$$H = \rho C_p \frac{(T_s - T_a)}{r_h} \tag{2.25}$$

with the subscripts s and a referring to the value of the atmospheric variable at surface and reference level, respectively.

d) Calculations of kB^{-1}

For estimates of H and L_vE with a single-layer equation as described above, a proper estimate of the resistance, r_h, is required. Unlike the resistance for momentum, the scalar resistance involves an extra resistance, which has been shown to be relatively large for sparse canopies (see Section 1.2.2f). For calculations of H and L_vE, reliable estimates of this excess resistance is of paramount importance. For this reason, quite a great deal of attention will be paid to this subject in this thesis (see Chapter 6).

According to Eq. 2.25, the turbulent transfer of sensible heat, H, can be parameterized with a bulk transfer equation, with r_h the resistance to heat transfer from a surface at the radiometric surface temperature, T_s. This surface temperature is theoretically located at a height z_{0h}, which is called the roughness length for heat in analogy with momentum transfer.

It is a commonly accepted fact that the transfer of heat and mass involves an excess resistance compared to the exchange of momentum. This is caused by the fact that transport of momentum not only involves viscous shear but also local pressure gradients, which are related to form drag on roughness obstacles, whereas the transport of heat and mass can only take place by molecular diffusion (Duynkerke, 1992). In this way the total resistance r_h is composed of

$$r_h = r_{ah} + r_r \tag{2.26}$$

With the formula for r_{ah} reading

$$r_{ah} = \frac{1}{ku_*}\left[\ln\left(\frac{z-d}{z_{0m}}\right) - \Psi_h\left(\frac{z-d}{L}\right)\right] \tag{2.27}$$

r_{ah} represents the resistance between the air temperature at a height z_{0m} and the reference temperature T_a. In combination with the logarithmic wind profile (Tennekes, 1973) and the fact that $u(0) = 0$ we find for u_*:

$$u_* = ku\left[\ln\left(\frac{z-d}{z_{0m}}\right) - \Psi_m\left(\frac{z-d}{L}\right)\right]^{-1} \tag{2.28}$$

where Ψ_m is the integrated stability function with L the Monin-Obukhov length, z_{0m} the roughness length for momentum and d the displacement height. The roughness length for momentum can be considered as a descriptor of surface roughness. Near the surface, the logarithmic wind profile needs a correction of its shape, which is accomplished by empirically introducing a displacement height, d. The physical significance of d is to account for the fact that for a dense canopy of surface-covering objects, only a small fraction of the total surface shear stress is taken up by the bottom surface at $z = 0$ (see Wieringa, 1993).

The excess resistance between z_{0h} and z_{0m} equals r_r and with knowledge of r_h and r_{ah} this resistance can be found from Eq. 2.26. Originally (Owen and Thomson, 1963; Chamberlain, 1968), this excess resistance was denoted by the dimensionless quantity kB^{-1} [= $\ln(z_{0m}/z_{0h})$]. Values of kB^{-1} can be derived from

$$kB^{-1} = kr_r u_* \tag{2.29}$$

In practice (for remote sensing purposes, for example), the value of r_r is not known. In such cases, kB^{-1} has to be derived from relatively simple formulae employing readily available parameters. Appendix 4 describes several of these formulae as found in the literature. In § 6.2.2 the performance of these equations will be investigated.

e) Bowen ratio energy balance method (BREB)

The Bowen ratio energy balance method (BREB) is derived from the flux-profile relations (assuming that $\Psi_h = \Psi_e$) and it combines measurements of temperature and humidity profiles with Eq. 1.1. It employs the Bowen Ratio, β, which is defined by

$$\beta = \frac{H}{L_v E} = \frac{C_p \Delta \overline{T}}{L_v \Delta \overline{q}} \tag{2.30}$$

where ΔT and Δq are measured temperature or humidity differences between levels on the mast, which are derived from dry and wet bulb temperature readings in combination with the psychrometer formula. Combination of Eq. 1.1 and 2.30 leads to

$$H = \beta \frac{R_n - G}{1+\beta} \tag{2.31}$$

and

$$L_v E = \frac{R_n - G}{1+\beta} \tag{2.32}$$

2.4.2 Soil evaporation

a) Introduction

Regions characterized by partial or sparse plant canopy cover occur seasonally in all agroclimatological zones. They may be the result of a lack of water, high or low temperatures or be part of a rotation scheme (fallow) designed to store soil moisture and fertility for the next growing season (Allen, 1990; Ten Berge, 1990; Massman, 1992; Van de Griend and Owe, 1994). Moreover, due to desertification, overgrazing and deforestation the area of bare or slightly vegetated soils world wide is increasing rapidly. In semi-arid areas water deficiency and high temperatures related to the relatively prolonged dry season are the main reasons for the absence of canopy cover or the presence of a partial canopy. Therefore, for various purposes and applications it is convenient to have a simple technique available to produce reliable estimates concerning the contribution of the soil sensible and latent heat of a crop or natural vegetation to total fluxes.

Analogous to Equation 1.1, the energy budget at the soil is given by (e.g. Garratt, 1992)

$$R_{n,s} = H_s + L_v E_s + G_s \tag{2.33}$$

where, $R_{n,s}$ is the net radiative flux of the bare soil (positive day-time; negative night-time), H_s and $L_v E_s$ are the soil sensible and latent heat fluxes, respectively, and G_s is the soil heat flux. Generally, it is difficult to directly estimate H_s and $L_v E_s$ at the soil surface. There is only one technique for making a direct assessment of the soil latent heat flux and this uses so-called micro-lysimeters (Boast and Robertson, 1982). However, this method only provides us with (daily) cumulated values and furthermore it is difficult to apply under certain circumstances (such as in very loose soil or in the hard, crusted tiger-bush soil). In order to estimate the sensible heat flux and vapour flux at the soil surface of the canopy in an indirect way, various techniques are available, ranging from simple formulae (Ritchie, 1972) to relatively complicated two component models (Shuttleworth and Wallace, 1985; Massman, 1992; Wallace and Holwill, 1996).

The most commonly used model to predict evaporation from bare soil is based on the Ritchie (1972) approach, which considers evaporation to occur in two distinct phases. Initially, evaporation from the soil proceeds at the potential rate during the 'first phase' immediately following re-wetting of the surface by rain. This lasts a number of days, t_l, until a certain total amount of water is evaporated, after which the second phase begins where the rate of soil evaporation declines according to the square root of time (Wallace and Holwill, 1996). The first phase evaporation is determined by a potential evaporation formula, such as those developed by Penman (1948), Priestley and Taylor (1972), or Penman and Monteith (Monteith, 1965), of which the last is usually assumed to yield the most reliable results (see Verhoef and Feddes, 1991). These formulas can be applied on a diurnal or daily basis. The diurnal evaporation values of the first phase have to be summed if we want to obtain cumulative amounts of soil evaporation. The formula describing the second drying phase produces only daily sums (in mm) and can be expressed mathematically as:

$$\Sigma E_{s2} = \alpha\sqrt{t-t_1} \qquad t > t_1 \tag{2.34}$$

where α is assumed constant for any particular soil and is a function of soil hydraulic diffusivity (Black et al., 1969; Wallace and Holwill, 1996).

In this thesis, a new procedure is suggested that is based on the assumption of free convective conditions (Jacobs and Verhoef, 1996). It can be used during both stages of soil drying and it has the advantage of also providing diurnal estimates of $L_v E$, even under relatively dry circumstances when lysimetry will become inaccurate. Under low wind conditions a free convective state often occurs which offers the opportunity for making a simple assessment of the contribution of the soil sensible heat to the total sensible heat flux. In this case there exists a unique relationship between the surface Rayleigh number and the surface Nusselt number. The same technique can be applied to the vapour flux by using a unique relation between the surface Rayleigh number and the surface Sherwood number, if the soil surface is wet. This latter condition occurs after a rainy period. Most times, however, the topsoil is dry and soil evaporation will be limited by the surface resistance to evaporation. If the relation between soil moisture and the so-called 'Soil Bowen Ratio Coefficient', c_W, as proposed by Massman (1992) is known, a simple correction to the estimated soil evaporation can be applied. Details of this theory will be described in Appendix 5. It will be applied to calculate the evaporation of the soil components of both Sahelian vegetation-types.

2.4.3 Bush transpiration

The energy balance of the vegetation component of a sparse canopy can be described with an equation analogous to Eqs. 1.1 and 2.33, although in this case the no-storage assumption becomes questionable. Furthermore, direct measurements (e.g. R_n) are hampered by the three-dimensional character of the vegetation elements. The transpiration component can be measured directly with several non-destructive techniques, like weighing (small pot experiments or lysimetry), sap flow measurements (Allen and Grime, 1995), deuterium estimates (Calder et al., 1991) or by a combination of porometry and calculations (Roberts et al., 1990). In some cases, destructive methods have been used to directly obtain transpiration (Calder et al., 1991). For this thesis, bush transpiration has been derived from sap flow gauges installed at the CWS savannah site.

During the 1980s, sap flow gauges, which use a heat balance principle to measure sap flow through intact plant stems were developed by Sakuritani (1981), Baker and Van Bavel (1987) and Steinberg et al. (1989). The gauges allow the transpiration from whole plants to be continuously measured, making it possible to measure transpiration from a single component of mixed vegetation. These first studies found an accuracy of better than 10 % for the gauges when comparing daily sap flow totals from potted plants with their daily weight loss (Allen and Grime, 1995). Since then many studies have been executed (see, for example, Lascano et al., 1992; Dugas et al., 1993; Allen and Grime, 1995).

Bush transpiration, L_vE_b (W m^{-2}), will be obtained from the following equation

$$L_vE_b = \sum_i^n \left(L_vF_iLAI_b / L_i\right) / n \tag{2.35}$$

where L_v is the latent heat of vaporization (J kg^{-1}), F_i the sap flow in stem i (kg s^{-1}), LAI_b the leaf area index (m^2 m^{-2}) of the bushes, L_i the leaf area of stem i (m^2) and n the total number of stems.

2.5 Effective parameters and fluxes

2.5.1 Background

Land-atmosphere interactions are strongly heterogeneous processes, at practically every scale from individual stomata to the whole earth. Between this lower and upper boundary, three spatial scales are of considerable interest to us: the leaf, the canopy, and the regional scale. Leaf-canopy scaling has been an issue for several decades, following the postulate by Monteith (1965) that a canopy acts as a 'big leaf' with a canopy conductance equal to the parallel sum of the leaf stomatal conductances (Raupach, 1995). Canopy-region scaling is important from the viewpoint of finding effective surface parameters which can serve as the lower boundary for meso-scale and general circulation models (GCM's) having characteristic grid sizes of one kilometre or more. This kind of scaling deals with small-scale (Blyth et al., 1993) heterogeneity, also called micro-scale (Raupach, 1993) or type A (Shuttleworth, 1988) heterogeneity for which it is assumed that the landscape variations do not affect the structure of the boundary layer. The surface is composed of a certain number of patches (for example a field or a forested area) and the convective boundary layer cannot adjust to successive surface types and develops as it would over homogeneous terrain with surface properties defined as averages of those of the individual surfaces (Raupach, 1991). For very small-scale heterogeneity, the distance between the patches is of the same order of magnitude as the height of the vegetation or less and heterogeneity can be treated as a sparse canopy (Blyth et al., 1993; Blyth, 1995; Blyth and Harding, 1995; Lloyd, 1995). This is the kind of heterogeneity that will be most often referred to in this thesis.

The two sparse canopies to be studied in this thesis consist of two major surface components: a canopy and an understorey. At the experimental sites, ground-based measurements were conducted at several scales: the leaf scale (porometry), the component scale (for example measurement of surface temperatures, net radiation or soil heat flux for bushes and understorey separately) and the field scale (such as eddy covariance measurements of H and L_vE, or measurement of R_n at 10 m producing an integrated value of R_n). Because we want to assess the total SEB we are in search of (field scale) area-averaged surface parameters. These can be used to calculate or check our radiation or energy balance, or as input parameters for evaporation models. Good and general averaging tools are therefore important. From recent literature (Raupach, 1991; Lhomme, 1992; Blyth et al., 1993; Malhi, 1993; McNaughton, 1994; Raupach, 1995; Braden, 1995) it became clear that there is no unique or single correct way for calculating the effective parameter values of a heterogeneous landscape or sparse canopy. The correct averaging procedure is always dictated by the chosen application.

Raupach (1995) found that scalar mass conservation requires elemental surface flux densities to be averaged linearly with area weighting across component surfaces. Area averages of other land-atmosphere interaction parameters (such as surface temperatures, conductances, albedo, emissivity) need to be consistent with this constraint to satisfy mass conservation. According to Raupach, linear averaging applies to net fluxes of conserved scalars, in particular H and L_vE and their sum, the available energy flux. It also applies to net irradiances in any spectral waveband, as these are also net scalar fluxes. However, it does not apply to inward and outward shortwave and longwave irradiances in cases where multiple scattering occurs between the surfaces as in a plant canopy or other non-planar surface. In this thesis, for calculation of area-averaged R_n and G-values and the surface parameters which are part of them, i.e. a, ε_s, and T_s , simple linear averaging procedures will therefore be used, as given by:

$$X_t = \Sigma \alpha_i X_i \qquad (2.36)$$

where X_t is the area average or total value of a certain variable composed of i component surfaces, with proportional coverage of α_i. This formula can be simplified for the savannah and tiger-bush vegetation, and for the majority of vegetated surface covers, by taking i=2, i.e.

$$X_t = \alpha X_u + (1-\alpha) X_b \qquad (2.37)$$

where the subscript u refers to understorey and b to bushes. The understorey represents the bare soil in the case of tiger-bush. The mixture of herbs, grasses and bare soil as encountered for most savannahs is blended into one average understorey value. This approach might prove sufficient for most fluxes (for example R_n), but in some cases the contribution of the several sub-surfaces will be necessary (like for the surface temperature). In some situations it may also be necessary to consider the separate contribution of sunlit and shaded surface elements. Similar averaging rules were applied by other authors (see Lloyd, 1995; Blyth and Harding, 1995).

Lhomme (1992), McNaughton (1994), Raupach (1995), and Braden (1995) discussed effective surface parameters for the proper calculation of sensible and latent heat fluxes using the Penman-Monteith equation. Their weighting procedures were not linear (due to the non-linearity of the PM-equation) and their weighting coefficients involved aerodynamic and surface resistances of the component surfaces. This kind of averaging will not be applied here, because evaporation is either measured directly or calculated from a sparse canopy model which allows for the interaction between the different surface components.

2.5.2 The energy balance and energy closure

To measure the energy balance, instruments (eddy covariance) installed at a single point above the surface are used to give values of H and L_vE. These instruments automatically provide field-averaged values, where the source area depends on measurement height, stability and wind direction. To obtain the available energy, ($R_{n,t}$ - G_t), a limited number of local measurements will usually be linearly combined. This sampling problem causes difference in source areas between the left and right side of Eq. 1.1, occurring over all kinds of surfaces, but predominantly for heterogeneous surfaces.

That the equality of available energy to the sum of atmospheric heat fluxes is difficult to achieve for a heterogeneous surface, has been shown by Culf et al. (1993) for the SEBEX tiger-bush site and by Lloyd (1995) for a HAPEX-Sahel tiger-bush site. To close the energy balance, an area-average net radiation which corresponds to the fetch of the flux measurements must be calculated. This value of net radiation will depend on the fractional vegetation cover in a certain sector around the mast, where the wind is coming from, and by the relative source strength in this sector. The distribution of vegetation and bare soil in the tiger-bush areas was mapped using aerial photography. Culf et al. (1993) found values between 27 and 45 % vegetation cover for the area enclosed by the 1 km circle centred on the tower (average 38 %). This was slightly higher than the value of 33 % derived from a digital image of the entire tiger-bush area (see Dolman et al., 1992). One kilometre long transects at 180 ° to the measurement towers gave bush to soil ratios of around 0.45 for the HAPEX-Sahel site (Lloyd, 1995). Whereas Culf et al. used a one-dimensional equation for calculation of relative source strength, leading to estimates of between 28 and 49 % effective vegetation cover, Lloyd used a two-dimensional model to produce relative flux density at any upwind distance. Both models depend on measurement height and roughness length, whereas the latter also employs stability. The models assume that the sources are at ground level. Lloyd calculated the ratio of fluxes from the bush and bare soil areas upwind of two towers, as effectively seen by the sensor, for different stabilities and measurement heights above the surface. Lloyds results, and those of Culf et al., (1993) showed that surface flux measurements made at a single point over heterogeneous terrain may be very different from the area average available energy which is usually calculated with simple averages based on component coverage areas. Furthermore, it may not even be possible to register similar flux measurements at adjacent positions. The difficulty arises when attempting to compare a linearly summed area estimation of available energy with a non-linear summation of flux sources from a non-static source area. Similar effects may occur in other micrometeorological experiments where measurements are made from a height over heterogeneous terrain which is of the same scale as the surface patches, of which the savannah is an example. According to Lloyd, it is also important to realize that the discrepancy between available energy and surface fluxes will diminish as the difference in energy balance between the surface types diminishes. Hence, a similar heterogeneous area but consisting of bush areas interspersed with grasses or herbs (a savannah surface) will create fluxes at the measurement point which should not be as markedly influenced by the spatial positioning of the component surfaces as they are in the tiger-bush area.

In this thesis, all calculations have been made with a single value of $(1-\alpha)$: 0.33 in the case of tiger-bush, 0.20 in the case of savannah, mainly because no detailed data of α as a function of wind direction were available. Furthermore, calculation of an effective fractional vegetation cover is still speculative and strictly speaking only necessary if we want to test energy closure. In these cases, note that α or $(1-\alpha)$ is a function of wind direction and stability.

3 FIELD EXPERIMENTS: BACKGROUND, DESIGN AND INSTRUMENTATION

3.1 Introduction

This chapter gives site descriptions, experimental set-up and data acquisition for the HAPEX-Sahel and SEBEX campaigns. First, in § 3.2 an extensive discussion of the climate of the Sudano-Sahelian zone (SSZ), where both experiments took place, will be given. This will be presented on an annual and interannual scale by using a long-term meteorological dataset gathered at the ICRISAT Sahelian Centre, where the SEBEX experiment has been conducted and which was the location of one of the measurement sites (southern super-site) during the HAPEX-Sahel experiment. To illustrate the strong N-S gradient occurring in the SSZ, which also determined the variation in the HAPEX-square, three locations were selected. The long-term seasonal behaviour of several meteorological parameters will be shown for each of these sites.

The lay-out of the HAPEX-Sahel experiment will be subsequently discussed in general terms and a short description of the three super-sites and the three main vegetation-types observed at each of these sites (savannah, tiger-bush and millet) will be given. The spatial variability in the square will be described on the basis of differences in rainfall, soil moisture and leaf area index as measured at the three savannah sites. These data are illustrative in the light of the results presented in Chapter 5. Finally, the experimental arrangement of the HAPEX-Sahel savannah and tiger-bush site and of the SEBEX experiment will be presented.

3.2 The Sudano-Sahelian zone (SSZ)

3.2.1 Location

The HAPEX-Sahel square (2-3 ° E, 13-14 ° N), is located in the so-called Sudano-Sahelian zone (SSZ). The SSZ is usually defined in terms of rainfall limits that range from about 400 to 1000 mm (Monteith, 1991). Sivakumar (1989), who reviewed several definitions of the SSZ that can be found in the literature, noted that authors used a wide variation of rainfall limits to define the SSZ. He argued that the length of the growing season should be the primary criterion for outlining the SSZ. According to this definition, the SSZ extends from Senegal to Gambia in the west to Chad in the east (see Fig. 3.1, reprinted from Sivakumar and Wallace, 1991). With a growing season that varies from 60-150 days, the region offers a wide range of growing conditions. However, a large part of the region has a growing season of less than 120 days (Sivakumar, 1989). The Sahel zone, from which the HAPEX-Sahel experiment takes its name, is usually used to delineate the area with annual rainfalls of 200-700 mm that extends from 13 to 17 ° N.

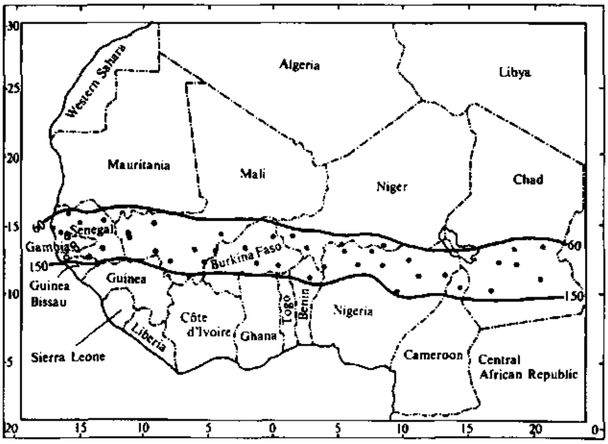

FIGURE 3.1. Geographical extent of the Sudano-Sahelian zone. Growing season lines of 60 and 150 days are shown (——). Reprinted from Sivakumar and Wallace (1991).

This large N-S rainfall gradient is illustrated in Fig. 3.2, which shows the mean annual rainfall (mm) in southern Niger. This area is located in the upper half of the Sudano-Sahelian belt, and it was here that the HAPEX-Sahel experiment was conducted. The average length of the growing season is related to the amount of rainfall and changes by more than one month over a distance of only 200 km. This has serious implications for the type of crops that can be grown in this region, because the date of the onset of the rains is important in planning agricultural operations, especially sowing.

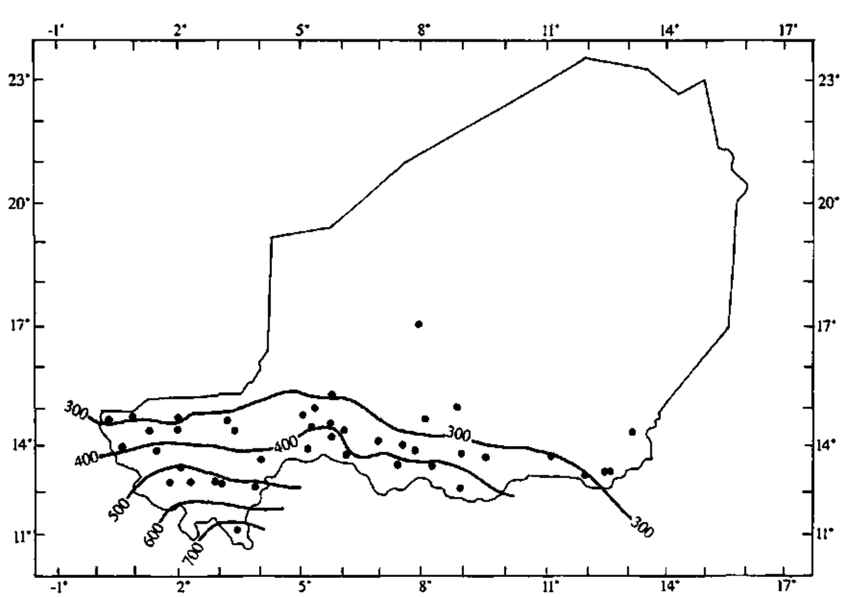

FIGURE 3.2. Mean annual rainfall (in mm) in the south of Niger. Figure reprinted from Sivakumar et al. (1993). Estimates are based on rainfall data from 1961-1990.

3.2.2 Rainfall

The rainfall distribution over Western Africa, and thus in the SSZ, is determined by the position of the meteorological equator and its two associated structures: the ITF (Intertropical Front) and the ITCZ (Intertropical Confluence Zone). The ITCZ, which is the ascending branch of the Hadley cell, is the zone along which two major air masses meet: the tropical continental air mass containing warm, dry air originating in the Sahara (the Harmattan or the Tropical Continental) and the warm, humid tropical maritime air originating from the Atlantic (Monsoon or Tropical Maritime). The ITCZ oscillates along the south-north axis, thus determining the start and length of dry and rainy periods. Its movement is related to the seasonal shifts in the relative position of the sun (Goutorbe et al., 1994). The ITCZ rarely extends its influence over continental areas north of 12 ° of latitude, a limit which is also (not coincidentally) the southern boundary of the Sahel. Thus rainfall in the Sahel (hence in the HAPEX-square) depends almost exclusively on the position and structure of the ITF. This is characterized by marked wind shears and moisture discontinuities, often at such low levels as below the 700 hPa surface, and is consequently not likely to produce extended and continuous rainfall. The Sahelian rainfall is therefore mostly of convective origin, either from isolated cumulo-nimbus phenomena or from organized cloud formations, often evolving in the form of squall lines. Such squall lines are the most characteristic feature of the Sahelian climate during the rainy season (Lebel et al., 1992).

The observation that rainfall in the SSZ since 1971 (some authors refer to 1969) has been considerably less than rainfall recorded before that period (Stewart, 1988; Nicholson, 1989; Lebel et al., 1992; Hare and Ogallo, 1993; Goutorbe et al., 1994; Lebel and LeBarbé, 1996), has led to the conclusion that this part of the globe, and areas such as north-eastern Brazil, western China, and eastern Australia (Hare and Ogallo, 1993), have been subject to a period of recurrent droughts which have lead to severe crop failures and declining national incomes and food production per capita (see Sivakumar and Wallace, 1991). This considerable reduction in rainfall, usually referred to as the Sahelian drought had its most intense period in 1972-73. The ongoing drought might be connected with the global climatic changes caused by changes in the general circulation that have little to do with Africa itself (in contrast with the ITCZ, SW-monsoon and connected disturbances). We can mention the anomalies observed in the space-time characteristics of rain-bringing systems such as the cyclones, jet streams, easterly/westerly winds, extra-tropical weather systems or the interrelated El Niño and the Southern Oscillation which are teleconnected with many climate anomalies around the world (Hare and Ogallo, 1993; Nicholson and Palao, 1993). Another possibility might be cycling which is normal in light of the history of this area (Stewart, 1988; Nicholson, 1989). According to Stewart (1988) this cycle is a long one, possibly the 100-year cycle shown to have held sway over Nile river flows for the past 300 years. It seems plausible that the SSZ may be following the Nile cycle (reaching its lowest point approximately 10 years after the turn of the century), and if so, we are presently well into the down slide (Stewart, 1988). An illustration of the long-lasting and until now irreversible drought afflicting the Sahelian zone is given in Fig. 3.3, which has been taken from Nicholson and Palao (1993).

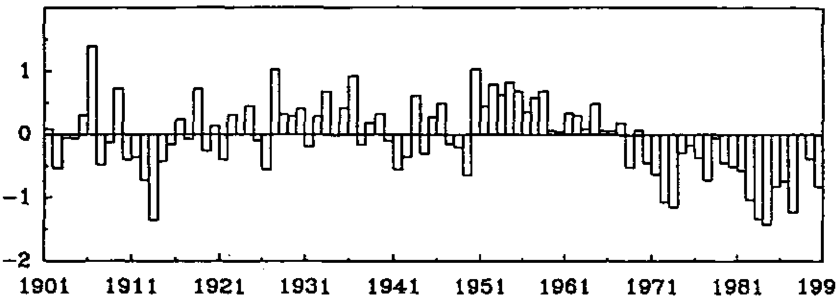

FIGURE 3.3. Rainfall fluctuations in the West African Sahel 1901-1990, expressed as a regionally averaged, standardized departure (departure from the long-term mean divided by the standard departure). Reprinted from Nicholson and Palao (1993).

This dry-out is also illustrated by Fig. 3.4, which shows the movement of the 400 and 600 mm isohyets in Niger after 1969 (Sivakumar et al., 1993). A clear decline in rainfall is illustrated by the isohyets being displaced 100-150 km southwards.

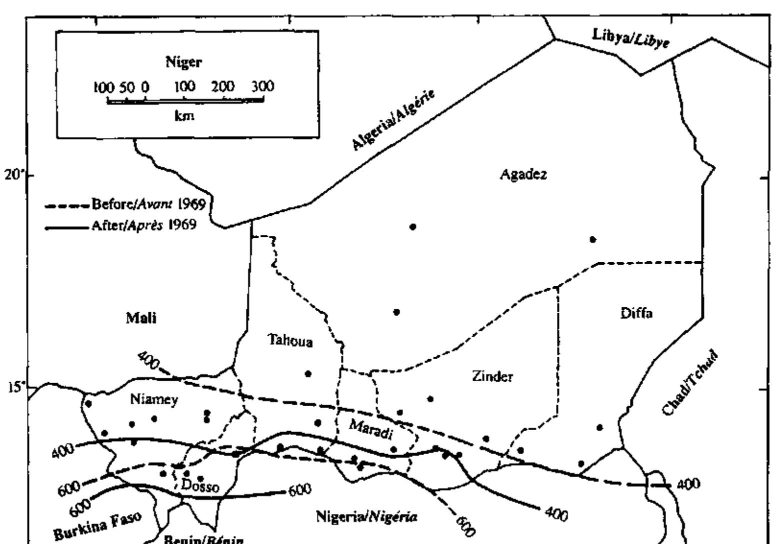

FIGURE 3.4. The location of the average rainfall isohyets in Niger for the periods 1945-1969 (dotted lines) and 1970-1990 (continuous lines). Reprinted from Sivakumar et al., 1993.

However, even though this long-term average rainfall gradient is uniform (rainfall increasing north to south, approximately 1 mm km^{-1}), rainfall in a single season can be markedly different because of the extremely large local variability. These large year-to-year changes in the isohyetal maps are the reason why no operational methods for the modelling of the Sahelian rainfall variability are available, either on annual or rain-event scale (Lebel et al., 1992).

If we focus on Niamey, which can be considered to be the centre of the HAPEX-square, the Sahelian drought is more than obvious: the total amount of rainfall, dates of the onset of the rains and the final rains themselves, duration and intensity (key factors for crop production) are all factors which reflect a deterioration since 1971. This can be readily seen in Table 3.1 (data from Stewart, 1988). Rainfall amount decreased by nearly 100 mm, duration of the monsoon cropping season by two weeks, the onset date by 11 days and rainfall intensity by nearly 1 mm/day.

TABLE 3.1. Niamey monsoon cropping season rainfall characteristics (from Stewart, 1988).

Period		Amount (mm)	Duration (days)	Onset (date)	Intensity (mm/days)
All:	1954-1983	494	99	20 June	4.68
Before 1971:	1954-1970	519	107	12 June	5.16
After 1971:	1971-1983	418	93	23 June	4.20

Stewart (1988) also indicated that seasons exhibiting a late onset (roughly after the third week of June) show the negative effects of climatic change very clearly, not simply in relative terms but in absolute reduction in rainfall amount. Prior to 1971, late seasons differed from early seasons only in duration. Late seasons were short, but had rainfall intensity indices as high or higher than early seasons. In the period from 1971 onward, both total rainfall and average intensity have declined catastrophically (Stewart, 1988). Another study however (Lebel and LeBarbé, 1996), claims that mean rainfall event varied little over recent decades. The main change that explains the rainfall deficit of the recent decades clearly appears to be the number of rainfall events rather than the average strength of the rainy events or the shortening of the rainy season. This illustrates that no consensus has been reached yet about the characteristics of Sahelian rainfall, a rainfall that is infamous for its high intermittence - 50 % of the annual rainfall falls in less than five hours (Lebel et al., 1996).

3.3 Climate of HAPEX-square and surroundings

3.3.1 Semi-arid regions

According to Heathcote (1983), the definition of 'arid region' before 1952 largely depended on the type of scientist involved. Different descriptions of semi-arid have been given for example by botanists, geohydrologists, soil scientists and climatologists. This led to classifications based on the natural vegetation types, geomorphologic characteristics, or amount and location of carbohydrates in the soil.

The climatologists initially had to rely upon the work of botanists because maps of world vegetation predated maps of global climates. Köppen had been trained as a botanist and used de Candolle's plant classification of 1874 as the basis for his climatic zones (1931), arguing that the natural vegetation reflected model climatic conditions (Heathcote, 1983). Finally Thornthwaite (1948) came up with an index which reflected the relationship between precipitation and evapotranspiration, a concept already introduced by Penck in 1894. From here Meigs (1953) developed his homoclimates, in which rainfall and climate figured as important factors. From Heathcote' s (1983) Table 2.3 it appears that the estimates (botanical and climatic) of global arid lands (< 500 mm rain) vary from 26.3 % (Köppen, 1931) to 36.3 % (Meigs, 1953) of the total land surface. However, according to the climatic definitions, the semi-arid regions cover approximately 15 %, whereas only about 6 % of the land surface appears to be occupied by semi-arid regions if we follow the botanical definition (Shantz, 1956). This discrepancy, as noticed by Heathcote (1983), leads to the conclusion that approximately 9 % of the world's vegetation considered by area is not in balance with its climate, a feature that might be caused by human activity.

The most recent attempt to map the dry climates of the world (see Hare and Ogallo, 1993), based on the P/PET ratios expressing precipitation (P) as a fraction of the potential evapotranspiration (PET), lead to percentages of 7.5, 12.5, and 17.5 for the hyper-arid, arid and semi-arid climate zones, respectively. In semi-arid regions P/PET is between 0.20 and 0.50 and this zone is suitable for sustainable pastoralism, whereas agriculture is susceptible to a high degree of interannual climate variability. The majority of the semi-arid zones are located in the western half of the United States and South America, on the African continent in the south and in a belt that runs below the Sahara and above the equatorial forests, in Central Asia and Northern Australia. In Western Europe only Spain has considerable areas that can be classified as having a semi-arid climate.

3.3.2 Interannual and seasonal variation

The semi-arid climate as observed in the HAPEX-square and its surroundings will be illustrated using the long-term (10 years: 1984-1993) variation of several main meteorological variables as monitored at the ICRISAT Sahelian Centre (ISC). This section provides the annual averages of rainfall, P, total downward solar radiation flux density, R_s, air temperature, T_a, and saturation deficit, D, at Sadoré, where the SEBEX experiment was located in the period 1988-1990 and the southern super-site of the HAPEX-Sahel experiment in 1992. The horizontal lines in the graphs denote the 10-year averages with the standard deviation next to them. Besides providing an overview of the average climate, the presented data also show how the conditions of the SEBEX and HAPEX-Sahel experiments compare with other years.

Furthermore, this section also gives the seasonal variation of these meteorological variables. The courses for a dry (1984), and a wet (1988) year are provided, to indicate the 'maximum possible' range. The decision whether a certain year had to be denoted as dry or wet was taken by calculating the P/E_p -ratios for all years with E_p the Penman potential evaporation. If we were to apply P-values only, 1986 and 1989 would be also considered as being extremely wet.

Fig. 3.5a shows that P varied from 260 mm in 1984 up to 699 in 1988. The first two SEBEX years - 1988 and 1989 - when compared to the average can be characterized as wet. The year 1990 was relatively dry. HAPEX-Sahel (1992) rainfall was close to the average of the past ten years. The bulk of the rainfall comes in showers that occur from May to September (see Fig. 3.6a), with a peak that usually occurs in August. The amount of rain in 1984 was much lower than in 1988 and 1992 for all months except May when no rainfall was recorded during 1988. For the dry year both the length of the rainy season and the intensity of the individual rain showers were clearly less.

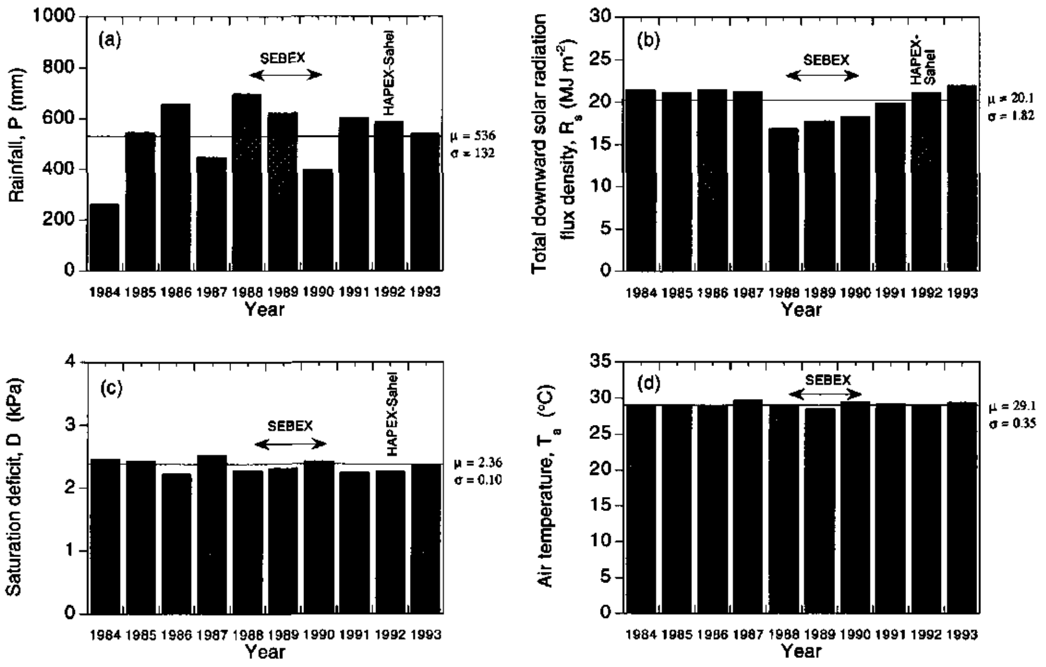

FIGURE 3.5. ***Inter-annual variation*** *of rainfall, P (a), total downward solar radiation flux density, R_S (b), saturation deficit, D (c) and air temperature, T_a (d) as calculated from a 10-year time series of meteorological data obtained at the ICRISAT Sahelian Centre.*

Fig. 3.5b shows that R_s was considerably lower (up to 25 %) than average for 1988, 1989 and 1990. This must partly be due to the high rainfall amounts, which are related to higher cloudiness. Occurrence of dust storms during the dry season may be another reason. The values for HAPEX-Sahel were slightly above average.

R_s was moderately variable during the season, as shown in Fig. 3.6b. A clear dip, correlated to large amounts of rainfall was observed during the rainy season of 1988. Low values were also observed during the 'winter' months. Values for 1988 are clearly lower both for the rainy and the dry period.

The high variation in rainfall amount appeared to have no major effect on the annual average of T_a, as shown in Fig. 3.5d; its value was fairly constant during the years (average = 29.1 °, σ = 0.35). SEBEX (1989) and HAPEX-Sahel years had slightly lower average air temperatures.

Saturation deficit, D, exhibited a higher variation through the years, as shown in Fig. 3.5c, which was only slightly correlated with rainfall (average = 2.36 kPa, σ = 0.10), although 1984 and 1988 had clearly higher and lower values than average. Below average rainfall years (1984, 1987 and 1990) had above average D-values.

From a seasonal point of view, D and T_a (Fig. 3.6c and d) exhibited a bimodal pattern. Differences between 1984 and 1988 were largest during the wet season. Maximum differences in D between a wet and a dry year were observed during the rainy period: after the dry-out of the vegetation the values are similar.

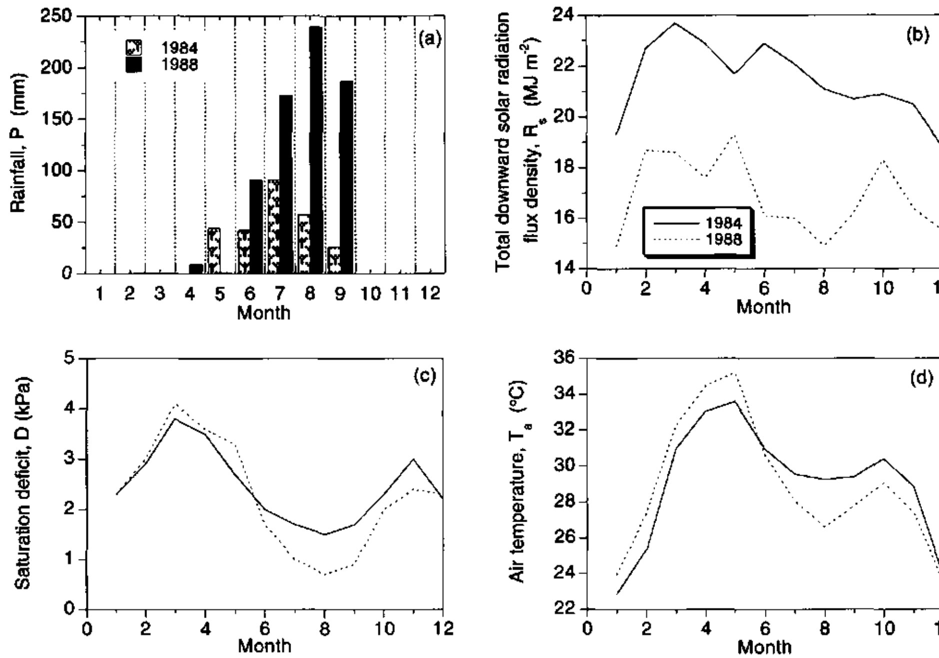

FIGURE 3.6. ***Monthly averages*** *of total rainfall, P (a), downward solar radiation flux density, R_S (b), saturation deficit, D (c) and air temperature, T_a (d) for a dry (1984) and a wet year (1988). The meteorological data were obtained at ISC.*

3.3.3 Spatial variation in the SSZ

Meteorological conditions, and thus the partition of available energy, change rapidly moving from north to south in the SSZ because of the large rainfall gradient. Three stations were chosen to illustrate the large spatial variation occurring over a distance of only 300 km. These meteorological stations were Tillabéry (14°12', 1°27'), Niamey (13°30, 2°08') and Gaya (11°59' , 3°30'). They are located in the vicinity of or in (Niamey) the HAPEX-grid square. Tillabery lies to the north-west of Niamey on the same latitude as Ouallam, where the original northern border of the grid-square was situated. Gaya lies to the south-east of Niamey, and thus of the HAPEX-grid square. All three stations are at similar altitudes (± 200 m). Data were taken from Sivakumar et al. (1993) and from the FAO agroclimatological database (*n/N*).

Monthly rainfall amounts for the three selected sites are shown in Fig. 3.7a. For all months, a clear ranking is observed; Tillabéry (north) having the lowest rainfall and Gaya (south) the highest. Long-term (1961-1990) annual totals are 393, 545 and 797 mm for Tillabéry, Niamey and Gaya, respectively. Largely related to this rainfall is the relative sunshine fraction (*n/N*) which is the ratio of the bright sunshine hours per day, *n*, and the total day length, *N*, (both in hours). This variable is chosen instead of R_S, because no direct measurements of R_S were available. The value of *n/N*, together with knowledge of the fraction of radiation on overcast (0.25 for an average climate) and clear days (0.50 for an average climate) and the extra-terrestrial radiation, yields an estimate of R_S. Highest dry season values (Fig. 3.7b) are found for Niamey. The lower values for Tillabéry are probably caused by the higher occurrence of dust storms in this drier area, whereas at Gaya more (convective) clouds will be present. The differences during the wet season are mainly caused by the presence of clouds.

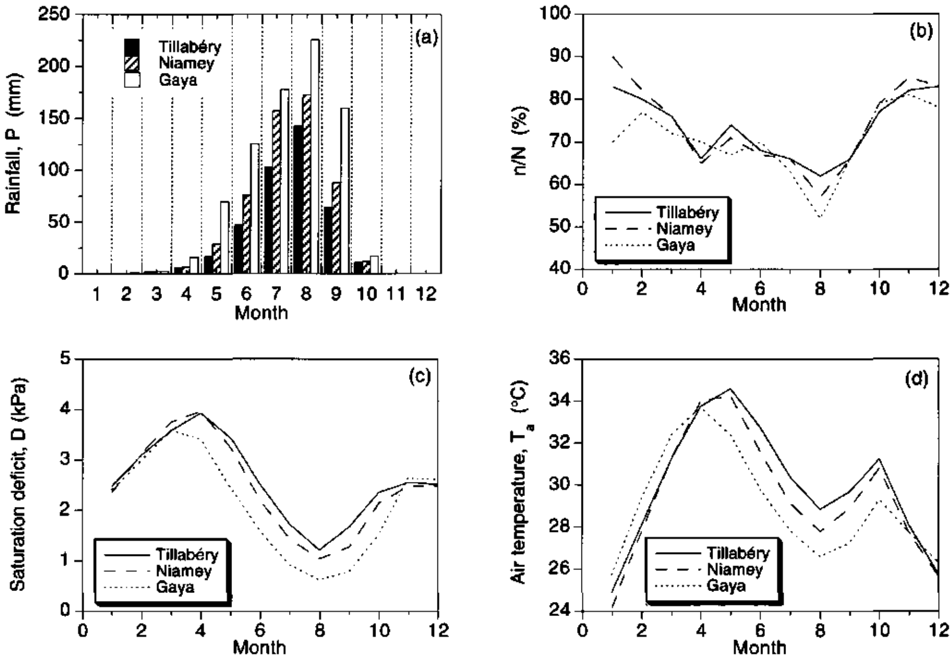

FIGURE 3.7. ***Monthly (long-term) averages*** *of rainfall, P (a), relative sunshine fraction, n/N (b), saturation deficit, D (c) and air temperature, T_a (d) for three locations in or in the vicinity of the HAPEX-square. The meteorological data were obtained from tables given in Sivakumar et al. (1993) and the FAO Agroclimatological database.*

The onset and severity of the rains is also reflected in Fig. 3.7c, which shows the seasonal course of D. Saturation deficit is lowest at Gaya during most of the months. When no rainfall occurs, spatial differences in D are negligible.

Average (long-term) monthly air temperatures (obtained from maximum, T_x, and minimum, T_n, air temperatures) are shown in Fig. 3.7d. Highest values of T_a are related to the station receiving the smallest amount of rainfall. Differences between the three stations are largest during the rainy season, whereas in the dry season the differences become negligible. Higher 'dry season' values at Gaya are caused by higher values of T_n (about 2 ° higher) .

3.4 The HAPEX-Sahel experiment

3.4.1 Introduction

The HAPEX-Sahel experiment was executed in Niger, West Africa during the years 1991-1992, as a follow-up of previously conducted large-scale international experiments in semi-arid regions (see § 1.1.2). The experiment had an intensive observation period (IOP) from August to October 1992.

The experiment aims at improving the parameterization of land surface atmospheric interactions at the GCM grid-box scale. It combines remote sensing with hydrological and meteorological modelling to develop aggregation techniques for use in large-scale estimates of the hydrological and meteorological behaviour of large areas in the Sahel. The experimental strategy consisted of a period of intensive measurements during the transition period of the rainy to the dry season, backed up by a series of long-term measurements in a 1° by 1 ° square in Niger. Three 'super-sites' were instrumented with a variety of hydrological and (micro) meteorological equipment to provide detailed information of surface energy exchange on the local scale. Boundary layer measurements and aircraft measurements were used to provide information at scales of 100 to 500 km^2. All the relevant remote sensing images were obtained for this period. The programme of measurements is now being analyzed and an extensive modelling programme is underway to aggregate the information at all scales up to the GCM grid box scale (Goutorbe et al., 1994).

3.4.2 Vegetation and soils around and in the HAPEX-square

a) General

The vegetation around and in the HAPEX-square consists of (semi-) natural vegetation: fallow savannah and tiger-bush (a sparse dryland forest) and several arable crops, of which millet, sorghum, groundnut and cowpea are the most important.

The fallow savannah contains diverse mixtures of naturally occurring perennial woody shrubs and herbaceous annual plants. Throughout the HAPEX-square the dominant woody shrub in the fallow savannah is *Guiera Senegalensis* (L.). The savannah areas will have been previously used for growing crops, but form part of a rotation system with a cycle which varies from a few years to 15 or even 20 years. In recent times the shorter rotations have become more common (see also Kowal and Kassam, 1978). Tiger-bush only occurs on the laterite plateaux. The tiger-bush vegetation is dominated by comparatively large woody perennials and trees. The vegetation grows in dense strips which are separated by areas of completely bare soil. The proportion of vegetation cover within the tiger-bush areas varies according to the rainfall such that the densest cover is at the southern most part of the square and this decreases towards the north (Goutorbe et al., 1994).

In Niger, and also in the HAPEX-square, millet is the most important staple crop. It is usually intercropped with cowpea, sorghum or groundnut. In the valley of the Niger river, rice is grown as a flooded or irrigated crop. Vegetable cultivation (tomato, onions) is also common in the Niger valley.

Visual inspection of a spot image for the 1° square suggests that tiger-bush occupies around 30 % of the land surface. The next most extensive land-cover type is millet, the dominant subsistence crop. Fallow land is an integral part of the rotation practised by local farmers, but occupies a smaller area than the millet fields.

The three sections below will give a more detailed description of the origin of the above mentioned main vegetation types. Millet will be described only briefly, because this thesis focuses on fallow savannah and tiger-bush vegetation and therefore no results pertaining to millet will be reported in the following chapters.

a) Fallow savannah

The *Guiera Senegalensis* J.F. Gmel. belongs to the family of the Combretaceae according to Von Maydell (1990). It can be described as a shrub, up to three meters high with a grey bark , grey-green oval to oblong ovate leaves of 2.5-6.0 by 1.5 - 3.5 cm. Its flowers have yellow greenish, globose heads. The fruit is elongate, 3-4 cm in size and covered by silvery-pink hair. It is found throughout Senegal, the Gambia, Mali, Niger and Burkina Faso and is linked with leached, sandy, and very dry soils. It can be found on fallow or as underwood in low savannah forests. It is an indicator of overgrazing. Its leaves, shoots and fruit are browsed by camels and goats, less by other livestock. Leaves persist a long time into the dry season. Branches and particularly roots are used as fuelwood. Slim branches are used for plaiting work, mats for sand stabilization and fencing material (Senegal), whereas the gum is marketed in Niger. The shrub has numerous medicinal applications (see Von Maydell, 1990).

b) Tiger-bush

As summarized by Cole (1986), several examples of linear vegetation patterns can be recognized in the SSZ. One of these linear vegetation pattern is the brousse tigrée or tiger-bush (bearing similarity to a tiger skin when viewed from the sky), that occurs in the Sahelian low tree and shrub savannah zone in the southern part of the Republic of Niger. It probably results from soil water variations related to termite activity in areas were shallow soils and limited rainfall cause intense root competition (White, 1965). The patterns occur on shallow gravely soils of plateaux with a massive cuirass of Tertiary age in areas where the rainfall is about 700 mm. They consist of alternating lines of *Combretum* (spp.) woodland about four metres high and intervening stripes of bare or sparsely covered soil. They occur close to and parallel with the escarpment edge of the plateau. Where not covered by patches of wind-blown sand the laterite plateau is remarkably level. It is covered by some 10 cm of sandy loam soil over ironstone gravel extending to laterite cuirass at a depth of 10-40 cm. The combination of shallow soil over impermeable laterite cuirass and level terrain inhibits percolation and results in the accumulation of surface water after rains. There are no significant differences between the soils of the woodlands and bare areas.

It has been suggested that the linear vegetation patterns formed when, with a change of climate, debris from degraded termitaria smothered adjacent vegetation. Trees, which were unaffected, benefited from the extra run-off from these collapsed termitaria and extended their roots beneath the bare areas. Once established the pattern became self-perpetuating for the compact soils of the degraded mounds and the root competition from the existing woodland trees discouraged seedling establishment on the bare stripes. The alignment of the woodland belts parallel to the escarpment edge and to large patches of sand are considered to be related to run-off from these areas (White, 1965).

The *Combretum micranthum* belongs to the family of the Combretaceae. It is a shrub (up to four meters) or a tree that can reach ten meters in height under favourable conditions. The brown-red, climbing branches may be as long as twenty meters. Leaves are light green when young, typically rust-coloured when mature (in the dry season). Leaf shape is variable, oblong- elliptic, and up to 10 cm in length. Small white flowers occur in dense racemes (2-5 cm long). The fruit has four wings and it is brown, scaly, and ferruginous, about 1.5 cm in diameter. This shrub is very frequent all over the Sahel (from Senegal to Niger, the Gambia, Burkina Faso, Nigeria, Sudan), where it often forms dense, pure stands. It is found on dry sites and related to sandstone, clay, laterite, crystalline rocks, on skeletal soils and on boulders in the Sudan zone. It is often associated with *Acacia machrostachya* and *Combretum nigricans*. This shrub is an indicator of extremely unfavourable (no longer cultivable) soils. Annual rainfalls between 300 and 1500 mm. The roots are very susceptible to termite attack. In many countries the leaves are used and traded as tea: the seeds are edible. The wood is used for fuel, and other domestic and medicinal uses (see Von Maydell, 1990).

Combretum nigricans also belongs to the family of Combretaceae, with var. elliotii mainly occurring in the Sahel. It is a small tree or shrub, up to ten meters in height, with a short bole, frequently spiral grained. The bark is beige-brownish-red and warty. The leaves are opposite and elliptic. Flowers are greenish-white, in axillary racemes, 3-5 cm long. Fruits are reddish, four-winged, glabrous, scaly or sticky in the centre, approximately 2.5 cm in diameter. This tree is widespread from the Atlantic coast to the Red Sea, particularly in the Sudan and Guinea savannahs. It is rarely found in the Sahel. It is frequently seen on clayey, loamy or lateritic soils or skeletal soils. The tree yields edible gum which is traded on local markets. The wood makes good fuelwood and charcoal, as well as pestles for mortars. The leaves are said to be unpalatable to livestock. Leaves, branches, bark and roots are used to cure various diseases.

Several uses and beneficial effects of trees and shrubs in the Sahel can be listed. These include the provision of fuelwood, timber, food, forage, medicines, raw materials, protective functions, soil improving functions and cultural functions. However, the trees can also have negative effects: competition with the annual plants (grasses and herbs) for water, nutrients and light, as has been shown in Chapter 1.

c) Millet

About one third of the world's millet is grown in Africa and about 70 % of this is grown in West Africa. Because of its adaptability to drought, pearl millet (*Pennisetum glaucum*) is the major millet type grown in Africa, and it is traditionally cultivated as an intercrop with a legume such as cowpea or groundnut. The harsh climate in West Africa means that farmers have to deal with a low and erratic rainfall that causes growing seasons of unpredictable length. Besides the problems associated with securing a reliable water supply, wind and water erosion damage crops and influence the fertility status of the soils. During the dry season, high values of air and soil temperature and of vapour pressure deficit inhibit optimal growth. The low fertility (low in organic matter, N and P), coarse textured soils often exhibiting a poor physical condition (low structural stability, low water holding capacity) are an extra constraint to the use of these soils for the growth of millet (Payne et al., 1990; Klaij and Vachaud, 1992; Wallace et al., 1993).

Millet is either grown as a pure crop (sole cropping) or intercropped with other cereals (usually sorghum) and/or a legume, usually cowpea. The percentage of sole crop millet increases from south to north in the SSZ. In the Northern Guinean zone of West Africa, sole crop millet is virtually unknown, whereas in villages of the Sahelian zone in Niger the proportion increases to 30-50 %. Most of the millet crop in West Africa is planted with virtually no prior land preparation. As a rainfed crop, pearl millet is sown with the first rains during the growing season.

3.4.3 The super-sites

a) General

The 1° by 1° HAPEX-square, located to the east of Niamey is shown in Fig. 3.8. In this square, three super-sites have been defined, the southern super-site, the central east super-site and the central west super-site. Limited measurements were also conducted at a experimental site at Danguey Gourou (in the northern part of the grid). From now on these sites will be referred to by a short mnemonic, SSS for southern super-site, CWS for central west super-site, CES for the central east super-site and NS for the northern (Danguey Gourou) super-site.

At the super-sites, the three vegetation types representative of the Sahelian vegetation in this area were sampled. This gave rise to three contrasting sub-sites: a millet site, a fallow savannah site and a tiger-bush site. In the case of the CWS, two extra sub-sites were added: a degraded fallow savannah and a cleared fallow savannah. At the first site the undergrowth was clearly less and more bare soil was present, whereas the second site had been stripped of all its bushes (June 1992) before the onset of the rainy period.

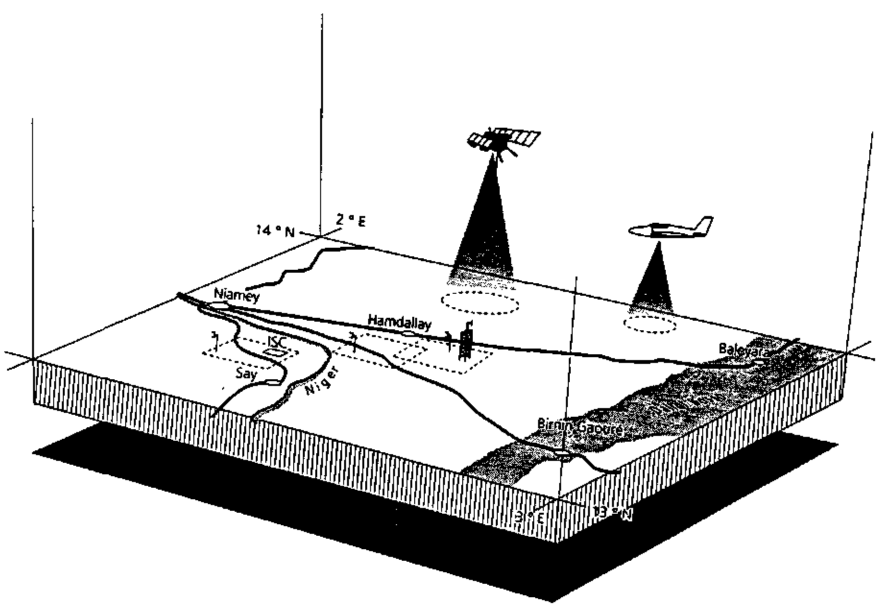

FIGURE 3.8. Diagram showing the position of the HAPEX-Sahel experimental square and the three super-sites. Reprinted from Goutorbe et al., 1994.

Each super-site has been described briefly in the HAPEX-Sahel overview paper (Goutorbe et al., 1994) and in more detail in a series of reports published elsewhere (the so-called super-site reports of Wallace et al. (1994) or Monteny (1993), for example). A summary of the relevant literature will be given here. The description of the other super-sites is necessary as later on in Chapter 5 and 7 some data from these sites will be used as comparative material.

b) Southern super-site - information taken from Wallace et al., 1994 and Moncrieff et al., 1996a):

The SSS was located near the right bank of the river Niger, and located around the ICRISAT Sahelian Centre (ISC) about 45 km south of Niamey. The area consists of a broad sandy valley next to the river Niger, bordered to the west by extensive laterite plateaux, on which the vegetation is mainly the above described tiger-bush. These plateaux occupy about half of the area within that part of the HAPEX-Sahel square that falls south of the river; a much larger portion than in the entire degree square (≈ 25-30 %, d'Herbes et al., 1992). The remainder of the area south of the river is predominantly agricultural land, containing either millet (*Pennisetum glaucum* (L.) R. Br. vc. Sadoré local) fields and fallow savannah in approximately equal portions (d'Herbes et al., 1992).

The millet is planted in a 400 x 400 m field at about 4600 ± 1260 pockets per hectare, each pocket contains about three plants after thinning. Cowpea (*Vigna ungiculata* (L.) Walp) is sown irregularly between the millet plants at about 900 ± 450 pockets per hectare. Soils are very sandy (structureless when moist, becoming massive when dry), chemically poor and sensitive to drought. They are underlain by hard laterite at a depth of 2.5-3 m and the water table is about 25 m deep.

The fallow savannah site (800 x 1000 m) had not been cropped since about 1986, allowing the natural vegetation to regenerate. The arid wooded savannah vegetation at this site consisted of a ground layer of annual herbs and grasses, including *Cassia mimosoides* (L.), *Cenchrus biflorus* Roxb. and *Mitracarpus villosus* (Sw.) DC. Scattered 2-3 m high shrubs (almost all Guiera Senegalensis L.) covered 16 % of the area and there were also occasional 4-8 m high trees (*Combretum glutinosum* Perrott. ex DC.) The site was occasionally grazed by cattle and sheep, except during the IOP. Soils at the fallow site were very similar to those at the millet site, although the laterite here often starts at 2 m and the water table is slightly deeper, at about 32 m.

The tiger-bush site was grown with an irregular shaped area of tiger-bush about 3 km across. The vegetation was confined to dense strips about 10-30 m wide by 100-300 m long, separated by completely bare crusted soil. The vegetated strips covered about 33 % of the area (calculated from areal photographs). The soil under the vegetation is well structured and permeable. Vegetation is dominated by two species of 2-4 m tall shrubs (*Combretum micranthum* G. Don and *Guiera Senegalensis L.*) and several single tree species (*Combretum nigricans* Lepr. ex. Guill. and Perrott. and *Acacia ataxacantha* DC. and *Acacia pennata* (L.) Willd.), typically 4-8 m tall. The soil is mainly 0.1-0.5 m of gravely sandy loam overlying weathered laterite. Solid laterite is found at depths starting at about 0.2-0.9 m.

c) Central east super-site (CES)

The CES was located 65 km east of Niamey. The region is covered by aeolian sand of Saharan origin, the depth depending on the underground relief. The fallow savannah consisted mainly of a grass cover interspersed with *Guiera senegalensis* bushes 3-3.5 m high whose position in the savannah is mostly due to the underground water storage at depths of 3 to 5 m in relation to the underground relief. The bushes cover about 17 % of the area. The grass layer composition is influenced by the rainfall chronology during the season. For the same total amount of precipitation, biomass production can be completely different because of the timing of the rain events during the wet season. This induces some differential succession in the dynamics of plant species. The grass layer is essentially made up of annual plants. Some of them are C_3 species, but most of them are C_4 species with greater photosynthetic potential. Different species are in competition at seedling after the first heavy rains: *Aristida mutabilis, Aristida adscensionis, Cenchrus biflorus, Mitacarpus scaber,* *Tribulis terrestris*. With more regular precipitation events during the rainy season, other plant species appear: *Zornia glochidiata, Ctenium elegans, Digitaria gayana, Eragrostis tremula, Dactyloctenium aegypticum, Indigofera aspera, Mitacarpus scaber*. Depending on the timing of the end of the rainfall events and the soil water content, young plants dry out without bearing fruit and for the other established plants, a senescence stage may occur one to three weeks after the rainy season is over (Monteny et al., 1996). Most of the savannah area in the valleys is used permanently or intermittently for growing pearl millet, often intercropped with cowpea. The millet is generally very heterogeneous due to the various depth of sand deposition upon the crust and the fact that millet is sown on two or three separate occasions with the arrival of the first rains.

Millet was sown at 7000 pockets per hectare, each pocket contains 3-4 plants after tilling. Depending on the rainfall distribution, cowpea was sown in between the millet when the latter had reached the heading stage.

d) Central west super-site (CWS)

This super-site was located 40 km east of Niamey, 15 km west of the CES and was centred on the village of Fandou Beri. It comprised four sub-sites: millet, fallow savannah, a more degraded fallow savannah and tiger-bush. The fallow savannah and tiger-bush sub-sites are the sites which are discussed in this thesis. The fallow savannah site consisted of a continuous herb layer which, early in the rainy season, contained C_3 herb species such as *Mitracarpus scaber*, Zucc. and *Indigofera* spp. During the season, however, C_4-grasses became increasingly important such that, by the end of the season, the herb layer consisted of approximately equal portions of herbs and grasses. Several grass species were present including *Digitaria gayana* (Kunth.), *Ctenium elegans* (Kunth.), *Eragrostis pilosa* (Linn.) and. *E. tremula* (Hochst.). The fallow site also supported a 1-3 m tall population of the woody shrub *Guiera senegalensis* (juss.)with a vertically projected canopy cover of around 10-20 %. The leaf area index, *LAI*, of the shrubs increased from zero at the start of the rains in June to about 0.32 at the end of October. Growth of the herb layer was slow at the beginning of the rains but increased rapidly during August and September to a *LAI* of 1.0 by the end of the season (Hanan and Prince, 1996). Figures of *LAI*, presented later, are based on growth curves fitted to the data (N. Hanan, personal communication, 1994).

The tiger-bush measurement area was located approximately ten kilometres south-east of the fallow savannah site. The vegetation consisted of *Guiera senegalensis* and several tree species (*Combretum nigricans, Combretum micranthum*) growing in long strips of 10 to 30 m wide. Vegetation height was on average four meters and the height of the trees was between six and ten meters. Vegetation strips covered approximately 30 % of the surface, the remaining 70 % was bare soil. *LAI* has not been measured but was estimated to be 1.0 by comparison to savannah bush values. Prior to the IOP (June) the trees and bushes that formed the vegetation strips were already lightly vegetated. From the beginning of the rains, the green leaf area developed rapidly. The tiger-bush leaf area remained high until the end of the IOP, unlike the herbaceous vegetation in the valleys which had largely senesced at this time.

The millet (*Pennisetum glaucum*) sub-site was planted in mid-July on sandy soil near the village of Fandou Beri. The vegetation cover was heterogeneous and further characterized by a low plant density of 3-10 plants per pocket at about 1100-2500 pockets per hectare (3629 clumps per hectare (± 585 per ha) according to Hanan and Prince (1996). Intercropping with cowpea (*Vigna unguiculata*, Savi.) and bisap (*Hibiscus sabdariffa*, Linn.) added to the heterogeneity, thus representing the traditional crop pattern on Sahelian cultivated soils. *LAI* increased from zero at planting to a maximum of about 0.3 in early

September. It then decreased as the crop matured and senesced before harvest in early October. The density and *LAI* of the intercrop species was clearly less than it was for millet (Hanan and Prince, 1996).

e) Northern super-site

The experimental site was located near the village Danguey Gourou, approximately 40 km north of Niamey. The sole-cropped millet cover at this site was also heterogeneous and of low density (3-10 plants per pocket at about 1100-1500 pockets per hectare). No other vegetation types have been sampled here.

3.4.4 Environment and leaf area index

The principal objective of the HAPEX-Sahel experiment is to improve the parameterization of the energy fluxes from Sahelian-type vegetation in GCMs (Goutorbe et al., 1994). The first requirement towards meeting this objective is to quantify the energy and water balance of the one degree study area, an area comparable in size to a GCM grid square. Such an area will inevitably contain a variety of vegetation and soil and, in a climate with spatially variable rainfall, a wide range of soil moisture conditions. (Gash et al., 1996). Even within the relatively small HAPEX-Sahel area, spatial variation is enormous. The gradient of rainfall of about 1 mm per km will manifest itself in the variability in the physiological stage achieved by the vegetation (Moncrieff et al., 1996a). The effect of rainfall on the vegetation development is illustrated by Fig. 3.9 which gives the normalised difference vegetation index (NDVI) for the three super-sites and the extra site (Danguey Gourou) during 1992. The early start of the rainy season at the SSS is reflected by the increase in NDVI about a month or so before the index increases for the other super-sites. Peak values for all sites are similar, apart from Danguey Gourou, being the most northerly of the stations. Difference in vegetation 'production' will thus mainly be caused by the length of the growing season.

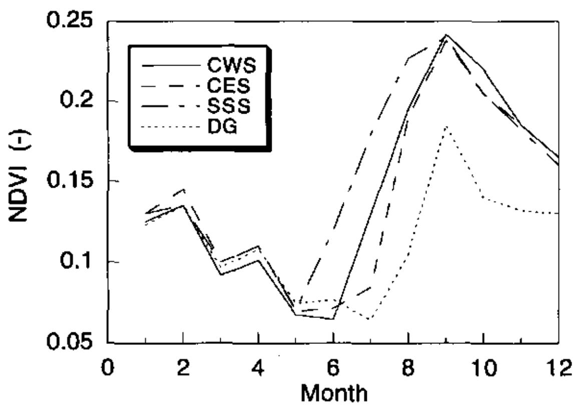

FIGURE 3.9. Observations of NDVI in 1992 over the HAPEX-Sahel experimental square.

Three important features monitored at the super-sites will be used to illustrate this aspect of spatial variation and to describe the environmental conditions and vegetation development during the IOP. They consist of rainfall, *P*, integrated (0-0.5 m) soil moisture content, Θ, and leaf area index, *LAI*. In this case only savannah data will be used because no measurements of *LAI* (and sometimes Θ) were available for the tiger-bush sites. Atmospheric conditions (Q_p, D and T_a) appeared to vary little among the super-sites (Moncrieff et al., 1996a). Therefore, the temporal variation of these variables will only be described for CWS.

Fig. 3.10a shows the rainfall as recorded at the three savannah sub-sites. The period shown extends from two weeks before the start of the IOP until the day of the last recorded rainfall. The last day at which rain was recorded was day 259 for the CES, day 262 for the SSS and day 264 for the CWS. During the period under consideration the CES received the smallest amount of precipitation (255 mm), whereas the SSS received 50 % more (total of 391 mm). The CWS received an intermediate amount of rain (312 mm).

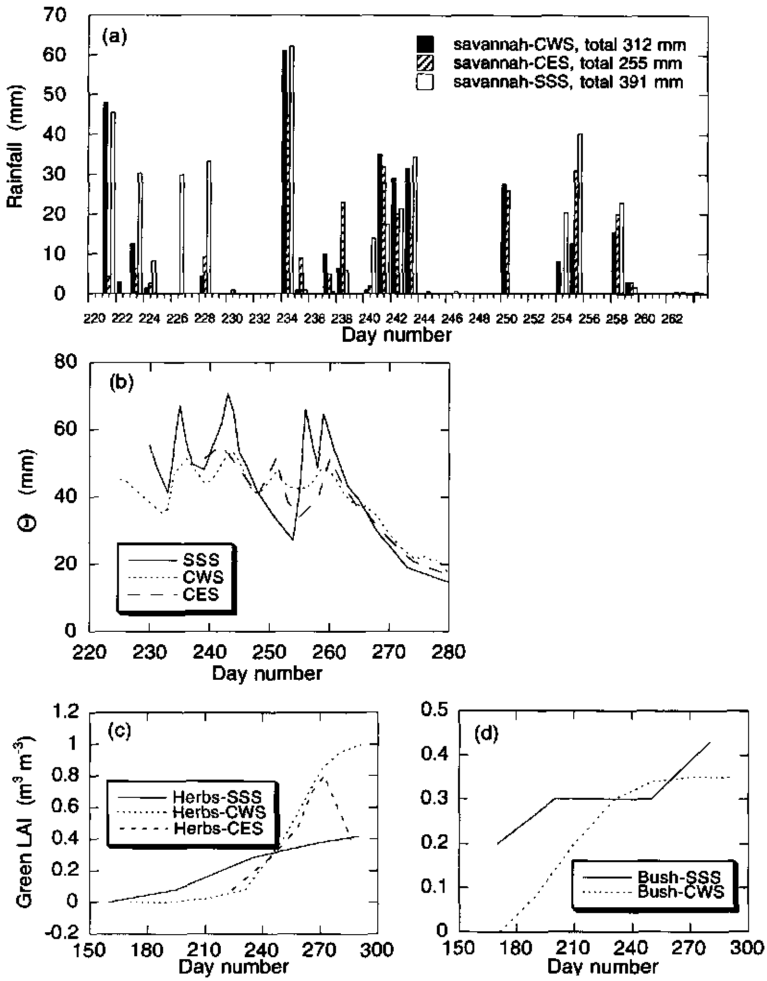

FIGURE 3.10. (a) Precipitation, (b) integrated soil moisture (0-50 cm), Θ and (c) + (d) measured leaf area index for the savannah vegetation components for the three super-sites during the IOP.

The consequences of this unequal rainfall distribution are illustrated by Fig. 3.10b, in which the integrated (0-50 cm) soil water content, Θ, is given for the three super-sites. The course of soil water content for the SSS and the central sites is similar until day 245, although the higher amount of precipitation per rainstorm for the SSS leads to generally higher values for this super-site. After day 246 however, Θ for the SSS falls below the values recorded for the CWS and CES. This is caused by the smaller cumulative SSS rainfall amount during days 241-243 and the fact that at day 250 at both the CWS and the CES a considerable rainstorm occurred, whereas no precipitation was gauged for that day at the SSS. Θ at SSS recovers after day 254, when it rains at the SSS and CWS. After the last rainfall, all super-sites show a similar course of Θ, with a declining drying-down rate after day 272 when milder atmospheric conditions (lower D, lower T_a) occur. At the end of the IOP the SSS topsoil appears to be the driest, but differences in sampling intensity between the three sites might have caused this effect.

The green biomass of the savannah is related to rainfall and soil moisture. Fig. 3.10c and d show the temporal changes in LAI for the understorey (grass/herb-layer), LAI_u, and the bushes, LAI_b, respectively, at the super-sites. At the CES no values of LAI_b were available. Both the bushes and the understorey at the SSS started to develop much earlier than at the central sites because of the large amount of rainfall occurring between March until July (305 mm). LAI_b and LAI_u for the SSS were clearly higher than the Central Sites values until day 230-240. Subsequently however, LAI_u for the SSS stagnated, whereas the values for the CES and CWS showed an exponential increase. The SSS LAI_b seemed to recover after day 254 when first rainfall occurred after a ten-day virtually rainless period. The LAI_u of the SSS however, stayed low in comparison to the central sites and showed no recovery. The central sites showed similar values of LAI_u. The observed senescense of the CES understorey is clearly visible in Fig. 3.10c by the sudden decrease in LAI_u after day 270. The unexpected asymptotic behaviour of the SSS LAI_u-course might be caused by the fact that no rainfall occurred at day 250, which led to a rainless period that lasted ten days with a serious decline in soil moisture, see Fig. 3.10b. This period might have been long enough to cause an irreversible stress-effect on this layer, which severely stagnated the growth of green leaf area. Verhoef et al. (1996b) measured a sharp decrease in leaf conductance (see § 6.3.1) and CO_2 flux (as described in Chapter 7) during the drying out stage of the CWS savannah vegetation. The decrease in moisture content for the SSS during day 244-254 was comparable to this dry-out and it might well be that this effect severely restricted the development of new green leaf area. Because of the increasingly drier atmosphere after day 260, thus inducing more vegetation stress, no recovery was possible.

3.5 Site description: HAPEX-Sahel CWS, savannah (WAUMET) site

3.5.1 General

The measurements of WAUMET took place at the CWS. The savannah consisted of scattered shrubs (*Guiera senegalensis*) with an understorey of several species of grasses and herbs as described in § 3.4.3. The undergrowth was rather sparse and low (maximum height 0.5 m), because of the late start to the rainy season (end of June). About 40 % of the understorey was bare soil.

The soil was classified as a loamy sand and the dry bulk density, ${}^b\rho_d$, was 1600, 1580, 1480 and 1400 kg m^{-3} for the depths of 0.05, 0.10, 0.25 and 0.45, respectively (Soet et al., 1995). The relatively large ${}^{b}\rho_d$ values are a result of high sand contents and a higher soil compaction possibly caused by the excrements of termites.

Fig. 3.11 shows seasonal trends of daily mean T_a, D, incoming photosynthetically active radiation, Q_p , and the amount of daily total rainfall, together with Θ. Values of D were mainly related to the rainfall events. Following rainstorms (see 22 August, day 235) D was less than 1 kPa. After the last rain of the wet season (20 September, day 264), D increased to 1.5 kPa and higher, with a peak of 3.1 kPa on 7 October (day 281). Changes in T_a were similar, but less pronounced. For most days incoming daily mean Q_p varied between values of 450 and 600 μmol m^{-2} s^{-1}. On cloudy days during the rainy season mean Q_p was less than 400 μmolm^{-2} s^{-1}. Θ was largest after the successive rainstorms of 27-30 August (days 240-243), that totalled nearly 100 mm of rain. After the last rainstorm on 20 September (day 264) the soil dried out quickly. The relatively cooler and more humid conditions from 28 September to 3 October (days 272-277) caused a temporary slow-down in the drying process.

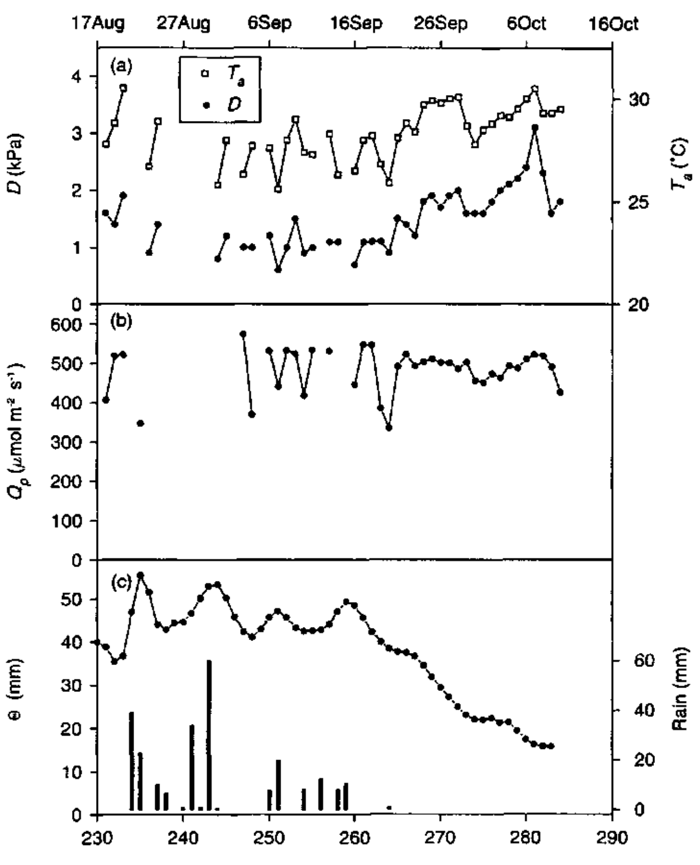

FIGURE 3.11. (a) Daily average vapour pressure deficit, D (closed circles), air temperature, T_a (open squares), (b) photosynthetically active radiation, Q_p , and (c) rainfall (bars) and integrated soil water content, Θ, for the WAUMET site at CWS during the HAPEX-Sahel IOP (17 August to 9 October 1992).

3.5.2 Micrometeorological measurements

The experimental site has been designed with the following purposes in mind. The main focus was on the measurement of the energy and CO_2 fluxes for semi-natural savannah vegetation. Furthermore, certain vegetation characteristics, such as leaf conductance and canopy temperature have been sampled to obtain a better insight in the physiological behaviour of the canopy, especially of its two different layers - the upperstorey of bushes and the understorey of grasses and herbs. The second aim was to verify and improve existing sparse canopy models. Because these models usually distinguish between the different surface components, the radiation and soil heat flux set-up involved separate measurements for bush and understorey. Measurement systems were designed in such a way that atmospheric fluxes could be calculated by several methods, to allow for testing the validity of the methods under these difficult environmental conditions. Note that in this thesis only the results of the EC method will be described. Information of the performance of the other methods can be found elsewhere. An overview of the WAUMET experimental site is given in Fig. 3.12.

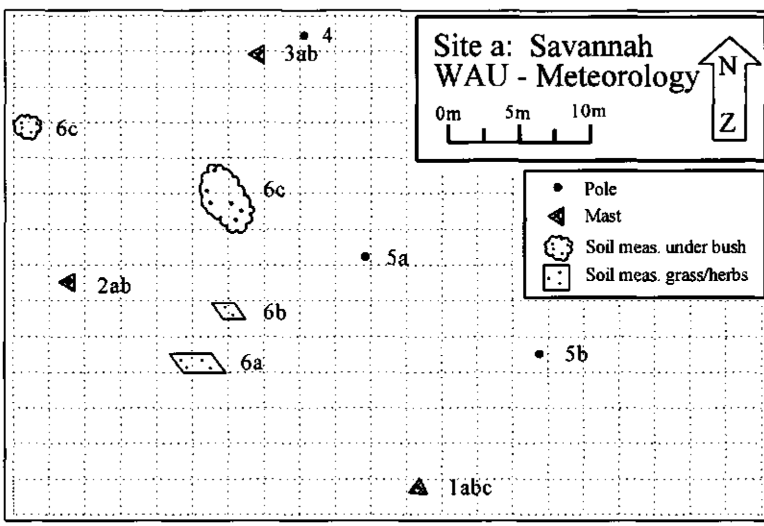

FIGURE 3.12. Experimental design of the WAUMET fallow savannah site. Mast 1 concerns the wind (u) profile (1a) and the total radiation components: R_s, $R_{n,t}$ and a_tR_s (1b), whereas in mast 2 the psychrometers were mounted, for measurement of dry and wet bulb temperature (T_a and T_w). Mast 3 contained the EC equipment, together with several radiation instruments (sampling a_uR_s and $T_{s,b}$) . An extra pole (location 4) was erected to allow measurement of $R_{n,u}$ and $T_{s,u}$. Poles 5a and 5b contained instruments to measure diffuse and longwave radiation, respectively. Two exposed soil plots were located between the EC and the psychrometer mast, where measurements of soil temperature, thermal conductivity and soil heat flux took place. Soil heat flux was also measured below a bush. Measurement heights and types of instruments are listed in Table 3.2.

Table 3.2 gives the sampled variables, together with the types of instruments, measurement height and the sampled surface component (if applicable) at the CWS WAUMET savannah site. The mentioned masts (between brackets) refer to Fig. 3.12.

TABLE 3.2. A list of the meteorological variables sampled at the WAUMET site, together with instrument type, measurement height and sampled surface component.

Variable	Instrument	Surface Component	Heights or depths (m)
	Wind speed (mast 1a)		
u	Cup anemometer		0.73, 1.46, 2.49, 3.46, 4.5, 6.0
u	Cup anemometer		1.15, 2.47, 3.44, 5.01, 7.08, 9.88*
Dir	Vane		6.0
	Air temperature and humidity (mast 2)		
T_a, T_w	Psychrometer		0.66, 1.47, 2.60, 3.58, 4.57, 6.06
	Atmospheric fluxes (mast 3a)		
H_t	Sonic anemometer	Total	5.0
L_vE_t	Sonic anemometer /IRGA	Total	5.0
F_c	Sonic anemometer/IRGA	Total	5.0
ρu_*^2	Sonic anemometer	Total	5.0
	Radiation (mast 1b, 3b and 4)		
R_s	Pyranometer		10.21
$a_t R_s$	Pyranometer	Total	10.08
$a_u R_s$	Pyranometer	Understorey	1.41
$R_{n,t}$	Net radiometer	Total	10.20
$R_{n,u}$	Net radiometer	Understorey	1.62
$T_{s,b}$	IRT	Bushes	2.45**
$T_{s,u}$	IRT	Understorey	1.60**
	Soil heat flux		
G_b (*9)	Heat flux plate	Bushes	-0.04
G_u (*2)	Heat flux plate	Understorey	-0.04
	Soil temperature		
T, Profile 1	PT-100	Understorey slightly vegetated	-0.03,-0.05, -0.10, -0.25, 0.50
T, Profile 2	PT-100	Understorey densely vegetated	-0.03,-0.05, -0.10, -0.25, 0.50
T, Plates (*3)	PT-100	Bush	-0.03
	Soil thermal conductivity		
λ, Profile 1	λ-needle	Understorey slightly vegetated	-0.015,-0.04, -0.075, -0.15
λ, Profile 2	λ-needle	Understorey densely vegetated	-0.015,-0.04, -0.075, -0.15

u = exposed understorey (mixture of grasses/herbs/bare soil), b = Guiera Senegalensis bushes, t = total vegetation (composite of bushes and understorey).
* Mounting height after day 266.
** Viewing directions were 180 and 90 ° for the bush and understorey, respectively.

a) Radiation

In order to capture R_n and its individual components, as given by Eq. 2.1, the following radiation flux densities have been measured: total downward solar radiation flux density, R_s net all-wave radiation flux density, R_n, reflected solar radiation flux density, a_sR_s, and surface temperature, T_s. All shortwave components have been measured with Kipp solarimeters (Type CM5, Kipp and Zn, Delft, the Netherlands), whereas for net radiation Funk net radiometers were used (Type Middleton, Funk)

With T_s, knowledge of the surface emissivity, ε_s, and incoming longwave radiation, $R_{l,\downarrow}$, the upward longwave radiation flux density, $R_{l,\uparrow}$, can be calculated (see Eq. 2.5). $R_{l,\downarrow}$ has not been recorded because of instrument failure. Downward diffuse solar radiation flux density, R_d, has also been measured. Problems with the shading ring caused a discontinuous time series for this variable and were therefore not used.

With the aim to distinguish the net and reflected shortwave radiation stemming from the undergrowth from that originating from the composite of the undergrowth plus the bushes, two net radiometers and two albedo meters (inverted Kipp solarimeter) have been installed. The instruments at a height of ten meters supplied average radiation values for the total vegetation, $R_{n,t}$ and $a_t R_s$. A net radiometer and an albedo meter installed at a height of 1.5 m provided the values of the understorey only, $R_{n,u}$. No attempt was made to measure the radiation originating from a single bush, because of the too large view angle of the radiation instruments. Separate surface temperatures of the understorey, $T_{s,u}$ and a bush, $T_{s,b}$ have been recorded continuously with two IRTs (type KT15, Heimann, Wiesbaden, Germany) operating in the 8-14 μm window. These IRTs were fixed instruments, one vertically pointing at the soil/herb surface, the other one viewing the bush from a horizontal position.

To obtain insight into the temperature distribution of the bushes, the differences between the shaded and sunlit understorey and the spatial variability of the field, a manually operated surface temperature sensor (Comet 8000, Mawi-therm, Monheim, Germany) was also used. A ground observation sequence conducted with this instrument consisted of collecting surface temperatures as follows: several observations looking off-nadir at the understorey, at the bare soil, looking from an 180 ° angle at the herbs , and looking from a 180 ° angle at the bushes. For all components, sunlit and shaded observations were made, resulting in about 40 measurements per sequence. Collection of these observations took approximately ten minutes, and therefore the time-dependency of the observations was neglected. This measurement sequence was in principle repeated each hour between arrival at and departure from the site, but only when enough observers were available. Measurements started at day 261.

It is illustrative to assess the surface areas actually detected by the instruments. Furthermore the disturbing influences of the masts, mounting arms and shore-lines have to be determined. According to theory dealing with view factors of radiation instruments (see Sparrow and Cess, 1978, for example) 90 % of the radiation seen by the sensors installed at a height of 10 m emanates from a circle with a radius of 30 m. Radiometers sampling the understorey have been monitoring radiation from an area with a radius of approximately 5.5 m. The fixed IRTs sampled areas with a radius of 0.20 and 0.15 m, respectively. A proper exposure is very important and downward facing radiation instruments should sample a typical section of the surface under investigation, as free as possible from artificial obstructions, including the instrument mounting itself, and unimpeded by shadows or reflected sunlight from metal surfaces. The mast which supported the instruments consisted of an open triangular framework. The sides of the triangle had a length of approximately 0.2 m. The maximum thickness of the aluminium poles and rungs was about 0.035 m. The rungs were spaced 0.25 m apart. The fraction obscured in the lower hemisphere by the vertical poles or rungs depends on the distance between the instrument and the mast, the width of the obscuring element and the height at which the net radiometer is installed. It was found that a mast with three vertical poles of approximately 10 m height (such as the net radiometer and inverted Kipp-solarimeter sampling the total vegetation) and 0.03 m width at a distance of roughly 0.7 m obscures a fraction of less than 1 % in the lower hemispheres. The rungs will also obscure a certain part of the radiation, depending on their distance to the instrument. A rung at the same height as the installed radiometer will obscure only 0.002 %, so the influence of all the rungs together will also be very small. The horizontal mounting booms had a width of about 10 cm. The booms did not influence the radiation measured by the instruments they were supporting because they had been placed in the same horizontal plane as the sensor surfaces. It can thus be concluded that the anomalous radiation received from objects other than the objects under consideration was small, especially if we take into account the fact that the poles, rungs or arms will emit radiation of approximately the correct intensity because of temperatures similar to the observed surfaces. Another source of error can be shading by the three guy-wires shoring each mast. Because of the small diameter of the guys (1 centimetre) this will affect the radiation of one 10-minute interval only.

The radiometers were cleaned about once a week or more frequently when rain fell. These intervals have been removed from the data series.

b) Air temperature and humidity

The radiation-shielded and ventilated psychrometers, as manufactured by the Department of Meteorology (WAU, The Netherlands), contained two thermometers (PT-100 resistance thermometers). One of the thermometers (yielding the wet bulb temperature, T_w) had been covered with a wet cotton wick in order to guarantee saturation. Continuous wetting of the wick was ensured by a syringe being filled from a plastic bottle and driven by a 12 V pump which were both installed in the mast. The humidity of the air was calculated from T_a and T_w with the psychrometer formula. Accuracy of the PT-100 thermometers was 0.01 K.

c) Wind speed

Profile measurements of wind speed, u, were necessary for the calculation of the roughness length of momentum, z_{0m} (see Section 6.2). Because of the growth of the bushes, the height of the cup anemometers was changed after day 266 in order to ensure measurements above the transition layer (see Table 3.2). All cup anemometers have been manufactured and calibrated (wind tunnel) at WAUMET. The cup anemometers had a stalling speed of 0.10-0.30 m s^{-1}. The accuracy was at least 3 % within the measuring range of 1-15 m s^{-1}. The cup rotation speed was measured with a photon-chopper system. The cup anemometers were fitted on rectangular booms of about 0.9 m long to avoid mast influences.

d) Soil temperature measurements

Soil temperatures have been measured with PT-100 resistance thermometers horizontally inserted at several depths at two plots, located approximately 5 m apart. The resistance elements had a diameter of about 3 mm. Both temperature profiles were located beneath the directly exposed understorey. One of the plots (Profile 1) was sparsely vegetated (soil coverage approximately 50 %) whereas the other plot exhibited more vegetation (grass and herbs) than average. Each temperature array consisted of five thermometers installed at depths of 0.03, 0.05, 0.10, 0.25 and 0.50 m. Transient λ-probes, developed by WAUMET (Van Loon, 1991) were placed in between the temperature sensors, at depths of 0.015, 0.04, 0.075, and 0.15 m. They were connected to a portable data logger several times per day (three times during the wet period, one or two times during the dry period) so they could be read. The temperature profiles have been installed for the calculation of soil thermal diffusivity, κ, for which the two upper PT-100 sensors have been used. Furthermore, in combination with values of heat capacity, C_h , and thermal conductivity, λ, they enabled calculation of the understorey soil heat flux, G_u, by the Calorimetric, Gradient and Analytical method (see Appendix 3).

e) Soil heat flux measurements

A direct measurement of soil heat flux has been made by thermopile flux plates (TNO, Delft, The Netherlands) at four locations. Thermopile plates were installed to the west, east and in the centre of a bush at an average depth of 0.04 m. Temperature sensors were placed above the plates at a depth of 0.03 m to calculate the heat storage for the soil layer overlying the thermopile plates (see Appendix 3). The fourth location was the exposed grass/herb layer. Per plot, three (bushes) or two (understorey) plates with similar calibration factors (C) and thermal conductivity (λ_{plate}) have been connected in series, as shown in Table 3.3, which gave four (averaged) output signals. The plates were 0.004 m thick and had a radius of 0.15 m. Mean below-bush G -values, G_b, were calculated by averaging the three results.

TABLE 3.3. Calibration factors (C) and plate conductivity, λ_{plate}, of the thermopile plates.

South of bush		West of bush		East of bush		Understorey plot	
C	λ_{plate}	C	λ_{plate}	C	λ_{plate}	C	λ_{plate}
12.0	0.25	12.2	0.25	7.5	0.45	7.3	0.45
11.6	0.25	12.2	0.25	7.5	0.45	7.8	0.45
11.7	0.25	12.5	0.45	7.7	0.45		

f) Sampling

All sensors, except the EC equipment installed in mast 3a have been sampled with a frequency of 0.1 Hz. Automatic averaging was done by two Campbell 21 X data loggers which were housed in a plastic box. This resulted in an output of ten minute averages. Instruments and dataloggers were powered by eight solar panels (SM55, Siemens, Germany).

g) Eddy covariance measurements

The momentum flux, ρu_*^2, sensible heat flux, H_t, total evaporation, L_vE_t, and the atmospheric CO_2 flux, F_c, were measured by eddy covariance using a three-axis sonic anemometer (Solent A1012R2, Gill Instruments Ltd., Lymington, Hampshire, UK) and a differential closed-path infra-red gas analyzer (model LI-6262, LI-COR Inc., Lincoln, NE, USA). This system has been developed jointly at a number of European laboratories and it was widely used in HAPEX-Sahel (see Chapter 7). The atmospheric CO_2 concentration, C_s, was also sampled with this analyzer. The sonic anemometer was mounted on a tower at a height of 5 m, with the inlet of the CO_2/H_2O-sampling tube located at its centre.

Two gases were used for CO_2 calibration: a zero calibration gas (dry nitrogen, which also allows the water vapour channel to be adjusted to zero) and dry air with 360 ppm CO_2. The infra-red gas analyzer was placed in a radiation-shielded box next to the mast, with the pumps and other power-consuming devices outside. A membrane pump was used to transfer the sample, from the inlet to the analyzer, via polyethylene tubing with a 3 mm inside diameter. This arrangement allowed the analyzer to operate just above air pressure, thus ensuring a higher signal-to-noise ratio and making the pressure less dependent on flow rate. Pressure fluctuations caused by the pump were sufficiently damped by the volume of the tubes (Heusinkveld et al., 1994). The system was controlled by specially-written software which calculates the surface fluxes in real-time. The raw turbulent records were stored on a portable computer for post-processing. The fluxes were sampled with a frequency of 20 Hz. Necessary corrections (co-ordinate rotation, correction for frequency response loss, and Webb correction) were made using the procedures described by Lloyd et al. (1996) and Moncrieff et al. (1996b).

The fetch was adequate for the majority of wind directions, ranging from 300 m (south) to several kilometres (north and east). However, data were rejected when winds were coming from directions ranging between 240-360 ° (because of a small millet field located within 50 m of the masts) and when it was raining.

h) Soil evaporation

Soil evaporation has been measured with micro-lysimeters following the description of Boast and Robertson (1982). They are brass cylinders with a height of 0.15 m and an inner diameter of 0.10 m. The cylinders were pushed into the soil and the soil sticking to the outside was wiped off after removal. Thereafter the cylinders were sealed with a plastic lid and their mass was determined. Then they were placed back into the holes. The maximum time of use was approximately two days. The lysimeters were then emptied and refilled at an undisturbed location.

i) Understorey fluxes

The shrubs adjacent to the savannah measuring site were cut early in 1992 in order to create a savannah grassland open site (area: 150 - 150 m) which is typical of the more northern parts of the Sahel. During the days 268 (24 September) to 274 (30 September) the EC mast of SC-DLO was moved to this adjacent site to measure evaporation, heat and CO_2 fluxes above natural grassland. The composition here was the same as the herbaceous sub-layer of the fallow savannah site (Kabat and Elbers, 1994).

j) Bush transpiration

Transpiration of the *Guiera senegalensis* shrubs was measured employing two constant power sap flow gauges (Dynamax Inc., Houston, TX, USA), which were operated by SC-DLO. The gauge's principle of operation is well described in several publications (Allen and Grime, 1995) and in the manufacturer's manual (Van Bavel and Van Bavel, 1990). Each gauge was wrapped around a stem and outputs from the gauges were recorded with automatic dataloggers, thus providing continuous measurement of transpiration. From the leaf area per stem and the LAI_b, L_vE_b was calculated (see Eq. 2.35).

k) Soil moisture content

Daily measurements of volumetric soil moisture content were made with a Time Domain Reflectometer (model FOM/m, Easy Test Ltd., Poland). Two twin-rod TDR-sensors were inserted horizontally into the soil to measure moisture content at depths of 0.05 and 0.10 m. Two more sensors were installed vertically, to measure mean water contents from 0.2-0.3 m and 0.4-0.5 m depths. The total soil water content from 0.05-0.45 m depth, Θ, was determined by integrating the measured moisture contents over the depth interval. Θ can be considered a reasonable index of the soil moisture available to the understorey, which hardly rooted below 0.6 m. For the *Guiera* bushes, fifty percent of the total roots were found in the top 0.5 m soil (Personal communication, N. Hanan, 1995).

3.5.3 Plant measurements

a) Stomatal conductance measurements

Leaf stomatal conductance, g_l , was measured with a diffusion porometer (model AP4, Delta-T Devices, Burwell, Cambridge, UK). At the beginning of the observation period only the leaves of the *Guiera* bushes were sampled, but during the second half the two main herb species (*Mitracarpus scaber* Zucc. and *Jacquemontia tamnifolia* (L.) Griseb.) were also sampled.

Measurements of g_l were done on most days for ten selected shrubs and random specimens of *Mitracarpus scaber* and *Jacquemontia tamnifolia*. The porometer was operated almost continuously from arrival at the site to departure, but some gaps in the measurements resulted from calibration periods, instrument failure, or change of operator. Four leaves (two sunlit, two shaded) were sampled from the shrubs at each of three levels, giving 12 measurements per bush. A difference between the layers was found, with the top layer having the highest conductance, but this difference was small enough (< 5 %) to use data from all layers to get an overall average of g_l. The difference between shaded and sunlit leaves was larger (± 15 %). However, for the purpose of finding an average diurnal course of leaf conductance or daily averages, a simple mean of all leaves, irrespective of the radiation receipt or location in the canopy, was considered sufficiently accurate. The sampled bushes were located about 25 m north to north-east of the eddy covariance mast. More information on the porometry measurements is given in Table 3.4.

TABLE 3.4. Species sampled by porometry at the WAUMET fallow savannah site (CWS), together with the start and end date of the measurements and the total numbers of half-hourly averages derived after screening and averaging the data for the individual leaves.

Species	Start date	End date	Number of half-hour averages
Guiera Senegalensis	12/8	10/10	283
Mitracarpus scaber	29/9	11/10	88
Jacquemontia Tamnifolia	29/9	11/10	86

b) Leaf area index, LAI

The *LAI* of the vegetation was determined through the 'specific leaf area' (surface area/dry matter) of the species and biomass measurements. The destructive measurements were made bi-weekly. Once the floristic composition of the herb layer was assessed, five samples of 0.5 m^2 were harvested on each plot, oven-dried and weighed. As far as the woody layer was concerned, the height and diameter of 12-30 bushes were measured and then harvested (see Begue et al., 1995).

3.6 Site description: HAPEX-Sahel CWS, tiger-bush (SC-DLO) site

The description of the measurement area has been given in § 3.4.3. The measurements and maintenance of the instruments at this site were carried out by SC-DLO, who erected a 16 m high tower in the vicinity of a vegetation strip. It was equipped with a 3D sonic anemometer (Solent A1012R2, Gill Instruments Ltd., Lymington, Hampshire, UK), and an automatic Thermometer Interchange System (TIS) measuring temperature and humidity gradients at two levels for estimation of Bowen ratios and wind speed at two levels. The components of radiation and soil heat flux were measured on the soil and vegetation strips separately. The measured meteorological variables, instruments and sensor heights are given in Table 3.5.

TABLE 3.5. Mounting details for sensors at the SC-DLO (CWS) tiger-bush site.

Variable	Instrument	Component surface	Sensor height (m)
	Meteorological fluxes		
H_t	Sonic anemometer	Total	14.7
L_vE_t	BR-system	Total	11.0
$u*$	Sonic anemometer	Total	14.7
	Radiation		
$R_{n,s}$	All-wave net radiometer	Soil	0.7
$R_{n,b}$	Net radiometer	Bushes	7.8
R_s	Pyranometer		7.2
$a_s R_s$	Pyranometer	Soil	0.7
$a_b R_s$	Pyranometer	Bushes	7.8
$T_{s,b}$	IRT	Bushes	7.8
	Soil heat flux		
G_s (*2)	Heat flux plate	Soil	-0.01
G_b (*2)	Heat flux plate	Bushes	-0.01
	Meteorological variables		
T_a	Sonic anemometer	-	14.7
T_w	Movable BR system	-	8.9 - 11.1
T_a	BR system	-	8.9, 11.0, 13.2
u	Sonic anemometer	-	14.7
u	Anemometer BR system	-	8.9, 11.0, 13.2
Dir	Vane	-	14.0
P	Air pressure transducer	-	1.5

importance in the validity of the long-term predictions of GCMs and therefore SVATs should provide a good description of these processes for a wide variety of surface types. At the same time, in order to limit computing time, the parameterization of the surface-atmosphere exchange processes should therefore be as simple as possible (Van den Berg, 1995a).

Nowadays, a wide range of SVATs are in use, varying from very simple models based on the big-leaf concept of Penman (1948) and Monteith (1965) to rather complex multi-layer/multi-component models (see Sellers et al., 1986; Viterbo and Beljaars, 1994). This study will concentrate on five existing models, which are based on the big leaf approach of Penman (1948) and Monteith (1965), on Shuttleworth and Wallace (1985), Choudhury and Monteith (1988), the two-layer model described in Huntingford et al. (1995) and Deardorff (1978). The latter also includes parameterizations taken from Dickinson et al. (1986) and Noilhan and Planton (1989). In the text these five will be referred to as BL, SW, CM, TL, and DD. BL, SW, CM, and DD have the advantage of being well-documented and widely used. They also represent an increasing complexity. The TL model has the advantage that it has been tested and calibrated for a savannah surface. It is based on SW with the modification that the component energy partitioning is determined by areal cover, as introduced by Dolman (1993). A compilation of 'the best parts' of CM and DD led to the Dual Component Model (DCM) and the Triple Component Model (TCM). In these cases, CM predominantly supplied the parameterization of the aerodynamic resistances. The scheme of DD was incorporated for the calculation of soil heat flux. Note that all models will use the same parameterization of average leaf conductance for the final model predictions given in Chapter 8. This will be the parameterization of the TL model, for reasons to be described in § 6.3. Hence, the equations for canopy conductance as proposed by CM and DD will not be considered here.

The SVATs used in this study are all one-dimensional and the majority of them distinguish between two surface components (SW, CM, TL, DD, DCM), whereas TCM allows for the description of three components. A three-component approach is necessary for the description of the savannah vegetation, especially if the undergrowth is relatively sparse and a considerable area of the understorey consists of bare soil. SW, CM and TL are based on the Penman-Monteith approach, which means that they are solved in a diagnostic way. DD, DCM, and TCM do not solve the energy balance equation at the same time as the surface flux equations, but they are based on the direct solution of the surface flux equations of latent and sensible heat. For this reason they have to be categorized as prognostic. Only CM and DD (and thus DCM and TCM) allow for heat and water flow in two separate soil layers. BL, SW and TL have no soil parameterization. All the models have in common the fact that they describe momentum, sensible and latent heat fluxes through networks of resistances, while the final values of the fluxes are restricted by the total (BL) or by the component available energy (others).

4.2.2 General terminology and structure of models

a) Terminology

In all descriptions given below using state variables, T stands for temperature, while q signifies specific air humidity. The subscripts a, c, s, and 0 denote whether the potentials have been determined for the air (at reference level), for the canopy (upperstorey, i.e. the bushes), at the soil surface, or at the mean canopy air flow (0). If SW and TL are used to describe the savannah, the soil and undergrowth are lumped together. To describe these models, both the tiger-bush and the savannah understorey (i.e. bare soil and a mixture of vegetation and soil) will be denoted with the subscript u for understorey. However, in Chapter 6 and 8, the separate subscripts s and u , may be occasionally used to distinguish explicitly between the bare tiger-bush and the vegetated savannah understories. In TCM the distinction between the canopy and undergrowth is made by using the letter u for undergrowth. If CM, DD or DCM are used to simulate savannah, the upperstorey and undergrowth are combined in one variable describing the total canopy (subscript c). The subscript s is sometimes used in combination with an extra subscript (1) for the DD, DCM and TCM models. Temperatures within the soil have been given the subscripts i and m in CM, where T_m is the lower boundary of the lower soil layer and T_i the temperature of the upper (dry) soil layer. The deep soil temperature in DD has the extra subscript 2. The subscripts a, c, s, and u will be used in a similar way for surface parameters such as albedo or emissivity (e.g. a_c or ε_s) and fluxes (for example L_vE_s, $R_{n,u}$).

All models utilize two types of resistances: **aerodynamic** resistances and **surface** resistances. The first group can be divided into resistances between the mean canopy air stream and the reference level air, between the understorey or soil and the mean canopy air stream and finally the resistances (generally referred to as boundary layer resistance) between the vegetated surface (upper canopy level or undergrowth) and the mean canopy air stream which is in series with the surface resistance. The second group comprises of canopy-related (canopy and undergrowth) and soil surface resistances. In the specific resistance networks, each resistance is specified by a subscript and a superscript. The subscript gives the type of resistance: aerodynamic (a), boundary layer (b) or surface resistance (s). The superscript describes the component: air (a), soil (s), canopy (c), or undergrowth/understorey (u). The last one only exists for SW, TL and TCM. All models assume that the aerodynamic resistance to heat and water vapour transfer equals the aerodynamic resistance to momentum, and that turbulent transfer can adequately be described by K-theory.

b) Symbols

Certain meteorological 'constants' are applied in the SVATs. To avoid superfluous description, their meaning, symbol and units will be given below. Δ is the slope of the vapour pressure temperature curve (Pa K^{-1}), γ is the psychrometric constant (Pa K^{-1}), ρ is the air density (kg m^{-3}), and C_p is the specific heat of air at constant pressure (J kg^{-1} K^{-1}).

An attempt has been made to use the same symbols, where possible, in all formulae. The symbols used here are consistent with those used in the other chapters. Therefore, certain variables or parameters are described by symbols which are different from the ones used in the original publications. Only the most important and distinguishing properties of the models will be explained. For further details the reader is referred to the original publications.

c) Visualization of models

In illustration of the above, Fig. 4.1 shows the above-ground resistance network of the DCM and TCM-models with their state variables.

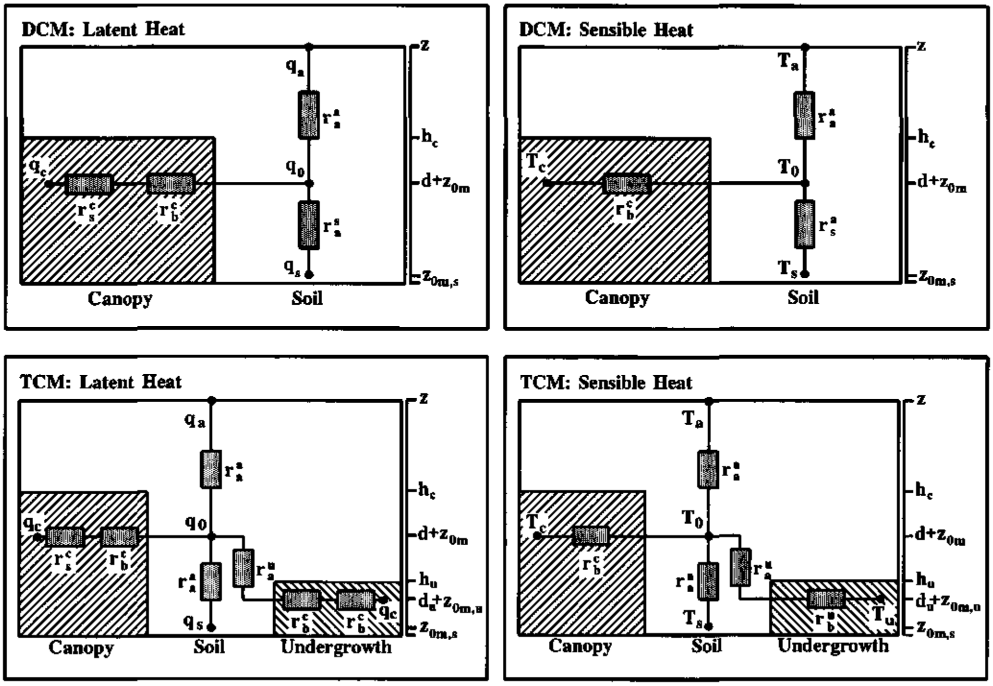

FIGURE 4.1. Schematic diagrams of the resistance networks of two of the models used. Latent and sensible heat fluxes for DCM and TCM.

4.2.3 Energy budgets

The factor limiting the exchange of sensible and latent heat is the available energy. In BL, a measured user-supplied value of $(R_{n,t} - G_t)$ is used. For SW the energy budgets for the complete canopy-soil system and for the understorey (soil or undergrowth) are given by

$$A_t = R_{n,t} - G_t = L_v E_t + H_t \tag{4.1a}$$
$$A_u = R_{n,u} - G_t = L_v E_u + H_u \tag{4.1b}$$

where A_t and A_u are the available energy of the total canopy-soil system and the understorey respectively. With analogous subscripts the net radiation, R_n, the soil heat flux, G, and the latent, L_vE and sensible, H, heat fluxes of the total system and of the understorey are described. TL employs a similar approach, but with energy partitioning being additionally determined by areal cover, α (see Eq. 2.37):

$$A_t = \alpha A_u + (1-\alpha) A_c \tag{4.2a}$$
$$A_u = R_{n,u} - G_u = L_v E_u + H_u \tag{4.2b}$$
$$A_c = R_{n,c} - G_c = L_v E_c + H_c \tag{4.2c}$$

For CM a distinction between the canopy surface and the soil surface is made in the following way

$$R_{n,c} = H_c + L_v E_c \tag{4.3a}$$

$$R_{n,s} = H_s + G_0 \tag{4.3b}$$

where $R_{n,c}$ and $R_{n,s}$ are the net radiation absorbed by the canopy surface and soil surface (W m^{-2}). G_0 is the heat flux into the dry soil layer (W m^{-2}). Part of this flux is conducted into the wet soil layer, so that the latent heat flux from the top of the wet soil layer is described by

$$L_v E_s = G_0 - G \tag{4.4}$$

where G is the soil heat flux (W m^{-2}). For SW and CM, $R_{n,s}$ (or $R_{n,u}$) is obtained from a Beer's law relationship

$$R_{n,s} = R_{n,t} e^{-\beta LAI_c} \tag{4.5}$$

where β is the extinction coefficient of the canopy for net radiation (-) and LAI_c is the leaf area index (m^2 m^{-2}). Variations in β as a result of variations in the structure and density of the vegetation and diurnal variations (Ross, 1975; Massman, 1992) are ignored in the present model. In TL, $R_{n,c}$ and $R_{n,u}$ are user-supplied. While in the SW and CM model, $R_{n,t}$ is assumed to be directly measured, the DD-model (and thus DCM and TCM) calculates the net radiation explicitly from the in and outgoing radiation terms. This yields the following energy budget for the vegetation layer:

$$(1-a_t)R_s + R_{l,\downarrow} - R_{l,\uparrow} - \left((1-a_s)R_s + R_{l,\downarrow,s} - R_{l,\uparrow,s}\right) = H_t + L_v E_t - (H_s + L_v E_s) \tag{4.6}$$

where R_s is the incoming shortwave radiation (W m^{-2}), a_t the shortwave albedo, and$R_{l,\downarrow}$ and $R_{l,\uparrow}$ the incoming and outgoing longwave radiation (W m^{-2}), respectively. H_t is the sensible heat flux (W m^{-2}) and $L_v E_t$ is the latent heat flux (W m^{-2}). The subscript s denotes the energy balance components of the soil surface. R_s and $R_{l,\downarrow}$ are user-supplied.

With the introduction of a vegetation area average shielding factor, σ_c, (Deardorff, 1978), which determines the degree to which the vegetation prevents short- and longwave radiation from reaching the ground, Eq. 4.6 can be rearranged to read

$$\sigma_c \left[(1-a_c)R_s + \varepsilon_c R_{l,\downarrow} + \frac{\varepsilon_c \varepsilon_s}{\varepsilon_c + \varepsilon_s - \varepsilon_c \varepsilon_s} \sigma T_{s,1}^4 - \frac{\varepsilon_c + 2\varepsilon_s - \varepsilon_c \varepsilon_s}{\varepsilon_c + \varepsilon_s - \varepsilon_c \varepsilon_s} \varepsilon_c \sigma T_c^4 \right] = H_c + L_v E_c \tag{4.7}$$

where a_c is the albedo of the canopy surface (-), ε_c and ε_s are the emissivities of the vegetation and soil surface, respectively (-) and σ is the Stefan-Boltzmann constant (W m^{-2} K^{-4}). To avoid too much complexity in Eq. 4.7 the subscript s, as introduced in Chapter 2 to indicate *surface* emissivities, has been left out.

Obtaining Eq. 4.7 from Eq. 4.6 involves interpolation, using σ_c, between the energy balance equations applicable above bare soil and those applicable above a dense vegetation. Eq. 4.7 is also applied in DCM and TCM. In TCM, however, σ_c is the sum of the component area shielding factors of the canopy and the undergrowth and a_c and ε_c are area weighted averages obtained in a similar way.

4.2.4 Parameterization of resistances

a) Aerodynamic resistances

In the BL-formula, the aerodynamic resistance is described by a single value, parameterized by Eq. 2.26 assuming that $r_e = r_h$, and $z_{0e} = z_{0h}$. As explained in Chapter 2, this approach asks for a value of $\ln(z_{0m}/z_{0h})$. In SW, $r_a^{\,a}$ and $r_a^{\,u}$ vary linearly with LAI_c between the values valid for the understorey only ($LAI_c = 0$) and with complete canopy cover ($LAI_c \geq 4$). In the extreme case of no upper canopy, the aerodynamic resistances are given by:

$$r_a^u(0) = \frac{\ln\left(\dfrac{z}{z_{0m,u}}\right)\ln\left(\dfrac{d + z_{0m}}{z_{0m,u}}\right)}{k^2 u} \tag{4.8a}$$

$$r_a^a(0) = \frac{\ln^2\left(\dfrac{z}{z_{0m,u}}\right)}{k^2 u} - r_a^u(0) \tag{4.8b}$$

where z is the reference height (m), z_{0m} is the roughness length of the canopy (m), $z_{0m,u}$ is the roughness length of the understorey (m), d is zero plane displacement height (m), k is Von Kármán 's constant (-) and u is the wind speed at reference height (m s^{-1}). Eq. 4.8 shows that stability effects are ignored. In the extreme case of complete canopy cover, the aerodynamic resistances are given by

$$r_a^u(4) = \frac{\ln\left(\dfrac{z-d}{z_{0m}}\right)}{k^2 u}\,\frac{h}{n(h-d)}\left\{e^n - e^{\left(n\left(1-\frac{d+z_{0m}}{h}\right)\right)}\right\} \tag{4.9a}$$

$$r_a^a(4) = \frac{\ln\left(\dfrac{z-d}{z_{0m}}\right)}{k^2 u}\left\{\ln\left(\frac{z-d}{h-d}\right) + \frac{h}{n(h-d)}\left(e^{\left(n\left(1-\frac{d+z_{0m}}{h}\right)\right)} - 1\right)\right\} \tag{4.9b}$$

where h is the canopy height (m), and n is an attenuation coefficient for eddy diffusivity (-).

Assuming a linear function of LAI_c between these limits, the actual aerodynamic resistances can be described by

$$r_a^u = \begin{cases} \frac{1}{4} LAI_c r_a^u(4) + \frac{1}{4}(4 - LAI_c) r_a^u(0), & 0 \le LAI_c \le 4 \\ r_a^u(4), & LAI_c > 4 \end{cases} \tag{4.10a}$$

$$r_a^a = \begin{cases} \frac{1}{4} LAI_c r_a^a(4) + \frac{1}{4}(4 - LAI_c) r_a^a(0), & 0 \le LAI_c \le 4 \\ r_a^a(4), & LAI_c > 4 \end{cases} \tag{4.10b}$$

The parameters d and z_{0m} are parameterized with d = 0.63h and z_{0m} = 0.13h and it is assumed that the effective source and sink height of the canopy will remain fixed with changing canopy cover. In TL, the in-canopy aerodynamic resistance is given by

$$r_a^u = \frac{e^n h}{nK(h)} \left[e^{-n\left(d_u + z_{0m,u}\right)/h} - e^{-n\left(d_c + z_{0m,c}\right)/h} \right] \tag{4.11}$$

and its above-canopy equivalent is calculated with

$$r_a^a = \frac{1}{ku_*} \left[\ln\left(\frac{z-d}{h-d}\right) - \Psi(z) + \Psi(h) \right] + \frac{h}{nK(h)} \left[e^{n\left(1-\left(d_c + z_{0m,c}\right)/h\right)} - 1 \right] \tag{4.12}$$

with the symbols described as above and Ψ the integrated stability function given in Eq. 2.24. The parameters d_u and $z_{0m,u}$ are the understorey displacement height and roughness length, respectively. In Eqs. 4.11 and 4.12, d_c and $z_{0m,c}$ denote the same parameters for the upper storey. $K(h)$ is the eddy diffusion coefficient at canopy height h. In CM, by integrating the reciprocal turbulent transfer coefficient over $z_{0m,s}$ and $z_{0m} + h$, $r_a{}^s$ can be described by:

$$r_a^s = \frac{e^n h}{nK(h)} \left[e^{-n\left(\frac{z_{0m,s}}{h}\right)} - e^{-n\left(\frac{d+z_{0m}}{h}\right)} \right] \tag{4.13}$$

In contrast to SW, Choudhury and Monteith (1988) accounted for buoyancy by using the relatively simple stability correction scheme of Choudhury et al. (1986). In this thesis, this scheme has been replaced by the parameterization of Louis et al. (1981) and Holtslag and Beljaars (1988), although no distinction is made between the aerodynamic resistance for momentum transfer and for heat transfer. Louis (1979) defined drag coefficients to describe the turbulent transfer of energy fluxes. The drag coefficients, C, can be written as a function of the bulk-Richardson number (Ri_B) and of z/z_{0m}. Functions of the drag coefficients are derived by fitting them to the Businger relations (Businger, 1973; Louis, 1979; Louis et al., 1981; Holtslag and Beljaars, 1988).

These functions read:

$$C = \begin{cases} a^2\left(\dfrac{1}{1+10Ri_B+80(Ri_B)^2}\right) & 0 \le Ri_B \le 1.4 \\ a^2\left(\dfrac{2bRi_B}{1+2a^2bc\sqrt{\dfrac{(z-d)}{z_{0m}}|Ri_B|}}\right) & Ri_B < 0 \end{cases} \tag{4.14}$$

where $a^2 = \dfrac{k^2}{\left[\ln\dfrac{(z-d)}{z_{0m}}\right]^2}$ (4.15)

being the turbulent drag coefficient in neutral atmospheric conditions. The empirical constants b and c are 5.0 and 7.5 for momentum transfer, and 5.0 and 5.0 for heat transfer (Louis, 1981). Finally, the aerodynamic resistance equals

$$r_a^a = \frac{1}{Cu} \tag{4.16}$$

CM used functions of canopy height and leaf area to describe z_{0m} and d. They calculated the values of z_{0m} and d by fitting functions to curves given by Shaw and Pereira (1982). If C_d is the mean drag coefficient for individual leaves and $X = C_d LAI$, these functions are

$$d = 1.1h\ln\left(1+\sqrt[4]{X}\right) \tag{4.17a}$$

and

$$z_{0m} = \begin{cases} z_{0m,s} + 0.3h\sqrt{X} & 0 \le X \le 0.2 \\ 0.3h\left(1-\dfrac{d}{h}\right) & 0.2 \le X \le 1.5 \end{cases} \tag{4.17b}$$

DD also takes atmospheric stability effects into account for the parameterization of r_a^s and r_a^a by using the same stability correction scheme as described above. The same approach is used for the calculation of z_{0m} and d as was adopted in CM. The resistance r_a^a is calculated by Eq. 4.16. In DD, r_a^s is a function of the Louis drag coefficient and a weighted mean wind speed, ranging from the mean wind speed of the canopy air flow in dense vegetation to the wind speed at reference height for bare soil surfaces:

$$r_a^s = \frac{1}{C\left[\sigma_c u_* + (1-\sigma_c)u\right]} \tag{4.18}$$

In DCM and TCM the parameterization of CM is used to find r_a^s (tiger-bush, with $z_{0m,s}$) and r_a^u (savannah, with $z_{0m,u}$). r_a^a is found from Eq. 4.16.

b) Boundary layer resistances

The aerodynamic resistance in BL is usually parameterized by Eq. 2.26-2.29. Here, the term kB^{-1} can be regarded as the boundary layer resistance (see Wallace, 1995). In SW the boundary layer resistance is given by

$$r_b^c = \frac{\overline{r_b^c}}{2LAI_c} \tag{4.19}$$

where $\overline{r_b^c}$ is the mean boundary layer resistance (typically 25 s m^{-1}). r_b^c will therefore not vary diurnally, only the seasonal change of LAI_c will influence its value. In TL a distinction has to be made between upperstorey and undergrowth boundary layer resistance, resulting in

$$r_b^c = \frac{100}{(1-\alpha)LAI_c}\sqrt{\frac{w_c}{u(h)e^{(n(z_{0m}+d)/(h-1))}}} \tag{4.20a}$$

$$r_b^u = \frac{100}{\alpha LAI_u}\sqrt{\frac{w_u}{u(h)e^{(n(z_{0u}+d_u)/(h-1))}}} \tag{4.20b}$$

with w_c and w_u (m) being the leaf width of both vegetation-layers and α the fractional coverage of the understorey (see Eq. 2.37). In CM, the *mean* boundary layer resistance per unit leaf area ($\overline{r_b^c}$) is assumed to be a function of wind speed and therefore of height within the canopy

$$\overline{r_b^c(z)} = \left(a\sqrt{\frac{u(z)}{w_c}}\right)^{-1} \tag{4.21}$$

where $a = 0.01$ (m s$^{-0.5}$), $u(z)$ is wind speed at height z (m s^{-1}). Ignoring stability effects in the canopy air flow, assuming K-theory and integrating over the canopy height, r_b^c can be expressed as:

$$r_b^c = \left(LAI_c\left(\frac{2a}{n'}\right)\sqrt{\frac{u(z)}{w_c}}\left[1-e^{\frac{-n'}{2}}\right]\right)^{-1} \tag{4.22}$$

where n' is an attenuation coefficient for wind speed (-).

In DD, DCM and TCM (using r_b^c and r_b^u) the parameterization scheme of Dickinson et al. (1986) is used to calculate the *mean* boundary layer resistance, $\overline{r_b^c}$. As in CM, the *mean* boundary layer resistance is assumed to be a function of wind speed within the vegetation.

However, the canopy is treated as one layer and therefore Eq. 4.23 can be simplified to

$$\overline{r_b^c} = \frac{1}{a\sqrt{\frac{u}{w_c}}} \tag{4.23}$$

where u_* is the friction velocity (m s^{-1}), assumed to represent the mean wind speed of the canopy air flow. As in SW, $\overline{r_b^c}$ is divided by LAI_c to obtain the bulk boundary layer resistance, r_b^c.

c) Surface resistances

c1) Canopy

Stomatal behaviour is influenced by many environmental conditions (CO_2, light, soil and air temperature, air humidity, soil moisture, pollution) and plant factors (leaf temperature, water status, plant hormones, leaf age or development, growth stage, and growth conditions) as has been summarized by Jacobs (1994). In the majority of the parameterizations the influence of environmental conditions only has been taken into consideration, because the other factors are difficult to gauge and it is not easy to express them in empirical or physiology-related parameters.

In the past decade many parameterizations to describe stomatal behaviour in response to environmental variables based on the empirical JS-approach have been developed. For example the original DD and the TL $r_s{}^c$ parameterizations are based on this approach. These kinds of models describe leaf conductance, g_l, as a combination of a maximum possible value and several stress factors, $f_1 ... f_n$. Each factor is a function of a single environmental variable. A factor has a maximum value of 1.0 when that environmental property does not cause any stress to the vegetation. If the environmental variable falls below a certain optimal value, stress is induced and f_x becomes smaller than 1.0 until finally a value of 0.0 is reached. This means that full stomatal closure occurs, even if the other factors are still > 0.0. This model can be expressed mathematically as

$$g_l = g_e + g_{l,\max} f_1 \cdot\cdot f_n \tag{4.24}$$

where $g_{l,max}$ is the maximum or potential conductance and g_e the cuticular conductance, usually taken as zero. Four variables are generally used to express the empirical relationship between stomatal conductance and environment: shortwave radiation, R_s, vapour pressure deficit, D, air temperature T_a and some measure of soil water status: soil moisture content, θ, or soil water potential, Ψ. Instead of R_s , often photosynthetically active radiation is used. Because of the interdependency between D and T_a, the latter variable is frequently omitted. Originally, the functional relationships were linear, whereas nowadays more complicated functions are used.

To calculate the canopy resistances for the Sahelian vegetation-types, to be used in all models, the functional relationships belonging to the TL model will be used. The TL parameterization was previously applied to describe the components (bushes and understorey) of a savannah (Huntingford et al., 1995). A similar approach was used by Hanan and Prince (1996) who gathered stomatal conductance data close to the WAUMET savannah site. In their paper the local climate was in fact described by the meteorological measurements conducted at the WAUMET-site. Because this parameterization will also be used in Chapter 6, their functions $f_1..f_4$ are described in Appendix 6.

In TL, the canopy and undergrowth surface resistances are parameterized with

$$r_s^c = \left(\frac{LAI_c}{1-\alpha} g_{l,\max} f_1 f_2 f_3 f_4\right)^{-1} \qquad \textit{and} \qquad r_s^u = \left(\frac{LAI_u}{\alpha} g_{l,\max} f_1 f_2 f_3 f_4\right)^{-1} \tag{4.25}$$

where $g_{l,\max}^{-1}$ is a minimal stomatal resistance and $f_1..f_4$ $(0 \le f_n \le 1)$ are described by

$$f_1 = \frac{R_s}{a_1 + R_s}\left(1 + \frac{a_1}{R_{s,\max}}\right) \tag{4.26a}$$

with $R_{s,max}$ the maximum value of R_s (W m^{-2}),

$$f_2 = \left(\frac{T_a - T_L}{a_2 - T_L}\right)\left(\frac{T_U - T_a}{T_U - a_2}\right)^{\frac{T_U - a_2}{a_2 - T_L}} \tag{4.26b}$$

where T_L and T_U represent the lower and upper limits of the possible temperature range,

$$f_3 = \exp^{-D/a_3} \tag{4.26c}$$

with D the vapour pressure deficit (mb) at reference level, and

$$f_4 = \begin{cases} 1 & \Delta\Theta < a_4 \\ \dfrac{a_5 - \Delta\Theta}{a_5 - a_4} & a_4 \le \Delta\Theta \le a_5 \\ 0 & \Delta\Theta \ge a_5 \end{cases} \tag{4.26d}$$

where $\Delta\Theta$ stands for soil moisture deficit (mm).

Here, a_1, a_2, a_3, a_4, and a_5 are fitted parameters representing the light saturation level, the optimum air temperature, the slope of the D-response curve, and the upper and lower critical soil moisture levels.

The other models employ the same parameterization of g_l. Hereafter, g_l is divided by LAI to obtain $r_s{}^c$ (see Eq. 4.27). Here, LAI may represent the upperstorey LAI (LAI_c) or a composite of LAI_c and LAI_u in the case of savannah (CM, DD, DCM), if the leaf conductances of the bushes and understorey are lumped together.

$$r_s^c = \frac{\left(g_{l,\max} f_1 f_2 f_3 f_4\right)^{-1}}{LAI} \tag{4.27}$$

c2) Soil

Shuttleworth and Wallace (1985) originally chose three constant values for r_s^s which in their opinion are typical of: very dry soils (2000 s m^{-1}), very wet soils (0 s m^{-1}) and an intermediate value of 500 (s m^{-1}). In this thesis, however, the parameterization of r_s^s as described in § 6.4 will be used for the tiger-bush bare soil. In this case, r_s^s is a function of soil moisture content. The same function will be used in the TL model. If an undergrowth is present (savannah), r_s^s is replaced by r_s^u (see Eq. 4.25).

The soil surface resistances in CM are parameterized as follows. For the saturated lower soil layer extending from depth l to l_m (m) the soil resistance to heat transfer ($r_{h,wet}^s$) can be expressed as:

$$r_{h,wet}^s = \rho C_p \frac{l_m - l}{\lambda_{sat}} \tag{4.28}$$

where λ_{sat} is the thermal conductivity of the saturated lower soil layer (W m^{-1} K^{-1}). Similarly, for the dry upper soil layer they used:

$$r_{h,dry}^s = \rho C_p \frac{l}{\lambda} \tag{4.29}$$

where λ is the thermal conductivity of the dry upper soil layer (W m^{-1} K^{-1}). To obtain an expression for the resistance to the diffusion of water vapour, Choudhury and Monteith (1988) assumed that evaporation occurs at the top of the wet soil layer, followed by molecular diffusion through pores within the dry soil layer. However, they found that the estimated evaporative flux departed significantly from the maximum rate after a few hours. This departure was ascribed to the effect that the effective molecular diffusion of water vapour is larger than the ordinary molecular diffusion due to atmospheric pressure fluctuations in a shallow sublayer of the soil. Therefore, the soil resistance to water vapour transfer of the dry soil layer (r_l^s) was assumed to be zero until l exceeds a limiting value l_0. In formula:

$$r_l^s = \begin{cases} 0 & l \le l_0 \\ \dfrac{\tau(l - l_0)}{\phi D_v} & l > l_0 \end{cases} \tag{4.30}$$

where τ is the tortuosity factor of the dry soil layer (-), ϕ is the porosity of the dry soil layer (-) and D_v is the molecular diffusivity of water vapour (m^2 s^{-1}).

4.2.5 Parameterization of atmospheric state variables and fluxes

In all models, the atmospheric variables T_a and q_a are boundary conditions. The other state variables are obtained in the following way.

Because Shuttleworth and Wallace (1985) assumed that the aerodynamic mixing within the canopy is sufficiently good to allow the existence of a mean canopy air flow with its own specific vapour pressure, temperature and wind speed, the in-canopy vapour pressure deficit can be expressed by

$$D_0 = D + \frac{\left[\Delta A_t - (\Delta + \gamma) L_v E\right] r_a^a}{\rho C_p} \tag{4.31}$$

where D_0 is the in-canopy vapour pressure deficit (Pa), D is the vapour pressure deficit at reference height (Pa), and $r_a{}^a$ is the aerodynamic resistance between a reference height and the mean canopy air flow (s m^{-1}). With D_0 it is possible to calculate the latent heat flux of the understorey- and canopy surface, using Penman-Monteith's equation:

$$L_v E_u = \frac{\Delta A_u + \dfrac{\rho C_p D_0}{r_a^u}}{\Delta + \gamma\left(1 + \dfrac{r_s^u}{r_a^u}\right)} \tag{4.32a}$$

$$L_v E_c = \frac{\Delta (A_t - A_u) + \dfrac{\rho C_p D_0}{r_b^c}}{\Delta + \gamma\left(1 + \dfrac{r_s^c}{r_b^c}\right)} \tag{4.32b}$$

with all the symbols as described and calculated in the above sections. D_0 can be eliminated, yielding:

$$L_v E = C_c PM_c + C_u PM_u \tag{4.33}$$

in which:

$$PM_c = \frac{\Delta A_t + \dfrac{\rho C_p D - \Delta r_b^c A_u}{r_a^a + r_b^c}}{\Delta + \gamma\left(1 + \dfrac{r_s^c}{r_a^a + r_b^c}\right)} \tag{4.34a}$$

$$PM_u = \frac{\Delta A_t + \dfrac{\rho C_p D - \Delta r_a^s (A_t - A_u)}{r_a^a + r_a^u}}{\Delta + \gamma\left(1 + \dfrac{r_s^u}{r_a^a + r_a^u}\right)} \tag{4.34b}$$

The coefficients C_c and C_u are functions of the resistances. For details about the mathematical derivation of Eq. 4.34 one is referred to Shuttleworth and Wallace (1985). An approach similar to the one described in Eqs. 4.31-4.34 is used in the TL model (TL is based on SW). However, in this case the proportional coverage of both components is taken into account (see Dolman, 1993 and Huntingford et al., 1995).

Eqs. 4.3 and 4.4 for CM contain six unknown fluxes. Of a total of eleven potentials in the system there are also five unknown; namely T_i, T_c, T_s, T_0, and e_0. Choudhury and Monteith (1988) established eight more flux equations to obtain the eleven unknown quantities. Penman-Monteith type equations for L_vE_s and L_vE_c were obtained, which included the unknown quantity of the in-canopy vapour pressure deficit (D_0):

$$L_vE_c = \frac{\Delta_1 R_{n,c} + \dfrac{\rho C_p D_0}{r_b^c}}{\Delta_1 + \gamma_2\left(1 + \dfrac{r_s^c}{r_b^c}\right)} \tag{4.35a}$$

$$L_vE_s = \frac{\zeta \Delta_2 R_{n,s} + \rho C_p\left(\dfrac{\Delta_2 (T_m - T_0)}{r_{h,wet}^s} + \dfrac{\eta D_0}{r_a^s}\right)}{\Delta_2 + \gamma_2} \tag{4.35b}$$

The coefficients ζ and η are functions of resistances, γ_2 is a function of the psychrometric constant and resistances (see Choudhury and Monteith (1988) for details). Δ_1 is the slope of the vapour pressure temperature curve at canopy level (Pa K^{-1}). Δ_2 is the slope at soil level (Pa K^{-1}). T_m is the temperature at the bottom of the wet soil layer (K) and $r_{h,wet}^s$ is the resistance to sensible heat transfer of the wet soil layer (s m^{-1}). These equations were then solved to give D_0, yielding:

$$D_0 = e_a^{sat} + \Delta_3 (T_0 - T_a) - e_0 \tag{4.36}$$

where e_a^{sat} is the saturated vapour pressure (Pa) and Δ_3 is the slope of the vapour pressure temperature curve (Pa K^{-1}), both at reference level. Similar equations were also established for the component sensible heat fluxes H_c and H_s. These read:

$$H_c = \frac{\gamma_1 R_{n,c} - \dfrac{\rho C_p D_0}{r_b^c}}{\Delta_1 + \gamma} \tag{4.37a}$$

$$H_s = R_{n,s} + \frac{\rho C_p (T_m - T_0) - r_a^s R_{n,s}}{\left(\dfrac{\eta}{\zeta}\right) r_{h,wet}^s} - \frac{\zeta \Delta_2 R_{n,s} + \dfrac{\Delta_2 \rho C_p (T_m - T_0)}{r_{h,wet}^s} + \dfrac{\eta \rho C_p D_0}{r_a^s}}{\left(\dfrac{\eta}{\zeta}\right)(\Delta_2 + \gamma_2)} \tag{4.37b}$$

where γ_1 is a function of the psychrometric constant and resistances. T_0 and e_0 are complex functions of the resistances, temperatures and vapour pressure deficits in the soil-canopy system (see Choudhury and Monteith (1988) for details). The quantities Δ_1 and Δ_2 can be replaced by Δ_3 without significant loss of accuracy of the model output.

DD assumed the mean vegetation air stream to take on properties intermediate between air properties at reference level, air properties at vegetation level and air properties at soil surface level. He defined a weighted mean temperature and specific humidity of the mean vegetation air flow. In this study the parameterization following Dickinson et al. (1986) is used. He solved the energy balance of the vegetation and soil surface for T_0 and q_0, obtaining:

$$T_0 = \left(\frac{T_a}{r_a^a} + \frac{T_c}{r_b^c} + \frac{T_{s,1}}{r_a^s}\right)\left(\frac{1}{r_a^a} + \frac{1}{r_b^c} + \frac{1}{r_a^s}\right)^{-1} \tag{4.38}$$

and:

$$q_0 = \left(\frac{q_a}{r_a^a} + \frac{\xi q_c}{r_b^c} + \frac{q_s}{r_a^s}\right)\left(\frac{1}{r_a^a} + \frac{\xi}{r_b^c} + \frac{1}{r_a^s}\right)^{-1} \tag{4.39}$$

where ξ is the fraction of potential evaporation (-), to be discussed later. In DCM and TCM the same equations are used, with the assumption (in TCM) that $T_c = T_u$. $r_b{}^c$ in TCM is parameterized with the following formula

$$r_b^c = \left(\frac{1}{r_b^c} + \frac{1}{r_b^u + r_a^u}\right) \tag{4.40}$$

where the superscript c on the right hand side denotes the bush canopy only. T_c can be found by solving Eq. 4.7 using the iteration scheme of Newton-Raphson. q_c is simply calculated by assuming that the air in the stomata of the leaves with temperature T_c is completely saturated. Expressions for all potentials in the system are established now and thus all component surface fluxes can be calculated using ordinary flux equations. Following Deardorff (1978) and Dickinson et al. (1986), the sensible heat flux is corrected for the amount of stems in the vegetation which do not transpire but do exchange heat, by:

$$H_c = \Gamma \rho C_p \frac{(T_c - T_0)}{r_b^c} \tag{4.41}$$

where Γ is a correction factor (-). Deardorff (1978) and Dickinson et al. (1986) accounted also for the wetness of the vegetation surface caused by dewfall or rainfall in the parameterization of the latent heat flux of the vegetation. They defined a coefficient representing the fraction of the total evapotranspiration which is evaporated at potential rate:

$$\xi = 1 - \delta\Psi\left(1 - \left(\frac{w}{w_{\max}}\right)^{\frac{2}{3}}\right) \tag{4.42}$$

where ξ is the fraction of potential evaporation (-), δ is a step function which is zero if condensation occurs onto the leaf ($q_0 \geq q_c$) and is otherwise unity ($q_0 < q_c$), w is the mass of water retained on the vegetation surface per unit ground area (kg m^{-2}) and w_{max} is the maximum value of w beyond which runoff to the soil surface occurs. The factor Ψ is the ratio between the stomatal resistance and the total resistance encountered by the evaporative flux from the vegetation surface. In DD and DCM it is defined as:

$$\Psi = \frac{\overline{r_s^c}}{\overline{r_s^c + r_b^c}} \tag{4.43}$$

In TCM we use:

$$\Psi = 1 - \left(\frac{\overline{r_b^c}\left(\overline{r_b^u}R_1 + r_a^u\left(R_2 + \overline{r_s^u}\right)\right)}{\overline{r_b^c}\left(\overline{r_b^u}R_1 + r_a^u R_2 + R_3\right) + R_4}\right) \tag{4.44}$$

with

$$\begin{aligned}
R_1 &= \overline{r_b^c} + \overline{r_b^u} + \overline{r_s^c} + \overline{r_s^u} + 2r_a^u \\
R_2 &= \overline{r_b^c} + \overline{r_s^c} + r_a^u \\
R_3 &= \overline{r_s^u}\left(\overline{r_b^c} + \overline{r_s^c}\right) \\
R_4 &= \overline{r_s^u}\left(\overline{r_b^u}\left(\overline{r_b^u} + \overline{r_s^u} + 2r_a^u\right) + \overline{r_a^u}\left(\overline{r_s^u}2r_a^u\right)\right)
\end{aligned} \tag{4.45}$$

(see Van den Berg, 1995b).

The water on wet vegetation surface (leaves and stems) evaporates according to:

$$E_c^{pot} = \Gamma\rho\frac{(q_c - q_0)}{r_b^c} \tag{4.46}$$

where E_c^{pot} is the maximum possible evapotranspiration of the vegetation (kg m^{-2} s^{-1}) The water vapour flux from partly wet vegetation can then be described by:

$$E_c = \xi E_c^{pot} \tag{4.47}$$

The amount of water extracted from the soil by transpiration is an important factor in the forcing of the soil moisture content. Assuming that transpiration occurs only from dry leaf surfaces and is directed outward, it can be expressed as:

$$E_{tr} = \delta(1-\Psi)E_c^{pot}\left(1-\left(\frac{w}{w_{\max}}\right)^{\frac{2}{3}}\right) \tag{4.48}$$

where δ is the same step function as in Eq. 4.42. The last term on the right hand side represents the fraction of dry leaves in the vegetation. Dewfall at, rainfall at, and runoff to the soil surface is added to the bulk soil moisture budget. Therefore, the evaporative flux of the soil surface can simply be expressed as:

$$E_s = \rho\frac{(q_s - q_0)}{r_a^s} \tag{4.49}$$

To account for the vegetation surface wetness in the calculation of the latent heat flux, the rate of change in surface wetness caused by precipitation or dewfall must be known. Deardorff (1978) treated precipitation intercepted by the vegetation as a part of dewfall. Therefore the rate of dewfall per unit surface area is dependent on the precipitation rate, the vegetation shielding factor and the 'real' dewfall rate. It can be described by:

$$\frac{\delta w}{\delta t} = \sigma_c P - (E_c - E_{tr}) \tag{4.50}$$

where the last term on the right hand side represents the 'real' dewfall rate. The precipitation rate at the soil surface is then:

$$\frac{\delta p}{\delta t} = (1-\sigma_c)P \tag{4.51}$$

The actual dewfall rate ($\delta w/\delta t$) is limited by a maximum dewfall rate beyond which runoff to the soil surface occurs ($\delta(w_{max} - w)/\delta t$) and by a minimum negative dewfall rate ($-\delta w/\delta t$), which corresponds to the maximum evaporation rate of the liquid water on top of the vegetation surface. If runoff occurs it is simply added to the precipitation rate at the soil surface. In formula:

$$\frac{\delta p}{\delta t} = (1-\sigma_c)P + \left(\frac{\delta w}{\delta t} - \frac{\delta(w_{\max} - w)}{\delta t}\right) \tag{4.52}$$

where the last term on the right hand side of Eq. 4.52 represents the runoff rate (kg m^{-2} s^{-1}). The infiltration rate into the upper soil layer is limited to the maximum forcing of the upper soil layer, i.e.:

$$\left(\frac{\delta p}{\delta t}\right)_{\max} = \frac{\rho_l d_{1,H_2O}}{C_1}\left(\frac{\delta\left(\theta_s - \theta_1\right)}{\delta t} + \frac{C_2}{\tau_1}\left(\theta_1 - \theta_{equ}\right)\right) + E_s + 0.1E_{tr} \tag{4.53}$$

4.2.6 Soil heat flux and soil temperatures

a) Soil heat flux

BL, SW and TL contain no soil layer(s) or soil state variables. In SW, G is a fixed fraction of the net radiation, whereas in TL measured values of G_c (G_b) and G_u are employed. In CM, the soil heat flux is explicitly parameterized. As can be seen from Eq. 4.4, part of the soil heat flux into the dry soil layer is used to sustain soil evaporation. The other part is conducted into the wet soil layer and is expressed as:

$$G = \lambda_{sat}\frac{T_l - T_m}{l_m - l} \tag{4.54}$$

where λ_{sat} is the thermal conductivity of the (saturated) lower soil layer extending from depth l to l_m (W m^{-1} K^{-1}).

The depths l and l_m and the temperature T_m are boundary conditions in CM. The depth l_m is constant in all model simulations. For short range studies l and T_m may be also held constant. However, for longer simulation periods, the evaporation front, l, will move progressively deeper towards l_m, as the soil dries out. Moreover, since heat is stored in or extracted from (depending on the direction of the soil heat flux) the wet soil layer, the temperature, T_m, will change according to the amount of stored or extracted heat. Changes in these parameters will effect the surface fluxes of the soil and, therefore, prognostic equations will have to be established to take these effects into account. The change in depth of the dry soil layer as a function of soil evaporation is modelled by Choudhury and Monteith (1988) according to:

$$l(t + \delta t) = l(t) + \frac{E_s(t)\delta t}{\theta_2} \tag{4.55}$$

where the term on the left hand side of the equation represents the depth of the dry soil layer in the next step of the simulation. E_s(t) is the evaporation from the soil (kg m^{-2} s^{-1}) and θ_2 is the (saturated) volumetric soil water content of the lower soil layer (m^3 m^{-3}), assumed constant with depth. δt is the time step in the simulation (s). The change in temperature T_m with the amount of heat storage and extraction can be described by:

$$\frac{\delta T_m}{\delta t} = \frac{1}{C_h}\frac{G}{\left(l_m - l\right)} \tag{4.56}$$

where C_h is the volumetric heat capacity of the wet soil layer (J m^{-3} K^{-1}).

DD, DCM and TCM use the Force-Restore rate equation of Bhumralkar (1975) and Blackadar (1976) to describe the change in temperature $T_{s,l}$ and humidity q_s at the soil surface. In this approach the temperature forcing by the soil heat flux is modified by a restoring term containing the deep soil temperature:

$$\frac{\delta T_{s,1}}{\delta t}=\frac{2\sqrt{\pi}G}{\rho_s c_s d_1}-\frac{2\pi\left(T_{s,1}-T_{s,2}\right)}{\tau_1} \tag{4.57}$$

where $T_{s,1}$ is the soil surface temperature (K), $T_{s,2}$ is the deep soil temperature (K), ρ_s is the soil density (kg m^{-3}), c_s is the soil specific heat (J kg^{-1}K^{-1}), $d_1 = (\kappa\tau_1)^{0.5}$ is proportional to the depth reached by the diurnal temperature wave (m), κ is the soil thermal diffusivity (m^2 s^{-1}), τ_1 is a period of one day (s). The quantity $T_{s,1}$ must be initialized. Further in the simulation $T_{s,1}$ changes with the rate given by Eq. 4.57. $T_{s,2}$ can be held constant and estimated from the mean air temperature over the previous 24 hours for short range studies. For longer periods, the change in $T_{s,2}$ can be calculated from:

$$\frac{\delta T_{s,2}}{\delta t}=\frac{G}{\rho_s c_s d_2} \tag{4.58}$$

where $d_2 = (365\kappa\tau_1)^{0.5}$ is $\pi^{0.5}$ times the e-folding depth of the annual temperature wave (m). The soil thermal diffusivity, κ, is derived from the soil heat conductivity and volumetric soil heat capacity. The soil heat conductivity is strongly dependent on the soil moisture content and thus on the *pF*-value. Al Nakshabandi and Kohnke (1965) established a relationship for soil heat conductivity as a function of the *pF* value of the soil. In their turn, Clapp and Hornberger (1978) established empirical relations between soil moisture content and pF value for different types of soil. The Clapp and Hornberger equations are implemented in DD, DCM and TCM.

The soil water content of the upper soil layer is forced by evapotranspiration and precipitation and restored by water movement in the soil. Water extraction by roots in this layer is limited to 10% of the transpiration, obtaining:

$$\frac{\delta\theta_1}{\delta t}=\frac{C_1}{\rho_l d_{1,H_2O}}\left(P_s-E_s-0.1E_{tr}\right)-\frac{C_2}{\tau_1}\left(\theta_1-\theta_{equ}\right) \quad 0\le\theta_1\le\theta_s \tag{4.59}$$

where θ_1 is the volumetric soil water content of the upper soil layer (m^3 m^{-3}), θ_s is the saturated soil water content (m^3 m^{-3}), P_s the precipitation rate at the soil surface (kg m^{-2} s^{-1}), E_s is the evaporation rate at the soil surface (kg m^{-2} s^{-1}), E_{tr} is the transpiration rate from the vegetation (kg m^{-2} s^{-1}), ρ_l is the density of liquid water (kg m^{-3}), and d_{1,H_2O} is an arbitrary normalization depth (m). The two dimensionless coefficients C_1 and C_2 are highly dependent upon soil moisture content and soil texture. Deardorff (1978) derived values for C_1 and C_2 which were restricted to a single soil type. Noilhan and Planton (1989) parameterized C_1 and C_2 for a wide variety of soil types, using a detailed multi-layer one-dimensional soil model. This parameterization is used in the present study. The coefficient C_2 characterizes the velocity at which the water profile is restored. As such, it contains the hydraulic conductivity, K_s. which is parameterized according to the Clapp and Hornberger (1978). Furthermore, following Noilhan and Planton (1989), θ_2 in the original restoring term of Deardorff (1978) has been replaced by θ_{equ} since this quantity takes gravity effects into account.

The time-dependent equation for the soil water content of the lower soil layer is

$$\frac{\delta\theta_2}{\delta t} = \frac{1}{\rho_l d_{2,H_2O}}\left(P_s - E_s - 0.9E_{tr}\right) \qquad 0 \le \theta_2 \le \theta_s \tag{4.60}$$

where θ_2 is the volumetric soil water content of the lower soil layer (m^3 m^{-3}) and $d_{2,\ H_2O}$ is the depth over which the soil water budget extends (m). It is assumed that no drainage occurs at the bottom of the lower layer and that 90 % of the transpiration is extracted from this layer, since it includes the root zone. The quantities θ_1 and θ_2 are boundary conditions of the model and their initial values in the simulation can be estimated or obtained from observations. Further in the simulation these values change with the rate given by Eqs. 4.59 and 4.60. It is now possible to calculate the specific humidity at the soil surface (q_s) with:

$$q_s = \left[0.5 - 0.5\cos(\alpha\pi)\right] q_s^{sat} \tag{4.61}$$

in which:

$$\alpha = \min\left(\frac{\theta_1}{\theta_{crt}}, 1\right) \tag{4.62}$$

where $\theta_{crt} = 0.75\theta_s$ is the critical value of the soil moisture content where the soil acts as if it is saturated (m^3 m^{-3}). Of course, q_s has an upper limit of $q_s{}^{sat}$.

b) Parameterization of soil properties.

Using curve-fitting, Al Nakshabandi and Kohnke (1965) established a relation for λ, which is a function of the soil water potential head, h. They demonstrated that the relationship between λ and h is virtually independent of the soil texture and structure. Its functional form reads:

$$\lambda = \begin{Bmatrix} 418e^{-(pF+2.7)} & pF \le 5.1 \\ 0.171 & pF > 5.1 \end{Bmatrix} \tag{4.63}$$

where pF is $^{10}\log(h)$ (in cm). However, the relation between moisture content and potential head is determined by soil structure and texture. Empirical and semi-empirical models have been proposed to express the moisture characteristics on the basis of these properties (Ten Berge, 1990). In this study the algorithms of Clapp and Hornberger (1978) are implemented in DD, DCM and TCM.

Clapp and Hornberger (1978) relate the potential head h to θ by using a simple relationship:

$$h = h_s\left(\frac{\theta_s}{\theta}\right)^b \tag{4.64}$$

The subscript s refers to saturation. The hydraulic conductivity, K_s, is a measure of the ability of the soil to conduct the flow of water. The hydraulic conductivity varies over many orders of magnitude between air-dryness and saturation. Clapp and Hornberger use the following parameterization. They relate K_s to the volumetric soil water content by using:

$$K_s = K_s^{sat}\left(\frac{\theta}{\theta_s}\right)^{2b+3} \tag{4.65}$$

where K_s^{sat} is the hydraulic conductivity at saturation (m s^{-1}), θ_s is the soil moisture content (m^3m^{-3}) and θ_s is the saturated soil moisture content (m^3m^{-3}). The variables h_s, θ_s, K_s^{sat} and the exponent b are functions of the USDA soil textural class (U.S. Department of Agriculture, 1951). Clapp and Hornberger (1978) provided a table of mean values for each of these parameters. Values used in this thesis will be given in Chapter 8.

4.3 The A-g_S model

As opposed to the semi-empirical JS approach, g_l can also be fitted according to physiology-based models. In this thesis the parameterization is based on the findings of Jacobs (1994) and it assumes a relationship between the photosynthetic rate of plants, A_n (mg m^{-2} s^{-1}) and their leaf conductance, g_l (m s^{-1}). It is mainly based on the photosynthesis model of Goudriaan et al. (1985). This strong correlation can be described by the following equation (Jones, 1983):

$$g_l = \frac{1.6A_n}{(C_s - C_i)} \tag{4.66}$$

Here, C_s and C_i (mg m^{-3}) are leaf surface and internal CO_2 concentration, respectively. Because of the relatively conservative C_i/C_s ratio (Wong et al., 1979; Morison, 1987; Jacobs, 1994) a change in g_l will be strongly linked with a change in A_n. Experimental evidence (see Jacobs, 1994) showed that the ratio between C_i and C_s is fairly constant:

$$\frac{C_i}{C_s} = k \tag{4.67}$$

This parameter k (-) is given by

$$k = f + (1-f)\frac{\Gamma}{C_s} \tag{4.68}$$

where Γ (mg m^{-3}) is the CO_2 compensation concentration which is parameterized as a function of temperature:

$$\Gamma = 80 * 1.5^{0.1(T_a - 25)} \tag{4.69}$$

and f (-) is a function of the specific humidity deficit, D_s (g kg^{-1}):

$$f = f_0\left(1 - \frac{D_s}{D_{s,max}}\right) \tag{4.70}$$

An empirical light response curve of A_n (mg m^{-2} s^{-1}) is used to combine the effects of CO_2 and light:

$$A_n = \left(A_m + R_{dk}\right)\left(1 - \exp\left(\frac{-\varepsilon I_a}{A_m + R_{dk}}\right)\right) - R_{dk} \tag{4.71}$$

where the dark respiration, R_{dk} (mg m^{-2} s^{-1}), is $A_m/9$ and $I_a = 0.5\ R_s$. A_m (mg m^{-2} s^{-1}) is the photosynthetic rate at saturating light intensity and I_a (W m^{-2}) is the absorbed PAR. The initial quantum use efficiency, ε (mg J^{-1} PAR^{-1}), quantifying the slope of the light response curve can be expressed as

$$\varepsilon = \varepsilon_0 \frac{C_s - \Gamma}{C_s + 2\Gamma} \tag{4.72}$$

and A_m is found from

$$A_m = A_{m,max}\left(1 - \exp\left(\frac{-g_m(C_i - C_s)}{A_{m,max}}\right)\right) \tag{4.73}$$

whereas $A_{m,max}$ and the mesophyll conductance, g_m (mm s^{-1}), are given by

$$X(T) = \frac{X(@25) * 2^{0.1(T-25)}}{\left(1 + \exp 0.3(T_1 - T)\right)\left(1 + \exp 0.3(T - T_2)\right)} \tag{4.74}$$

where $X(T)$ is either $A_{m,max}$ or g_m, at any temperature T, with specific values of $X(@25)$, and reference temperature T_1 and T_2. $X(@25)$ is the value of X at 25 °.

4.4 Evapoclimatonomy model

The evapoclimatonomy submodel as developed by Lettau and described and tested for Sahel data in Nicholson and Lare (1990) is in essence a numerical solution to the integration of the simple hydrologic budget equation

$$P = L_v E + N + dm/dt \tag{4.75}$$

where N is runoff and dm/dt is the change in soil moisture storage. The model uses two important assumptions (Nicholson and Lare, 1990):

1) For a stable climate the long-term mean of dm/dt is zero, i.e. there is no net change in soil moisture storage, which leaves the right hand side of Equation 1 with only two terms. For most years this is a reasonable assumption.

2) L_vE and N can both be partitioned into immediate and delayed processes. The model requires input of monthly precipitation and solar radiation absorbed by the ground. For a detailed description see Nicholson and Lare (1990).

4.5 Model for calculation of roughness parameters

4.5.1 Introduction

Drag can be defined as the total shear stress on a rough surface or the downward flux density of streamwise momentum to the surface (Raupach, 1992). The total drag on a surface, τ, may be specified with a drag coefficient (which is z-dependent) or better by the roughness length, z_{0m}, in the logarithmic wind profile (see Eq. 2.28). The latter depends only on geometric properties of the surface, such as roughness element height (h), breadth (b) and element spacing D. They define the so-called roughness density λ:

$$\lambda = bh / D^2 \tag{4.76}$$

which was proposed by Lettau (1969) and formally justified by Wooding et al. (1973) (Raupach, 1992). Shaw and Pereira (1982) tested the dependence of z_{0m}/h and d/h on λ by using a model based on second-order closure principles.

The total drag can be divided into two components; the drag acting on the scattered elements, τ_R, (in our case the shrubs) and on the substrate surface below the elements, τ_S :

$$\tau = \tau_R + \tau_S \tag{4.77}$$

The partition of the stress depends on the above-defined density of the obstacles, λ, and on the drag coefficient for the substrate surface, C_S, and C_R , the drag coefficient for an isolated, surface-mounted roughness element.

Several theories about the calculation of drag partition concerned with determining the aerodynamic properties of a plant canopy have been developed in the past decades. The drag partition equation was introduced by Schlichting (1936) and it was tested by Marshall (1971) using wind tunnel experiments. Follow-up studies were conducted by Wooding et al. (1973), Seginer (1974), Arya (1975) and Kondo and Akashi (1976). From here on, Raupach (1992) developed a simple analytical treatment of drag partition theory based on scaling and dimensional analysis. Raupach's model will be applied (see Chapter 6) to find out whether the experimentally derived z_{0m}- and d values of fourteen selected sparse canopies are plausible, because the model's geometry fits very well with these types of sparse canopies. Furthermore, a sensitivity analysis will be executed in order to test which combination of model parameters gives the best description for these sparse canopies.

4.5.2 Raupach's drag partition model

A sound analytic treatment of drag partition on rough surfaces is given by Raupach (1992). It describes vegetation with isolated surface elements which makes it a useful tool for calculating the roughness characteristics of the bush-like sparse canopies that are being considered in this paper. The lay-out of the model is illustrated in Fig. 4.2.

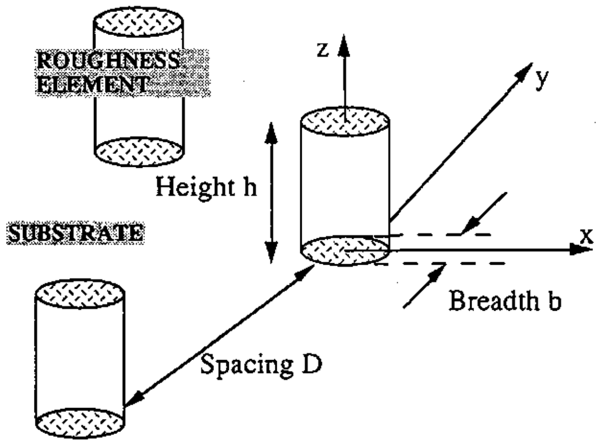

FIGURE 4.2. Lay-out of Raupach's drag partition model showing isolated, cylinder-shaped, roughness elements with height, h, breadth, b and spacing, D.

Two hypotheses are needed for the description of τ_R and τ_S. The first specifies the external scales controlling the shelter area A and volume V for a single roughness element, whereas the second describes the interactions between the roughness elements. From these hypotheses the following equations were derived. For the unobstructed ($\lambda = 0$) shear stress for the substrate surface:

$$\tau_S(\lambda = 0) = \rho C_S u_h^2 \tag{4.78}$$

With C_S the drag coefficient for the substrate surface and u_h the mean velocity at canopy height h. The shear stress on the underlying surface with the elements present is given by

$$\tau_S(\lambda) = \rho C_S u_h^2 \exp\left[-c_1\left(\frac{u_h}{u_*}\right)\lambda\right] \tag{4.79}$$

The stress on the isolated roughness elements reads:

$$\tau_R(\lambda) = \lambda \rho C_R u_h^2 \exp\left[-c_1\left(\frac{u_h}{u_*}\right)\lambda\right] \tag{4.80}$$

Here c_1 is a function of b/h. C_R is the drag coefficient for an isolated, surface-mounted roughness element. For vertical-axis cylinders $C_R \approx 0.25$, for cubes a values of 0.4 can be assumed. Raupach suggested a value of 0.3 for all bushes. The factor u_h/u_* accounts for the sheltering of the surface and the roughness elements. If $\gamma = u_h/u_*$ and if we sum Eq. 4.79 and 4.80, γ can be solved for every λ from the following implicit function:

$$\gamma = \frac{u_h}{u_*} = \left(C_S + \lambda C_R\right)^{-1/2} \exp(c_1 \lambda \gamma / 2) \tag{4.81}$$

The partition of stress is summarized by the following two formulae:

$$\frac{\tau_S}{\tau} = \frac{1}{1+\beta\lambda} \qquad \frac{\tau_R}{\tau} = \frac{\beta}{1+\beta\lambda} \tag{4.82}$$

with

$$\beta = C_R / C_S \tag{4.83}$$

The stress partition is thus entirely controlled by β.

For the prediction of z_{0m} and d from drag partition theory, as stated by Raupach, not only the flow within the canopy but also the flow above has to be taken in account. For the determination of the roughness length, z_{0m}, a so-called profile influence function (not to be mistaken with stability correction), Ψ, has been added to the logarithmic wind profile which accounts for the dynamic effects of the canopy on turbulence. Ψ is a function of the height above the canopy, z, displacement height, d, and the height up to which the influence of wake diffusion is noticeable, z_w. Thus

$$\frac{\kappa u(z)}{u_*} = \ln\left(\frac{z-d}{z_0}\right) + \Psi\left(\frac{z-d}{z_w - d}\right) \tag{4.84}$$

The profile-law applied for the wind speed at canopy height h is

$$\frac{\kappa u_h}{u_*} = \left[\ln\left(\frac{h-d}{z_{0m}}\right) + \Psi_h\right] \tag{4.85}$$

According to Raupach et al., (1989), Ψ_h is a function of one constant only, c_w. This constant (greater than 1) determines Ψ_h through the following equation

$$\Psi_h = \ln(c_w) - 1 + c_w^{-1} \tag{4.86}$$

In Raupach's original paper of 1992 the + and - were interchanged. Formula 4.86 was obtained from a personal corrigendum (dd. 23-10-1992). This means that the adopted value for Ψ_h of 0.74, was obtained with c_w being approximately 4, not 1.5 as given in the paper. An argument for the fact that c_w has to be considerably higher than 1.5 will be given in § 4.5.3.

According to Raupach the z_{0m} to height ratio may be finally written as

$$\frac{z_{0m}}{h} = \frac{h-d}{h}\exp(\Psi_h)\exp(-\kappa\gamma) \tag{4.87}$$

The following formula has been applied for calculation of d/h:

$$\frac{d}{h} = \left(\frac{\beta}{1+\beta\lambda}\right)\left(1 - c_d\left(\frac{b}{h\lambda}\right)^{1/2}\gamma^{-1}\right) \tag{4.88}$$

4.5.3 Model constants

The constant c_l depends on *b/h*. Raupach takes $c_l = 0.37$ for the cylinder-like obstacles with $b/h \approx 1$. For the tiger-bush, with large values of *b/h* , a higher value seems more appropriate, which is why c_l will be set to 0.37 and to 0.5 in the sensitivity analysis to be presented in Chapter 6.

The constant c_w is related to the introduction of Ψ. Originally (Raupach et al., 1980), Ψ was a function of z, d and z_w, with z_w the upper height limit of the layer of wake influence. Two external governing length scales - the inter-element separation D (Garratt, 1980) and the element breadth (b) - failed to described the datasets analyzed by Raupach (1992). For this reason the following formula was introduced

$$c_w = \frac{z_w - d}{(h-d)} \tag{4.89}$$

Raupach (1992) originally derived values for c_w ranging from 1.4-1.8 based on velocity profile data in the roughness sublayer (O'Loughlin, 1965; Raupach et al., 1980). However, applying formula 4.89 to Table II of Raupach et al. (1980), where z_w in combination with d is given for several artificial rough surfaces, yields values for c_w ranging from 1.8 - 13 for low, high and best d-estimates. The constant c_w appears to be a function of λ; the higher λ, the higher c_w. The corrigendum of Raupach made clear that higher values of c_w (around 4.0) are necessary to obtain proper values of Ψ_h by using Eq. 4.86. A value of 4.6 will be used for the model calculations.

In Raupach's paper, a C_S of 0.003 is assumed. This describes the unobstructed drag coefficient for a relatively *smooth* substrate surface (such as bare soil). This value is correct in the case of the selected row crops (vines and cotton) and tiger-bush (see Table 6.1). However, it is too low for savannah-type vegetation, which has an understorey of high grasses (0.5-0.75 m). For these surfaces C_S should be higher than 0.003. The exact value of C_S is given by $C_S = u_*^2/u_h^2$. However, these variables are not available for the savannah experiments. If we make use of values for h, z_{0m} and d as given in the literature for long grass and heather (Wieringa, 1993), a value of about **0.018** can be deduced by using Eq. 4.84 and setting Ψ_h to 1.0. For the model runs, a value of **0.010** was thought appropriate for all savannah surfaces because the grass was assumed to be rather sparse. The element drag coefficient, C_R, was varied between values of 0.25 (vertical-axis cylinders), 0.3 (as used by Raupach, 1992) and 0.4 (cubes).

According to Raupach (1992) a value of 0.6 for c_d is most appropriate for the majority of the canopies. This assumption is based on the results of several wind tunnel models of canopies (Raupach et al., 1980; O'Loughlin, 1965) and closed vegetation canopies (Raupach, 1992). It is possible that different c_d values are necessary to describe different types of vegetation (closed versus sparse or, within the sparse range, row-crops versus scattered crops). For the model runs c_d values of 0.3, 0.6 and 1.2 will therefore be used and any vegetation-type dependency will be looked for.

5 THE SURFACE ENERGY BALANCE

5.1 Introduction

This chapter will discuss the observed temporal, and occassionally spatial, variation of the surface fluxes. Both diurnal and seasonal/annual results will be considered. The diurnal results, covering all components of the radiation balance, the SEB, and parameters such as surface temperature, will mainly refer to the HAPEX-Sahel CWS savannah and tiger-bush locations. For these sites, daily averages of some parameters have also been calculated in order to illustrate the effect of the dry-out on the exchange processes. From the SEBEX-experiment, daily (24 hour) averages of all important fluxes and surface or atmospheric variables will be used to get an annual picture. This is illustrative, because the HAPEX-experiment only yielded two months of data, which were primarily obtained during the wet season. Furthermore, the results (mainly L_vE) of the CWS savannah and tiger-bush sub-sites will be briefly compared with the data obtained for the same vegetation at the other super-sites (CES and SSS) to get an impression of spatial variability. The most likely cause of this variation is the large rainfall variability leading to variable plant development (see Fig. 3.9).

In each section, the diurnal HAPEX-Sahel savannah and tiger-bush data (and sometimes variation during the IOP) will first be shown and discussed. More emphasis will be put on the savannah data as this was the site were the WAUMET activities took place. Next, the fluxes or variables will be considered from a seasonal point of view using the SEBEX data. Note that the experiments took place during different years. Differences between wet (June, July, August, and September) and dry season (remaining months) values will be considered.

A distinction will be made between fluxes originating from the bushes (savannah, tiger-bush surfaces), from the understorey layer (vegetation plus soil) or undergrowth (savannah) and from the bare soil surface (tiger-bush). These will denoted by the subscripts b, u, and s, respectively. In some cases (for example, surface temperature), extra subscripts will be used to indicate whether the variable had been measured under sunlit (s) or shaded (sh) conditions.

The following order has been chosen for the presentation of the results. First, the net radiation, R_n, will be discussed in § 5.2. The soil heat flux, G, will be described in § 5.3 and the available energy, $(R_n - G)$, will be summarized and compared with the sum of H and L_vE in § 5.4. Thus, the energy closure of the different datasets is considered here. In § 5.5 the results for H and L_vE will be presented. A summary and concluding remarks about data relevant for Chapters 6 and 8 will be presented in § 5.6.

5.2 Radiation

As described by Eq. 2.1, R_n consists of four terms. Hence, this section will deal with shortwave incoming radiation, shortwave outgoing radiation, longwave incoming radiation, longwave outgoing radiation and net radiation. This order is chosen because certain phenomena observed for R_n can not be explained without prior knowledge of the course of the fluxes which make up R_n. In the sections on longwave incoming and outgoing radiation, sky emissivity, surface emissivity and surface temperature will also be discussed.

5.2.1 Shortwave incoming radiation

Fig. 5.1 shows the diurnal variation in R_S for a typical cloudy and a typical clear day for the HAPEX-Sahel savannah site. R_S reaches maximum values of just over 1000 W m^{-2}. These high values are common for semi-arid areas close to the equator (Kowal and Kassam, 1978). Note the two peaks in R_S on 10 September. During those clear periods the reflection of direct solar radiation from the clouds causes R_S to be slightly higher than the values recorded on the clear day.

It appeared that R_S values for the tiger-bush site were lower (≈ 10 %) than those for the savannah area. Both sites were relatively close together (10 km apart) and no evidence existed for a generally dustier or cloudier atmosphere above the tiger-bush site. In addition, sensor shading, caused by guylines, the mast or other instruments, occurred two times a day at the tiger-bush site. The tiger-bush R_S-data used in the remainder of this thesis have been corrected with the R_S-data obtained at the savannah site.

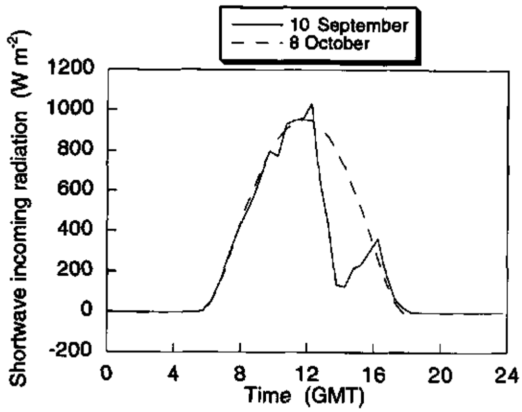

FIGURE 5.1. Diurnal variation in R_S for a typical cloudy day (——) and a typical clear day (- - - -) for the HAPEX-Sahel savannah site.

In Fig. 5.2 the seasonal course of daily mean values of R_S over the SEBEX savannah and tiger-bush surfaces is shown. The incoming shortwave radiation as received by both surfaces is very similar. Differences will be caused by local cloud occurrence and sensor or set-up differences. Although seasonal R_S exhibits distinct minimum (December and January) and maximum values (March, April) the differences between the wet and the dry season is relatively small as is shown in Fig. 3.6b.

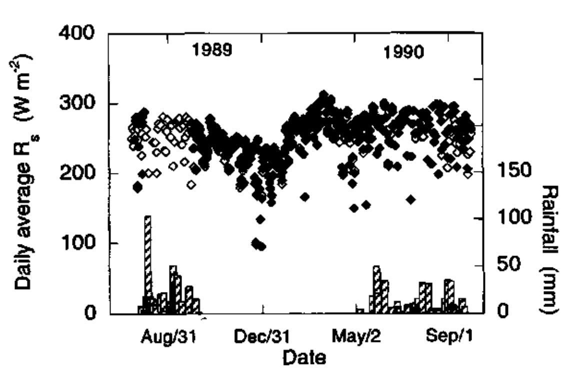

FIGURE 5.2. Seasonal variation in R_S over the savannah and tiger-bush surfaces during the wet and dry seasons of the SEBEX 1989-1990 experiment. Savannah rainfall is also indicated (bars).

5.2.2 Shortwave outgoing radiation

There is a surprising lack of albedo measurements over the Sahel region (Allen et al., 1994), even though various studies have been undertaken to investigate the influence of an increase of albedo on rainfall in this specific area (see Charney, 1975; Laval and Picon, 1986). Diatabé et al. (1989) describe Sahelian albedo values found from Meteosat visible data. The albedo displayed a zonal trend, increasing from south to north as the vegetation density decreases. In order to enable a more detailed study of the, still poorly understood (see Novak, 1990), interaction between Sahelian albedo and rainfall, this surface property has been monitored extensively during the SEBEX and HAPEX-Sahel campaigns.

Fig. 5.3 shows the HAPEX-Sahel albedo values for all component surfaces for a day in the middle of the wet season (8/9 September) and a day which occured three weeks after the last rainfall (8 October). Owing to sensor problems, no tiger-bush soil albedo data were available after day 260. No direct measurements of bush albedo, a_b, have been made at the savannah site for reasons described in Chapter 3 (view angle problems). Instead, a_b was calculated from measurements of total vegetation (bushes plus understorey) albedo, a_t, and knowledge of the percentage of bush coverage (see Eq. 2.37).

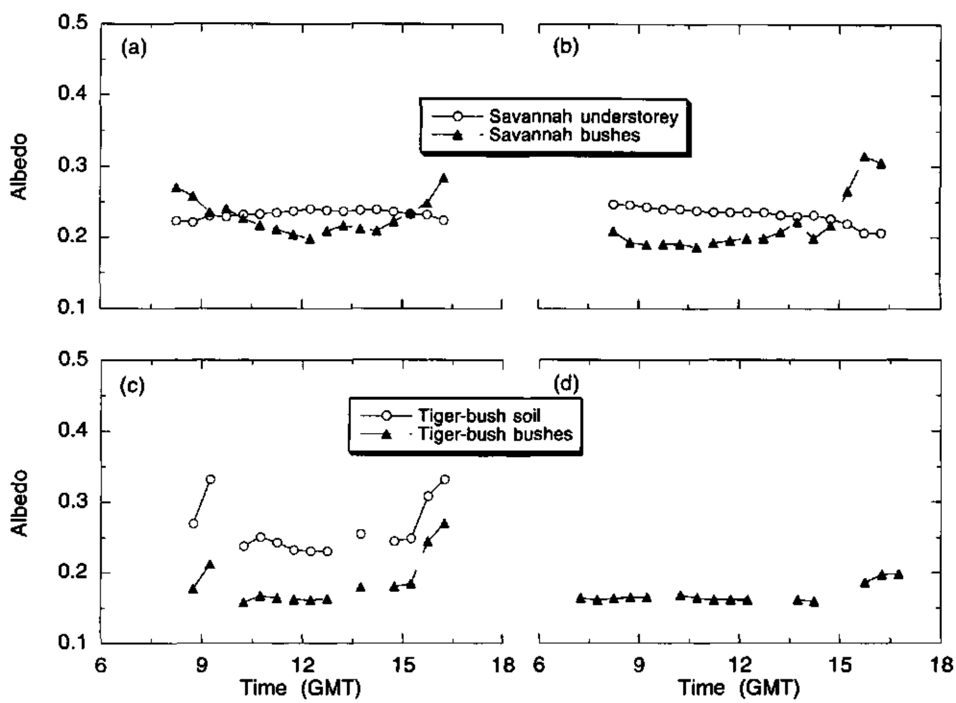

FIGURE 5.3. Variation in half-hourly mean albedo for the component surfaces at the HAPEX-Sahel savannah (a + b) and tiger-bush (c + d) sites for a day during the rainy period (8/9 September) and a day occurring three weeks after the last rainfall (8 October).

The albedo for the two component surfaces at the tiger-bush was directly measured with downward-facing solarimeters. The heights of these sensors were 0.7 and 7.8 m for bare soil (a_s) and bushes (a_b), respectively. This probably means that the sensor installed above the bush was also 'seeing' bare soil.

For all days and for all component surfaces, most albedo values were below 0.3. Lowest values were observed for the tiger-bush vegetation strips. During most of the day, values for a_u were slightly larger than those for (savannah) a_b because of the presence of bare soil (approximately 40 %) between the relatively sparse undergrowth. The onset of the dry season did not change a_u or a_b (savannah/tiger-bush) values noteworthily. However, from observations by Allen et al. (1994), it can be estimated that (midday) a_s values would have reached values of 0.3, which is an increase of 25 %. The vegetation values were very low, the tiger-bush bushes having values less than the average reported value of 0.20 (see Stull, 1988). The dense bushes appear to be very efficient in trapping the incoming radiation as also observed by Allen et al. (1994).

Results of the seasonal variation in albedo for the SEBEX savannah and tiger-bush component surfaces are presented in Fig. 5.4, where daily averages are shown. The annual means of Allen et al. (1994), were also obtained from these data. For the 1989-90 SEBEX campaign, lowest values of albedo were measured for the vegetation strips at the tiger-bush site, whereas the highest values were recorded for the bare soil between the linear vegetation patterns. The albedo of the tiger-bush vegetation strips remained very constant during the year, which indicated that major leaf-shedding did probably not occur. The savannah bush albedo is slightly higher than the albedo of the undergrowth, especially during the wet period. The small difference between both surface components shows that the surface was densely overgrown with grasses and herbs, leaving little bare soil exposed.

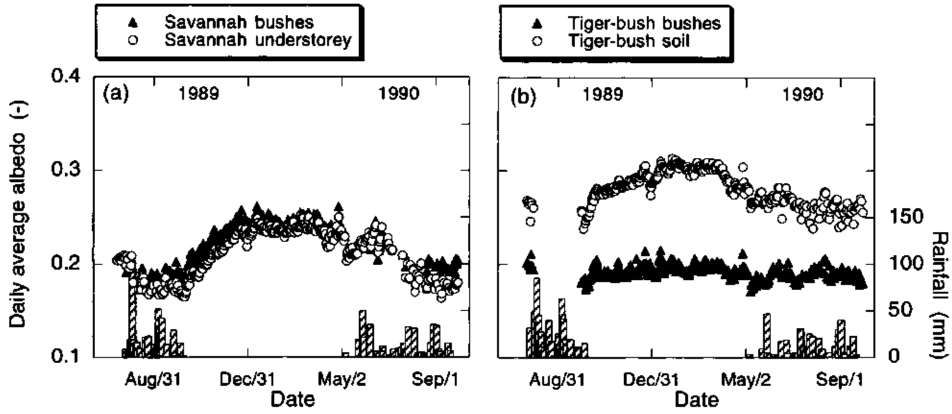

FIGURE 5.4. Seasonal variation in daily mean albedo for the SEBEX savannah herb layer and bushes (a) and the tiger-bush bushes and soil (b) from July 1989 to September 1990. Rainfall (bars) at both sites is also given.

This is all in agreement with the conclusions drawn from Fig. 5.3. According to Allen et al. (1994) the ranking of these surfaces is a consequence of the differing quantity of plant material present to trap radiation by multiple reflection and absorption. Fig. 5.5 gives the average albedo of both natural vegetations when the fractional coverage of the component surfaces is taken into account. In other words, the values shown in Fig. 5.5 were calculated according to Eq. 2.37, with α set to 0.80 and 0.67 for savannah and tiger-bush, respectively.

The average albedo value for both surfaces is highest during January and February when green vegetation is almost entirely absent (savannah), or the soil surface is very dry (tiger-bush) . After that, a gradually decreases after the occurrence of the first rains. A distinct dip in a is observed for the savannah in August/September. The values for the tiger-bush were similar between April and September, indicating that no significant increase in green LAI takes place during the growing season. The difference between both surfaces is about 0.03 during the dry season, until 0.06 for August and September. For a detailed description and explanation of course of a through time and differences between both surfaces, see also Allen et al. (1994).

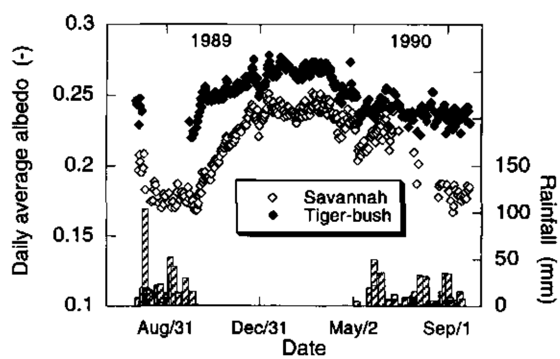

FIGURE 5.5. Variation in area-averaged daily mean albedo for the savannah and tiger-bush sites during the SEBEX campaign. The average is calculated with $a_t = \alpha a_{u/s} + (1-\alpha)\, a_b$. The parameter α equals 0.8 and 0.67 for the savannah and tiger-bush, respectively. Savannah rainfall is also indicated (bars).

The observed albedo values agree well with values given in the literature (Stull, 1988; Garratt, 1992). Sellers (1965) found values between 0.15-0.20 and 0.20-0.25 for wet season and dry season savannah, respectively. Oguntoyinbo (1970) found yearly averages for Sahelian savannas to be around 0.20. The wet season value for the understorey was 0.17, whereas during the dry season values between 0.21 and 0.25 were observed. Durand et al. (1988) measured values around 0.25 for the dry season of 1984. Rowe (1993) reported values ranging from 0.16 to 0.25 for shrub and scrub savanna, which can be considered representative for the Sahel. Bare soils display a large range of albedo values, mainly depending on soil type and especially the soil moisture content of the topsoil (see § 2.2.4). No values are available in the literature for the tiger-bush (except Allen et al., 1994), but the soil and bush albedos are well within the range of values found in the literature. Ten Berge (1990) gives 'wet' values ranging from 0.14 (loamy soil) to 0.21 (sandy soil), wheras the dry values are 0.28 and 0.39, respectively. Menenti (1986) found values of around 0.3-0.4, for dry desert soils.

Diabaté et al. (1989) established that albedo, deduced from Meteosat visible data, changed less than 0.025 between February and May (in 1984). From February to October decreases of 0.025-0.10 were observed. Those seasonal variations agree well with the data presented in Fig. 5.5. However, note that the year 1989 was considerably wetter than 1984.

5.2.3 Longwave downward radiation flux density

For the HAPEX-Sahel CWS savannah and tiger-bush sites, $R_{l,\downarrow}$ was not directly measured. It was calculated according to Eq. 2.2 with a value for ε_a as found from Eq. 2.3 (Brutsaert, 1975a). The constant in this equation was taken as 1.24 because replacement by 1.31 (Culf and Gash, 1993) is only necessary for calculations concerning the dry season. Furthermore, ε_a (0) has not been corrected for the occurrence of clouds for reasons explained in Chapter 2.

During the IOP, $R_{l,\downarrow}$ calculated in this way was fairly constant, with an average value of around 400 W m^{-2}. As a result of diurnal changes in T_a and D, values varied between 360 and 450 W m^{-2}. During the SEBEX-campaign, $R_{l,\downarrow}$ was only measured for the tiger-bush site, but differences between both sites were expected to be small. Fig. 5.6 indicates that it has an unmistakable seasonal pattern. This was also observed by Culf and Gash (1993). Low values occur from December until March, after which a sharp increase is observed during April, caused by increasing sky emissivity, $\varepsilon_a(0)$, and cloud amount (see Eq. 2.4). The increasing values of ε_a were the result of markedly decreasing e_a and T_a-values (see Fig. 3.6c and d). The abrupt decline of $R_{l,\downarrow}$ after the last rain is induced by the opposite effect. Incoming longwave radiation is also influenced by atmospheric dust (see Nicholson and Lare, 1990; Durand et al., 1988).

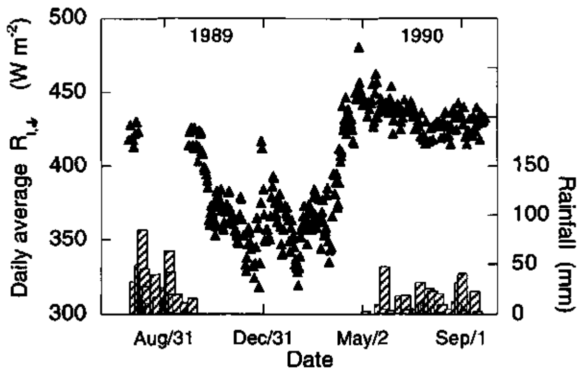

FIGURE 5.6. Seasonal variation in daily mean $R_{l,\downarrow}$ as directly measured at the SEBEX tiger-bush site. The bars represent rainfall at this site.

Fig. 5.7 shows a comparison between ε_a as calculated from Eq. 2.2 (i.e. from measured values of $R_{l,\downarrow}$ and $T_a{}^4$) and $\varepsilon_a(0)$ as estimated from Eq. 2.3. Both emissivities exhibit a similar seasonal course comparable to the one observed in Fig. 5.6. However, ε_a-values calculated from $R_{l,\downarrow}$ and $T_a{}^4$ are usually higher and they stay relatively constant during the dry season. This difference is most likely caused by the fact that Brutsaerts equation is only valid for a clear sky and therefore neglects the influence of dust or clouds, which explains its lower values. However, differences between ε_a and $\varepsilon_a(0)$ were apparent during all seasons which indicates that not taking cloud cover into account may not be the only source of deviation. There is a possibility that Eq. 2.3 does not work satisfactorily under these tropical circumstances.

Values for the ratio $\varepsilon_a/\varepsilon_a(0)$, which theoretically should always be larger than 1.0, were calculated. During most of the days $\varepsilon_a/\varepsilon_a(0)$ was larger than 1.0, with maximum values of 1.2. The ratio was largest during January, February, and March 1990. The cloud cover, c, which was back-calculated from Eq. 2.4 taking a value of 0.2 for n (Ten Berge, 1990), ranged from 0.1 to 0.9. Surprisingly, high cloud covers were observed during the 'spring' months. Although large (rain) cloud covers were not very likely for those months, the high values may have been caused by dust storms. However, this does not correspond with the relatively high R_s values shown in Fig. 5.2, for example. The rather unexpectedly persistent nature of the high $\varepsilon_a/\varepsilon_a(0)$-ratios might indicate an instrument failure. Consultation of the diffuse radiation data did not reveal a significant increase of diffuse radiation (and thus of percentage of overcast skies) during the winter months which also raises questions about the high observed ε_a values during those months. However, installation of the shading ring and maintaining its right position is not an easy task near the equator. So there is a possibility that the R_d data is not entirely trustworthy. From this limited analysis, it can not be concluded whether it was the theory (i.e. Eq. 2.2-2.4), the measurements, or both, which were responsible for the failure to describe the course of ε_a through the seasons. Nevertheless, it underlines the fact that determination of $R_{l,\downarrow}$ for these highly variable climates is a complicated matter.

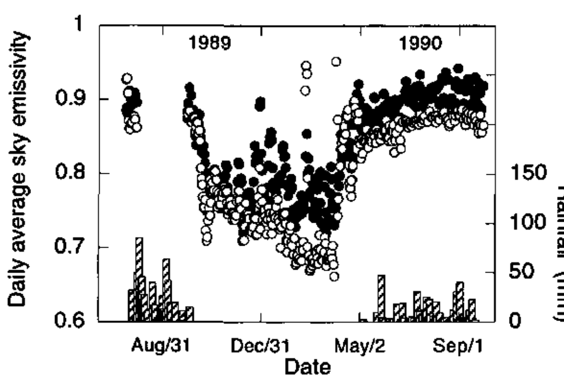

FIGURE 5.7. Seasonal variation in daily mean ε_a and $\varepsilon_a(0)$ as calculated for the SEBEX tiger-bush site. The variable ε_a was calculated from $R_{l,\downarrow} = \varepsilon_a \sigma T_a^4$, whereas $\varepsilon_a(0) = 1.24\,(e_a/T_a)^{1/7}$. Rainfall (bars) is also plotted.

5.2.4 Longwave upward radiation flux density

a) General

In hot, semi-arid climates longwave upward radiation flux density, $R_{l,\uparrow}$ (as given by Eq. 2.5), constitutes a large part of the radiation balance. In the infra-red part of the spectrum most natural surfaces behave as a grey radiator. This means that this radiation component will be predominantly determined by the average surface temperature, T_s, and by the average surface emissivity, ε_s, following the corrected Stefan-Boltzmann law. The second term in Eq. 2.5, describing the reflected part of incoming longwave radiation, involves estimates of $R_{l,\downarrow}$ and ε_s. As a result of the usually high values of ε_s for vegetated or bare soil surfaces, its portion will be relatively small.

T_s and ε_s will be first dealt with in separate sections after which final values of $R_{l,\uparrow}$ will be calculated and depicted. Separate surface component values and area averages of $R_{l,\uparrow}$ are important for the component calculation of R_n as calculated in most higher order SVATs (see, for example, Deardorff, 1978).

b) Component surface temperatures

As shown in Chapter 2, surface temperature is a key parameter in the SEB. Furthermore, infra-red measurement of canopy temperature can serve as an indicator of plant water stress, as was recognized already in the early 1960's (Tanner, 1963). Since the world-wide application of remote sensing, determination of T_s has again become an important issue .

This section describes the surface temperatures of the various components of the savannah and tiger-bush sites. Surface temperature has been measured on a continuous (Heimann IRTs) and a discontinuous (handheld IRT, Comet 8000) basis. All radiometric surface temperatures have been corrected to yield 'true' surface temperatures using the procedure described in Appendix 1. The distinction between the components is illustrative and also useful for physiological studies or to check the outcomes of multi-component SVATs. Many simple canopy/soil models assume that the soil surface and the foliage are at the same temperature (Noilhan and Planton, 1989) and it is interesting to know how far this is from the truth for the surface under consideration. For those models which do allow for different canopy and soil surface temperature (Deardorff, 1978; Shuttleworth and Wallace, 1985) directly measured component surface temperatures supply important material to substantiate the results. In the case of two vegetation layers - savannah composed of bushes with a distinct understorey of grasses and herbs- only one average canopy temperature will be calculated (see Dolman, 1993). So it has to be verified whether the different vegetative components (bushes, herbs, grasses) have similar values of T_s, which means that the assumption of one single vegetation temperature is valid.

From the individual components, an effective T_s has been reconstructed for the entire surface, as explained in Appendix 7. This latter value will be used in the gradient-resistance formulation for calculation of r_h, using a proper description of kB^{-1} (see § 2.4.1 and § 6. 2.2), and for computing values of $R_{l,\uparrow}$.

Fig. 5.8 shows the observed range of temperatures for the four surface types during day 269. The results of sunlit and shaded objects are shown in Fig. 5.8a and 5.8b, respectively. Data were taken from the ground observation sequence as obtained with the hand-held IRT (Comet 8000, see § 3.5.2). Averaging of all measurements yielded 41 half-hour averages for each surface component. Temperature differences between vegetative surfaces were small. Herb layer temperatures tend to be slightly higher than bush temperatures, especially under directly exposed circumstances. For the plant material, the increase in temperature from early morning to noon is small: around five degrees K. As expected, and proving the correctness of the measurements, surface temperatures were very similar for all surfaces during the early morning. Peak values occured approximately one hour after noon.

As anticipated, highest surface temperatures were found for sunlit bare soil. For low sun angles, however, understorey temperatures were sometimes higher. Surface temperatures for the mixture of bare soil, grasses and herbs, were intermediate between bush/herbs and soil temperatures, but generally closer to the soil temperatures, indicating that a large part of the understorey was non-vegetated. Correlation between sunlit and shaded temperatures is high ($r^2 = 0.88$ for the bushes and 0.78 for the herb layer).

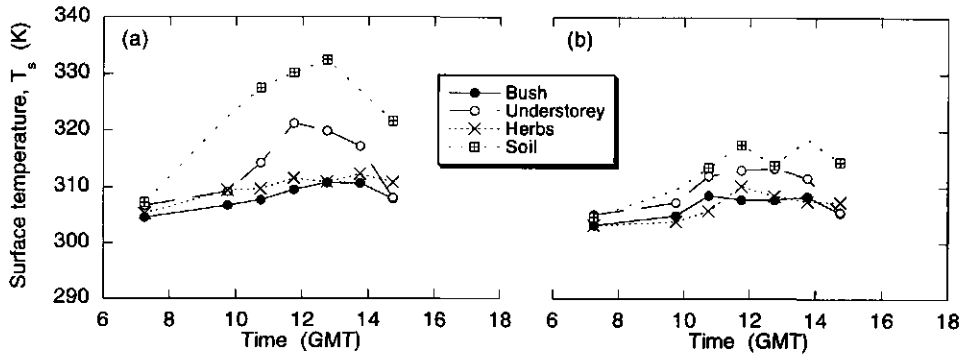

FIGURE 5.8. Diurnal variation in T_S (half-hourly averages) over savannah bushes, a mixture of herbs, grasses and bare soil (HAPEX-Sahel) and bare soil alone as measured with a hand-held IRT (Comet 8000) for day 269 (27 September). (a) Sunlit objects, (b) shaded objects.

Table 5.1 gives the ensemble averages for the 41 half-hourly averages (Comet 8000) for the four, simultaneously observed, individual surfaces. Heimann values averaged over the same 41 half hours, are given for comparison. Average differences between sunlit and shaded vegetation were small, which may mean that the effect of shading on temperature, presumably leading to lowered plant stress, will be small. However, the effect of diminished radiation load on plant stress may be more important than the lower temperature.

Bush surface temperatures as measured with the Heimann, were 3° lower than the values recorded by the hand-held Comet, which may have been the result of spatial variability or because of the fact that the instrument pointed to the north face of the bush. Their view angles were similar (approximately 90 °). Heimann values of the understorey, $T_{s,u}$, were clearly higher than the Comet equivalent for reasons described below.

TABLE 5.1. Average (n=41) surface temperatures for directly exposed and shaded surface components as measured with two types of IRTs. Variance is given between brackets.

Surface type	Instrument	sunlit T_S	shaded T_S
Guiera bushes	Comet 8000	307.4 (10.0)	306.3 (8.6)
" "	Heimann KT15	304.4 (13.2)	
Herb layer	Comet 8000	308.9 (11.7)	307.0 (10.7)
Understorey	Comet 8000	314.3 (36.0)	309.9 (16.6)
" "	Heimann KT15	319.0 (78.4)	
Bare soil	Comet 8000	321.4 (77.0)	312.1 (29.2)

A more detailed comparison was made between the results of the fixed and the hand-held instruments by calculating the relationship between the radiometric temperatures as measured by the hand-held and the fixed IRTs (see Appendix 8). Correlation for the bush temperatures was good ($r^2 = 0.74$). Heimann recordings were slightly lower, as was probably caused by one or more of the reasons described above. However, the correlation between the grass/herb/soil values as measured by the two types of IRTs was considerably lower ($r^2 = 0.61$) and it appeared that individual Heimann output could be up to 10 ° larger than Comet data.

The major difference between the way in which the temperatures were recorded was related to their view angle. The Heimann was installed vertically (see Table 3.2), whereas the manual measurements taken from the transect resulted in view angles of around 45 °. Therefore, the Heimann was seeing between the blades of grass to the soil below, thus missing the majority of the vegetation. This phenomenon was also observed by Malhi (1993) for the same type of vegetation. This statement is proven by Fig. 5.9 which shows the Heimann understorey surface temperatures against the soil and herb layer Comet surface temperatures. Correlation between Comet $T_{s,s}$ and Heimann $T_{s,u}$ is very high ($r^2 = 0.93$) and the points are close to the 1:1-line. Correction of the surface temperatures as measured continuously with the Heimann with the help of readings recorded with the Comet is described in Appendix 8.

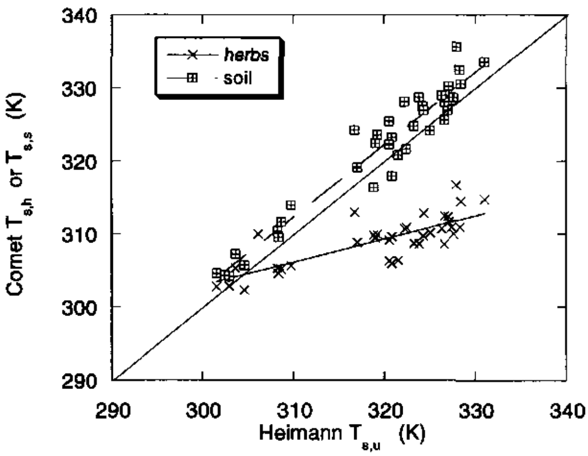

FIGURE 5.9. Relationship between the Heimann understorey surface temperatures and the Comet soil and herb surface temperatures for the HAPEX-Sahel savannah site.

c) Composite surface temperatures

The savannah vegetation consists of three main surface types: *Guiera senegalensis* bushes, an undergrowth of herbs and grasses and bare soil. Deriving a composite temperature from the separate measurements performed on the various surfaces is a delicate matter (see Kustas et al., 1989; Malhi, 1993). The procedure followed to arrive at an effective value of T_s is given in Appendix 7.

The recalibrations performed on the directly measured Heimann T_s-values, as described in Appendix 8, appeared to be very important. A comparison of $T_{s,t}$ with the direct composite obtained with the uncorrected temperatures of $T_{s,u}$ and $T_{s,b}$ showed that proper correction lowers peak values by nearly 10 °K and increases early morning values by up to 5 °K. This will have serious implications for calculations of net radiation, sensible heat flux and kB^{-1}. It illustrates that measurement of surface temperatures by nadir-looking instruments can lead to serious overestimations (see also Malhi, 1993; Stewart et al., 1994).

Fig. 5.10 shows recalibrated surface temperatures of the savannah bushes and understorey as measured with the fixed IRTs. Day 253 represents wet surface conditions, day 282 shows a situation when herbaceous vegetation had started to wilt and the upper soil layers were dry.

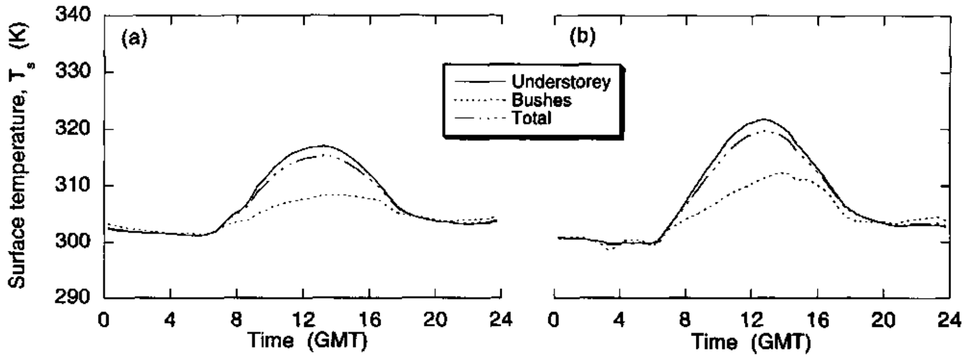

FIGURE 5.10. Diurnal variation in T_s over the savannah component surfaces (HAPEX-Sahel) and the area average, $T_{s,t}$, as measured with fixed IRT's (Heimann KT15) for (a) a typical wet day (253, September 10) and (b) a typical dry day (282, October 8).

Values of understorey T_s were much higher than the values for the bush. Increase during the morning and decrease during the evening is more pronounced for the IRT representing a mixture of soil, grass and herbs. Maximum values for the understorey were up to 320 °K (47 °C) , whereas the values for the bush were close to air temperature. It appears that bush temperatures were usually slightly higher than T_a at 2.5 m (height at which bush IRT was installed). However, errors in surface temperatures are reported (Ten Berge, 1990) to be up to 1 K, which means that no real conclusion can be drawn from this observation. Fig. 5.10 shows that the areal average is very close to $T_{s,u}$.

Fig. 5.11 gives an illustration of the seasonal course of T_s for both the savannah (a) and the tiger-bush (b) surface components. As in the previous SEBEX graphs, 24 hour averages are shown. All day-time temperatures were obtained for directly exposed objects. As expected from the above described results, the savannah shrubs were always cooler than the savannah understorey. Peak values for the savannah components were observed just before the first rains (around June). The tiger-bush component surfaces had a similar course, with the surface temperatures of the soil being generally higher than the bush temperatures. During the dry season, differences between both components got smaller because of the senescense of the vegetation and because of lower night-time soil surface temperatures. Although during the wet season, T_s for the tiger-bush bare soil patches was significantly higher than the T_s for the understorey, area-averaged values (Fig. 5.11c) were only slightly higher because of the larger savannah α-value(0.8 compared to 0.67). T_s values for the bushes (single *Guiera* bushes and the tiger-bush clusters) were very similar, which lowers the T_s relatively for tiger-bush because of the larger coverage with bush vegetation (33 % against 20 %).

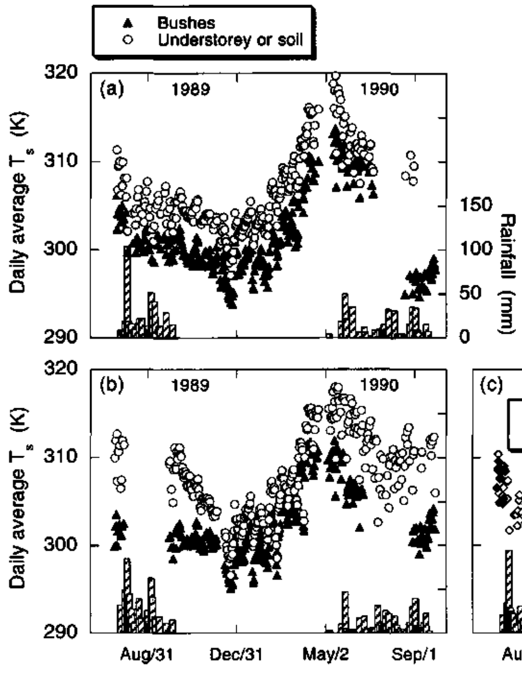

FIGURE 5.11. Component (a + b) surface temperatures, $T_{s,b}$, $T_{s,u}$ and $T_{s,s}$, and area-average (c) surface temperature, $T_{s,t}$, during the SEBEX experiment. It is assumed that all surface components were exposed. α is 0.8 and 0.67 for the savannah and tiger-bush, respectively.

d) Surface emissivity

Direct measurements of ε_s have not been made for the HAPEX-Sahel and SEBEX savannah or tiger-bush surfaces. Therefore, well-considered estimates have to be made based on past experiments for similar vegetation types or surfaces. Reliable values of ε_s are necessary for calculation of $R_{l,\uparrow}$ (see Eq. 2.5) and for the correction of surface temperatures (see Appendix 1) which are also needed in this same equation.

With the guide values from past experimental data (Hipps, 1989; Ten Berge, 1990; Van de Griend et al., 1991; Labed and Stoll, 1991; Garratt, 1992), the following wet season values were selected for the savannah and tiger-bush surfaces, which were assumed to be valid during the whole HAPEX-Sahel IOP. Savannah/tiger-bush bushes: 0.98; savannah understorey: 0.96 (0.95 for HAPEX-Sahel as a result of less undergrowth); savannah herbs and grasses: 0.97; and tiger-bush bare soil: 0.95. It is awknowledged that ε_s will exhibit a seasonal dependency. Therefore, ε_s has been ascribed a seasonal course for the SEBEX-experiment by introducing a dependency on the month during which the data were collected. In this way ε_s reached its lowest values from February to March: 0.952, 0.945 and 0.935 for the bushes, savannah understorey and tiger-bush bare soil respectively. The savannah soil ε_s values have been fixed at 0.91 because of the sandier character of the soil and the fact that no ponding (with accumulation of organic matter on the soil surface), but instead a very rapid drying occured. The tiger-bush soil was generally darker than the savannah soil.

e) Longwave upward radiation density, $R_{l,\uparrow}$

Finally, longwave upward radiation density, $R_{l,\uparrow}$, has been calculated using Eq. 2.5. The fluxes for the component surfaces were found by applying their respective surface temperatures and emissivities and are shown for the HAPEX-Sahel experiment in Fig. 5.12, together with the area-averaged value for two specific days. Data for the tiger-bush are not shown because bush values are expected to be similar to the ones observed for *Guiera senegalensis,* whereas surface temperatures for the bare soil in between the strips were not recorded so that $R_{l,\uparrow}$ could not be calculated. Differences between $R_{l,\uparrow}$ found for the understorey and bushes were large, notably during day 282. Night-time values were not much influenced by the dry-out, whereas day-time values increase markedly for both component surfaces. Bush $R_{l,\uparrow}$ peaks later than understorey $R_{l,\uparrow}$.

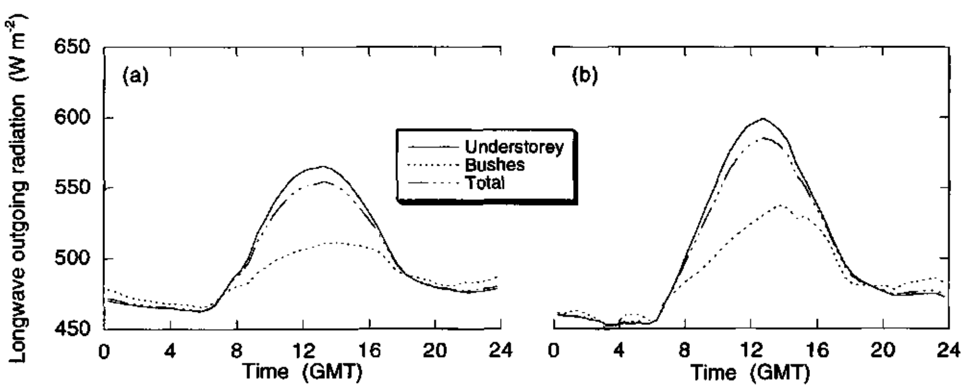

FIGURE 5.12. Longwave outgoing radiation, $R_{l,\uparrow}$, for the HAPEX-Sahel savannah surface components for a day during the wet period (a, day 253) and during the dry period (b, day 282), together with the area average obtained from $R_{l,\uparrow,t} = \alpha R_{l,\uparrow,u} + (1-\alpha)R_{l,\uparrow,b}$.

Fig. 5.13 shows SEBEX seasonal values of $R_{l,\uparrow}$ for both surfaces. A seasonal variation of up to 150 W m^{-2}, for daily averages, was observed. $R_{l,\uparrow}$ is highest just before the onset of rains because of the high surface temperatures. After the rains begin, a steady decline occurs, both through increasing green biomass and wetter soil conditions. Seasonal courses were similar for both surfaces (this is not the case for albedo, for example) and both surfaces reached comparable values. The tiger-bush surface appears to 'lose' less longwave radiation, because of slightly lower average surface temperatures (see Fig. 5.11) and a lower value of ε_s (wet season values of 0.96 as opposed to 0.97).

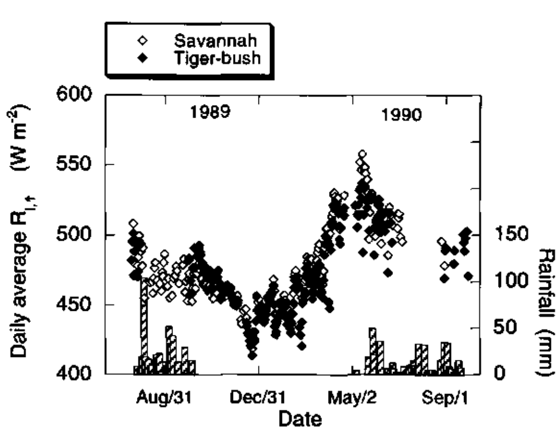

FIGURE 5.13. SEBEX average seasonal values of $R_{l,\uparrow}$, for savannah (open diamonds) and tiger-bush (closed diamonds). For savannah: $T_{s,t} = 0.2*T_{s,b} + 0.8*T_{s,u}$, for tiger-bush: $T_{s,t} = 0.33*T_{s,b}+0.67*T_{s,s}$. $R_{l,\uparrow,t} = \alpha R_{l,\uparrow,u} + (1-\alpha)R_{l,\uparrow,b}$. Rainfall at the savannah site is also given (bars).

5.2.5 Net radiation

Fig. 5. 14 shows the HAPEX-Sahel net radiation over the four sub-surfaces and for two typical days in the wet and the dry period, respectively. $R_{n,u}$ and $R_{n,s}$ -values were measured directly. Although direct measurements were available, the values for $R_{n,b}$ in the case of tiger-bush were derived from the individually measured radiation components following Eq. 2.1. This was done because it was suspected that the view area of the radiometer was too large compared to the area of the vegetation strip. For the same reason no direct measurements were made for the (much smaller) savannah bushes.

Both the savannah and tiger-bush bushes have a higher net radiation, reaching peak values of 800 W m^{-2}. The understorey or bare soil R_n-values were up to 200 W m^{-2} lower. This is mainly caused by the fact that the bushes have lower surface temperatures and slightly lower albedos. For both surface types $R_{n,u/s}$ is somewhat lower during the dry-out period. The net radiation received by the tiger-bush soil is higher than that received by the savannah herb layer. This may have been caused by lower ε-values for the bare soil or by spatial variability because the radiation sensors sampling bare soil had been installed at a height of 0.7 m only.

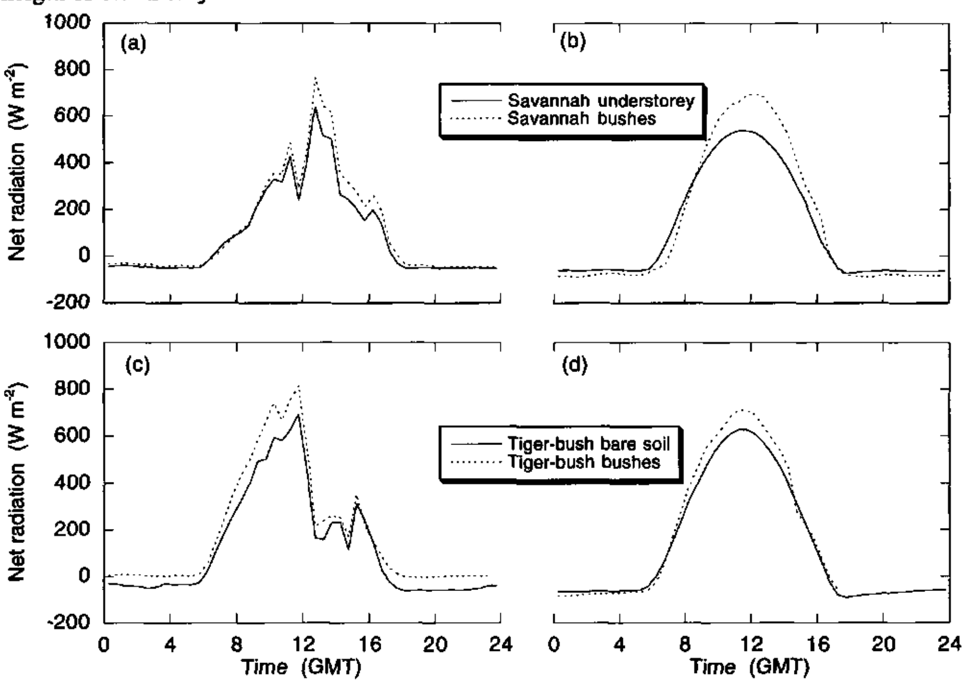

FIGURE 5.14. Diurnal variation in R_n over HAPEX-Sahel savannah (a+b) and tiger-bush (c+d) component surfaces for a typical cloudy day (4/10 September) and a typical clear day (8 October) during the wet and the beginning of the dry season, respectively.

Fig. 5.15 shows the daily R_n for the savannah and tiger-bush vegetation components during the SEBEX 1989-1990 campaigns. Minimum values of around 50 W m^{-2} were observed during the dry season (December, January), whereas during the wet season (July/September) maximum values close to 200 W m^{-2} were reached. Lowest values were found for the tiger-bush soil, especially for the rainy months. For the tiger-bush bushes the highest R_n values were recorded. The savannah upper- and understorey components have similar values, particularly for the dry months when the bushes were leafless and the grasses and herbs were dead. During the wet period of 1989, the understorey values are larger than the bush values. This is rather unexpected looking at Fig. 5.14, which represents the HAPEX-Sahel data. However, the SEBEX undergrowth was reported to be much denser, which might have caused the higher $R_{n,u}$ values. Sampling problems again may have been the reason for this phenomenon. $R_{n,s}$ is consistently lower than the tiger-bush $R_{n,b}$ values.

$R_{n,t}$ for both surfaces is plotted in Fig. 5.16a. It appears that for the majority of the days the savannah receives a higher net radiation load.

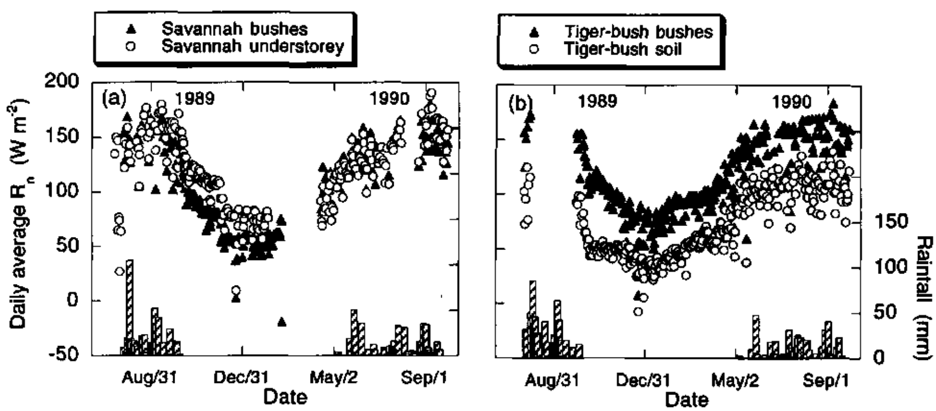

FIGURE 5.15. Seasonal variation in directly measured R_n over all component surfaces during the wet and dry seasons of the SEBEX 1989-1990 experiment. Bars represent rainfall.

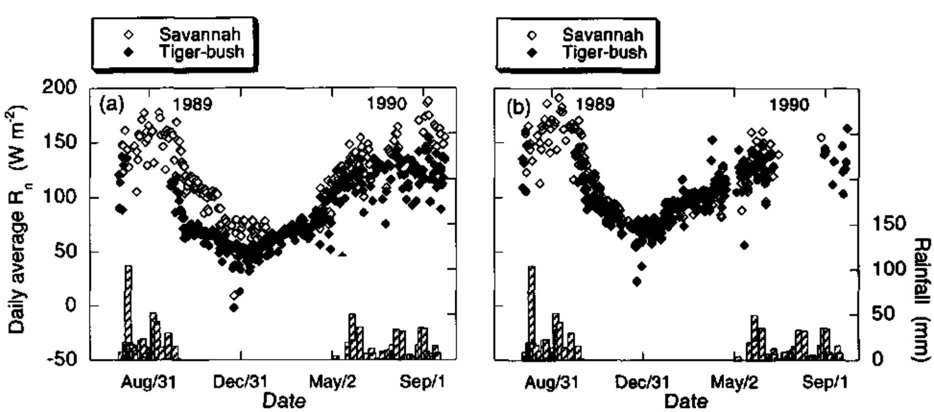

FIGURE 5.16. Seasonal variation in $R_{n,t}$ over the savannah and tiger-bush surfaces during the wet and dry seasons of the SEBEX 1989-1990 experiment. (a) 'Directly' measured components and (b) indirectly calculated net radiation obtained from the ingoing and outgoing shortwave and longwave radiation terms for both surfaces as given by Eq. 2.1. For both surfaces and both graphs $R_{n,t}$ is obtained with $R_{n,t} = \alpha R_{n,u/s} + (1-\alpha) R_{n,b}$.

b) Composite R_n

From the separate measurements of the four components of net radiation described in § 5.2.1-5.2.4, i.e. incoming and outgoing shortwave and longwave radiation fluxes, a composite value of R_n was calculated. This value should be in close agreement with the data presented above, both on a diurnal and a seasonal scale.

Spatial variability and instrument set-up can account for a certain difference between measured and composite R_n. Keeping this in mind, the best and most plausible value of R_n has to be selected and used for further model input (TL, for example, requiring separate values of $R_{n,b}$ and $R_{n,u}$) or for validation of the SVAT-models (e.g. DCM, see § 8.4).

For the HAPEX-Sahel savannah site, the bush, understorey and total R_n, of which the last two have been measured directly, have been compared with the R_n as composed of the four radiation components. Agreement between the directly measured and composite values of $R_{n,t}$ and $R_{n,u}$ was very satisfactory ($r^2 = 0.96$ for both cases). Peak values were slightly overestimated by the composite R_n estimates, especially during the rainy period, probably because of a too low ε_s-value. The peak values for the bushes, for which $R_{n,b}$ and a_b have been calculated indirectly, agreed well, but there appeared to be a small lag between both estimates: the composite $R_{n,b}$ lagging behind the 'direct' estimate of $R_{n,b}$. For the HAPEX-Sahel tiger-bush site no $T_{s,s}$ measurements (and thus no outgoing longwave radiation) were available and neither were values for $R_{n,t}$. Therefore, the only comparison made was between direct and composite $R_{n,b}$. As already mentioned above, the net radiation sensor installed above the bush had been also sampling bare soil, which led to large differences between both R_n-values. The composite values of $R_{n,b}$ were used for further calculations.

Fig. 5. 16b shows the net radiation for the SEBEX surfaces as calculated from the four radiation terms. It appeared that the savannah data exhibited a large correspondence (r^2=0.96), with an average overestimation of measured compared to composite R_n of only 6 %. For the tiger-bush however, the directly measured R_n was 20 % lower than the composite R_n, although the trend between both R_n-estimates is similar ($r^2 = 0.88$). This is partly affected by the fact that the bush net radiometer sees too much bare soil. This phenomenon was already acknowledged for the HAPEX-Sahel tiger-bush site, and it illustrates how large errors may be if radiometers are not installed at a correct height because the view factor is not taken into account. However, the directly measured $R_{n,s}$ values were also quite low compared to component values of $R_{n,s}$. This might have been caused by spatial variability, which will be much larger for the bare soil patches than for the vegetation strips. Spatial variability will cause the surface temperature and albedos to be non-representative. Fig. 5.16b shows that, according to composite radiation calculations, the savannah and the tiger-bush surface have a very similar seasonal course in $R_{n,t}$. On average, the tiger-bush site appears to receive slightly more net radiation. Because this is in agreement with the HAPEX-Sahel findings, the composite $R_{n,t}$ values for the SEBEX tiger-bush will be used from now on.

5.3 Soil heat flux

5.3.1 Introduction

G is determined by meteorological forcing and by thermal soil properties. The theory behind G, λ, C_h and κ has been given in § 2.3 and in Appendix 2 and 3. Paragraph 5.3.2 will describe the behaviour of topsoil thermal properties during the HAPEX-Sahel and the SEBEX experiments. An appraisal will be made of the temporal variability resulting from soil drying. The values of λ, κ and C_h, derived in this section, will be used for calculation of G (§ 5.3.3) and as input for SVATs (Chapter 8). Furthermore, they are useful for GCMs, for which soil-related input data for all kind of global biomes are required. Five methods (the Amplitude, Arctangent, Logarithmic and Harmonic equation, see Appendix 2) have been used and compared for the derivation of κ (see Appendix 9). The results of the Harmonic (HAPEX-Sahel savannah), and the Amplitude (SEBEX, savannah and tiger-bush sites) have been selected for further calculations. Values of C_h were derived from measurements of soil moisture content, θ, and dry bulk density (see Eq. A2.1). For the HAPEX-Sahel savannah site, λ was either measured directly by the non-stationary probe method (Van Loon, 1991) or alculated from $\lambda = \kappa C_h$ (see Eq. 2.9). The λ-values found from measurements at several pths for two plots are given in Appendix 10.

Paragraph 5.3.3 will describe the soil temperature measurements. These data are rtant for the calculation of κ and λ and for calculation of the soil heat flux. A comparison made for the soil temperatures beneath the various surface components (bushes, rey and bare soil), because an existing difference can cause a variability in, for soil evaporation or soil CO_2 flux.

empt has been made to pinpoint the most suitable method for determination of G EX-Sahel savannah site under these harsh, remote circumstances (see Appendix e HAPEX-Sahel tiger-bush site was determined by the plate method only. The for the SEBEX experiment. If a reliable G is found the next step is averaging component coverage areas. Thus, to find an area-representative value of G omplicated calculation-phases, in contrast with the other fluxes of SEB, for s are relatively easy to obtain by present-day meteorological techniques, if t and choice of fetch are properly taken care of. Recently conducted -arid regions (HAPEX-MOBILHY, EFEDA-I and HAPEX-Sahel) d for a sound procedure for determining the area averaged soil heat v focussed on the accurate determination of R_n, H and L_vE, whereas or a good understanding of the exchange processes for sparsely lculation of G is indispensable. These efforts will be rewarded by balance.

ies

soil properties at the savannah site during the HAPEX-Sahel 5.17, where Fig. 5.17a shows the heat capacity, C_h, for four these four depths are illustrative of the vertical variation encountered s. These values, and interpolations, will be used in the Calorimetric method.

During the rainy period values were relatively constant with C_h attaining maximum values of 1.7 MJ m^{-3} K^{-1}. The minimum value for C_h was about 1.2 MJ m^{-3} K^{-1} for the upper depth, and occurred three weeks after the last rainstorm.

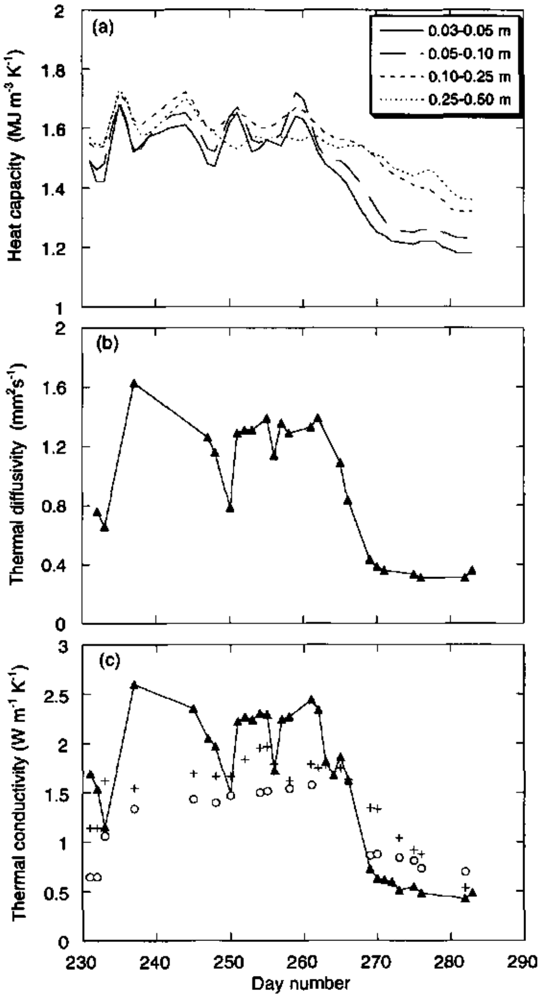

FIGURE 5.17. Thermal soil properties at the savannah site during the IOP of the HAPEX-Sahel experiment.. (a) Heat capacity, C_h, (b) thermal diffusivity, κ, at 0.05 m depth as calculated with the Harmonic method and (c) thermal conductivity, λ, at 0.075 m depth as calculated from $\lambda = \kappa C_h$ with κ obtained from linear interpolation of the κ–values between 0.05 and 0.10 m. Also shown are the measured λ-values at the same depth for two soil plots (o = densely vegetated plot, + = slightly vegetated plot).

Fig. 5.17b gives the topsoil (0.05 m) κ–values obtained from the Harmonic method using hourly mean values for soil temperature (see Appendix 9). During the rainy period, κ was relatively constant, which is in agreement with Fig. 5.17a. κ reached maximum values of around 1.5 mm^2 s^{-1}. This value is high but not unusual for wet sandy soils. It agrees with the high λ-values found for this soil at relatively low θ-values (see Fig. 5.18b). A few days without rainfall (between day 244 and 250, for example) lead to a considerable decrease of κ. This is caused by the high evaporative demand of this region, which lowered θ rapidly. After the beginning of the dry season, κ rapidly declined to values around 0.3 mm^2 s^{-1}. A clear relationship between κ and θ was found, as shown in Fig. 5.18a (r^2 = 0.80), supporting the validity of the calculations. Note that the relationship between θ and κ can not be extrapolated linearly towards higher moisture contents - at a certain value of θ, κ will decrease again. Due to the rapid drying of the savannah soil no θ-values higher than 0.12 were recorded.

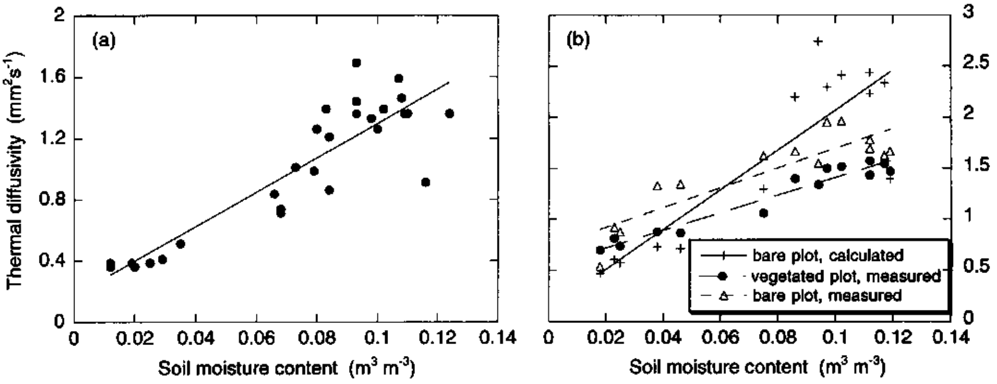

FIGURE 5.18. (a) Relationship between soil moisture content, θ, and diffusivity (as calculated with the Harmonic method, see Eq. A2.7), κ, and (b) measured and calculated thermal conductivity , λ, (at 0.075 m depth) as a function of θ for the HAPEX-Sahel experiment.

Fig. 5.17c shows the course of thermal conductivity during the IOP. The continuous line represents the λ-values at 0.075 m depth as calculated by Eq. 2.9, i.e by multiplying κ by C_h. Its course is very similar to the one observed for κ. Wet period values were frequently higher than 2.0 W m^{-1} K^{-1}, whereas λ decreased rapidly to values of 0.5 W m^{-1} K^{-1} after the last rainfall. The scattered symbols indicate **measured** λ-values (also at 0.075 m) as found for a vegetated and nearly bare soil plot. These points were taken from the data presented in Appendix 10. The measured wet season values were clearly lower than the calculated values and exhibited less scatter, especially for the densely vegetated plot. However, measured dry season values were higher than the calculated ones.

Despite the absolute differences between measured and calculated λ, correlation was satisfactory ($r^2 = 0.85$ and 0.78 for the vegetated and bare plots, respectively). Differences between measured and calculated thermal conductivities may be caused by two phenomena. In the first place, soil heterogeneity, causing differences in soil moisture content and thus in thermal properties. Another possibility might be the problem of contact resistance, already mentioned in Appendix 10, leading to measured values that are too low. It appeared, however, that differences between λ-measured and λ-calculated increased with increasing θ which makes the latter cause less plausible. Horton (1982) argues that transient methods (the λ-probes) for determining the thermal conductivity are more applicable for measuring λ of moist soils because a long waiting period for thermal gradients to become constant is not required (in contrast to steady-state methods). Thus water movement in response to temperature gradients is minimized, and the mechanism of heat transfer is almost exclusively conduction. This might imply that measured λ-values in moist soils are closer to true conductivity values than they are in dry soils, thus explaining the phenomena described above.

Fig. 5.18b shows that the conductivities (measured and calculated) were a clear function of θ. The vegetated and bare plots show similar slopes. The slope of the calculated λ-θ function is significantly higher (for reasons suggested above) whereas the intercept is smaller. A reason for this might be that C_h and/or κ-estimates were too high during wet periods.

There were no data on soil thermal properties available for the HAPEX-Sahel tiger-bush site. Unfortunately, this prevented a comparison between soil thermal properties typical for HAPEX-Sahel savannah and tiger-bush surfaces.

The annual course of C_h, κ, and λ, calculated on the basis of SEBEX data, is given in Fig. 5.19. Here, κ was found from soil temperatures at two depths (0.01 and 0.10 m) according to the Amplitude method. These sensors were installed below the understorey and bare soil, respectively. The Amplitude method has been chosen for its simplicity, which seriously reduced calculation time, and for good performance. For unknown reasons the calculated tiger-bush κ-values were very high (up to 2 mm s^{-1}) from November 1989 until April 1990, which was highly unlikely because of the low θ-values. Therefore, tiger-bush κ and λ are not shown. This implausible trend must have been caused by measurement problems, either in the case of the T_s (used to calculated T_{soil} at 0.01 m) or T_{soil} (0.10 m depth) data. The daily means of both variables show satisfactory values (see § 5.2.4 and 5.3.2), but this does not guarantee that the diurnal courses from which the maximum and minimum temperatures were taken were correct. During the dry season, the variables were sampled at hourly intervals which might have caused the problem. Furthermore, the calculated value of κ is very sensitive to the depths z_1 and z_2 (see Eq. A2.3). A shift of the soil temperature sensor due to reinstallation (at a shallower depth than 0.10 m) or soil movements (cracks, animal activity) might be another reason for the anomalous κ-values for tiger-bush. Another possibility may be that the methods used to calculate κ simply do not work in this heterogeneous, stoney soil.

C_h was found from Eq. A2.2 with $\theta_s = 0.36$ and 0.32 for the savannah and the tiger-bush site, respectively. The average for the layers extending from 0-0.05 and from 0.05-0.10 m depth was taken for the soil water content, $\theta\,(=\phi_l)$. Consequently, λ (calculated with $\lambda = \kappa\, C_h$ because directly measured values for λ were not available), also represented 0-0.10 m. Calculation of C_h and λ depended on the availability of θ-data. For both sites, soil moisture content had been measured with an average frequency of one week, which restricted the number of calculated C_h and λ-values. The savannah and tiger-bush C_h-data (Fig. 5.19a and d) show a similar seasonal course. Tiger-bush C_h-values were higher during the dry season (higher θ-values), and they show more variation. This is caused by the relatively fluctuating θ-values, which can not really be explained as no rainfall occurred during the dry season. Savannah C_h-data, ranging from 1.3 to 1.8 MJ m^{-3} K^{-1}, were very similar to the values observed during HAPEX-Sahel (see Fig. 5.17a).

Fig. 5.19b shows savannah κ-values throughout the year. The bulk of the data ranged from 0.3 to 1.2 mm^2 s^{-1}. During the HAPEX-Sahel campaign (1992) values ranged between 0.3 and 1.5 mm^2 s^{-1}. This shows that during the relatively short drying period of the HAPEX-Sahel experiment the topsoil had already dessicated down to its dry season values. Apparently, the transition period between dry and wet season during which most of the changes in surface properties occur, is very short.

Fig. 5.19c shows the seasonal course of thermal conductivity. λ stayed roughly constant during the dry season for the savannah surface, which is to be expected given Figs. 5.19a and b. Values are highly comparable to the values obtained during the HAPEX-Sahel campaign.

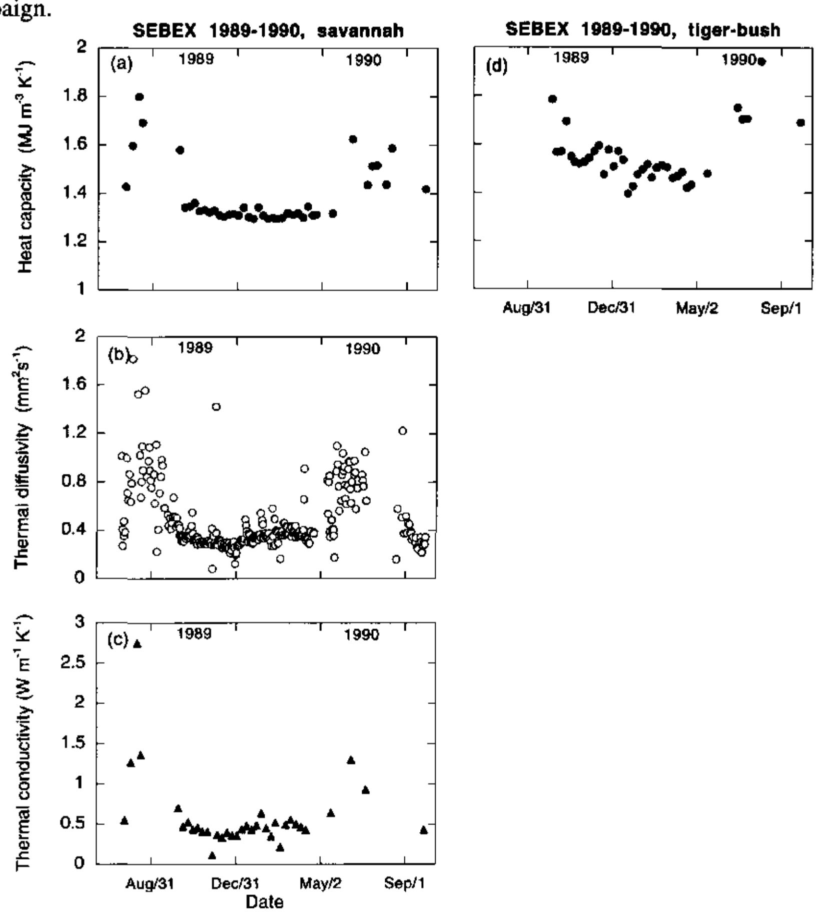

FIGURE 5.19. Thermal soil properties at the savannah site during the SEBEX experiment. (a) Heat capacity, C_h, for 0-0.10 m depth, (b) thermal diffusivity, κ, for 0-0.10 m depth and (c) thermal conductivity, λ, for 0-0.10 m depth as calculated from $\lambda = \kappa C_h$. Fig. 5.19d gives C_h for the SEBEX tiger-bush site.

As a result of the (technical) problems described above, it appears that we are facing a general lack of tiger-bush κ and λ-data. Luckily, additional soil temperatures for tiger-bush have been recorded during the 1989 wet season of the SEBEX-campaign, which made calculation of κ for two soil layers (0.05-0.10 and 0.10-0.20 m) at two plots possible. The agreement between κ-values of both layers of the two plots was satisfactory. The upper layer of Plot 2 had comparatively high κ values.The average thermal diffusivity of Plot 1 compared well to the average of Plot 2 ($r^2 = 0.78$), which guaranteed the reliability of the calculations.

Fig. 5.20 shows the variation of κ (average first layer of Plot 1 and 2) at the tiger-bush site during the 1989 wet season in which the SEBEX savannah values were added for comparison. Both surfaces have a similar range in κ values during the first part of the wet season, whereas after day 260 the tiger-bush κ stayed at a higher level. The main reason for this will be the higher soil moisture content and the different soil composition. It appeared that the wet values for both surfaces were similar, whereas the dry values were higher for the tiger-bush. One has to be careful though: a difference of 0.01 m between the intended and the true sensor depth may give a 40 % difference in κ.

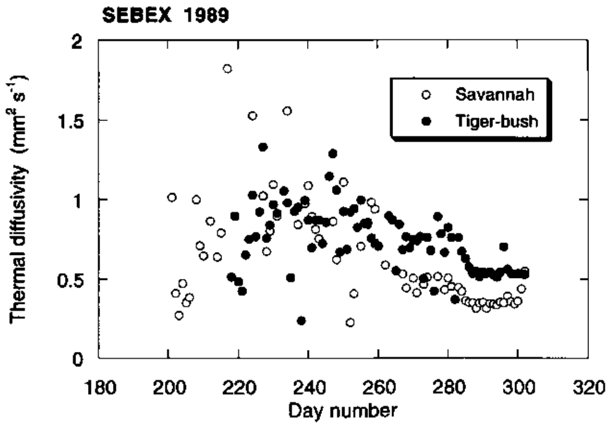

FIGURE 5.20. Thermal diffusivity for the SEBEX tiger-bush site. Soil temperatures of the 'extra' bare soil plots have been used. SEBEX savannah values are shown for comparison.

5.3.2 Soil temperatures

Proper measurements of soil temperature are important for meteorological projects because they are necessary for calculating soil thermal diffusivity and soil heat flux. Moreover, knowledge of the soil temperature is vital for agricultural purposes. It will govern processes like seedling germination and biological activity (see Veenendaal, 1991). For these natural vegetations, spatial variability of soil temperature will be very large. Certain soil patches will be bare, others are lightly or densely vegetated with grasses and herbs and at further locations the soil is shaded by scattered bushes or vegetation strips.

Fig. 5.21 shows the diurnal variation of three soil temperatures as measured at the HAPEX-Sahel savannah site. All sensors were approximately at a depth of 0.03 m. The first two sensors were installed beneath the sunlit understorey. One of them was beneath lightly vegetated soil, whereas the other lay under a densely vegetated plot. The third one had been placed below a bush. Differences were very large even between the two understorey plots, which shows that estimating the soil heat flux can be problematic if only one temperature profile has been sampled. As expected, the temperatures beneath the bush are even lower during the day-time. The lightly vegetated plot has been chosen for the understorey estimates of κ and G, as it was thought to represent an average falling as it did between the densely vegetated and bare soil patches ($\approx$ 40 % of total understorey area). In order to obtain a better area average, more temperature profiles would be preferable but this is not feasible under these remote conditions where experiments are usually driven by solar power.

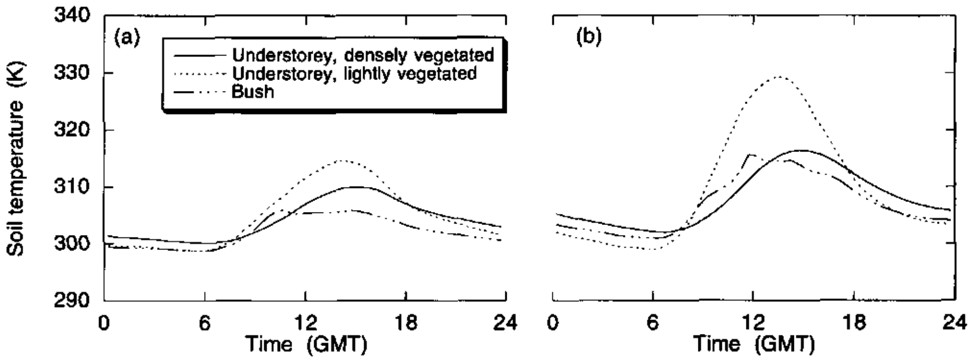

FIGURE 5.21. Soil temperatures at 0.03 m depth for the lightly vegetated, densely vegetated and bush plot of the HAPEX-Sahel savannah site during day 252 (a) and day 282 (b).

Fig. 5.22 shows the 24-hour averages of soil temperature at 0.10 m depth for the SEBEX savannah and tiger-bush component surfaces. The course of these temperatures was clearly related to air temperature (see Fig. 3.6d) - lowest values were observed during the winter months (DJF) and during the wet season. Peak values were reached just before the start of the rainy season. The soil temperatures of the two savannah components show a very similar seasonal behaviour. The temperature beneath the understorey is generally higher. During the wet season the difference is around two degrees, whereas during the dry season a maximum difference of four degrees is reached (April). A large difference between both components was recorded in the case of tiger-bush with the bare soil values being significantly higher, especially during the wet season (up to ten degrees).

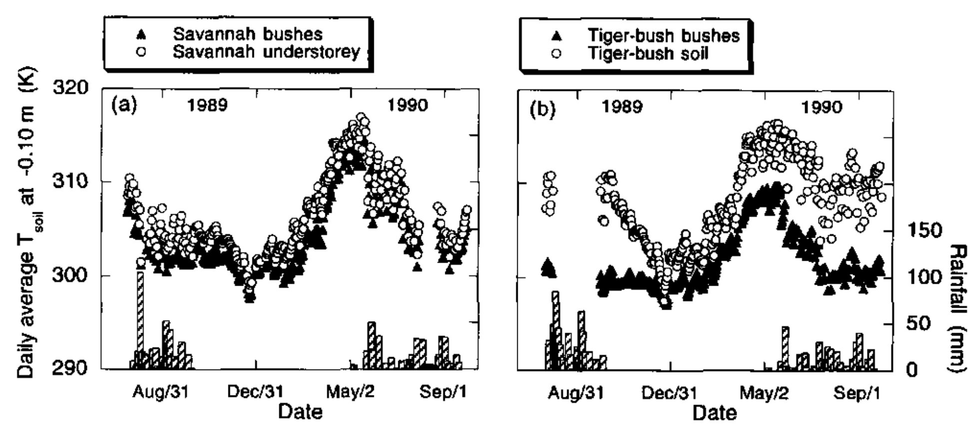

FIGURE 5.22. Daily averages of soil temperature at 0.10 m depth beneath the SEBEX savannah (a) and tiger-bush (b) component surfaces. Rainfall at both sites is indicated by bars.

Difference in soil temperature will be caused by two processes: direct shading of the surface, and higher soil moisture contents owing to reduced evaporation and possibly to so-called hydraulic lift. Separate measurements for θ underneath the bushes and below the herb layer were not available, but differences are assumed to be small, because of the size and density of the bushes. For the tiger-bush, θ was measured independently below both surfaces. Values were lower during the dry season and usually higher during the wet season for the bare plot because of the umbrella-effect of the very dense vegetation strips. Bare plot dry season θ-values were approximately 0.05 m^3 m^{-3} lower than those for the vegetated plot.

As shown in Fig. 5.22, differences in soil temperatures between the savannah components will be small during the wet season because both surfaces are vegetated (bushes and undergrowth, respectively). Although more or less leafless, the bushes will still offer some protection during the dry season, during which the understorey will be effectively bare, which explains that the highest differences occur just before the onset of the rains. For the tiger-bush, the difference will always be quite large, because one component surface is densely vegetated whereas the other is bare. This difference in vegetation cover will be clearest during the wet season, during which time the largest differences were observed.

5.3.3 Soil heat flux calculations

Mean below-bush G values, G_b, are shown in Fig. 5.23a and 5.23b, together with the understorey, G_u , or bare soil value, G_s, and total soil heat fluxes, G_t , as calculated with an analogy of Eq. 2.37 ($\alpha = 0.8$ or 0.67, for savannah and tiger-bush, respectively). For G_u, the results of the Calorimetric method were used, whereas G_b and G_s were obtained by using thermopile plates, as explained in Appendix 3. Fig. 5.23 only shows the results for days 282 and 283. During most of the other days a similar course was observed with the largest variation recorded during the rainy period (clear versus cloudy days, dry versus wet soil). The dry-out caused a slight decrease in understorey and area-averaged soil heat flux, whereas hardly any change was recorded for the G_b values.

Savannah G_t was similar to G_u, because of the small G_b-values and because of the fact that only a small percentage of the total area is occupied by the *Guiera* bushes. G_b was clearly less than G_u, because the soil was shaded by the bushes: peak values were approximately 150 W m^{-2} lower. The same phenomenon, however, meant that positive G_b-values continued approximately two hours longer than the understorey and total G-fluxes. This shadow-effect also caused the relatively broad peak observed for G_b. In addition, during the night G_b -values are less negative than G_u or G_t-values.

For the tiger-bush site an analogous pattern was observed as shown in Fig. 5.23b. Differences between G_t and G_s are larger than for the savannah surface because the tiger-bush has a vegetation coverage of 0.33. It appeared that the day-time $G_{u/s}$ values of the savannah and tiger-bush were highly comparable, although a small phase shift occured which was probably caused by the fact that the tiger-bush heat fluxes had been measured with shallowly installed (-0.01 m) thermopile plates after which no storage correction had been applied. This also explains the relatively small negative night-time values for the tiger-bush soil. Day-time soil heat fluxes for the tiger-bush soil were expected to be higher than G_u. That this was not the case may have been caused by the location of the sensors, or by the different properties of both soils. The G_b-values of tiger-bush and savannah were also very similar and again tiger-bush night-time G-values were higher than the savannah. However, this might have been the result of the fact that the tiger-bush vegetation strips were denser that the *Guiera* bushes, although this should have resulted in lower day-time values, too.

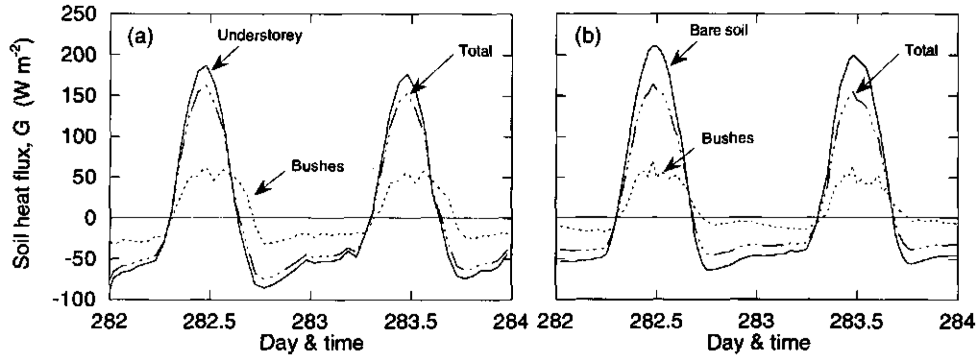

FIGURE 5.23. (a) Component, G_u and G_b, and total soil heat flux, G_t, for the HAPEX-Sahel savannah site and (b) component, G_s and G_b, and total soil heat flux, G_t, for the HAPEX-Sahel tiger-bush site. Two days during the dry period (282 and 283) are shown.

The area-averaged soil heat flux, G_t, for the tiger-bush was very similar to the savannah values which means that the possible differences in available energy will mainly be determined by differences in R_n.

Studying the course of the maximum soil heat flux (12.00 GMT) of the exposed savannah understorey during the IOP revealed that (peak) soil heat flux only declined to 75 % (from 250 to 200 W m^{-2}, which is from 0.4 to 0.3 R_n) of its maximum value, whereas the soil thermal properties rapidly fell to 25 % (κ) or less (15 % for λ) during the dry period. This is caused by the increasing temperature gradient which counteracts the decreasing λ-values. Soil heat flux will therefore keep on consuming 30-40 % of the total available energy. Concurrent changes in E/R_n (0.6 to 0.3) and H/R_n (0.15 to 0.4) are much more pronounced (see § 5.5), which shows that G accounts for a relatively constant portion of the radiant energy.

The SEBEX G-fluxes have been measured with shallowly (-0.005 m) installed soil heat flux plates. This may give radiation errors when the overlying soil is blown away by the wind or removed by water motion. In addition, soil heat flux plates are known to underestimate soil heat flux during the night, which is why they are usually installed at a certain depth (0.05 m, for example) with at least one temperature sensor placed between the sensor and the surface in order to calculate heat storage in that layer. This shallow installation caused the vast majority of the daily averages to be positive, suggesting an apparent warming of the ground. Besides, if the evaporation front is below the plate, part of the measured G will originate from the evaporation process (see also Mayocchi and Bristow, 1995). This is an extra reason for measured G to be too positive during the wet season. Therefore, SEBEX G-fluxes were regarded with caution. The annual course of the daily averaged G-values is given in Fig. 5.24. In both figures, the data points have been shifted downwards (-10 W m^{-2} for G_u and G_s, -5 W m^{-2} for G_b) to ensure negative values during the dry season and thus an annual G-value of ≈ 0 W m^{-2}. This shift resulted in a range of (wet season) values that was similar to the daily averages calculated during the HAPEX-Sahel campaign (not shown).

Fig. 5.24a shows the daily average soil heat flux for the 'between-vegetation' plots for the savannah and the tiger-bush. For this graph, five-day averages of G have been calculated to tackle the rather irregular character of this flux. Results from 1989 and 1990 have been combined and Fig. 5.24 therefore shows G against the day of year. Highest positive values are observed during the wet season, both for the savannah and tiger-bush. Fig. 5.24b shows G as measured beneath the bushes. Values are much smaller than for the bare/herb layer plots and seasonal variation is hardly present. Values are similar for the Guiera bushes and the tiger-bush vegetation strips. Fig. 5.24 shows that the daily values of G were quite small (maximum 5 -10 W m^{-2} compared to around 100 W m^{-2} for R_n), as are differences between wet and dry season and between savannah and tiger-bush.

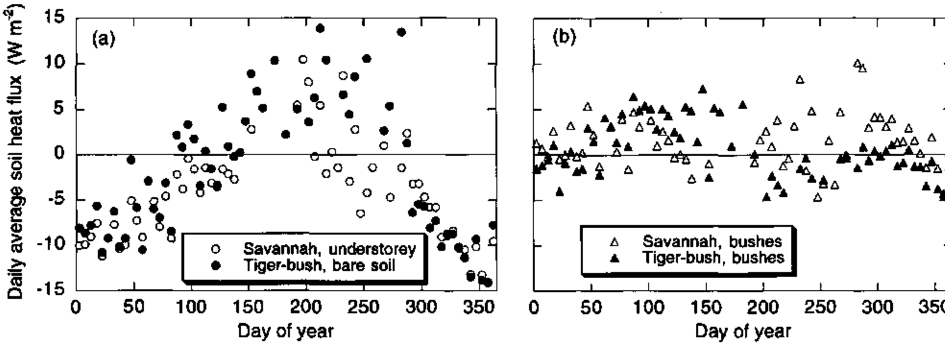

FIGURE 5.24. (a) Daily averages of G_u, G_s and (b) G_b for the SEBEX savannah and tiger-bush surfaces. Daily averages were averaged over five-day intervals and assigned to the middle of this interval (for example, at day 2.5 the average of day 1-5 is plotted). No distinction was made between the years 1989 and 1990.

5.4 Available energy and energy closure

The total available energy, A_t, for a certain surface determines the value of the sensible and latent heat fluxes. A_t will depend on the difference between the total net radiation, $R_{n,t}$, and the total soil heat flux, G_t, which have been specified in the previous two paragraphs. It was concluded by Gash et al. (1996), that the primary factor determining the variability of the evaporation during the HAPEX-Sahel campaign was the available energy rather than the value of the resistances representing the surfaces, which shows that proper calculation of A_t is important.

Fig. 5. 25 shows a comparison between the total available energy of the HAPEX-Sahel savannah and tiger-bush surfaces. It appears that for the tiger-bush site more energy was available, occasionaly up to 50 W m^{-2}. The available energy for the four subsurfaces is also given. Differences between the vegetated and non- or less-vegetated components was large (up to 300 W m^{-2}). (R_n - G) was highest for the tiger-bush vegetation strips, the tiger-bush bare soil received the smallest amount of available energy.

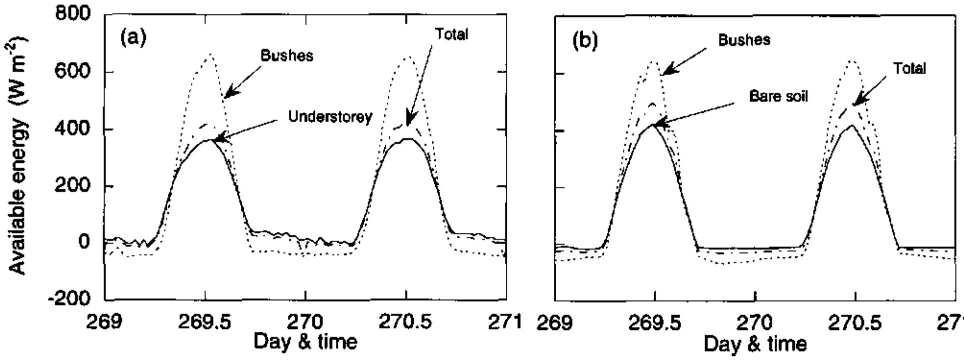

FIGURE 5.25. Total available energy, A_t, and the energy available for the separate components of the HAPEX-Sahel savannah (a) and tiger-bush (b) sites.

These findings agree with the results presented by Gash et al. (1996) who calculated A_t for the three major surface types occurring at the SSS. In their paper, A_t was calculated as the sum of evaporation and sensible heat flux in order to avoid the problem of the different vegetation samples of radiometers and micrometorological fluxes in this heterogeneous vegetation as observed by Lloyd et al. (1996). It appeared that cumulative totals, chosen in order to remove random variations and errors and to emphasize systematic trends of A_t, were highest for tiger-bush. The savannah A_t was some 10 % less than tiger-bush, whereas for the millet some 20-25 % less A_t was received. These differences were not related to the amount of rainfall received as the lowest rainfall had been recorded for the tiger-bush site.

Energy closure for HAPEX-Sahel was evaluated by comparing half-hourly values of $(R_n - G)$ and $(H + L_vE)$. Composite $R_{n,b}$ was used for the tiger-bush site instead of the directly measured values, for reasons described in § 5.2. Closure was assumed to be satisfactory for those times during which the absolute difference between $(R_n - G)$ and $(H + L_vE)$ was less than 50 W m^{-2}. This number was thought adequate because a detailed error analysis of Lloyd et al. (1996) revealed that H and L_vE can be measured with an accuracy of about 20 %. With this criterion, 22 % of all savannah data and 25 % of the tiger-bush data had to be rejected, which left enough data for analysis. These checked H and L_vE-fluxes will be used in the next section and to verify the model results given in Chapter 8. For the SEBEX data set the same criterion (50 W m^{-2}) was used, but in this case hourly flux values were screened (before the calculation of daily averages). The percentage of closure for the savannah site was similar to the one calculated for HAPEX-Sahel, whereas closure for the SEBEX tiger-bush was less (≈ 35 % rejection). This was partly caused by the fact that values of $R_{n,t}$ that were originally used to check the closure were obtained from direct measurements found from area-weighted averaging of the individual land cover components. These values were later found to be possibly too low compared to composite values of $R_{n,t}$. Furthermore, $R_{n,t}$ was calculated with a single value of α in stead of using an effective vegetation cover (see Culf et al., 1993; Lloyd, 1995) which changes with wind direction and stability, as explained in § 2.5. This resulted in rejection of a considerable amount of L_vE-data.

5.5 Sensible and latent heat fluxes

5.5.1 Introduction

Total sensible and latent heat fluxes have been measured with several methods (for an explanation of the methods see Chapter 2) including the Bowen ratio method, the profile method and the eddy covariance technique. This section will be confined to the outcomes of the EC method as this method is most reliable and because it was applied at most of the HAPEX-Sahel and SEBEX sites (see Lloyd et al., 1996; Gash et al., 1996; Moncrieff et al., 1996a, b).

The sensible and latent heat fluxes have been measured for several component surfaces in the following way. At the HAPEX-Sahel (CWS) and SEBEX savannah sites, the transpiration coming from the bushes was estimated by using sap flow gauges. Knowledge of the leaf area index, *LAI*, and the total leaf area per sap flow stem was needed to calculate an average L_vE_b in Wm^{-2} (see Eq. 2.35). At the CWS savannah site, micro-lysimeters were used to estimate the average (bare) soil evaporation, L_vE_s. The lysimeters were only used during the wet period (days 244-254), for which daily cumulative values were obtained. A simple evaporation model (see Appendices 5 and 12, partly summarized from Jacobs and Verhoef, 1996), based on Sherwood numbers, was used to extrapolate the results of this ten-day period. An estimate of evapotranspiration originating from the understorey was obtained by EC measurements at the grassland sub-site (see 3.5.2i). No component measurements of H and L_vE were performed for the CWS tiger-bush. However, at the HAPEX-Sahel SSS tiger-bush site, separate measurement of H_s and L_vE_s were obtained with a micro-Bowen ratio system (see § 3.7 and Wallace and Holwill, 1996), which will be used for illustration.

First, total H and L_vE for the HAPEX-Sahel and SEBEX savannah and tiger-bush vegetations will be described. A summary is also given of the findings of Gash et al. (1996), who analyzed the spatial variability of the micrometeorological evapotranspiration fluxes during the IOP of HAPEX-Sahel. This is presented and then the available component surface fluxes will be given.

5.5.2 Total sensible and latent heat fluxes

a) Results HAPEX-Sahel

Fig. 5. 26 shows the total sensible, H_t, and latent, L_vE_t, heat fluxes as measured for the HAPEX-Sahel CWS savannah and tiger-bush sites, for two consecutive days during the transition period and two days which occurred in the dry period. The interruptions in the plotted lines are due to missing data because Fig. 5.26 only shows the results for which the absolute difference between (R_n -G) and (H + L_vE) is less than 50 W m^{-2} (see § 5.4).

H is clearly less than L_vE during the transition period (Fig. 5.26a) for the savannah site, their ratio is approximately 0.3. During the dry period (Fig. 5.26b), however, H-values are very similar to the L_vE-values. Furthermore, H-fluxes attain negative values roughly three hours before the L_vE-fluxes cross the zero-line. The atmosphere changes from an unstable to a stable stratification very early and the extra energy resulting from this is used by the vegetation to continue its transpiration. When the surface dries up this time lag between H and L_vE appears to diminish. Most of the time, night-time L_vE appears to be slightly positive, which might indicate that the stomata are somewhat opened. This phenomenon has been observed by several groups, also for savannah, although it might be an artefact of the EC set-up. For the tiger-bush site, H and L_vE were of similar magnitude during the relatively wet period (Fig. 5.26c: days 269-270). However, a clear phase shift was observed: although both fluxes peaked roughly at the same time, L_vE was considerably higher during the morning hours. During the afternoon, both fluxes had a comparable course. During the dry-out (Fig. 5.26d: days 282-283), with generally higher H-fluxes, this pattern was also observed, though it was less pronounced. L_vE appeared to be positive during most of the night-time.

Fig. 5.26 illustrates that H was smaller at the savannah than at the tiger-bush site, whereas L_vE had corresponding values, thus making the sum of H and L_vE larger for the tiger-bush site. Differences between the wet and the dry period were much more pronounced for the savannah. In addition, the phase shift between H and L_vE occurred at entirely different times. It seems that the sensible heat flux produced at the tiger-bush bare soil patches was used for the evaporation of the bush strips. After partial stomatal closure (presumably around 10 GMT) H appeared to 'recover'. This means that a lateral exchange of fluxes between the two surface components occurred, because there was a considerable distance between them. This phase shift between tiger-bush H and L_vE was not as obvious at the SSS tiger-bush site (data not shown), which indicates that this phenomenon may be an artefact of the combination of the EC (H) and BREB (L_vE) method employed at the CWS. However, a comparison of H obtained by the BREB approach and by the EC method (Kabat and Elbers, 1994) showed a good agreement between both fluxes which supports the findings.

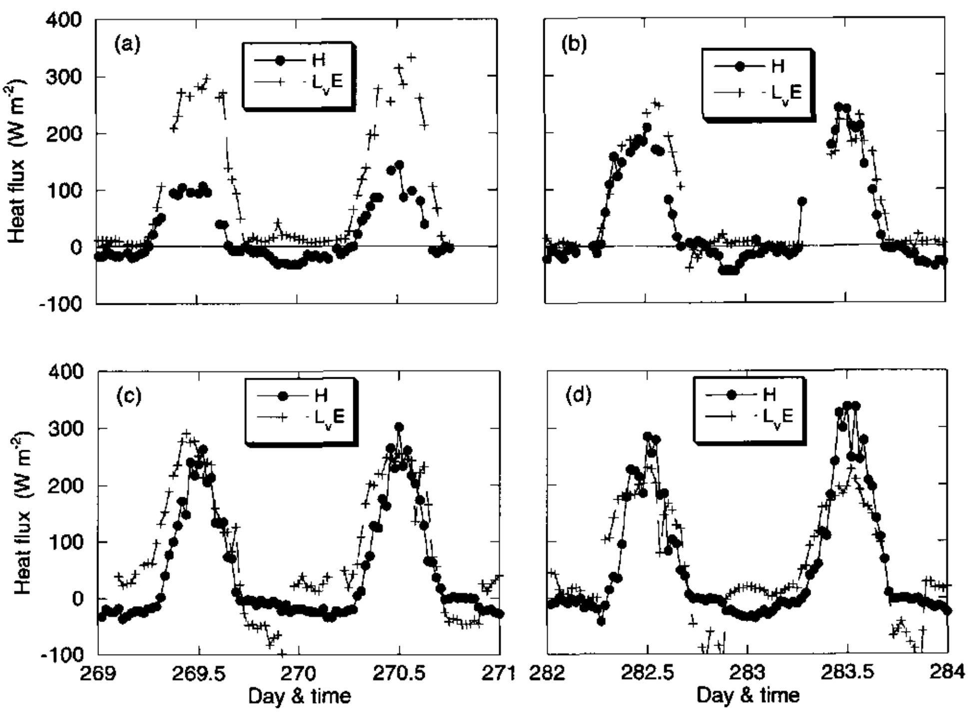

FIGURE 5.26. Total sensible, H_t, and latent heat, L_vE_t, fluxes for the HAPEX-Sahel savannah (a+b) and tiger-bush (c+d) sites. Figs. 5.26a and c show the results for days 269 and 271 occurring approximately one week after the last rainfall, whereas Figs. 5.26b and d represent two days during the dry period (day 282 and 283).

The evolution of H/L_vE (from here on referred to as Bowen ratio) during the IOP has been calculated for savannah and tiger-bush by, for example, Goutorbe et al. (1994) and Kabat and Elbers (1994). As expected from Fig. 5.26, Bowen ratios were considerably smaller for the savannah site. For the wet season, values as low as 0.10 have been observed with the majority of the values being around 0.25. Ratios of up to 1.2 were found during the last week of the IOP (around day 282). The tiger-bush Bowen ratio values ranged from 0.25 to 0.8 in the wet and between 1.0 and 2.0 in the dry season.

It is interesting to see how the fluxes observed at the CWS compare to the results for the other super-sites. For this purpose, the findings of Gash et al. (1996) will be summarized here. These authors selected three days to illustrate the spatial variability of evaporation, as measured by ten participating groups at the various sites, in the HAPEX-square. Day 233 (20 August) was early in the IOP, when the vegetation at the SSS was already well developed (Wallace et al., 1994). The millet *LAI* was close to its maximum value and the fallow site vegetation was already well developed. In contrast, the vegetation at the other sites was relatively poorly developed because of the later start to the wet season, with the millet at the central sites still being at the seedling stage. Day 261 (17 September) was selected as an example of a day with wet soil, there having been rain on both days 258 and 259 at all sites. Day 282 fell after the wet season had ended, and was chosen to represent dry conditions, there having been no rain at Danguey Gourou during the previous 10 days or at the three main sites during the previous 23 days (Gash et al., 1996).

The day-time evaporative fraction, $\Sigma L_vE/(\Sigma L_vE + \Sigma H)$, and the day-time average evaporation rate were calculated for 9 to 16 GMT for each system operating on those days. It appeared that, when the data were presented as evaporative fraction, the variation between the systems at the same site, and over the same vegetation type was of the same size as the difference between sites and vegetation types. Gash et al. (1996) concluded that any interpretation of differences between sites and vegetation types must therefore be speculative, especially bearing in mind the differences of up to 20 %, which were typically to occur between instrument systems at the different sites. The data had been arranged as the average of each site, regardless of vegetation type and as the average for each vegetation type, regardless of site. There was no day when there appeared to be a great difference in evaporative fraction, although the millet sites appeared to be evaporating a smaller fraction of A_t on day 261 than the other vegetation types. The actual evaporation showed little difference between the three main sites, although L_vE at Danguey Gourou was consistently low, as was expected from the lower rainfall amounts. Note that at DG there was a millet field only.

When plotting data from the whole IOP as a time series it appeared that during the rainy period the evaporative fraction was approximately constantb - between 0.7 and 0.8 for the fallow savannah and tiger-bush, and between 0.6 and 0.8 for the millet. Evaporation started to diminish rapidly after about day number 260 for the millet and the tiger-bush, and after about day number 270 for the fallow. During the dry-down the evaporative fraction at the CES was consistently less than the values observed at the CWS and SSS (some 30 %). Tiger-bush values of evaporative fraction as observed for the CWS and the SSS were very similar. During the dry-down the values appeared to be slightly less than the values observed for fallow savannah. A similar trend was found for the SEBEX fallow savannah site (Gash et al., 1991).

b) SEBEX, annual course for savannah and tiger-bush

As stated in the previous paragraph, energy closure for the SEBEX tiger-bush site was moderate. Therefore, the L_vE -flux shown and used in Figs. 5.27 and 5.28 is the rest term of the energy balance for which the directly measured H and G, and the composite $R_{n,t}$ have been used.

Sensible heat fluxes, H_t, and latent heat fluxes, L_vE_t, are given in Fig. 5. 27 for both surface types. H roughly varies between 10 (end of wet season) and 100 (end of dry season) W m^{-2}. A large scatter is observed, but a clear downward trend after the beginning of the rains occurs (see 1990). During the rainy season, H of the tiger-bush appears to be similar or slightly higher than H observed for the savannah. During the dry-out period (1989), however, H for the tiger-bush is considerably lower than H for the savannah, for reasons explained below. The savannah latent heat flux shows an opposite course - L_vE ranges from nearly zero W m^{-2} before the rains until 150 W m^{-2} at the peak of the rainy season. Well after the rainy season, L_vE of the tiger-bush is higher than the savannah values. This is probably caused by the fact that the tiger-bush vegetation also consists of deeper rooting trees (such as *Combretum Nigricans*) which allows the usage of deeper soil water (see also Wallace et al., 1992; Culf et al., 1993). The higher density of the vegetation strips also ensures less soil evaporation, thus enabling the vegetation to stay green longer. L_vE already increases before the beginning of the rains which suggests that vegetation already starts to develop in the dry season. This is a regularly observed phenomenon in these semi-arid regions (Wallace et al., 1992; Von Maydell, 1990). It is supposed that some savannah species (among them *Guiera Senegalensis*) have underground storage organs from which they extract water before and during the beginning of the wet season.

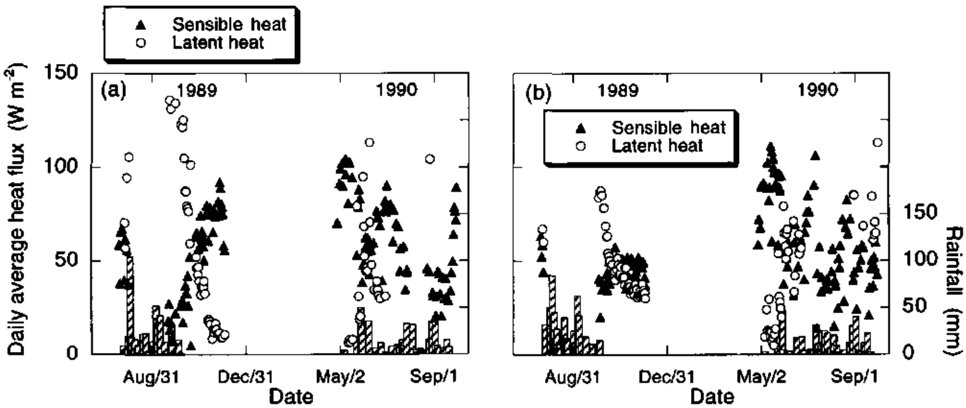

FIGURE 5.27. Sensible and latent heat fluxes for the SEBEX savannah (a) and tiger-bush (b) surfaces. L_vE is the rest term of the energy balance.

The fact that H above the tiger-bush is very low compared to the values for savannah is probably caused by the fact that part of the sensible heat is used for transpiration. This was also observed during the HAPEX-Sahel campaign.

Fig. 5.28 shows the evolution of Bowen ratio during the SEBEX campain. A 40-fold difference between wet and dry season was observed. Although tiger-bush values are similar to or higher than values observed for the savannah during the rainy period (as for the advantage of this type of model is that in practice the soil evaporation is connected to simple environmental conditions which are easily measured.

In this study, a simple evaporation model has been developed based on the assumption of the occurrence of free convective conditions which often prevail in semi-arid regions. Moreover, it incorporates the soil resistance to evaporation as proposed by Massman (1992). The modelled soil evaporation has been verified by micro-lysimeter data (CWS savannah, see Jacobs and Verhoef, 1996) and micro-BREB data (SSS tiger-bush), as summarized in Appendix 12. From the results presented in Appendix 12 the following main conclusions can be drawn.

1) If the soil exchange processes of heat and vapour are in the free or mixed convection state, the sensible and latent soil heat fluxes can easily be estimated by using Nusselt and Sherwood numbers for free convection.
2) By using the analogy between heat and moisture transport the vapour transport can also be estimated by using the Nusselt number along with the equilibrium Bowen ratio at the soil surface. The latter technique is simpler and often more accurate to execute under experimental field circumstances.
3) By using this technique the dependency of the Soil Bowen Ratio Coefficient, c_w, as a function of the soil moisture content of the topsoil must be known. This relation for a particular soil can be obtained by using micro-lysimeters or a micrometeorological method like the BREB method.
4) From the limited micro-lysimeter data available it appeared that the installation location, whether sunlit or shaded, hardly affects the evaporation rates obtained with the lysimeters.

The new method worked very satisfactorily (see Fig. A12.4) and it has been used to calculate the daily cumulative evaporation amounts for the savannah, because direct measurements (micro-lysimetry) were only obtained during a limited period of the IOP (days 244-254). Fig. 5.30a shows the cumulative values as calculated with the Sherwood-resistance model and the simple relationship (Eq. 2.34) where E_S is only a function of time (in days) for the last month (day 265-285) of the IOP. Results for the tiger-bush are given in Fig. 5.30b. It appears that all methods yield similar results (differences are within 10 to 20 %), especially when the soil becomes drier.

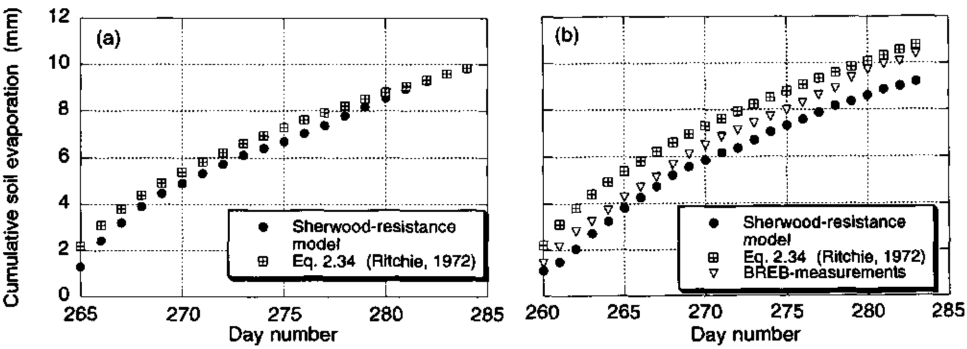

FIGURE 5.30. A comparison between the cumulative daily evaporation amount as calculated by the the Sherwood-resistance model, the Ritchie (1972) approach (Eq. 2.34), with α given a value of 2.2, and direct measurements (BREB method) for (a) savannah (CWS) and (b) tiger-bush (SSS).

b) Vegetation component latent heat fluxes

The stripped savannah surface (CWS a') provided the possibility of measuring the flux exchange above the grass/herb layer component only. However, strictly speaking, the results gathered here cannot be assumed to represent the understorey as encountered for the total savannah. Plots a and a' have a different source-sink distribution and resistance network because at plot a the separate components influence each other.

A comparison between H and L_vE for the 'grassland' site and the undisturbed WAUMET site showed a good agreement between both sites ($r^2 > 0.80$) which is encouraging. However, values of the grassland site were approximately 30 % lower, indicating that the relatively small bush coverage of 20 % at the savannah site, had a considerable influence on the total evaporation. This is supported by sap flow measurements and model calculations (§ 8.4, L_vE_b being larger than L_vE_u). The fact that H-values were also 30 % lower, probably resulted from the fact that the herb/grass layer at the grassland site was denser, therefore having less bare soil, and thus lower surface temperatures. Furthermore, as can be seen from Fig. 5.25, A_u is considerably less than A_b, which also contributes to the occurrence of lower fluxes. Accordance between $(H_u + E_u)$ and $(R_{n,u}\text{-}G_u)$ was less than for the total fluxes especially during the morning, when $(H_u + E_u)$ was much lower than $(R_{n,u}\text{-}G_u)$. E_u will be used later on in § 6.3.3 to inversely calculate the herb layer resistances, $1/g_{cs}$. However, note that the results may deviate from values found for an understorey with accompanying bushes, because g_{cs} does not represent plant physiology alone.

c) Partiononing of L_vE_t over all components

Fig. 5.31 shows the ratios of daily component evaporation (in mm to make it comparable to results presented by Allen and Grime, 1995 or Wallace and Holwill, 1996, for example), E_s, E_b or E_u (i.e. soil, bushes or undergrowth) and total evaporation as a function of day number for savannah (a) and tiger-bush (b). The tiger-bush data (EC and micro Bowen ratio system) were taken from the SSS, because no values on soil evaporation were availabe at CWS. Savannah E_b-values were obtained from two sap-flow gauges, whereas the E_s-values were calculated from the Sherwood-resistance model (see Appendices 5 and 12). Values for E_u were calculated from $(E_t - E_s - E_b)$. During the days 240-250 no E_t-data were available for the savannah due to instrument failure. It is realized that the limited number of two sap flow gauges (i.e. one stem on two bushes) will not yield a very representative sample of the *Guiera* vegetation. Allen and Grime (1995), for example, employed seven gauges to calculate an area-averaged transpiration for their fallow savannah (SEBEX 1990). Nevertheless, correlation between both gauges was high ($r^2 > 0.90$, both on a diurnal and daily basis) and flux magnitudes were very similar. Therefore, sap flow measurements will be used here as an estimate of E_b, although they have to be regarded with a certain amount of skepticism.

It appears that savannah E_b accounted for 20-35 % of the total evaporation - the lower percentages being representative for the wet period. At the end of the IOP, E_b/E_t gradually increased to 35 %, as a result of the undergrowth starting to senesce. Allen and Grime (1995) concluded that total seasonal transpiration from their *G. senegalensis* bushes was 35 % of the seasonal rainfall total. If we assume that under these semi-arid conditions approximately 100 % (for a normal to dry year) of all rainfall will be returned to the atmosphere as evaporation, this value of 35 % is similar to our values.

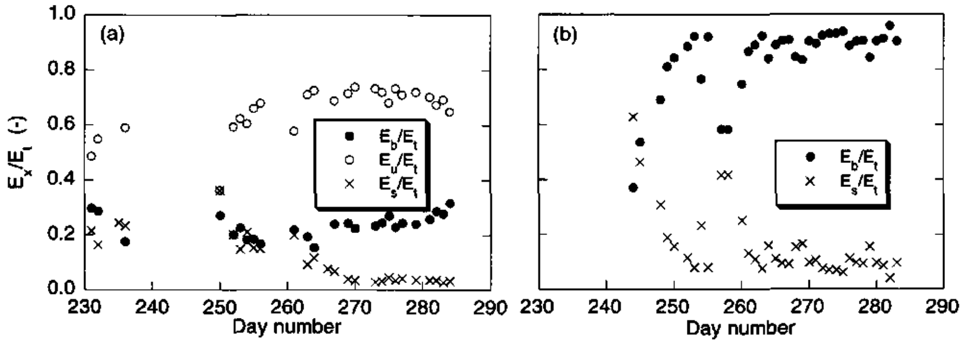

FIGURE 5.31. (a) Daily average ratios of bush, herb-layer and soil evaporation to total evaporation for the HAPEX-Sahel CWS savannah site and (b) daily average ratios of bush and soil evaporation to total evaporation for the HAPEX-Sahel SSS tiger-bush site.

Despite the same percentage of bush coverage (≈ 20 %) their values were slightly higher because of the higher values of LAI_b (peak values of 0.6 compared to 0.4 for the CWS savannah). As also observed by Allen and Grime (1995) and Dugas and Mayeux (1991), the bushes transpired more than expected on the basis of their areal cover. Savannah E_s accounted for ≈ 20 % during the wet season to ≈ 5 % at the end of the IOP. E_s/E_t was relatively large immediately after rain, but very rapidly decreased thereafter. Fig. 5.31a shows that application of a three component SVAT-model would be useful during the wet period. However, it would mean an unnecessary complication during the transition or dry period. The portion of the herb/grass layer, E_u/E_t, remains rather constant. At the beginning of the IOP (only few points available), LAI_u is still low, resulting in E_u/E_t-values of 0.5. At full development, values of 0.7 are reached, whereas at the end of the IOP (early senescence) a slight decline seems to occur.

In comparison with the savannah, the soil portion of total tiger-bush evaporation varied largely during the IOP. After rainfall, values of around 0.6 were attained, which diminished rapidly. At the end of the IOP, soil evaporation still acounted for 10-20 % of total evaporation. Values of E_b were not obtained from sap flow, but calculated from E_t-E_s. On most days E_s/E_t was higher than 0.8, except for those days on which rainfall occurred. The sharp decrease in E_t at the end of the IOP was mainly caused by the drying vegetation component and not by the drying soil. Again, the bush component accounted for a larger part of E_t than expected from its areal cover (33 %).

5.6 Conclusions

a) Radiation

To ensure proper values of $R_{n,b}$ for this sparse Sahelian vegetation, necessary to evaluate A_t and for separate component input in multi-layer SVATs, it is of vital importance to place the radiometers in close proximity to the scattered vegetation elements. Although this leads to a smaller area being seen by the instruments, it will avoid cross-sampling of the adjacent surfaces. In both the HAPEX-Sahel and the SEBEX experiments, this condition was not met, especially for the tiger-bush sites. Difference between directly measured $R_{n,b}$ and $R_{n,b}$ based on the sum of the individual shortwave and longwave radiation components, were therefore considerable. It is advised to actually install the radiometers measuring outgoing $R_{n,u/s}$ and $a_{u/s}R_s$ at a greater height for the bare and understorey radiation measurements, to ensure a larger representative area and to diminish the influence of spatial variability.

It became clear that the large difference between daily averaged tiger-bush and the savannah R_n as observed during SEBEX (savannah having predominantly higher values of R_n) is apparent and probably caused by the measurement design. Calculation of $R_n = (1-a)R_s + R_{l,\downarrow} - R_{l,\uparrow}$ leads to the conclusion that values of tiger-bush R_n are generally slightly higher than the values observed over savannah, being in agreement with the observations made during HAPEX-Sahel. Although tiger-bush albedo is higher, $R_{l,\uparrow}$ is lower for the majority of the days observed. Although intuitively higher values of $R_{l,\uparrow}$ are expected for the tiger-bush, because of relatively large patches of bare soil, this does not appear to be the case for most of the year. This is mainly caused by the different partition of vegetated and less vegetated/unvegetated areas for both surfaces and by the fact that during the dry season the undergrowth of the savannah disappears, mainly leaving bare soil and therefore T_s-values similar to the tiger-bush soil.

Measurements of surface temperature, T_s, for sparse vegetations featuring a large percentage of high grass (FIVE, 1989; HAPEX-Sahel, 1992) should be considered with care. Vertically installed, nadir viewing IRTs are very likely to look between the blades of grass, thus seeing mainly bare soil. This phenomenon was also observed by Malhi (1993). This will lead to too high values for T_s which may have serious implications for the values of the excess surface resistance (kB^{-1}) when it is inversely calculated from H and (T_s-T_a) and thus for the fluxes calculated for this area such as those derived by a combination of remote sensing and a bulk transfer equation.

b) Soil heat flux

For the soil heat flux a simple linear summation of the component heat fluxes G_u, G_s and G_b, multiplied by their relative coverage fractions, yields a good estimate of G_t. However, to find the individual values of $G_{u/s}$, which are most important because they occupy the largest area and exhibit values roughly three times as high as G_b, a robust method has to be selected. It appeared that the Calorimetric method met requirements best - it was relatively insensitive to used values of top soil thermal soil properties and it ensured the best SEB closure. However, it required the most sensors, in comparison to the other methods, which may be a disadvantage when used at remote sites. However, 'investing' in a reliable estimate of G may be worthwhile, as there is increasing evidence that the differences in evaporative fraction and actual evapotranspiration as observed over the HAPEX-square and probably over other (semi-arid) areas, are largely caused by differences in available energy.

The dry-out of the upper soil layers, which determine the surface soil heat flux, occurs during a relatively short transition period of approximately one month. After that, soil thermal properties already reach the dry-period values. Sensible and latent heat flux, being dependent on much deeper soil moisture, exhibit a much more gradual decrease, but still appear to reach their dry season values in a relatively short time.

c) Available energy

Tiger-bush appeared to have the highest values of available energy, A_t, as confirmed by findings of Gash et al. (1996). This was mainly caused by higher values of $R_{n,t}$, being the result of a higher bush coverage (33 % as opposed to 20 %) for which considerably higher values of net radiation (up to 300 W m^{-2} more than $R_{n,u}$ and $R_{n,s}$) were found and by lower values of G_t. $G_{u/s}$ and G_b for tiger-bush and fallow savannah were very similar, but again the higher proportion of bushes observed for the tiger-bush lead to these slightly lower values of G_t for tiger-bush, thus also contributing to higher values of A_t. The differences in A_t between fallow savannah and tiger-bush were about 10 % on a diurnal and on a cumulative basis. However, taking into account the differences of up to 20 %, which were typically observed to occur between instrument systems (see Lloyd et al., 1996), this difference must be considered speculative. On the other hand, it has been found for all three supersites and in Chapter 8 it will be shown that this difference is plausible.

d) Sensible and latent heat fluxes

Differences between savannah and tiger-bush sensible and latent heat fluxes are pronounced. During the rainy period, evaporation of the tiger-bush will be largest, because of the contribution of soil evaporation. During approximately a month after the last rainfall, the savannah will be evaporating more owing to the green understorey. After senescense of the undergrowth, L_vE for savannah is rapidly reduced to values near zero. However, there are indications that tiger-bush evaporation continues (see also Culf et al., 1993), probably during the whole dry season, although at a relatively low rate.

The method propsed by e.g. Søgaard and McAneney (1994), where daily values of sensible heat flux can be found from maximum air temperature and surface temperature at 1400 GMT appears to give very plausible results for the savannah and tiger-bush.

For calculation of daily or cumulative soil evaporation the square-root formula (Ritchie, 1972) works very satisfactorily. For both the savannah and the tiger-bush, as well as for the millet soil component (See Wallace and Holwill, 1996), the constant equals 2.2. This is very convenient for obtaining large-scale areal estimates of E_s.

e) General

Besides being confusing, using erroneous R_n-data may yield wrong values of sensible and latent heat fluxes (if the BREB method is used), it may lead lead to unnecessary rejection of other SEB fluxes (L_vE or H as measured by the EC technique, because of failing SEB-closure) or even cause rejection of entire SVATs because they were run with or checked with the wrong input data. Hence, for further calculations concerning the HAPEX-Sahel experiment the directly measured R_n-values will only be used for the bare soil and understorey surfaces. The 'indirect' R_n will be used in the next chapters for the SEBEX-experiment only.

The hypothesis that differences in evaporative fraction and actual evapotranspiration as observed over the HAPEX-square are mainly caused by differences in A_t and not by significant differences in surface resistances (Blyth, 1995; Gash et al., 1996) will be tested in Chapter 8. This assumption may be valid during the wet or transition season but might not be during the dry season.

6 THE RESISTANCE NETWORK

6.1 Introduction

This chapter describes the components of the resistance network forming the basis of the SVATs described in Chapter 4, by employing a combination of field measurements and model parameterizations. Furthermore, the diurnal or seasonal course of a particular conductance or resistance can give insight in the behaviour of the canopy as a result of changing environmental (atmospheric and soil) or intrinsic (flowering, leaf shedding) conditions.

First, the surface parameters necessary to calculate aerodynamic resistances for single-layer bulk transfer models (z_{0m}, z_{0h} and d) and two-layer SVATs (z_{0m} and d) will be considered. In § 6.2.1, the parameters z_{0m} and d will be calculated with a detailed drag partition model (Raupach, 1992) in order to asses the agreement between these predictions and previous, simpler estimates and the 'measured' values. These calculations include the HAPEX-Sahel and SEBEX surfaces, but also three other savannah estimates and similar types of surfaces also vegetated with bush-type, sparse canopies (vineyards, cotton crops and low orchards) serving for comparison. Next, the scalar roughness length (here taken as z_{0h}) for heat will be studied, by considering the quantity kB^{-1}. Section 6.2.2 will present values of kB^{-1} for two sparse canopies, together with a bare soil acting as a (smooth) reference surface. In Section 6.2.3 the conclusions on the previous two sections will be given.

Section 6.3 describes the leaf and canopy conductance, the latter having being obtained by both the bottom-up and top-down technique. § 6.4 gives some values of the soil surface resistance (r_s^s in Chapter 4). Finally, Section 6.5 summarizes the surface conductances for the two stories (upper canopy and understorey, the latter being a herb-grass layer or soil) encountered for the savannah and tiger-bush. There is a growing consensus among scientists that for most vegetation-types, but especially for (semi)-arid rainfed agriculture crops or natural vegetation, canopy surface resistances are the most important ones (Van den Hurk et al., 1996; Huntingford et al., 1995). This means that measurements of leaf conductance and LAI_c (to scale-up from the leaf to the canopy scale) have to be executed with great care as the canopy conductance largely determines the final transpiration estimate.

6.2 Parameters for calculation of aerodynamic resistances

6.2.1 Roughness length and displacement height for momentum

a) General

Reliable values of z_{0m} and d are indispensable for a check on the measured (with the EC-technique) momentum fluxes and for calculation of aerodynamic resistances. We therefore need reliable methods or adequate working relationships to estimate z_{0m} and d that will also work in the case of sparse canopies.

Many articles about the determination and evaluation of z_{0m} and d for closed canopies are available in literature. Early results were summarized by the relations $d = 0.66h$ and $z_{0m} = 0.13h$ (Monteith, 1973). So far as the roughness parameters for vegetation under incomplete canopy cover are concerned, fewer experiments have been conducted and their

z_{0m}/h and d/h-ratios seem to vary widely. As an illustration: Garratt (1978) found a z_{0m}/h -ratio of 0.05 for a natural savannah, whereas Hatfield (1989) calculated ratios close to 0.5 for a cotton canopy. Ratios of d/h were usually around 0.6 (sometimes d was set to 60 % of canopy height instead of calculated, see Garratt, 1978, for example), although several authors assumed (Hicks, 1973) or calculated (Riou et al., 1987) a negligible zero plane displacement. Both these authors studied the aerodynamic properties of flat, extensive vineyards. They claimed that the aerodynamic properties of their row crops will vary with wind direction. This led for the vineyard of Riou et al. to d=0.75 and z_{0m} = 0.20 for winds blowing across the rows, whereas parallel flow resulted in d = 0 and z_{0m} = 0.55. However, for other row crops (for example, Hatfield, 1989) no significant effect of wind direction on values of z_{0m} and d has been recorded. A possible cause for the occasionally observed change of z_{0m} and d with wind direction, may be found in the boom on which the anemometers are mounted and the direction in which it points. Another complication of row crops is the fact that they are frequently placed on furrows. According to Kustas et al. (1989), who measured z_{0m} and d over an incomplete canopy cover of cotton, the furrows seem to contribute significantly to the magnitudes of d. The problem of non-homogeneity was studied by Dolman et al. (1992) for a tiger-bush vegetation.

The aim of Section 6.2.1 is therefore to assemble data from sites with sparse vegetation (including the HAPEX-Sahel and SEBEX experiments) and to compare this new collection of z_{0m} and d values with previous experimental results and Raupach's (1992) drag partition theory (see § 4.5), originally established for medium-sparse canopies. This defines whether z_{0m} and d can be estimated from vegetation characteristics such as canopy height, h, and density, λ. Roughness estimates with the relationships z_{0m}= 0.13h and d= 0.66h are given for comparison, because there are circumstances where no data on vegetation characteristics are available and because these relationships are simple and still widely used (see Eq. 4.8 - 4.10).

Before the new data can be used to extend existing knowledge, their quality has to be assessed thoroughly. The 'rules' by which the data are judged are described in Appendix 13. They comprise of available fetch, site homogeneity and the height of the instruments compared to z^*.

b) Summary of experiments and quality assessment

Table 6.1 gives 14 experimental values of z_{0m} and d, as well as vegetation characteristics (h, b, D, λ), and a qualification of fetch, homogeneity and measurement height plus an overall quality rating. All savannahs exhibited an undergrowth of (sparse) grasses, the row crops and tiger-bush were situated on bare soil (except for the orchard, R7, which had a ground cover of grass).

The fetch was evaluated by comparing the fetch as calculated with Eq. A13.1 with the fetch available during the experiment. With Eq. A13.1, minimally necessary fetches were calculated using estimated roughness lengths and maximum height of wind speed measurements as input. Sometimes, experimental fetches were explicitly stated, while in other cases the fetch was given as 'several kilometres' (S2, S3). Occasionally the fetch varied with wind direction (see, for example, S4 and R5). For this quality-column + means that the experiment fetch was larger than the calculated fetch, 0 denotes that the available fetch was equal or slightly less than the value calculated by Eq. A13.1 and - means that the experiment fetch was considerably smaller (< 50 %) than the calculation. The homogeneity of the experimental sites was judged qualitatively as good (+) or moderate (0) mainly depending on the variety of surrounding surface types. Canopy types R5 and R7 appear twice, because they had two different values of z_{0m} depending on wind direction (R5) or LAI_c (R7). In this study z^* was calculated with $z^* = 20z_{0m} + d$ (given in De Bruin and Moore, 1985, see Appendix

13), after which its value was compared with measurement height of wind speed to obtain the quality rating. Other formulas, mainly using spacing *D*, were tested but they appeared to give unreliable z^*-values for reasons explained in Appendix 13. When all *u*-levels were higher than z^*, + was given to the experiments. With no levels above z^* the experiment was given -. With two or three levels above z^* the experiment was rated as average (0). For the final quality rating + is only given to those data sets with three plus signs in the foregoing columns, whereas - designates that one of the three criteria was not met. All the intermediate cases are assigned 0.

TABLE 6.1. Summary of canopy and roughness characteristics plus quality rating of 14 bush-type sparse canopies.

Vegetation-type	h [m]	D [m]	b [m]	λ	z_{0m} [m]	d [m]	Fetch	Homo-geneity	z^*	Data Quality	Reference
Scattered crops											
Savannah, S1	2.3	5.0	3.5	0.32	0.44	1.80	+	+	0	0	Chen Fazu and Schwerdtfeger, 1989
Savannah, S2	8.0	20.0	2.0	0.03	0.40	4.80	+	+	+	+	Garratt, 1980
Savannah, S3	9.5	10.0	2.0	0.19	0.90	7.10	+	+	+	+	Garratt, 1980
Savannah, S4	2.3	3.4	3.0	0.60	0.17	0.93	-	0	0	-	Lloyd et al., 1989
Savannah, S5	2.5	6.6	3.0	0.17	0.25	1.14	+	0	0	0	This thesis
Tiger-bush,T1	4.0	40	20	0.05	0.44	2.00	0	+	+	0	Dolman et al., 1992
Tiger-bush,T2	4.0	40	20	0.05	0.15	3.70	0	+	-	-	This thesis
Row crops											
Vineyard, R1	0.90	1.5/5.0	0.70	0.04	0.095	0.0	+	+	-	-	Hicks, 1973
Vineyard, R2	0.90	2.5	0.90	0.13	0.08	0.31	+	+	0	0	Van den Hurk, 1995
Cotton, R3	0.49	1.0/0.5	0.25	0.19	0.066	0.31	+	0	0	0	Kustas et al., 1989a
Cotton, R4	0.38	1.0	0.30	0.10	0.16	0.10	+	+	-	-	Hatfield, 1989
Vineyard, R5	1.5	1.75	0.30	0.16	0.55	0.0	0	0	-	-	(a) Riou et al., (1987) parallel flow
Vineyard, R5	1.5	1.75	0.30	0.16	0.20	0.75	-	0	0	0	(b) Riou et al., (1987) across flow
Vineyard, R6	2.0	2.0	1.0	0.50	0.25	1.40	-	+	-	-	Weiss and Allen (1976)
Orchard, R7	3.7	7.3	4.0	0.28	0.23	0.92	-	0	0	-	(a) Randall (1969) leafless
Orchard, R7	3.7	7.3	4.0	0.28	1.22	0.92	-	0	-	-	(b) Randall (1969) full leaf

Most experimental sites appear to have a sufficient fetch except for the S4, R5 (across flow), R6 and R7 experiments. We know that the calculated fetch is a function of maximum measurement height and of roughness length. Because the S4, R5, R6 and R7 fetches were most likely too small, the z_{0m}-values should be distrusted. However, even if we change the z_{0m}-values of S4, R5, R6 and R7 experiments to more realistic values, the calculated fetches are much larger than the experimentally achieved fetches. Therefore, the validity of the z_{0m} and *d*-values of the experiments labelled with - may be doubted. According to calculated values of z^* all levels for the surfaces S2 and T1 were acceptable: surfaces with a very low value for λ.

For the S1, S4, S5, R2, and R3 case, level 1 and/or level 2 turned out to be unreliable. For T2, R1, R4, R5 (a), R6 and R7 (b) no cup-level seemed to be high enough. For the cases R5 (b) and R7(a) only 2 out of 5 and 7 levels, respectively, appeared to be valid.

c) Comparison of data with drag partition model (Raupach, 1992)
In this section an attempt is made to answer the following questions.

- How well are the roughness parameters presented in Table 6.1 predicted by the model as summarized in § 4.5 ? And what is the influence of parameters like b/h, c_d, C_S, C_R. For example: do we really need estimates of b instead of taking b/h=1 as assumed by Raupach ? Or : is $C_R = 0.30$ the best value for the sparse canopies considered in this paper ?
- Is its predictive performance better than the simple rules of thumb; $z_{0m} = 0.13h$ or $d = 0.66h$?
- Are the collected good/fair quality sparse canopy data a useful extension of existing closed-canopy knowledge ?

The model performance (with different parameters as input) will be tested by comparing predicted with measured values of z_{0m} and d. Only the reduced data set (+, 0) will be considered for this purpose. To find the best combination of parameter values two sums of squares (SSQ_{z0m} and SSQ_d), being the squared differences between predicted and measured values of z_{0m} and d , respectively, will be used as the criterion. The minimum (i.e. best) SSQ-value will be labelled with a performance index equal to one, the second lowest value with a two, et cetera.

However, changing a particular model parameter may increase predictability of one roughness parameter, whereas it may cause the predictions of the other to be less accurate. For this reason the SSQ-values of z_{0m} and d-predictions were multiplied and also ranked according to performance. Note that the model estimate of z_{0m} is dependent on d (see Eq. 4.87), which means that a certain parameter combination leading to a suboptimal d-prediction may give the best z_{0m}-prediction. In all cases we will aim for more accurate z_{0m} predictions, because this parameter represents the drag at the surface, whereas d is a structure parameter only. Furthermore, from Eq. 4.8, for example, it appears that a small difference in z_{0m}, compared to d, might cause a large change in calculated aerodynamic resistance. In addition, for practical purposes (such as meso-scale models), the first model level, z, is usually much higher than d. Hence, it is always preferable to target for the best estimate of z_{0m}, even if this means a suboptimal d-prediction.

A total of 72 parameter-combinations were used as input for the model, by allowing b/h, c_d, C_S, C_R and c_l to vary. The used options were $b/h = 1$ or $b/h \neq 1$, $c_d = 0.3$, 0.6 or 1.2, $C_R = 0.3$ (as used by Raupach), 0.4 (cubes) and 0.25 (cylinders), $c_l = 0.37$ or 0.50, and C_S = standard (0.003 and 0.01) or double the standard (0.006 and 0.02).

Table 6.2 gives the parameter combinations for the five runs having the lowest values of $SSQ_d{*}SSQ_{z0m}$ and their ranking, according to SSQ-values, if the model's performance for predicting z_{0m} and d is considered separately. The SSQ-values for the predictions with two widely-used formulas are given for comparison. In case a, z_{0m} and d are only a function of h, in case b, z_{0m} is related to d by an expression suggested by Thom (1971) with the constant 0.26 as given by Moore (1974). This is done to have an analogy with the drag partition model, where z_{0m} is also a function of d (see Eq. 4.87). Furthermore, this relationship is claimed to provide better results than $z_{0m} = 0.13h$ (Jacobs and Van Boxel, 1988).

*TABLE 6.2. Parameter combinations and their SSQ-values for z_{0m} and d-predictions yielding the best five model performances for the reduced (fair/good quality data, n=8) data set. The last three columns give the quality ranking if SSQ_d*SSQ_{z0m}, SSQ_d and SSQ_{z0m} are considered, respectively. The * indicates the standard parameter combination as used by Raupach (1992).*

							performance index		
b/h	c_d	C_S	C_R	c_l	SSQ_d	SSQ_{z0m}	combi	d	z_{0m}
≠1	0.3	st.	0.40	0.37	1.102	0.113	1	1	4
≠1	0.3	st.	0.40	0.50	1.177	0.166	2	2	10
≠1	0.6	st.	0.40	0.50	3.107	0.078	3	18	1
≠1	0.6	st.	0.30	0.37	3.069	0.079	4	17	2*
≠1	0.3	st.	0.30	0.37	1.277	0.215	6	4	12
a.	$z_{0m} = 0.13h$		$d = 0.66h$		1.577	0.555	15	7	28
b.	$z_{0m} = 0.26(h\text{-}d)$		$d = 0.66h$		1.577	0.168	5	7	11

The lowest SSQ_d (1.102) is obtained with $b/h \neq 1$, $c_d = 0.3$, C_S = standard, $C_R = 0.4$ and $c_l = 0.37$. The standard combination (*) ranks 17. Predictions with d=0.66 h are the seventh best. If we only consider the SSQ-values for z_{0m}-predictions, the best parameter set would be $b/h \neq 1$, $c_d = 0.6$,C_S = standard, $C_R = 0.4$ and $c_l = 0.50$. In this case the standard parameter set ranks second. The predictions with $z_{0m} = 0.13h$ lead to a high SSQ and are therefore unfavourable, although the inclusion of d in Eq. b make z_{0m}-predictions much better compared to z_{0m}=0.13h. Considering the trade-off between z_{0m} and d-predictions (i.e. the combined performance index), it appears that a combination of $c_d = 0.3$, $C_R = 0.4$ and $c_l = 0.50$ appears to give the best results, whereas the standard data set as proposed by Raupach (1992) ranks fourth.

A graph of predicted versus measured z_{0m} and d, using the best parameter combination, is given in Fig. 6.1a and 6.1b, respectively. The symbols reflect the good, fair and poor data. Fig. 6.1 shows that for the majority of the surfaces the measured and predicted values for z_{0m} and d are rather close, especially if we bear in mind the large values for standard deviation which are a result of most methods. See, for example Garratt (1978) giving $z_{0m} = 0.4 \pm 0.2$ m and $d = 4.8 \pm 1.0$ m, or $z_{0m} = 0.066 \pm 0.043$ m and $d = 0.31 \pm 0.20$ m (Kustas et al., 1989). S4, T1, R1, R4, R5 and R7 exhibit large differences between their values of 'measured' and predicted displacement heights. This does not come as a surprise if we look again at the quality rating column presented in Table 6.1. The surfaces with relatively high discrepancies between the experimental values and the predicted values have either a bad fetch and/or one or more wind speed levels situated within the roughness sub-layer. If we were to omit the lower two levels for the S4-surface, for example, we would arrive at a higher z_{0m} and d-value (see Fig. 4 in Lloyd et al., 1989).

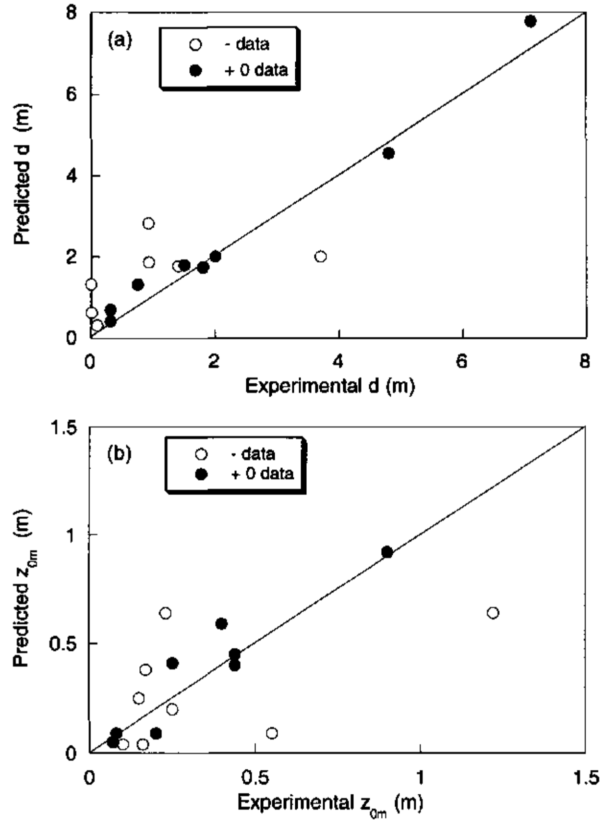

FIGURE 6.1. Relationship between predicted and experimentally obtained values of displacement height (a) and roughness length (b). Predictions were found from the best parameter combinations as given in Table 6.2. For d this means $b/h \neq 1$, $c_d = 0.3$, $C_S = st.$, $C_R = 0.4$, $c_l = 0.37$, whereas for z_{0m} $b/h \neq 1$, $c_d = 0.6$, $C_S = st.$, $C_R = 0.4$, $c_l = 0.50$. The closed circles represent the fair/good quality data, the open circles the - data. Correlation coefficients (+ data only) are 0.98 and 0.89 for d and z_{0m}, respectively. If we use the z_{0m}-parameter set to predict d too, r^2 decreases to 0.93.

Finally, we skipped the '-' experiments and we combined the remaining eight values with Raupach's data set (closed triangles). The behaviour of this combined data set is depicted in Fig. 6.2.

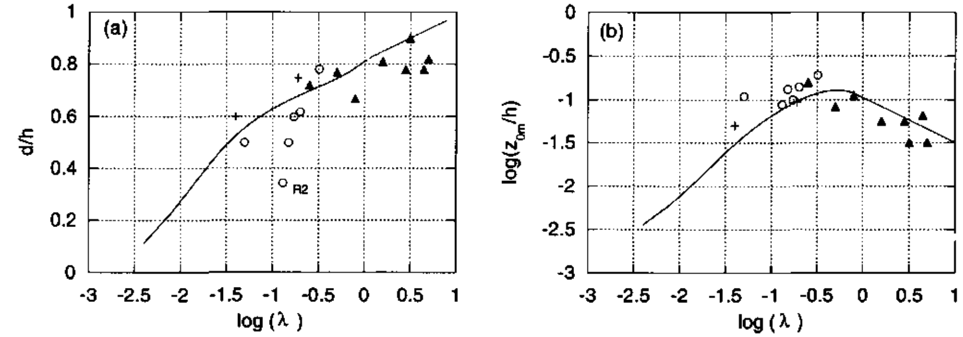

FIGURE 6.2. Experimental values of d/h and $\log(z_{0m}/h)$ as a function of $\log(\lambda)$ for the selected (sufficient fetch, enough measurements above z^*) vegetation-types of Table 6.1. The closed triangles represent the data of Raupach et al. (1980). The line designates model predictions with $c_d = 0.6$ and $b/h = 1.0$.

The solid line represents drag partition theory with the parameter values set to Raupach's original values and it serves for comparison only. It appears that the sparse canopies presented in Table 6.1 enable verification of Raupach's theory until values of $\log(\lambda) = -1.5$. The limited amount of data points per surface type (four savannahs, four row crops) makes the assumption of different parameter combinations for specific canopy types unwarranted, especially because optimal z_{0m} and d -predictions require different parameter sets.

6.2.2 Roughness length for heat transfer

a) Literature overview

Garratt and Hicks (1973) presented an overview of experimental data on z_{0h} and kB^{-1}. They tested the relationship for z_{0h} proposed by Sverdrup (1937) and Sheppard (1958) for aerodynamically smooth surfaces that is based on the assumption that eddy and molecular diffusivities are additive. In addition, they considered the relationship obtained from wind tunnel experiments by Owen and Thomson (1963) that relates kB^{-1} to the roughness Reynolds number (see Eq. A4.3). They collected data about a wide range of surface types, varying from smooth surfaces such as water, snow and bare soil, to vegetated ones covered with grass (short vegetation), vineyard and trees (tall vegetation). It was assumed that in the case of a water surface the roughness lengths for water vapour and heat transfer are the same. Also, data from wind tunnel experiments were collected refering to towelling, rough glass, artificial grass and surface arrays of cylinders and spheres. They found that for smooth natural surfaces the bulk of the data lies close to values resulting from the assumption that eddy and molecular diffusivities are additive, but the data do not unambiguously support the mathematical form predicted from this assumption. Also, it was found that for kB^{-1} a modified Owen-Thomson relation holds for $5 < Re^* < 100$. It was found that for values of $Re^* > 100$, kB^{-1} increases further with increasing Re^* for so-called bluff bodies. Recently, Kohsiek et al. (1993, see also the corrigendum, 1994) analysed data for a large flat terrain in La Crau (southern France) covered with scattered piles of bluff bodies, i.e. one m high piles of stones. Between these stone piles the surface is flat and covered with stones and sparse grass and herbs. They found that kB^{-1} increases with Re^*, but less than the bluff body curve of Garratt and Hicks (1973) indicates. The La Crau terrain apparently behaves as a transition between a real bluff body and permeable rough obstacles.

For natural surfaces covered with fibrous roughness elements Garratt and Hicks (1973) found that the 'kB^{-1} versus Re^* -curve bends slightly down for larger values of Re^*, but kB^{-1} is virtually constant over a wide range of Re^*. The latter is in agreement with the findings of Thom (1972) and those of Brutsaert (1982) who reviewed studies made before 1982. In many meteorological models containing a sub-model for the vegetation-atmosphere interaction the results of Thom (1972) and Garratt and Hicks (1973) are used and kB^{-1} for vegetation is taken as a constant at about 2 (see, for example, Jacobs and De Bruin, 1992). Note that Rider and Robinson (1951) found a much higher kB^{-1}.

In a recent study Beljaars and Holtslag (1991) analysed a micrometeorological data set on grass land near the Cabauw tower in the Netherlands and they found a kB^{-1} of almost 9. However, they based their calculations on the effective roughness length for momentum that is needed to derive the area-averaged momentum flux on a scale of 10-50 km. At Cabauw the effective z_{0m} appears to be significantly larger than its local value (on a scale of about 100 m); in some wind directions the effective z_{0m} is 10-20 cm, whereas its small-scale value is about 1 cm (De Bruin, 1982). In an earlier (unpublished) study by Keijman and De Bruin (1979) in which a local z_{0m} was used, a kB^{-1}-value significantly greater than 2 was also found for a similar grass field near the Cabauw tower. Recently, Duynkerke (1992) also found a much higher kB^{-1} for another Cabauw data set (also grass). He discovered a clear dependence of kB^{-1} on u_*, while he used only meteorological data observed close to the ground ($z < 2$m). We conclude that even for a simple surface such as a grass, there is in the literature no unanimity about kB^{-1} (see also the review by Hewer, 1993).

Where there is sparse canopy things become even more complicated. During day-time the temperature difference between the various surface elements can be very large. For instance, the transpiring vegetation will have a temperature close to air temperature at reference height, whereas the non-evaporating bare soil can easily be 25 °C warmer. The temperature distribution at the surface will be determined also by shading effects, for example, which can cause kB^{-1} to become dependent on the solar angle. Several authors have considered the roughness lengths for heat and momentum of partial canopy surfaces (e.g. Verma and Barfield, 1979; Garratt, 1980; Hatfield et al., 1985; Kustas et al., 1989; Malhi, 1993; Stewart et al., 1994; Blyth and Dolman, 1995). Again, the results are to some extent conflicting.

Experimental determination of kB^{-1} requires independent observations of the fluxes of momentum and sensible heat flux, as well as the air and surface temperature. The latter is difficult to obtain. First of all, the exact location of T_s is difficult to define, while conventional thermometers are in fact useless, because close to the ground the vertical and horizontal temperature differences are large. In all recent studies T_s is obtained with an IRT. However, IRT data require corrections for emissivity of the surface, view angle and atmospheric effects.

An objective here is to discuss various features relating to z_{0h}. Using a coupled vegetation-PBL-model (Jacobs, 1994), it will be shown that surface temperature and surface conductance are sensitive to z_{0h} or kB^{-1}. Next, experimental data on kB^{-1} of three different surface types will be presented, namely smoothened bare soil (FLEVO-I experiment, Ten Berge, 1990), a vineyard (EFEDA-I) and a fallow savannah (HAPEX-Sahel, CWS). The first surface type is chosen for reference. In contrast to the roughness length for momentum z_{0m}, there does not exist a simple rule of thumb to determine z_{0h}, while it is also difficult to derive this quantity from field observations. Therefore, this section will also compare the measured values of kB^{-1} with various parameterizations that have been proposed in the literature (see Appendix 4).

b) A small sensitivity study

In order to get an impression of the sensitivity of T_s and related parameters to kB^{-1}, the coupled vegetation-PBL model used by Jacobs (1994) has been applied. The PBL part is the same as used by De Bruin and Jacobs (1989) and Jacobs and De Bruin (1992) and originates from Troen and Mahrt (1984). The vegetation sub-model is essentially the big-leaf approach by Monteith, in which the surface conductance is dependent on environmental conditions. The g_l-parameterization is physiology-based (see Jacobs, 1994). For the test case, the model has been initialized with fair weather Mid Latitude Summer profiles for a hypothetical vegetation (z_{0m} = 0.10 m, LAI = 3.0, equivalent to grass) near De Bilt (The Netherlands). Values for kB^{-1} were varied from 2.0 to 12. A value of 9.0 was found by Beljaars and Holtslag (1991), whereas Duynkerke (1992) found a value of 6.0 for the same vegetation.

It appeared that for values of kB^{-1} of 8 or higher the stomata started to close around 8 GMT. A kB^{-1} value of 12 halved the canopy conductance, compared to kB^{-1} = 2 or 4. When radiation, and thus temperature, decreased the stomata reopened again. This decreased g_c will lower the transpiration considerably (although transpiration at the same time is increased by the higher surface temperatures). It might be clear that too high values of kB^{-1}may lead to anomalous results for the energy balance of the vegetation under consideration. Surface temperature and surface conductance appear to be sensitive for variation of kB^{-1} indicating that it is important to know kB^{-1} fairly accurately and that uncertainties about this parameter must be solved.

c) Results: Average kB^{-1}

In this section, values of kB^{-1} were calculated with Eq. 2.29 for the vineyard, savannah and bare soil surface. Determination of kB^{-1} was not possible for the HAPEX-Sahel tiger-bush, because bush temperatures were not available. Effective surface temperature, $T_{s,t}$, was calculated as described in Appendix 7. To avoid anomalous outcomes due to small flux values, kB^{-1} for the vegetated surfaces was computed for those cases where T_s-T_a > 0.05, $w'T'$ > 0.05, and u^* > 0.1. The $w'T'$ and u^*-constraints were set to 0.01 for the bare soil surface.

Table 6.2 gives the number of observations for the time slots satisfying the constraints and the average values of kB^{-1} for the three surfaces, when improper fetch conditions and erroneous data are neglected. The values for the vegetated surfaces are high compared to the values as given by Stewart et al. (1994) for similar surfaces. For the SEBEX savannah experiment (see Table 4, Stewart et al., 1994) an average kB^{-1} value of 5.8 was found. This is about twice as low as the value found for the HAPEX-experiment, even though canopy and roughness characteristics are comparable. However, Malhi (1993) reported a value of 13.5 for a similar type of savannah at the HAPEX-Sahel SSS. His value for a vineyard located in the vicinity of the site instrumented by WAUMET during the EFEDA-experiment was 6.5 which is considerably lower than the value listed in Table 6.2. The value found for the bare soil (FLEVO-I) is in accordance with values gives by Garratt and Hicks (1973) for bare soil surfaces (mainly small negative values). Table 6.2 shows that a large variation in kB^{-1} occurred during the observation periods, the difference between minimum and maximum values being the largest in the case of the savannah.

TABLE 6.2. Average values of kB^{-1}, together with its standard deviation and minimum and maximum values as found for three surfaces.

Experiment	Surface	No. of observations (half hours)	kB^{-1} (avg.)	kB^{-1} (std.)	min	max
EFEDA	Vineyard	247	11.7	2.4	6.2	22.1
HAPEX-Sahel	Savannah	294	12.4	6.7	2.6	31.4
FLEVO-I	Bare soil	80	-0.7	3.3	-7.9	6.7

Average 'measured' values of kB^{-1} given in Table 6.2 are found from measured H-fluxes. In practise, however, we need estimates of kB^{-1} to find H from, for example, remote sensing measurements of T_s (Stewart et al., 1994) and simple meteorological measurements of T_a and wind speed. Therefore, the values given in Table 6.2 have been compared with the results as produced by simple formulae stated previously in the literature (see Appendix 4). These average values were plotted in Fig. 6.3, which has the same design as the graph given by Garratt and Hicks (1973), as a function of Re^*. It appears that the measured values of savannah and the vineyard are located in between the permeable rough and bluff-body branch, as Stewart et al. (1994) also found.

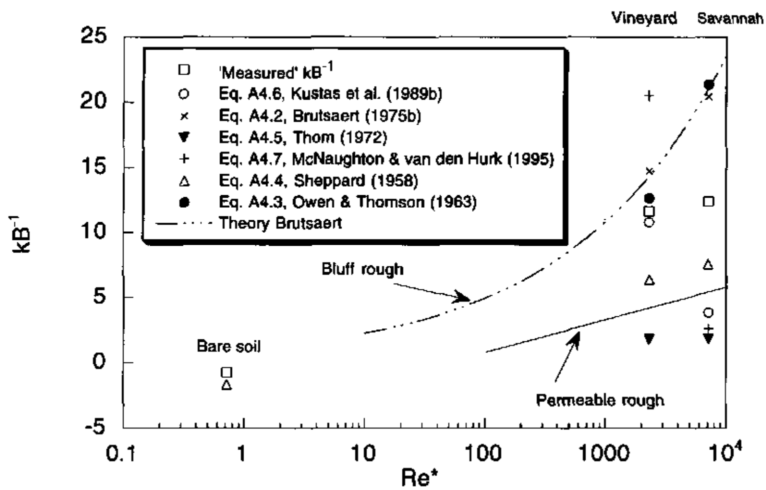

FIGURE 6.3. Average values of kB^{-1} as obtained from H, $(T_s\text{-}T_a)$ and u and as calculated by various empirical formulae (see Appendix 4).

A large deviation between the empirical equations and 'measurements' existed. For the vineyard, comparable estimates of average kB^{-1} were obtained with Eq. A4.6 (Kustas et al., 1989b), Eq. A4.3 (Owen and Thomson, 1963) and Eq. A4.2 (Brutsaert, 1975b). None of the formulae yielded values around 12 for the savannah; they were either lower (Eq. A.4.4, Sheppard, 1958), much lower (McNaughton and van den Hurk, 1995; Kustas et al., 1989b and Thom, 1972) or much higher (Brutsaert, 1975; Owen and Thomson, 1963). The Sheppard formula (Eq. A4.4), being developed for the whole range of Re^*-values, gives a negative value for the bare soil surface. The other formulas either do not apply (for example, Eq. A4.7, because no leaf width or *LAI* can be determined) or because they were specifically developed for rough (vegetated) surfaces. The formulae for smooth or transition surfaces (Eq. A4.8, A4.9 and A4.10), not shown in Fig. 6.3, yielded values of kB^{-1} of -1.17, -1.16 to -0.16 and -0.60, respectively. This is close to the 'measured' average of -0.73. The procedure of Thom (Eq. A4.5) yielded very low values of kB^{-1} for all surfaces. However, this formula was derived for a bean crop and should possibly be evaluated with appropriate values for *LAI* and mean leaf chord length.

c) Prediction of sensible heat flux

A proper value of kB^{-1} is important for a reliable estimate of the sensible heat flux by a simple, single layer model, i.e. a bulk transfer equation as given in Eq. 2.25. The performance of a kB^{-1}-estimate for a particular data set can therefore be tested by calculating the sensible heat flux and comparing these values to the measurements. This procedure has been followed for the three data sets and is summarized in Table 6.3. Differences between estimates are expressed as a sum of squares (SSQ = $\Sigma(w'T'_e\text{-}w'T'_m)^2$, where $w'T'_e$ and $w'T'_m$ are calculated on a **half-hourly** basis). The lowest SSQ-value will represent the best kB^{-1} estimate, although different criteria may lead to different ratings. For method 1, which yields the measured value of kB^{-1}, the difference between measurements and estimates should naturally be zero. The second best estimate will be found when we assign to kB^{-1} the average, constant value of all calculations. Table 6.3 shows that Methods 3 and 7 were performing best.

For the EFEDA data set the second method (Kustas et al., 1989b) also yielded low SSQ-estimates. The estimate following Kondo (1975), see Eq. A4.10, for the FLEVO-set yielded comparable values of SSQ.

Another way to express the performance of the various equations is to compare the **average measured** $w'T'$-value with the **average estimated** $w'T'$-value. In this case we use: $\Delta w'T' = \overline{w'T'}_e - \overline{w'T'}_m$. To express the influence of kB^{-1} in a percentage, in order to make it comparable to other computations, this difference is divided by the average measured flux, i.e. $\%w'T' = \frac{\Delta w'T'}{\overline{w'T'}_m}$. The same can be done for kB^{-1}, i.e. $\%kB^{-1} = \frac{\Delta kB^{-1}}{kB_m^{-1}}$, where $\Delta kB^{-1} = \overline{kB_e^{-1}} - \overline{kB_m^{-1}}$. A similar exercise was done by Stewart et al. (1994) who estimated that taking a kB^{-1} of 7 instead of the calculated value found for eight experiments conducted in semi-arid regions, yielded a percentage difference between $\overline{H_e}$ and $\overline{H_m}$ varying from 10 to 40 %. kB^{-1} for these surface varied between 3.8 (grass) and 12.4 (shrubs), which would be a percentage difference in kB^{-1} of +84 and - 44 %. These calculations were executed for the three surfaces studied here and plotted in Fig. 6.4 together with data from Stewart et al. (1994).

TABLE 6.3. The difference between the measured kinematic sensible heat flux ($w'T'$) and the sensible heat flux as calculated with a bulk transfer equation, $w'T' = (T_s-T_a)/r_h$. For the calculation of r_h several estimates of kB^{-1} were used, as computed by the various empirical equations listed at the bottom of this table. The numbers refer to these equations. The difference between measurements and estimates is expressed as a sum of squares, $\Sigma(w'T'_e-w'T'_m)^2$, where e stands for estimate and m for measured. kB^{-1} was either variable for each time slot (see e.g. Eq. A4.6 where kB^{-1} is a function of u, T_s and T_a measured during a certain time interval) or kept constant at the average value measured for the whole data set (i.e. the values represented in Fig. 6.3). Best performance is marked with an asterisk.

	EFEDA SSQ's (measured versus predicted $w'T'$)							
	1	2	3	4	5	6	7	
kB^{-1} variable	0	1.03	0.62	36.74	1.96	2.99	0.43*	
kB^{-1} constant	0.20	0.29	0.46	38.46	1.64	3.24	0.24*	
	HAPEX-Sahel SSQ's (measured versus predicted $w'T'$)							
	1	2	3	4	5	6	7	
kB^{-1} variable	0	5.25	0.89*	21.05	11.90	1.04	0.98	
kB^{-1} constant	0.39	6.88	0.87*	22.94	13.87	1.15	0.94	
	FLEVO-I SSQ's (measured versus predicted $w'T'$)							
	1	2	3	4	5	6	7	8
kB^{-1} variable	0	0.13	0.03	0.035		0.045	0.028*	0.035
kB^{-1} constant	0.029	0.073	0.027*	0.033		0.049	0.027*	0.027*

1 = 'Measured' kB^{-1} (Eq. 2.29)
2 = Kustas et al. 1989b (Eq. A4.6)
3 = Brutsaert, 1975b (Eq. A4.2)
4 = Thom, 1972 (Eq. A4.5)
5 = McNaughton and Van den Hurk, 1995 (Eq. A4.7)
6 = Sheppard, 1958 (Eq. A4.4)
7 = Owen and Thomson, 1968 (Eq. A4.3)
8 = Kondo, 1975 (Eq. A4.10 with λ=3 and measured Re^*)

All values representing vegetation appear to fall along a single curvilinear relationship in Fig. 6.4. The values for bare soil follow a straight line with a much smaller slope. The x-axis for the bare soil extends to + 800 % (the value found from the 'Kustas' method) which cannot be shown in this graph. The grass data point (the most right crossed square) from Stewart et al. (1994) deviates from the line. It is the only permeable rough surface used in the comparison, the other experiments concerned savannah, open forest (tiger-bush), shrubs and a mixture of stone piles and grass. It is therefore closer to the line of the bare soil, representing smooth/transition surfaces.

It can be deduced that using the 'wrong' value of kB^{-1} results in a much larger error for a rougher (bluff body) surface than for a smooth or permeable rough surface. An overestimation of kB^{-1} with 800 % yielded an error in H of -20 % only, for the bare soil. In the case of bare soil surfaces, the value of kB^{-1} is not of great importance for proper H-estimates because of the much larger value of r_{ah} compared to r_r.

Furthermore, it appeared that using a **larger** value of kB^{-1} than the 'actual' value for the vegetated surfaces leads to **smaller** differences between estimated and measured H (or $w'T'$) than when a too low value is used. This is especially apparent when the percentage difference is larger than 50 % and this is caused by the fact that H_e can never attain negative values because of the positive values of $(T_s$-$T_a)$ and r_h. It has therefore to be concluded that the widely-used value of 2.0 should be raised to at least 7.0.

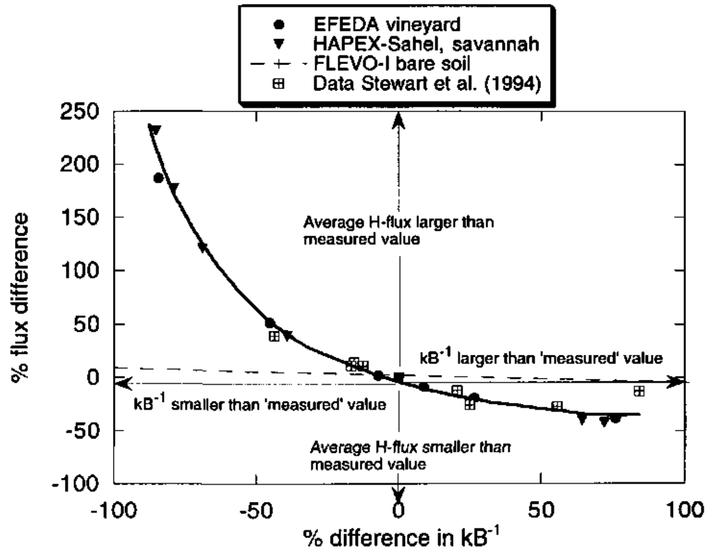

FIGURE 6.4. The result of a percent difference in kB^{-1} on the percent difference in H or w'T' expressed as $\frac{\Delta w'T'}{w'T'_m}$ for the various empirical estimates of the EFEDA, HAPEX-Sahel and FLEVO-I experiments and for the experiments as summarized by Stewart et al. (1994) where H as calculated with the actual value of kB^{-1} (i.e. measured H) is compared to values calculated with an average of 7.0.

d) Diurnal course of kB^{-1}

An examination of the diurnal course of kB^{-1} revealed that, in the case of the two vegetated surfaces, kB^{-1} exhibited a distinct variation with time. This variation was less for the bare soil, but still recognizable. Highest values were observed around noon for the vineyard, and lowest values during the morning and afternoon. In the case of the savannah, the same course was found for some days, but on other days the course was reversed or not clear. A possible explanation for this variation of kB^{-1} during the day for a sparsely vegetated surface was given by Kustas et al. (1989b). They suggested that in their study of a vegetation composed of a mixture of bushes (30 %) and bare soil, the rapidly drying soil became the major source of sensible heat, thereby increasing kB^{-1} (smaller z_{0h}). At the same time, the larger u-values also increased kB^{-1} because momentum transfer became more efficient relative to sensible heat transfer. This chain of reasoning may be used for the vineyard but it would not explain the reversed course observed for the savannah, unless we argue that the closure of the stomata after a certain time in the morning causes the herbs and grasses to exchange more sensible heat, thereby lifting the average source of heat to a higher level (and thus reducing kB^{-1}). The fact that kB^{-1} for the bare soil varies diurnally is not so obvious. The moving-source theory is not a very plausible explanation where this very smooth rolled soil is concerned (see Ten Berge, 1990). Nevertheless, the small soil crumbs may be compared to canopy elements, thus ensuring a diurnal change in source height on a micro-scale.

According to Garratt and Hicks (1973) a bluff-rough surface is characterized by a kB^{-1} being dependent on the roughness Reynolds number, whereas for a surface covered with roughness elements of a fibrous character this relationship is not evident (lower branch in Fig. 6.3). It appeared (not shown here) that none of the two vegetated surfaces exhibited a pronounced correlation between kB^{-1} and u_* (or wind speed, u). This is probably caused by the rather permeable character of the branches. Surprisingly, Malhi (1993) found a "very strong trend from $z_{0h} \sim 10^{-3}$ m at wind speeds of 1 m s^{-1} to $z_{0h} \sim 10^{-10}$ m at 6 m s^{-1} " for a similar savannah site. Correlation between u_* and kB^{-1} was practically negligible for the FLEVO-I bare soil. This is in accordance with the definition for B^{-1} (Eq. A4.8) for smooth surfaces as given by Von Kármán (Goldstein, 1938) and to the summary of formulae as listed by Brutsaert (1982).

For sparse canopies, that do not necessarily have the same sources and sinks for momentum and heat fluxes, it is questionable whether the concept of kB^{-1} resulting from the single-layer bulk-transfer approach is still physically sound. Blyth and Dolman (1995) compared z_{0h} found by a single source model to that calculated from a dual source model. They found a large discrepancy between both values and it appeared that z_{0h} varied strongly with available energy and humidity deficit. This effect may cause the observed diurnal course in kB^{-1}. However, in their test case they kept all resistances in the network constant, which may have influenced the outcome. More insight into the process of changing source height for heat during the day might be achieved by applying higher order closure models (see Meyers and Paw U, 1989).

e) Experimental considerations

Absolute values and diurnal courses of kB^{-1} have to be evaluated in the light of several calculation procedures.

1. The applied corrections, especially for surface temperature (see Appendix 1). It appeared that using the '8-14 µm'-correction instead of the 'whole-spectrum'-correction yielded slightly lower estimates of kB^{-1} for all surfaces. It was found that the correction had hardly any influence on the diurnal course of kB^{-1} for the bluff-bodied surfaces (savannah,

vineyard). It does, however, obscure the low-high-low course for the bare soil surface to such an extent that the variation of kB^{-1} during the day almost disappeared.

2. If we would introduce a higher emissivity (because of higher θ-values) for the bare soil during morning and evening compared to midday, this would enlarge the values of kB^{-1} relative to the midday values. This effect would also cause bare soil kB^{-1} to be more constant during day.
3. Considering the averaging procedure for surface temperature: T_s has been recorded with several methods for the vineyard. A comparison between fixed sensors and moving cable systems indicated that a simple line-averaging procedure, such as $T_s = 0.10T_{plant} + 0.90\,T_{soil}$, yields satisfactory results. Application of the cable surface temperatures instead of the fixed surface temperatures appeared to have a small effect on the course of kB^{-1}. However, the fixed IRTs installed at the savannah site were seriously overestimating T_s due to their nadir-viewing set-up, as explained in Chapter 5. Therefore, their values have been corrected with the help of the transect T_s-measurements (see Appendix 8). Omitting this correction leads to a large overestimation of kB^{-1}, which illustrates the importance of using correct average values of T_s.
4. The reference height of temperature and wind: ideally, measurements of u and T_a at the same heights should be applied for an intercomparison between different sites. If such data are not available, wind speed should be extrapolated downwards or upwards (see Stewart et al., 1994). However, this procedure is not possible for T_a because an estimate of z_{0h} is necessary in this case .
5. The constraints set in calculation procedure: it appeared that the constraints for H, $(T_s$-$T_a)$ and u_* used in the iteration procedure have considerable influence on the final (average) value of kB^{-1}. In the case of the savannah, for example, relaxing the $w'T'$-constraint increased kB^{-1} by nearly 50 %.

6.2.3 Conclusions

a) Parameterization of z_{0m} and d

Taking into account that we aimed for the best z_{0m}-predictions, the optimal parameter set to be used in Raupach's drag partition model would be $b/h \neq 1$, $c_d = 0.6$, $C_S =$ standard, $C_R = 0.4$ and $c_l = 0.50$. We need explicit estimates for b to arrive at satisfactory d and z_{0m}-estimates. We do not recommend the use of simple rules of thumb ($z_{0m} = 0.13h$, $d = 0.66h$), unless z_{0m} is parameterized as a function of d too, by $z_{0m} = 0.26(h - d)$, for example.

b) kB^{-1}

Average values for the three surfaces considered in this thesis are reasonably close to values reported previously in the literature. The values are best described by the well-established formulas of Brutsaert (1975b), Owen and Thomson (1963) and Sheppard (1958).

kB^{-1}-values as reported in the literature for similar sites are in some cases contradictory. This is predominantly the result of different measurement levels, data handling (such as corrections for T_s) or calculation procedures (constraints for $w'T$, u^*, T_s-T_a). Comparing kB^{-1} between different sites is useless, unless a joint approach like the one in Stewart et al. (1994) is pursued.

It appeared that overestimation of kB^{-1} leads to smaller errors in prediction of H than in the case of underestimation of the excess resistance. The widely applied value of 2.0 is too low for the majority of the surfaces occurring in nature, as has been shown by recent literature. Therefore, we propose that it should be increased to 7.0, for example.

Half-hourly values of kB^{-1} show a scatter during the day. This scatter cannot satisfactorily be removed by using a different average of surface temperatures or different corrections. It is neither possible to describe the diurnal course of kB^{-1} with the existing theory. Therefore, it can be concluded that it is better to avoid calculation of sensible or latent heat flux with a bulk transfer equation during early morning and late afternoon. It may be better to distrust calculation of H and L_vE with a flux-gradient type relationship for these times of the day, instead of searching for physical explanations for deviating kB^{-1}-values. This still leaves us with a problem, because single-layer models are indispensable in GCMs and remote sensing applications.

6.3 Vegetation-related conductances

6.3.1 Measured leaf stomatal conductance

a) General

Average leaf stomatal conductance, g_l, has been measured and calculated according to the procedure given in § 3.5.3. Its values can be upscaled to canopy conductances, g_c, following the bottom-up approach mentioned in Chapter 1. The diurnal course can also be fitted with several empirical formulae involving environmental variables. This ensures values of g_l for those periods when no direct measurements are available or parameterizations which will be used for incorporation into a SVAT (see Eq. 4.26). Sections 6.3.1 and 6.3.2 describe the results of these exercises. They only concern the HAPEX-Sahel savannah site because for the HAPEX-Sahel tiger-bush and the SEBEX experiment no porometry data were available.

b) Diurnal course

The average diurnal course of g_l for *Guiera senegalensis* as observed during the 'wet' period (days 234-267) and during the 'dry' period (days 270-284) is shown in Fig. 6.5.

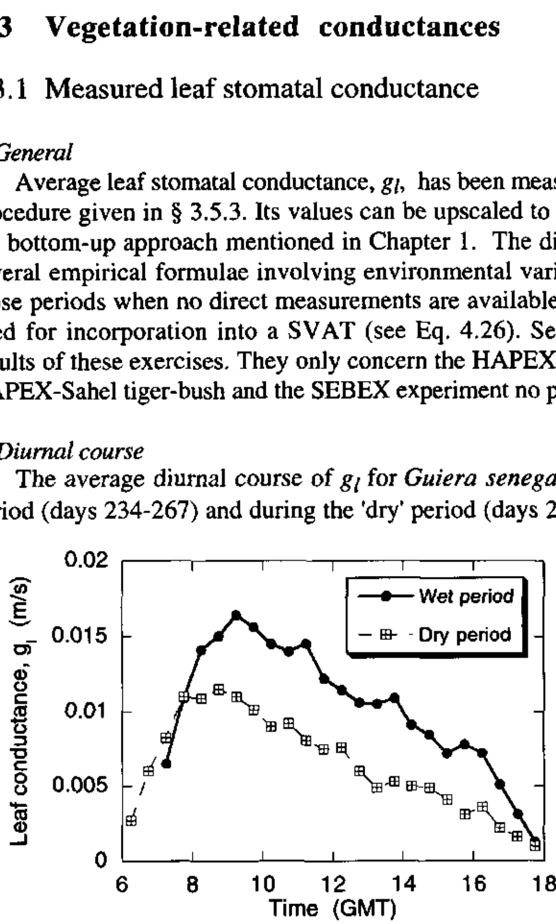

FIGURE 6.5. Average diurnal course of Guiera senegalensis leaf conductance during the 'wet' period (Θ =30-50 mm, D < 2.0 kPa) and during the 'dry' period (Θ < 20 mm , D > 2.0 kPa). The wet curve is an average of 150 half-hourly values observed from day 234 to 267. The curve representing the dry period was derived from 120 half-hourly averages (day 270-284).

Fig. 6.5 illustrates a different diurnal g_l-pattern as both soil and atmosphere became drier. This pattern can roughly be divided into two types. The first (see wet period curve) shows a broad peak between 8-11 GMT after which the stomata partially close as a result of the high radiation load, contributing to increases in leaf temperature and consequently to increases in humidity difference between leaf and air. However, g_l stays relatively high and for some days g_l seemed to recover later in the day. This pattern occurred only during the rainy period until about one week after the last major rainfall. The second type, characterized by generally lower values and by an earlier and narrower peak in g_l (see dry period curve), occurred mainly during the dry period at the end of the IOP. Similar patterns were found for the two understorey herbs-species.

These patterns are associated with moderate leaf water stress and they are characteristic for species of arid habitats that are regularly confronted with drought stress. Well-watered vegetation would show two distinct peaks (morning and afternoon) during the day with a midday depression in stomatal opening. This pattern was occasionally observed for *Guiera Senegalensis.* When stress is more severe, stomata open widest during the early morning, diminish their opening at midday and tend to reopen less during the afternoon. These types of stomatal behaviour are frequently described in the literature. Tenhuenen et al. (1987) describe several experiments. For a *Quercus suber* in Portugal, the height and timing of the peak changed through the season, which is similar to the behaviour observed in *Guiera*. They found midday stomatal closure for nearly all woody species of Mediterranean maquis vegetation, with species-specific differences in sensitivity to high leaf temperatures and large humidity deficits.

The *Guiera* bushes always exhibited one (morning) peak, indicating that the bushes were under continuous moderate water stress (even during the rainy period), as a result of the relatively hot and dry atmospheric conditions. In order to prevent excessive water loss towards the end of the IOP, the stomata began to close earlier in the day.

Fig. 6.6 shows the diurnal variation in g_l for two herb species (*Mitracarpus scaber* and *Jacquemontia tamnifolia*) during days 277 (6.6a) and 282 (6.6b). The cloudier conditions in combination with lower values of D and higher values of Θ cause g_l to be higher during day 277. The half-hourly averages for *Guiera senegalensis* are plotted for comparison. The conductances for the herbs are generally higher and have a more variable character which was partly caused by the fact that fewer measurements per half hour were conducted on the herb species.

Comparison of the WAUMET stomatal conductance data and the data presented by Hanan and Prince (1996) revealed that *Guiera*-values were roughly of the same magnitude (WAUMET data were ≈ 25 % higher). However, the differences in g_l for *Mitracarpus scaber* were much larger (on average around 100 %). These differences may have been created by local differences in soil water content, but more likely by instrumental or sampling procedure differences. The porometers were both of the same type (transient porometer) and make (DeltaT devices). However, the instrument used by Hanan and Prince (1996) was older (Mark II compared to AP4) and did not allow for automatic calibration of the measurements in the field. Sampling procedures used by the two teams were very similar. The discrepancy found between the results of both groups underlines that measured stomatal conductance data should be considered with care. No measurements on the grass species were conducted by WAUMET. Therefore, for calculation of canopy conductance (see next paragraph), the conductance parameterization and parameters derived from direct measurements on *Digitaria gayanus* (Hanan and Prince, 1996) were used to describe bottom-up grass conductance during the IOP.

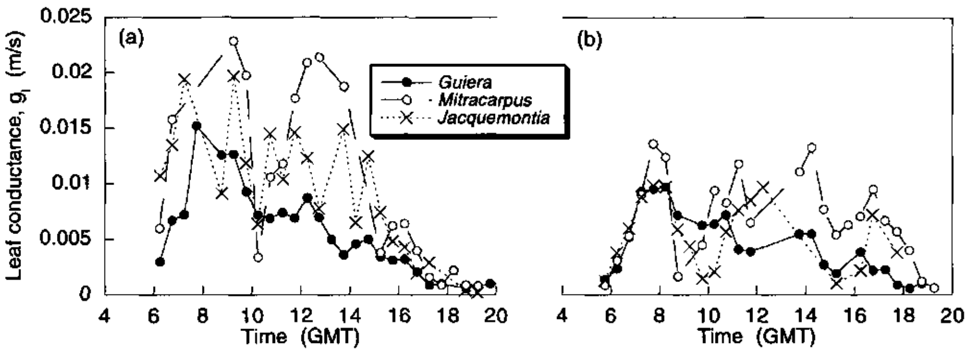

FIGURE 6.6. Half-hourly values of leaf conductance of Mitracarpus scaber, Jacquemontia tamnifolia and Guiera Senegalensis during days 277 (a) and 282 (b).

c) Seasonal variation

Fig. 6.7 shows the mean day-time (8-14 GMT) leaf stomatal conductances for *Guiera senegalensis* (with standard deviation), *Mitracarpus scaber* and *Jacquemontia tamnifolia*. This particular time interval was chosen to ensure a maximum number of day-time averages, as measurements were not always available after 14 GMT. A clear trend in g_l with time was observed: the conductances decreased towards the end of the IOP. The *Guiera* bushes reached maximum conductances on 4 September (day 248). Leaf conductances observed for *Mitracarpus scaber* were generally twice as high as those for *Guiera*, while conductances for *Jacquemontia tamnifolia* were in between.

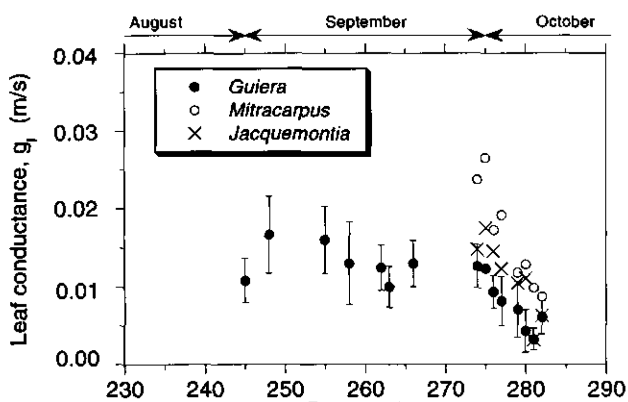

FIGURE 6.7. Day-time average (8-14 GMT) of leaf conductances for three predominant species at the HAPEX-Sahel savannah site from 1 September to 9 October 1992.

d) Relationship to environmental variables

Fig. 3.11 showed the pronounced seasonal trends of daily mean T_a, D, incoming Q_p and the amount of daily total rainfall, together with Θ. The daily average leaf conductances depicted in Fig. 6.7 were evidently related to these variables as shown in Fig. 6.8.

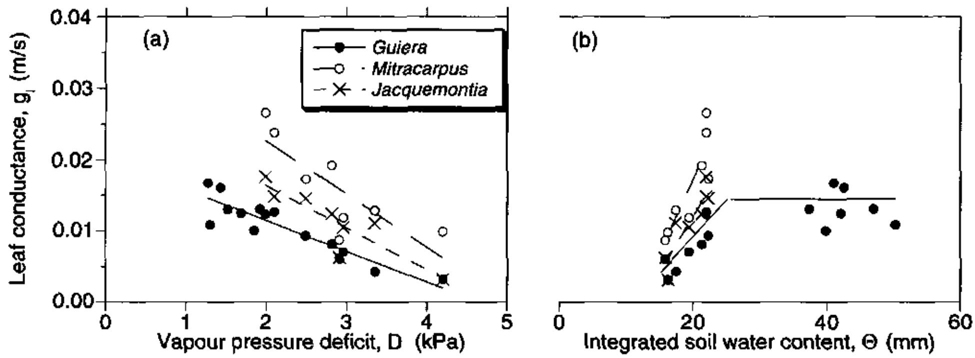

FIGURE 6.8. (a) Relationship between daily average leaf conductance and D for three predominant species at the savannah site. (b) relationship of daily average leaf conductance to Θ for the same species.

Average day-time conductances were clearly related to day-time (8-14 GMT) mean D, as reported by other authors (see, for example, Ludlow, 1980; Schulze et al., 1987; Price and Black, 1990; Roberts et al., 1990). The very low conductances on 7 October (day 281) were caused by warm, very dry air reaching the field site: instantaneous measurements of D exceeded 6 kPa. As soon as D decreased to 2.9 kPa on the following day, and even lower values on the next day (2.0 kPa, not shown in Figs. 6.7 and 6.8, because of incomplete conductance data) g_l instantaneously recovered for all sampled species. This suggests that no severe plant water stress had yet occurred during the drying period. The bushes and the undergrowth still behaved as a relatively resilient system when more humid atmospheric conditions returned, so apparently responded directly to D.

Fig. 6.8a also shows the negative relationships between D and daily average conductance found for *Guiera*, *Mitracarpus* and *Jacquemontia* (r^2 = 0.83, 0.65 and 0.78 respectively). The g_l of the two undergrowth species showed a larger response to D, the relationship for *Mitracarpus* being the strongest. This agrees with the results of Ludlow (1980) that species with high maximum conductances (like the two sampled undergrowth species) respond more strongly to D than species with lower conductances. Changes may occur in plants exposed to water stress to make stomata either more or less responsive to D. Tenhuenen et al. (1987) claim that soil water stress modifies the characteristics of stomatal behaviour: increased water stress resulting in greater sensitivity to high values of leaf temperature and D. This statement does not seem to apply for the savannah data presented here, as a linear response was observed. However, exposure to water stress does not always alter the relationship between g_l and D (Ludlow, 1980). Fig. 6.8a does not show a change in the response with decreasing plant water status (towards the end of the IOP, with decreasing Θ), although few data are available for the two herb species.

The relationship between Θ and g_l (Fig. 6.8b) shows asymptotic behaviour for the *Guiera* bushes with rapidly decreasing g_l values as Θ falls below 25 mm. Similar asymptotic behaviour was not observed for *Mitracarpus* and *Jacquemontia* (r^2 = 0.75 and 0.81 respectively) because no measurements were made before the last rain. It is not possible to determine whether the decrease in g_l is caused by a response to dry atmosphere, as Θ and D are correlated (r^2=0.77). The response of the canopy conductance of *Guiera* to vapour pressure deficit, soil water deficit, and solar radiation was also studied by Huntingford et al. (1995), using data from a similar savannah site nearby. They found that a discontinuous linear function, similar to the two lines shown in Fig. 6.8b, between canopy conductance and soil moisture deficit, fitted their measurements well. They also found that it was difficult to clearly separate the response of conductance to soil water and vapour pressure deficit, as these tend to be well correlated in the environment of the Sahel.

6.3.2 Parameterization of leaf stomatal conductance

a) Introduction

Average leaf stomatal conductance, from which a canopy resistance r_s^c can be derived, is an important variable in many SVAT models. As indicated in Chapter 4, it is usually not available as a direct input parameter (like R_s or T_a), but it is parameterized as a function of easily obtainable meteorological parameters. Estimates of g_l are then derived from a parameterization describing the response of the individual leaves to controlling environmental properties. This approach entails fitting a suitable model to the measured leaf conductances thus yielding a set of parameter constants representative for the specific canopy. In most cases the empirical multiplicative model of Jarvis (1976) is used, but recent investigations applied mechanistic models (see, for instance, Jacobs, 1994; Friend and Cox, 1995).

b) Optimizations

The response to the environment has been illustrated in Fig. 6.8 for daily estimates of g_l. A multiple non-linear regression technique has been used for the determination of a functional relationship on a half-hourly basis. The equations as described in § 4.2.4 and 4.3 have been applied, i.e. the (TL) formulations of Huntingford et al. (1995), Hanan and Prince (1996, see Appendix 6) and Jacobs (1994). The parameters of the three models, together with the coefficient of determination, are given in Tables 6.4-6.7. The coefficient of determination is a measure of the fraction of the total variance accounted for by the model.

TABLE 6.4. Optimized parameter values for a stomatal conductance (JS-type) model (JSH). Measurements of g_l have been obtained for several savannah species during the HAPEX-Sahel experiment. Model as described by Huntingford et al. (1995), see § 4.2.4. In Eq. 4.26b, T_L= 5.0 and T_U = 55 °C. $R_{s,max}$ = 1000 W m^{-2}.

Species	$g_{l,max}$ (m s^{-1})	a_1 (R_s) (W m^{-2})	a_2 (T_a) (°C)	a_3 (D) (mb)	n (-)	c.o.d.
*Guiera**	0.018199	191.57	25.76	59.514	248	0.62
*Mitracarpus***	0.0238	186.65	n.a.	95.87	81	0.33
*Jacquemontia***	0.0236	123.36	n.a.	41.23	84	0.31

* D and T_a at 2.5 m

** D and T_a at 0.7 m

n.a.: not applicable

Table 6.4 shows that values of c.o.d. were very low for the herb species. For the latter, T_a has not been used as a fitting parameter because of the relationship between T_a and D and instability of the optimization procedure (Huntingford et al., 1995; Wright et al., 1995; Hanan and Prince, 1996). Values for $g_{l,max}$ are higher in case of the herb species, as expected from Figs. 6.6 and 6.7.

TABLE 6.5. Parameter values in a JS-type model as proposed by Hanan and Prince (1996) and described in Appendix 6. Dependence on intercepted PAR per unit leaf area, R_p, vapour pressure deficit, D, and root-weighted soil water potential, Ψ_r.

Species	$g_{l,max}$ (m s^{-1})	a_1 (R_p) (W m^{-2})	a_3 (D) (mb^{-1})	a_4 (Ψ_r) (cm)	c.o.d.
Guiera	0.0335	62.84	0.0531	-1986.19	0.58
Mitracarpus	0.0677	55.89	0.0347	-1497.81	0.39
Jacqemontia	0.0894	31.19	0.0846	-1265.34	0.45

When fitting with the parameterization of Hanan and Prince (1996), c.o.d is considerably higher for the herb species (see Table 6.5). Slightly lower values are observed for the bushes. These higher values of c.o.d. are affected by the incorporation of soil moisture as illustrated in Table 6.6, which gives the sequential c.o.d.-values when degrees of freedom are increased step-wise.

TABLE 6.6. Model results, expressed as the coefficient of determination, for sequential fitting with the Hanan and Prince (1995) JS-type model. $f_1 = f(R_p)$, $f_3 = f(D)$, $f_4 = f(\Psi_r)$.

Model	*Guiera*	*Mitracarpus*	*Jacquemontia*
	c.o.d.	c.o.d.	c.o.d.
$g_l = f_1\ g_{l,max}$	0.14	0.13	0.06
$g_l = f_1 f_3\ g_{l,max}$	0.58	0.30	0.30
$g_l = f_1 f_3\ f_4\ g_{l,max}$	0.58	0.39	0.45

The conductance data were also fitted by the A-g_s model of Jacobs and given in Table 6.7. This model also requires values of C_s, which reduced the total amount of data points (n=139), because of failure of the IRGA on a number of days. The model was fitted with four independent variables (R_s, T_a, D, and C_s) and allowed eight parameters to vary: g_m(@25), $A_{m,max}$(@25), $g_m(T_1)$, $g_m(T_2)$, $A_{m,max}(T_1)$, $A_{m,max}(T_2)$, $D_{s,max}$ and f_0. For *Guiera senegalensis,* agreement between measurements and model estimates was good (c.o.d. = 0.736) and the found parameter values were physically possible and similar to the values found by Jacobs. However, if this reduced data set was used to find the parameter values of the JSH-model, an equally good fit was attained (c.o.d. = 0.728). In addition, it was found that running the A-g_s model with a *constant* value of C_s hardly influenced the final parameter values. In this case the goodness of fit was even slightly better (c.o.d = 0.737).

Using the A-g_s model for the two herb species yielded maximum c.o.d.-values of around 0.40. The parameters thus obtained are not shown in Table 6.7, because consistency in the parameter estimates was difficult to obtain. In our case, using the physiological approach instead of the semi-empirical approach did not lead to a better agreement between data and model-estimates.

TABLE 6.7. Parameters in the A-g_s model (see § 4.3) derived from the porometry data for Guiera Senegalensis (HAPEX-Sahel). X(@25) denotes the parameter value at 25 °C.

Guiera Senegalensis	Parameter (X)	*X(@25)*	T_1 (°C)	T_2 (°C)
	g_m (m s^{-1})	0.0032	0	30
	$A_{m,max}$ (mg m^{-2} s^{-1})	5.2	29	48
	$D_{s,max}$ (g kg^{-1})	73.8		
	f_0 (-)	0.852		

Fig. 6.9 shows the diurnal course of simulated g_l of *Guiera Senegalensis* as obtained by the parameterizations given in Tables 6.4, 6.5 and 6.7 for a day during the wet period (a) and during the dry period (b). The patterns are comparable to those shown in Figs. 6.5 and 6.6. A slight difference between the parameterizations can be observed, especially during the dry day.

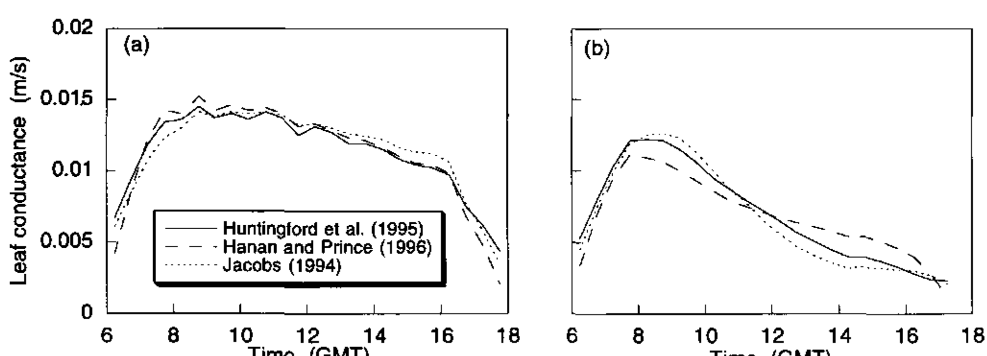

FIGURE 6.9. Comparison of the diurnal course of g_l, (a): day 245, (b): day 282, as obtained with the three different g_l-parameterizations derived for the same vegetation (Guiera senegalensis).

c) Conclusions

It is difficult to capture the g_l-measurement for the herb species in any kind of model (whether empirical or physiological) which utilizes the functional relationship between conductance and environment. This was also found by Hanan and Prince (1996). Several reasons for this discrepancy may be put forward:

1. The limited amount of available data (days 273-284) which, furthermore, were mainly obtained during the dry-out. This restricts the available range of especially D and θ. Hanan

and Prince (1996) obtained data for *Mitracarpus scaber* during a much longer period. Even though they obtained a much wider range of meteorological and soil conditions, their fit also resulted in low values of c.o.d. (0.44).

2. The influence of non-environmental factors, such as plant hormones as induced by the low θ-values, or the fact that the herbs had somewhat hairy leaves.
3. The fact that the leaves were very close to the ground (maximum height of the herbs was approximately 20 cm) which resulted in dust-covered leaf surfaces and a considerable micro-climatological influence.

The fairly elaborate and physically sound physiological approach to calculate g_l from environmental variables does not improve the goodness of fit. If a model selection criterion were applied, which relates the coefficient of determination to the number of parameters (i.e. the number of degrees of freedom) the physiological model would be deemed less appropriate than the empirical approach. The influence of C_s on the final parameter values was negligible as was its influence on the correlation between measurements and estimates of g_l. However, the well-founded physiological approach has unmistakable advantages when built into a PBL-model used to describe feedback between the atmosphere and the vegetation, as shown in Section 6.2.2b.

To describe the environmental influence for both the bushes and the understorey at least R_s and D should be taken into account. Adding T_a improves the estimates only marginally in case of the *Guiera* bushes and obscures the relationships for the herb species. The introduction of soil moisture, by e.g. Ψ_r as proposed by Hanan and Prince (1996), has proven indispensable for the description of the shallow-rooting understorey species. For the *Guiera* bushes, rooting until several meters, adding soil moisture to the model variables does not increase the c.o.d. This indicates that the bushes were mainly experiencing atmospheric stress.

Simple radiation variables (e.g. R_s) are good enough. Parameterizations accounting for PAR-interception (Hanan and Prince, 1996), leaf area or physiological processes (Jacobs, 1994) do not result in better model estimates.

6.3.3 Canopy surface conductance

a) Introduction

In Chapter 1, two approaches for estimating canopy stomatal conductance, g_c, were introduced: the 'bottom-up' and 'top-down' scaling methods (Baldocchi et al., 1991). A special issue of Agricultural and Forest Meteorology (no. 54, 1991) was dedicated to the topic of determining g_c. First of all because of the importance of the subject for estimating evaporation on the leaf, plant, canopy and landscape scale. Secondly, because of the (sometimes large) discrepancy found between both approaches.

The lack of correlation between environment and g_l for the understorey species and the fact that only a few of these species have been sampled, make up-scaling from leaf to canopy scale a difficult task in the case of the savannah. On the other hand, the top-down approach will be seriously hampered by the layering of the total vegetation. No measurements of g_l were available for the tiger-bush, which meant that the top-down approach was the only feasible method of obtaining values of tiger-bush g_l or g_c. This paragraph intends to determine the best estimate of g_c (or g_{cs}) to be used in the SVATs (presented in Chapter 4) which will be evaluated in Chapter 8.

b) Bottom-up approach

The *LAI* is needed for scaling up from the leaf to the canopy level. In the most simple case, the entire canopy is treated as a single giant leaf. In the case of a single species natural vegetation or crop, multiplication of the leaf conductance by *LAI* will yield the canopy conductance:

$$g_c = \gamma g_l \, LAI \qquad (6.1)$$

where γ is 1 for hypostomatous leaves, while for amphistomatous leaves $\gamma = 2$. Most plants will have stomata on both sides of their leaves, but with adaxial conductance being less than abaxial conductance, so γ will have a value lower than 2.

Other parameterizations add extra complexity by distinguishing between sunlit and shaded leaves, taking into account sunlit and shaded leaf area indices and by dividing the canopy into several (usually three) horizontal layers. Rochette et al. (1991b) tested six different methods for scaling up from g_l to g_c for a maize canopy, which they then compared to surface conductances as estimated by the PM-method. They concluded that not distinguishing between the sunlit and shaded leaf area index does not produce different g_l-values for medium density canopies, such as the maize canopy they studied, if sampling is made in the sun and in the shade at different levels in the canopy. They state, however, that this conclusion could be different for a denser or a sparser canopy, where sunlit and shaded *LAI*-fractions over the whole canopy are significantly different, and when sampling is random or incomplete. Sampling of only the top sunlit leaves (Whitehead et al., 1981) led to g_l-values that were sometimes double those obtained using other methods. They found that scaling-up methods requiring a weighting based on sunlit and shaded *LAI* and canopy level tend to overestimate g_{cs} in this particular study.

The use of scaling up with effective *LAI*, LAI_f (Szeicz and Long, 1969), where $LAI_f = LAI$ if $LAI < LAI_x/2$ and $LAI_f = LAI_x/2$ if $LAI > LAI_x/2$ (with LAI_x being the maximum *LAI*), had a good correspondence with g_{cs} when the canopy was incomplete, but the method failed to estimate g_{cs} when the canopy is fully developed. However, early in the season and for dry soil surfaces this method gave the best approximation of g_{cs}, indicating that this may be a useful approach for the conditions encountered during HAPEX-Sahel. The most complete method also incorporates leaf inclination angle classes (see Sellers et al., 1986).

In order to calculate evaporation for the savannah site, the leaf conductances of the different components have to be scaled up to component canopy conductances if a dual source or two-layer SVAT is used and from here on to one single value for the big-leaf approach. Field measurements by Hanan and Prince (1996) at the same experimental plot suggested γ to be 1.2 for *Guiera senegalensis*. Similar measurements for *Mitracarpus scaber* and *Digitaria gayanus* were not available so *Mitracarpus*, being a C_3-plant like *Guiera senegalensis*, was assigned a value of 1.2 whereas *Digitaria*, a C_4-grass, was given an γ-value of 1.55 similar to millet.

Estimates of *LAI* per species are also needed to calculate the total canopy conductance. As described in Chapter 3, separate measurements of *Guiera* leaf area index, LAI_b, through the IOP were made. The vegetation of the sub-layer, composed of several species of (annual and perennial) grasses and herbs, was lumped together giving the mixed herb layer LAI_u. However, the contribution of the herbs and grasses to this understorey *LAI* has been roughly recorded during the IOP, which provided coarse estimates of the separate contribution for grasses and herbs.

The total canopy conductance for the savannah vegetation can thus be induced from:

$$g_c = 1.2\ LAI_b\ g_{l,b} + 1.2\ LAI_h\ g_{l,h} + 1.55\ LAI_g\ g_{l,g} \qquad (6.2)$$

where the subscript b stands for the main canopy (bushes), h for herbs and g for grasses, and with the last two terms giving the understorey conductance. To calculate g_c for the tiger-bush, the first term of Eq. 6.2 can be used with LAI_b set to 1.0

c) Top-down approach

The PM big-leaf model is usually used for the 'top-down' approach (Finnigan and Raupach, 1987; Baldocchi et al., 1991). This method yields values of g_{cs}, which are relatively reliable when the surface is dry and the sources or sinks of momentum, latent and sensible heat fluxes are indeed at the same level, as assumed by the PM-model. Furthermore, soil evaporation has to be negligible, although some scientists (e.g. Paw U and Meyers, 1989) incorporated soil surface conductance in g_{cs} by considering the soil as another big leaf with a LAI of 1.0. Some controversy exists about the true meaning of g_{cs} and its applicability to a real canopy. In 1966 Philip described it as "an artefact of a somewhat unrealistic analysis" and claimed its physiological significance is questionable (Lhomme, 1991). When using the PM-model, special attention has to be paid to correct estimation of r_a^a: a proper value of the excess resistance, B^{-1}/u^*, needs to be added to $r_{am} = u/u^{*2}$ (Lhomme, 1991; Kim and Verma, 1991). See § 6.2.2 for more information on how to describe this excess resistance and some typical values for sparse bush-like canopies.

In contrast to the single-layer approach as described above, the multi-layer approach treats the stand as a continuous or discrete set of horizontal planes, each one absorbing net radiation and transferring sensible and latent heat (Lhomme, 1991). Another approach is to derive a general combination equation, similar in form to that produced by the single layer approach, from a multi-layer approach as done by Shuttleworth (1976) and Lhomme (1988). Huntingford et al. (1995) conducted the top-down approach by comparing calculated L_vE, as found by a single-source, a two-source and a two-layer model, with measured values of L_vE for a savannah surface. Stomatal conductance was described by a Jarvis-Stewart (JS) type model as given in § 4.2.4 (according to the TL approach). Whereas values for g_{cs} found for the bushes by the two-source and two-layer model were similar, g_{cs} for the herb layer found by the two-layer model was considerably lower compared to the two-source model. Shuttleworth (1976) introduced the so-called shelter factor, $F = g_c / g_{cs}$, where g_c is the bottom-up value and g_{cs} the top-down estimate. Rochette et al. (1991b) found mean shelter factors ranging from 1.3 to 2.1. Finnigan and Raupach (1987) suggested that F could be expressed as a function of the ratio of the aerodynamic and stomatal conductances at the top of the canopy, as verified by Rochette et al. (1991b).

A comparison was made between bush, understorey and total g_c, as found from upscaling and from inverted forms of the PM and TL models, for the HAPEX-Sahel savannah. For the top-down values of the understorey, the data obtained at site CWS a' were used. Top-down values for the *Guiera* bushes have been calculated from the TL model (see Huntingford et al., 1995). The reason for not using the sap flow measurements at the CWS site, was that the number of gauges was considered insufficient to give a representative value of L_vE_b. It appeared that the matching between the bottom-up and top-down approach was satisfactory for the understorey if the *Mitracarpus* and *Digitaria* g_l-estimates of Hanan and Prince (1996) were used. The parameterization found from fitting the WAUMET data yielded too high values, as a result of the high values for *Mitracarpus*. The understorey surface conductance appeared to be comparable to the values given by the TL parameterization with the parameters listed in Huntingford et al. (1995).

By contrast, the top-down values for the bushes, as well as for the total canopy, were considerably lower than the bottom-up calculations. The ratio g_c/g_{cs} was more than two for the majority of the half-hour values. High ratios were also found by other authors (see, for instance, Finnigan and Raupach, 1987; Rochette et al., 1991b). The difference between both approaches, while using the PM-equation, is usually flattered because too low values of B^{-1}, and thus of r_h, are taken.

Fig. 6.10 shows values of L_vE/A_t, g_c/g_{cs} and the ratio between L_vE (obtained with g_{cs}, i.e. measured values of L_vE) and L_vE (obtained with g_c, i.e. using the PM equation in a bottom-up approach) as a function of g_a/g_{cs}. In this figure, g_a is the reciprocal of the bulk aerodynamic resistance against heat or moisture transfer (see Eq. 2.26). A_t is found from ($L_vE + H$). Figure 6.10 is arranged in analogy with Fig. 5.15 of Finnigan and Raupach (1987). They proved theoretically that the 'intuitive' (i.e. g_c) and the 'correct' (i.e. g_{cs}) values can easily differ by a factor or two. For their calculations they used an extensive, mature cereal crop with a total *LAI* of 3.0. The outcomes were dependent on the shape of the stomatal conductance (or transpiration) profile and on *D* (expressed by values of g_a/g_i, where $g_i = R_n/L_vD$).

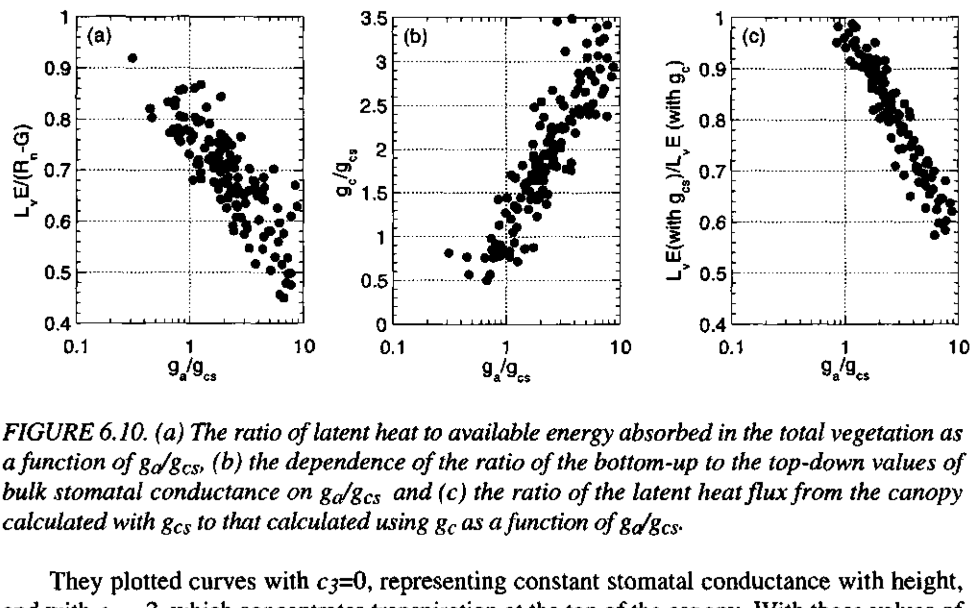

FIGURE 6.10. (a) The ratio of latent heat to available energy absorbed in the total vegetation as a function of g_a/g_{cs}, (b) the dependence of the ratio of the bottom-up to the top-down values of bulk stomatal conductance on g_a/g_{cs} and (c) the ratio of the latent heat flux from the canopy calculated with g_{cs} to that calculated using g_c as a function of g_a/g_{cs}.

They plotted curves with c_3=0, representing constant stomatal conductance with height, and with c_3 = 2, which concentrates transpiration at the top of the canopy. With those values of c_3 and g_a/g_i ranging from 0 to 2, g_c/g_{cs} ranged from 0.4 to 1.3. The consequences of this 'error' were an over- or underestimation of L_vE of maximally 20 %. Following their reasoning, our savannah should have a negative value of c_3, because the major source of evaporation is from the grass/herb layer. The result is that a canopy like a savannah with the major evaporation source (undergrowth) close to the ground will lead to a large discrepancy between sources/sinks of momentum (near the top of the bushes) and evaporation.

Therefore, it is highly unlikely that the top-down and bottom-up approaches would roughly generate the same outcome, which results in the comparatively large differences (up to 50 %) between measured and calculated L_vE presented in Fig. 6.10c.

Furthermore, it appeared that the total savannah vegetation, but especially its upper canopy layer (bushes) was strongly decoupled from the atmosphere. This fact has already been mentioned by Allen and Grime (1995). Values of the decoupling factor, $\Omega = (\varepsilon + 1)/(\varepsilon + 1 + g_a/g_c)$, as introduced by Jarvis and McNaughton (1986) and tested by Price and Black (1991), for example, were always higher than 0.5 and on many occasions higher than 0.9, yielding an average of 0.78. The decoupling was probably caused by shape, size and the slightly hairy character of the leaves resulting in low boundary layer conductance compared to stomatal conductance. This effect was enhanced by the predominantly low wind speeds, which caused free convection to be predominant (see also Appendices 5 and 12). High values of Ω enhance the difference between D at the reference and D at the leaf level, D_l (with the latter approaching zero in the extreme). If canopy conductance is inferred from an inverted equation using a (too high) value of D, its values will be seriously underestimated. When Ω is close to 1.0, D_l tends to a local equilibrium value, De_q. Following the parameterization of Jarvis and McNaughton (1986), it was found that D_{eq} was up to two or three times lower than D. Using this value in the inverted PM-equation would yield more plausible results of g_{cs}.

It can be concluded that under the free convection conditions observed here, the use of the PM-approach in its single or even in its multi-layer form may lead to serious overestimations of L_vE if intuitive or upscaled values of g_c are used. For this reason, only top-down values will be used for further calculations (see Chapter 8) to make sure that reliable values of L_vE are obtained. The final parameter values are shown in Table 6.8.

TABLE 6.8. Parameter values for the TL stomatal conductance model. Values of g_l were obtained from inverting the TL-model with measured L_vE and available energy as input. This procedure was executed for the vegetated component surfaces. The values of r_s^s required for this approach will be presented in the next section .

Vegetation	$g_{l,max}$ (m s^{-1})	a_1 (R_s) (W m^{-2})	a_3 (D) (mb)	a_4 $(\Delta\Theta)$ (mm)	a_5 $(\Delta\Theta)$ (mm)
Savannah understorey*	0.0115	-8.83	80.5	0.0	138
Savannah bushes*	0.0110	62.9	20.3	61.5	106
Tiger-bush** bushes	0.030	349.9	14.14		

** Parameterization and parameter values as given in Table II of Huntingford et al. (1995).*
*** Obtained from inverting the TL-model using CWS evaporation and micrometeorological data.*

6.4 Soil surface resistance

a) Introduction

The soil surface resistance can be imagined as the diffusive resistance of a dry soil layer of some thickness (usually several mm), overlying a wet soil layer. As the soil dries, the depth of the layer increases, reducing vapour flux from the wet layer (Ham and Heilman, 1991). Although sometimes the use of a soil surface resistance is considered impractical or not in accordance with theoretical calculations (e.g. Fuchs and Tanner, 1967), its use is widespread in the majority of the resistance-based canopy models and reliable values are therefore requisite for proper estimates of evaporation.

Surface resistance can be measured directly with a so-called fast air circulation chamber (Kohsiek, 1981; Van de Griend and Owe, 1994), but in most cases a rather arbitrary value is chosen. In the Shuttleworth and Wallace model, for example, $r_s^s = 500$ represents a wet soil, whereas $r_s^s = 2000$ represents a dry soil. Furthermore, even if r_s^s is changed during the measurement period (i.e. lower values after rain) it is usually kept constant during the day (Massman, 1992). This means that for several hours after rainfall or dewfall, the results of the used method are unreliable. Soils with a pronounced capillary rise (i.e. loamy soils) will also show a large variation in diurnal soil moisture, thus making a constant value of r_s^s relatively ineffective.

b) Measurements

For this thesis, values of r_s^s were derived by inverting the TL-model using a combination of measured total and soil evaporation (and meteorological variables needed in the TL model) obtained at the SSS tiger-bush site. These were the same data used in § 5.3.3 to evaluate soil evaporation. Fig. 6.11 shows the large variation observed for tiger-bush r_s^s. On days were rainfall occurred (e.g. 246) r_s^s was very small (< 100 s m^{-1}) but several days without rainfall caused r_s^s to increase to values around 2000 s m^{-1}. New rainfall (days 256, 258 and 259) caused r_s^s to diminish again. After the last rainfall (day 259), r_s^s started to increase rapidly to values around 8000 s m^{-1} at the end of the IOP. These values are within the range reported by other scientists e.g. $r_s^s = 278$ and 1592 s m^{-1} for θ=0.22 and 0.08 m^3 m^{-3}, respectively (Ham and Heilman, 1991). Massman (1992) found values < 100 s m^{-1} during and just after rainy days, whereas his values of r_s^s increased up to values of > 80000 during dry periods. Van de Griend and Owe (1994) reported values of r_s^s ranging from 10 ($\theta = 0.15$) to 2000 s m^{-1} ($\theta = 0$). These comparatively low values were measured with a fast air circulation chamber.

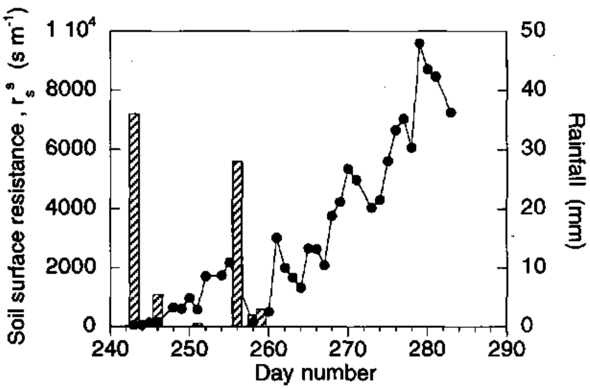

FIGURE 6.11. Soil surface resistance for evaporation, r_s^S (at 12 GMT), as inversely calculated from L_vE (EC), L_vE_s (Bowen ratio), $R_{n,b}$, $R_{n,s}$, G_b, G_s, T_a, D and u using the TL-model as described by Huntingford et al. (1995). Meteorological data were obtained from the Institute of Hydrology, SSS. Also indicated is the daily amount of rainfall in mm.

Fig. 6.12 compares values of r_s^s with values derived for the soil Bowen ratio coefficient, c_w (see Appendix 5 and 12). Both resistances were highly correlated ($r^2 = 0.96$) even though they were calculated by different methods, although both methods employed measurements of L_vE_s in a certain way. Massman (1992) also found a good and linear correlation between r_s^s and c_w ($r_s^s = 160[c_w - 1]$ with r_s^s in s m^{-1}) for a soil between a sparse short-grass steppe. However, in this case r_s^s and c_w were found from a non-linear regression approach (employing the SW model and measured values of **total** L_vE) in which r_s^s and c_w were part of the same equation. Therefore, as suggested by Massman, this result could have been an artefact of the model. Fig. 6.12 indicates that this was probably not the case.

FIGURE 6.12. Relationship between r_s^s, as calculated by inverting the TL model using measurements of L_vE_t and L_vE_s, and c_w as found from the Sherwood-resistance approach explained in Appendix 5 and 12 (adapted from Jacobs and Verhoef, 1996).

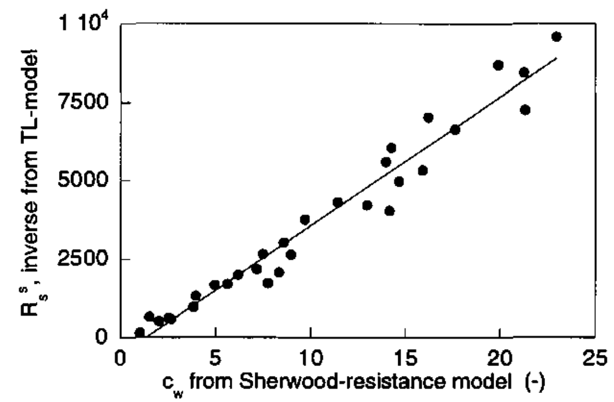

6.5 Summary for savannah and tiger-bush surfaces

Fig. 6.13 shows the bush, understorey and total surface conductances for the savannah and tiger-bush. Half-hourly values of leaf conductance, which were averaged between 8-16 GMT, were obtained from the parameter values listed in Table 6.8. Effective surface conductances were calculated by taking into account the *LAI* and the coverage of a certain component (α or $1-\alpha$) by using the formulae given in Eq. 4.25. For the calculation of the total surface conductance the following formula was applied:

$$r_s^t = \frac{\frac{LAI_b}{1-\alpha} g_{l,b} + \frac{LAI_u}{\alpha} g_{l,u}}{LAI_b + LAI_u} \tag{6.3}$$

Savannah values for LAI_b and LAI_u were given in Fig. 3.10, whereas the parameters were set to 1.0 for the tiger-bush surface components.

Tiger-bush bush conductance appears to be considerably higher than the values found for the scattered *Guiera senegalensis* bushes forming the savannah upperstorey. Tiger-bush reacted strongly to changes in *D*, as also reported by Gash et al. (1996), which caused the high variation compared to the savannah bushes. The tiger-bush vegetation seems to be more resilient after a decrease in *D*. Fig. 6.13b shows that the ranking for the understories was opposite - the herbaceous undergrowth of the savannah resulted in high conductances compared to the tiger-bush bare soil. Both conductances clearly diminished during the last three weeks of the IOP. The consequences for the total surface conductance are illustrated in Fig. 6.13c. During most of the days savannah conductance is higher, although the more resilient character of the tiger-bush vegetation strips cause tiger-bush conductance to be higher than the savannah values during the last two days of the IOP.

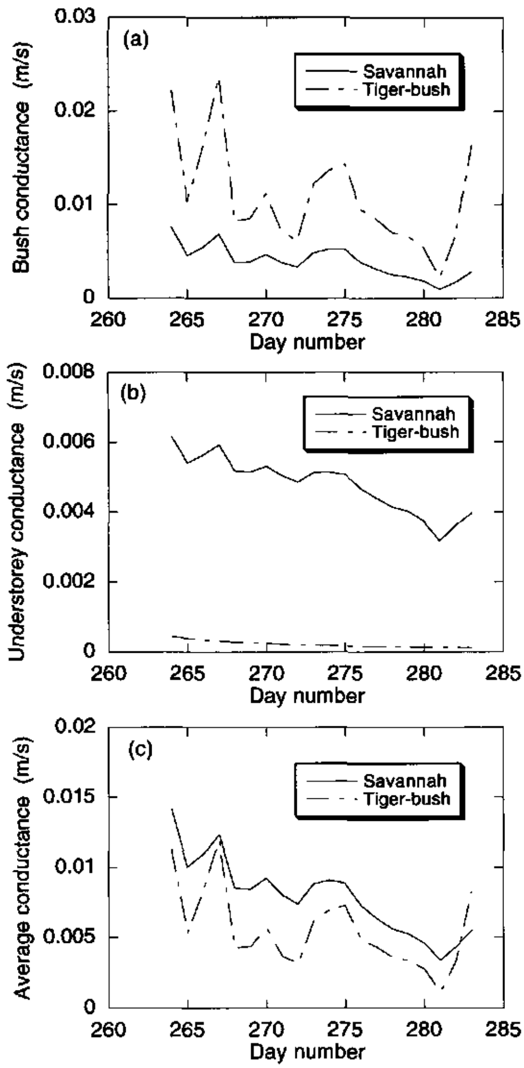

FIGURE 6.13. Seasonal course of savannah and tiger-bush $g_{cs,b}$ and $g_{cs,u}$ and total g_{cs} during the last three weeks of the HAPEX-Sahel IOP.

7 CO2 fluxes

7.1 Introduction

This chapter presents measurements of CO_2 fluxes, F_c, of a deciduous savannah (HAPEX-Sahel). The water use efficiency (amount of CO_2 assimilated per unit amount of water transpired) will be also considered. This is interesting in two respects. Firstly, to allow comparison of the efficiency with those measured for other vegetation and crops both for the HAPEX-Sahel experiment and during other experiments. Secondly, to allow the possibility of calculating the net canopy CO_2 uptake from more widely available evaporation measurements using empirical relationships between water use efficiency and environmental variables. Water use efficiency is normally defined as the ratio of photosynthesis and transpiration. At the field scale, it is difficult to measure canopy photosynthesis and transpiration rates directly (Baldocchi, 1994) because evaporation from the soil and respiration are also taking place. The latter is unknown and we will use $|F_c / E|$ as a measure for water use efficiency. This chapter also describes some results on radiation use efficiency (amount of CO_2 assimilated per unit of solar radiation absorbed), expressed as F_c/Q_p.

The influence of soil moisture content, vapour pressure deficit and photosynthetic photon flux density on E, F_c and $|F_c / E|$ are analysed on two time scales. Daily (24 hours) or 'day-time' (i.e. 8-16 GMT) means or integrals are used to investigate longer-term patterns through the IOP. Half-hourly means or instantaneous measurements are used to study short-term variations over diurnal cycles.

The savannah surface was composed of a mixture of several C_3- (*Guiera* bushes and herbs) and C_4- (the majority of the grasses in the area) species. This study therefore offers the possibility of investigating, for a mixed community of C_3 and C_4-plants, how F_c, E and $|F_c / E|$ behave with respect to important environmental variables. Most previous studies of this kind have been made for closed mono-species canopies of C_3 or C_4 crops. In this study, no attempt was made to partition F_c into contributions of the individual C_3 and C_4-species or the soil. However, separate measurements of g_l for *Guiera* and two herb species were made. These results have been described in § 6.3.1.

Because of some problems with the eddy covariance instruments, and to avoid confusing the effect of soil evaporation with transpiration, no CO_2 flux data observed prior to the last major rainfall of the wet season (day 261, 17 September) will be analyzed in this chapter.

7.2 Results and discussion

7.2.1 General

Day-time CO_2 fluxes will have a negative sign to comply with the micrometeorological convention that fluxes towards the surface are negative per definition. The most negative (lowest value) will therefore represent the highest physiological activity. Strictly speaking this should be referred to as the minimum F_c-value. However, to avoid confusion in the description of the diurnal CO_2 flux, the negative values are regarded as absolute values. This

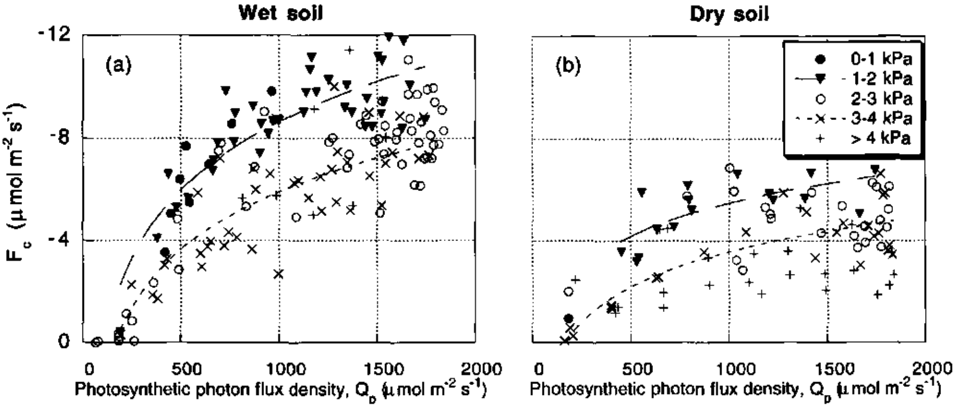

FIGURE 7.2. Half-hourly values of F_c as a function of Q_p for different classes of D: (a) 'wet soil' conditions, $\Theta > 30$ mm, (b) 'dry soil' conditions, $\Theta < 20$ mm. Data points in figure (a) were before 3 October (22/9 - 3/10), whereas data in (b) represent 5 October until 12 October. Logarithmic fits to the data are given for $1 < D < 2$ kPa ((a) $-F_c = -17.9 + 8.8 \log Q_p$, $r^2 = 0.74$; (b) $-F_c = -16.7 + 7.5 \log Q_p$, $r^2 = 0.64$) and for $3 < D < 4$ kPa ((a) $-F_c = -7.6 + 4.4 \log Q_p$, $r^2 = 0.50$; (b) $-F_c = -10.3 + 4.6 \log Q_p$, $r^2 = 0.76$). Reprinted from Verhoef et al., 1996b.

Moncrieff et al. (1996a) arranged the radiation use efficiency for the three super-sites in a way similar to the one given in Fig. 7.2, i.e. according to the evaporative demand of the atmosphere and also by soil water content. For the SSS, F_c against PAR was plotted for days 241-249, a relatively wet period, and the stand apparent quantum efficiency was about 54.5 incident photons per mol CO_2 fixed. Measurements made on *Guiera* leaves by porometry showed a leaf scale quantum efficiency of about 66.7 incident photons per mol CO_2 fixed. Similar measurements on Egrostis tremula (the main species in the savannah ground flora) showed a leaf scale quantum efficiency of about 40 incident photons per mol CO_2 fixed (Levy et al., 1996). For the CWS only day 247 was available and it appeared that, for both sites, F_c increased almost linearly with PAR. A slight hysteresis was observed for the SSS. This probably also occurred at the CWS, but no afternoon values were available due to overheating of the IRGA.

Fig 7.2 shows a clear hysteresis - the morning (low D) F_c-values being higher than the afternoon (high D) values. This hysteresis is explained by Haverkort and Goudriaan (1993) who argue that the stomata of a vegetation open in response to a photosynthetic demand, but they close in response to a higher D. Air humidity has a direct effect on stomatal conductance and not through the water potential of soil or leaf. Because D is very small during the first hours of the morning and the photosynthetic demand high, a sharp peak in conductance will be observed for this situation. The direct reaction to D leads to an asymmetric course of photosynthesis during the day (see Fig. 7.1). The photosynthesis-light response curve shows two branches; the upper (closed triangles and circles in Fig. 7.2) refers to open stomata, whereas the lower stands for stomata with C_i -regulation (the stomatal opening is adapted to keep the internal CO_2 concentration constant during day-time). It appears that plants with D-regulation follow the upper branch during the morning (open stomata because of low D-values) and the lower branch during the afternoon. According to Haverkort and Goudriaan, a strategy of constantly open stomata mainly occurs for a combination of sufficient soil water and moist air. If slight water stress occurs, the *D*-response comes into effect.

The relationship between Q_p and F_c at the CES (not shown) was not as clear as for the other two sites which may have been related to some of the difficulties of using the Bowen ratio method. The fact that many near-zero values occurred even for high Q_p values, may have been caused by the circumstance that during day 282 the Q_p -effect is overruled by the influence of *D*. The radiation use efficiency for the SSS tiger-bush stand on day 260 was only about 170 photons per mol CO_2 fixed, considerably smaller than that measured at either the millet or savannah sites (Moncrieff et al., 1996a). By day 276, radiation use efficiency had decreased to about 350 photons per mol CO_2 fixed. Leaf-scale measurements of assimilation reported by Levy et al. (1996) show that light saturation occurs at Q_p-levels of about 500 μmol m^{-2} s^{-1} in both the dominant tree species (*Combretum nigricans* Lepr. ex. Guill. et Perott) and the dominant shrub (*Combretum micranthum*) (Moncrieff et al., 1996a).

b) Respiration

Generally, the vegetation and soil lose CO_2 through respiration. During the IOP, a gradual decline in night-time respiration of the savannah was observed, which is illustrated by the differences recorded for days 262 and 282 (see Fig. 7.1). Night-time respiration rates of the soil/root/canopy system were lower on 8 October (day 282) than on 18 September (day 262). F_c was positive longer on 18 September than 8 October, again implying that respiration had diminished. During the rainy period average values were about +3.5 μmol m^{-2} s^{-1}. Following the assumption (Goudriaan, 1982) that canopy dark respiration was < 10 % of maximum observed F_c, which was -10 μmol m^{-2} s^{-1}, then by difference, the sum of soil and root respiration was approximately +3.5 - 1.0 = 2.5 μmol m^{-2} s^{-1}.

Hodges and Kanemasu (1977) cite bare soil respiration rates equalling 1.6 μmol m^{-2} s^{-1}. For soil with roots under a corn canopy, Rochette et al. (1991) reported soil respiration ranging between 2.3 and 3.4 μmol m^{-2} s^{-1}, when soil temperatures were near 30 °C and soil moisture varied from 0.13 to 0.18 m^3 m^{-3}. Under a wheat crop soil respiration reached values between 1.2-2.3 μmol m^{-2} s^{-1} for dry conditions and up to 6.8 μmol m^{-2} s^{-1} after a rainfall event (Baldocchi, 1994). These values suggest that the sum of microbial and root respiration estimated for the fallow savannah are comparatively low, probably as a result of fewer roots and less organic matter in the soil. Although increased temperature (as observed towards the end of the IOP) is said to increase plant maintenance respiration (Kirschbaum and Farquhar, 1984; Price and Black, 1990; Baldocchi, 1994), the drying of the soil apparently counteracts this process. Respiration is reported to be sensitive to soil water deficits, though both increases and decreases have been reported (Jones, 1983). The increase in night-time air temperatures during the IOP was relatively small, however; less than 2 °C. Therefore, large changes in respiration would not be expected.

c) Spatial variability

A comparison between the values of F_c measured at the spatially separate super-sites has been described by Moncrieff et al. (1996a). A summary of their findings concerning differences in diurnal variation in F_c as gauged for the three super-sites will be given here. A direct comparison of the above described F_c as recorded at the CWS with the other HAPEX-Sahel super-sites was hindered because some of the equipment was out of action during the IOP (measurement problems related to moisture or too high temperatures, calibration problems or material failure). For this reason no period could be found in which F_c has been measured at all super-sites simultaneously. Therefore, during the wet period only a comparison between the SSS and the CWS was possible, whereas during the dry period a comparison between the CWS and the CES could be made. Comparison of the diurnal variation of F_c during day 247 as observed at the SSS and CWS, revealed similar peak values of F_c (-10 to -12 μmol m^{-2} s^{-1}), which is supported by Figs. 3.10c and 3.10d, showing similar bush and grass/herb layer *LAI* -values around day 240-250. However, the vegetation of the CWS seemed to reach its photosynthetic maximum at an earlier stage. This was not caused by a difference in atmospheric properties, as recorded values of *D* and Q_p were highly comparable. Night-time respiration values are also similar.

Another comparison for F_c , together with *D* and Q_p, this time during the dry-out, was made between the two central sites. It appeared that *D* at the CES was clearly higher. Q_p was also higher, but this might have been caused by the relationship applied to calculate Q_p from R_s. No night-time/early morning F_c-values were available for the CES, because F_c was measured using a Bowen ratio method. The small gradients during the night and during the transition hours prevented accurate measurement of F_c. During the morning hours, the fluxes at the CES appear to be smaller than at the CWS. This may also be due to problems during the transition hours. During the remainder of the day, values for both sites were in close agreement for days 261, 269 and 277. Some of the peaks coincided, but the F_c-values at the CES showed a more irregular pattern which may be a function of the method used or else may be due to problems of inadequate fetch in some wind directions. On day 269 both sites showed high values. Around this day, the vegetation at both sites reached its maximum development and sufficient soil moisture was apparently still available. One week later (day 277), soil moisture content was lower, and reduced incoming Q_p also reduced the exchange of CO_2. On day 282, F_c for both sites was clearly lower than on previous days. The vegetation had started to suffer as soil water depletion continued.

Verhoef et al. (1996b) observed a very sharp decline in leaf conductance of both bushes and herbs during the last ten days of the IOP (see also Fig. 6.7), in combination with a low moisture availability. For the CWS, the rate of increase in green *LAI* (grass/herbs) has obviously diminished (see Fig. 3.10c), whereas for the CES clearly senescence occurred (*LAI* decreases after day 270) because of higher *D* values and slightly lower Θ values as compared to the CWS. This led to considerably lower F_c-values at CES for day 282 compared to the values measured at the CWS. Besides the environmental influence, the different understorey species composition at the CES may also have caused the early senescense observed there.

Measurements of F_c over tiger-bush were made only at the SSS during the IOP. In order to get some insight into the different behaviour of savannah and tiger-bush vegetation, Moncrieff et al. (1996a) compared CWS and CES savannah and SSS tiger-bush F_c on selected days. Even though the diurnal courses of the environmental variables were very similar, the tiger-bush F_c appeared to decrease more rapidly after the last rain, having peak values of only 3 μmol m^{-2} s^{-1} on day 282 which is about half the flux obtained at the savannah sub-sites. This difference is probably caused by the fact that there are no grasses or herbs present at the tiger-bush site. These 'spenders' have a large photosynthetic activity when compared to the bushes, which keeps the savannah F_c relatively high. After the senescence of the herb/grass layer, however, (as observed at the CES), the F_c of the savannah will rapidly diminish, whereas the tiger-bush vegetation with its deep-rooting vegetation of shrubs and trees may be able to utilise drainage (Wallace et al., 1994) to maintain green leaves (and thus transpiration and CO_2 exchange) well into the dry season. For these reasons the carbon and water exchange of the tiger-bush landscape is important in the overall response of the Sahel to atmospheric forcing (Moncrieff et al., 1996a).

7.2.3 Seasonal variation

Earlier it was illustrated how the CO_2 flux varies through the day at the different super-sites. However, because the carbon balance is of interest, it is also important to know how the CO_2 flux changes through the season.

a) Seasonal course of F_c and E at CWS

Fig. 7.3 gives the daily total F_c for the CWS savannah site over the last month of the IOP, to illustrate the effect of the gradual drying of the vegetation from the start of the dry season. Here, daily total evaporation, E, is given for comparison. Micro-lysimeter measurements showed that between three and four days after a large rainstorm, soil evaporation was negligible at < 0.5 mm day^{-1}, so the eddy covariance measurements of E from 22 September (day 266) onwards can be considered to represent canopy transpiration only. Between the last rainfall event on 20 September (day 264) and the end of the IOP on 9 October (day 283), daily total values of E and F_c decreased by 50 % and 70% respectively, in response to the decreasing conductances as will be shown in Fig. 7.4.

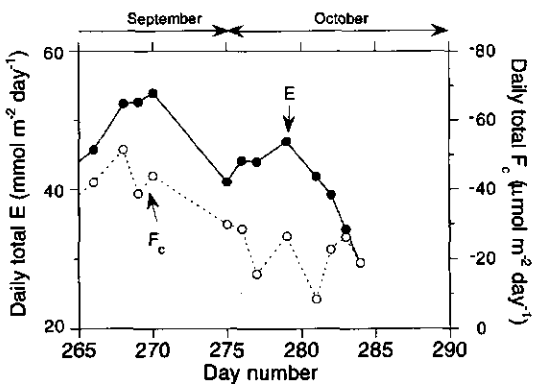

FIGURE 7.3. Daily total E and F_c during the last half of the IOP. Daily totals were obtained from 48 half-hourly fluxes, expressed in mmol m^{-2} s^{-1}. Reprinted from Verhoef et al. (1996b).

b) Direct relation with mean leaf conductance

Fig. 7.4 shows the relationship between daily total F_c and day-time mean g_l (as presented in detail in § 6.3) for *Guiera* during the last three weeks of the IOP. The relationship is fairly linear (r^2=0.73) and strongly positive. The relationships for *Mitracarpus* and *Jacquemontia* were less clear (r^2 = 0.21 and 0.57). However, it has to be kept in mind that F_c is determined by the canopy stomatal conductance, whereas g_l is the conductance of individual leaves. Furthermore, only two species of the undergrowth were sampled, and F_c also includes soil respiration which was not measured.

The increase of green *LAI* levelled off somewhat during the last part of the IOP, but did not decrease which makes it unlikely that senescence was a major cause of decreasing CO_2 uptake. Decreases in E were mainly caused by decreasing stomatal conductances. They were smaller than the decreases in F_c as the driving force for latent heat transfer increased towards the end of the IOP, as a result of decreasing atmospheric humidity and higher air temperatures.

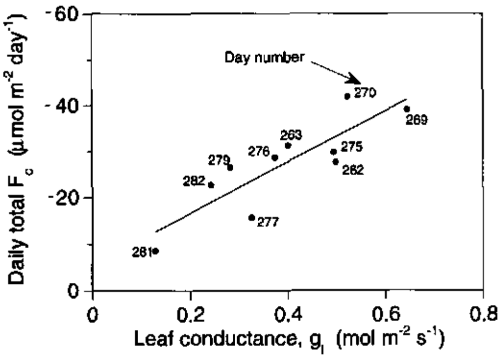

FIGURE 7.4. Relationship between mean leaf conductance, g_l, and daily total F_c for Guiera senegalensis. Reprinted from Verhoef et al. (1996b).

c) Differences between super-sites

F_C-values were integrated from 8-16 hours to compare the above described observation with temporal F_C variation at the other super-sites. These are the hours of largest photosynthetic activity and also the only hours for which we have data available for the CES. Fig. 7.5 shows the integrated F_C-values (hereafter referred to as ΣF_C) for the three sites during the IOP. A rapid increase is observed for the available days at the SSS, the central sites show a sharp decline after day 272. ΣF_C for the CES is clearly less than values calculated for the CWS, especially during the last two days sampled (277 and 282), which is to be expected from the *LAI* development of the undergrowth (Fig. 3.10c). This is in agreement with the findings of Gash et al. (1996) who found the evaporative fraction at the CES to be significantly lower during the last three weeks of the IOP.

FIGURE 7.5. Integrated F_C (8-16 GMT) for the three super-sites by day of IOP, savannah. Reprinted from Moncrieff et al., 1996a.

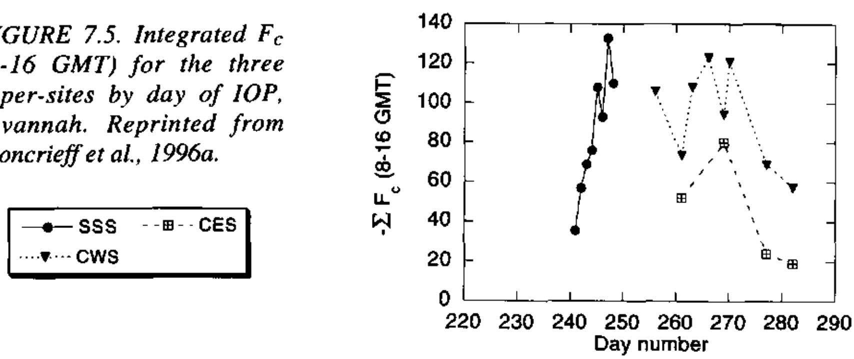

Fig. 7.6 shows a more detailed picture of the seasonal course of F_C as measured over fallow bush at the CWS and SSS in two contrasting weeks where soil moisture status was changing markedly. At the SSS, there had been five periods of rain in the few days before day 243 and about 200 mm of water was stored in the soil profile down to a depth of 150 cm. A further shower on day 246 increased soil moisture storage. We can regard the net CO_2 flux at the SSS therefore as being representative of a period when soil moisture was not limiting and the increase in net CO_2 flux as the week progressed is clear. Maximum *D* on the days shown varied from 0.8 kPa on day 241 to 2.1 kPa on day 247, but there was no obvious indication that evaporative demand by the atmosphere influenced the assimilation over this period. The contrast is clear with the CWS data as soil moisture and increasing evaporative demand act in the way described earlier to suppress net carbon exchange towards the end of the IOP at the CWS (Moncrieff et al., 1996a).

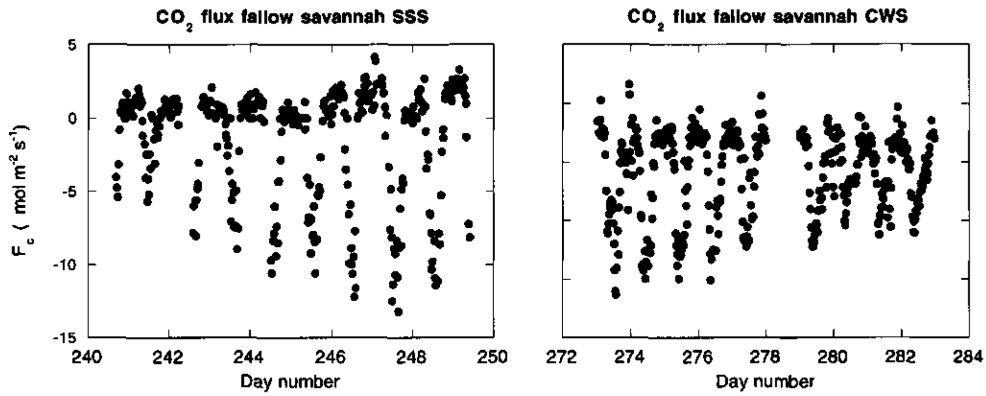

FIGURE 7.6. F_c at SSS and CWS over two contrasting weeks during IOP. Reprinted from Moncrieff et al. (1996a).

d) Influence of environment

The value of ΣF_c, as given in Fig. 7.5, appears to be clearly related to D (averaged between 8 and 16 GMT) as indicated in Fig. 7.7a. An interesting phenomenon can be observed in this graph. The measurements of the SSS indicate that ΣF_c is positively correlated with D (more CO_2 exchange during days with higher D), whereas the measurements at the central sites yield lower values of ΣF_c with increasing D. It is likely that this is just a Q_p-effect as Q_p for the SSS also increases as D increases over the period shown.

Fig. 7.7a can be divided into two parts: one where the exchange of CO_2 is reduced by low D and one where the stomatal opening is regulated by a combination of high D and relatively low soil moisture content. The breakpoint between the driving force restricting and the conductance restricting effect of D seems to be around 1.5-2.0 kPa. Still, this graph has to be interpreted with care as the vegetation is in a different development stage for the ascending and descending part of the 'curve'.

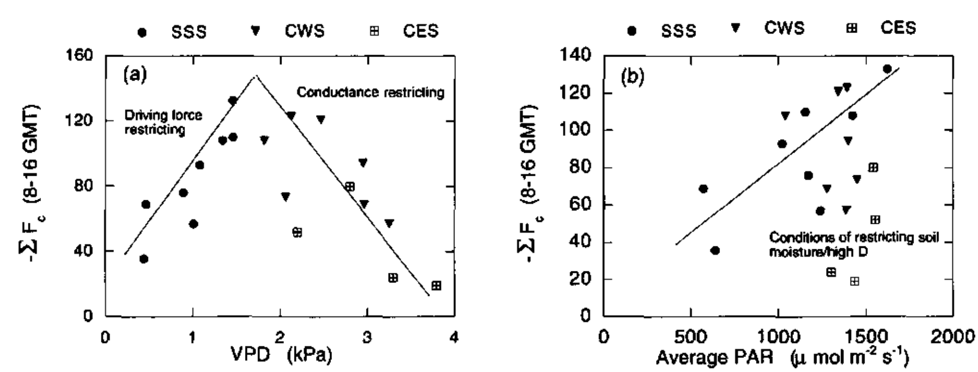

FIGURE 7.7. Integrated F_c (8-16 GMT) for the three super-sites against D (a) and against Q_p (b), savannah. Reprinted from Moncrieff et al., 1996a.

The influence of Q_p (averaged between 8 and 16 GMT) on ΣF_c is given in Fig. 7.7b. This graph shows that increasing Q_p-values only lead to a higher CO_2 exchange under mild and relatively well-watered conditions. When the vegetation experiences more stress, either by high D-values and/or low soil water content, higher Q_p values do not guarantee higher F_c-values.

7.2.4 Water use efficiency

a) Introduction

Water use efficiency characterizes the capability of the vegetation to utilize the resources available (Monteith, 1972; Jarvis, 1986). On a daily basis, F_c is dominated by solar radiation, when no water stress is present. The evapotranspiration, E, is dominated by the amount of available energy, which is also strongly dependent on R_s. Because of this common dependency on R_s, the relationship between the two parameters as expressed in $|F_c / E|$ becomes highly influenced by D (Moncrieff et al., 1996a).

b) Diurnal variation of $|F_c / E|$

This is illustrated by Fig. 7.8 which shows the dependence of $|F_c / E|$ on D for half-hourly averages. In this figure, only values with $R_s > 300$ W m^{-2} were used because it is reported that water use efficiency indices are sensitive to low levels of irradiance (Baldocchi et al., 1985). The relationship can be described by: $|F_c / E| = 0.00327\ D^{-0.935}$ ($r^2 = 0.82$), which is different from the findings of Baldocchi et al. (1985) and Baldocchi (1994), who reported a linear response of $|F_c / E|$ to D. The non-linearity was presumably caused by the harsh environmental conditions, in contrast to their experiments, where the soil was generally wet. The curvilinear shape of the response curve agrees with theory, both as derived from a big-leaf model (Bierhuizen and Slatyer, 1965; Tanner and Sinclair, 1983) and from calculations with the CANWHT-model, as shown by Baldocchi (1994).

The vegetation appeared to be most efficient when D was low (which occurs during early morning), and stomata were still wide open. When D increased $|F_c / E|$ declined rapidly, after which the stomata diminished their opening (between 8 and 10 GMT). After partial stomatal closure, $|F_c / E|$ decreased at a smaller rate, which was followed by a section (see Fig. 7.8) where $|F_c / E|$ stayed relatively constant with D. Baldocchi et al. (1985) call the decrease of $|F_c / E|$ with increasing D (at least on a daily basis) an artefact of water-stress induced stomatal closure. However, if C_i decreases, F_c will decrease too. This causes F_c to decrease more than proportionally at high D compared to E (see also Jacobs, 1994). Furthermore, the fact remains that D is much easier to measure than g_l. The clear relationship between D and $|F_c / E|$ could be used to calculate CO_2 fluxes from measurements of D and E only, which means that long-term estimates of F_c can be obtained without expensive EC equipment (if E is measured with, for example, the BREB method).

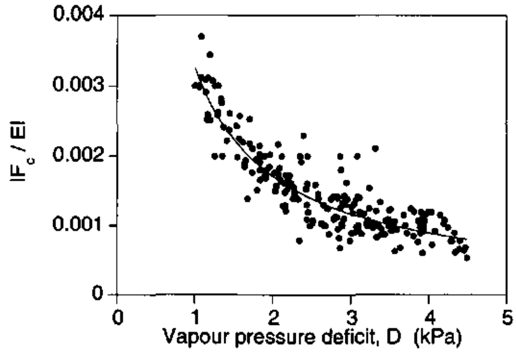

FIGURE 7.8. Relationship between half-hourly values of $|F_c / E|$ and D at the CWS fallow savannah site. The plotted curve is described by $|F_c / E|$ = 0.00327 $D^{-0.935}$ (r^2 = 0.82). Reprinted from Verhoef et al., 1996b.

The response of $|F_c / E|$ to D has been observed by several authors (Bierhuizen and Slatyer, 1965; Rawson et al., 1977; Overdieck and Strain, 1981; Schulze and Hall, 1982; Meinzer, 1982; Baldocchi et al., 1985). Baldocchi (1994) found that $|F_c / E|$ of a wheat crop increased as the absolute humidity deficit of the atmosphere decreased. $|F_c / E|$of a corn crop on the other hand, was relatively insensitive to humidity deficits. He calculated $|F_c / E|$ values of -5 to -15 mg g^{-1}, whereas the values calculated for the savannah range from -5 to -45 mg g^{-1}, indicating that the savannah behaves more efficiently, especially at high atmospheric humidity.

There was only a slight difference (< 10 %) between values of $|F_c / E|$ for days with high and low soil moisture status, again underlining the fact that soil water status does not change the vegetation's response to changing atmospheric conditions. However, this may have been caused by the fact that the soil water measurement depth was rather shallow, which means that perhaps the plants were still able to get sufficient water from below 50 cm.

Moncrieff et al. (1996a) compared diurnal variations in $|F_c / E|$ for the SSS and CWS super-sites. Again, no data were available that covered exactly the same period. $|F_c / E|$ was greatest in mid-afternoon for the days 240-249 at the SSS, whereas at the CWS, for day numbers 269, 277 and 282, $|F_c / E|$ was greatest in the early daylight hours. The afternoon values at the CWS appeared to be relatively constant but lower than in the morning. This has also been explained with reference to Fig. 7.8. An explanation for this is the different stomatal behaviour observed during the wet and transition periods (see § 6.3). Conductance measurements made on the *Guiera* bushes (see Fig. 6.5) show that stomata keep on opening until around 11 GMT during the rainy period, and then partially close as increased D and radiation loads cause stress. During some of the wet days, stomata start to re-open in the early afternoon thus causing the maximum in $|F_c / E|$. On the other hand, in the drier period (CWS) the reduced soil moisture and increased D-values restrict stomatal conductance and after the early-morning peak stomata tend to stay less open later in the day, which results in the lower afternoon values. The vegetation at the CWS during this period is thus optimizing its exchange with the environment early in the day and protecting itself against atmospheric and soil-moisture induced stress throughout the rest of the day (see Moncrieff et al., 1996a).

Calculations of $|F_c / E|$ were also made for the SSS tiger-bush stand by Moncrieff et al. (1996a) for the days 261-283. It appeared that its values were similar to the ones observed over the savannah sites. As for the CWS, the maximum $|F_c / E|$ was always obtained in the morning, usually before 11 GMT with a decline in $|F_c / E|$ into the afternoon. There was no secondary peak in the late afternoon, indicating that tiger-bush, like the savannah vegetation, was optimising exchange of water and CO_2 in the morning and then decreasing stomatal conductance to avoid desiccation for the remainder of the day.

c) Seasonal variation of $|F_c / E|$

On a daily basis, $|F_c / E|$ is also influenced by D and Θ, as shown in Fig. 7.9 which gives the relationships between $|F_c / E|$ and D and Θ. The highest correlation ($r^2 = 0.67$) was observed for $|F_c / E|$ against D. For Θ the correlation was much lower ($r^2 = 0.50$). In this case the relationship between $|F_c / E|$ and D is linear because the different response to D, observed during morning and evening as a result of stomatal closure, will disappear because of the averaging procedure.

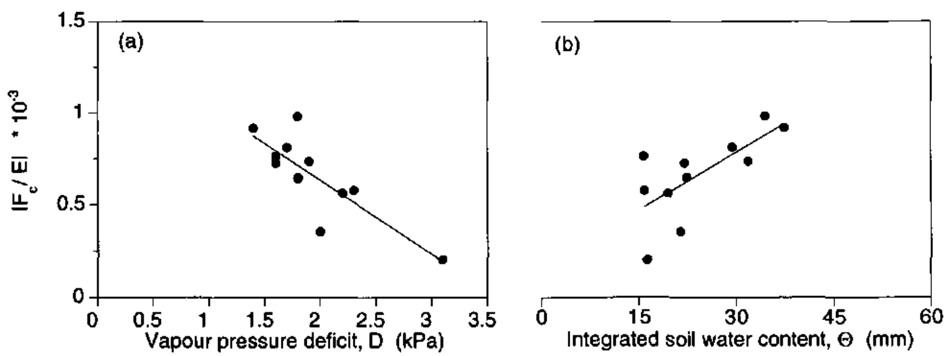

FIGURE 7.9. Daily averages of $|F_c / E|$ against D (a) and Θ (b) for the CWS fallow savannah site. Reprinted from Verhoef et al., 1996b.

7.3 Conclusions

The surface flux of CO_2 varied across the area both in space and time. Much of the difference in flux, measured on the same type of vegetation on the same day but at different super-sites, was largely a function of the developmental stage of the plants, which in turn was dictated by the timing of the arrival of the rains earlier in the year. This was particularly apparent with fluxes over millet (see also Jacobsen, 1995), whereas differences in F_c over the different savannah sites were less affected, but evidence that the grass and herb layers were at different stages was apparent. Thus, difference in F_c will be a function of the relative proportion of C_4-grasses to C_3-plants which are most active. There was a clear indication that savannah (and tiger-bush) vegetation optimized stomatal conductance to mitigate against stress caused either by high evaporative demand or soil moisture induced stress. All surface types showed decreasing F_c as the region became progressively drier after the termination of the seasonal rains. Models which seek to scale up from measurements at the scale of individual super-sites must take into account the heterogeneity of the type of surface vegetation, and also the variability in life cycle stage of the vegetation which is rainfall-dependant (Moncrieff et al., 1996a).

Water use efficiency, $|F_c / E|$, appeared to be a function of atmospheric vapour pressure deficit, D, both on a diurnal and a daily scale. This observation, made on all vegetation types and super-sites, may be a useful tool if we want to make estimates of F_c for (potential) production calculations or (global) carbon balance calculations. Measurement of E by a relatively simple and cheap method like the BREB method, or calculation of evapotranspiration by the Penman-Monteith method, for example, thus yielding a value of actual E, will allow for calculation of F_c if the D-response curve for a particular vegetation at a particular site is known.

8 MODEL RESULTS

8.1 Introduction

One of the main aims of the HAPEX-Sahel project is to develop aggregation techniques for estimating the large-scale hydrological and meteorological behaviour of extensive areas in the Sahel. These aggregation techniques involve a combination of remote sensing, to provide information on the spatial variability of surface properties such as albedo, aerodynamic roughness and soil moisture, and adequate meteorological modelling.

As can be deduced from the earlier chapters in this thesis, the final values of sensible and latent heat fluxes depend on the combination of available energy, the resistance network, the environmental conditions and the state of the vegetation or substrate. In order to ensure proper upscaling, we want to understand the underlying causes of flux differences between different vegetation types. Hence, it is necessary to make a good estimate of these influences and of their relative importance. A SVAT, dealing with the above described factors is, in this context, an essential expedient. Atmospheric state variables like temperature, humidity and wind speed can be relatively easily and accurately monitored. The determination of available energy, i.e. net radiation and soil heat flux, involves more problems especially for a sparse vegetation as expounded in Chapters 2 and 5. As resistance values are calculated, the path gets even more slippery, notably when dealing with the within-canopy or surface resistances which are still poorly defined. Nevertheless, in the next sections an attempt will be made to understand the combined effect of the complicated interplay between vegetation, soil and atmosphere on the latent heat flux of savannah and tiger-bush. This chapter will therefore address the following topics.

First (§ 8.2), the results of a **pre-study** (Van den Hurk et al., 1996) concerning a **vineyard,** will be briefly presented. Van den Hurk et al. (1996) tested the performance of three SVATs, which led to several recommendations, mainly concerning the resistance network and the soil heat flux. These conclusions can be partly transferred to the model configurations used for savannah and tiger-bush. However, the vineyard, although it was also sparse and grew under semi-arid conditions, was very different from the Sahelian vegetation. The savannah and tiger-bush shrubs have a more scattered nature, in contrast with the row structure of the vineyard. In addition, the Sahelian shrubs are much higher (up to four times as tall) and, as in the case of the tiger-bush, cover a larger percentage of the surface area, which may seriously influence the resistances. Finally, the savannah had a vegetated understorey, which may also lead to conclusions different from those given in Van den Hurk et al. (1996).

Based on the findings described above, two models (**DCM** and **TCM**) have been developed (Van den Berg, 1995b) to describe exchange at the sparse savannah and tiger-bush surfaces (see also Chapter 4). These models combine the best parts of single SVATs. Where possible, their results will be compared with the outcomes of the original models (**CM, DD**), in order to check the performance of the **DCM** and **TCM** -models. In addition, the behaviour of two other models was tested. The well-known **SW** model was chosen because of its simplicity, making it useful for larger-scale applications and possibly for prediction of evaporation on a longer time scale. The second model is the **TL**-model, based on the findings of Dolman (1993) and Huntingford et al. (1995). This model has already proven effective for savannah vegetation and it has the advantage of a 'non-extinctive' treatment of radiation.

Because of the introduction of two extra models, it was considered justifiable to perform **some preliminary analyses** (including simple sensitivity studies), as presented in § 8.3, mainly to illustrate the differences between the resistance estimates of the various models. Furthermore, we are aiming to create a model that is physically correct, but which does not put an unnessecary burden on computer time and user-supplied input (both data and parameters). Only such a model will be practical for one of the main aims of the HAPEX-Sahel project: aggregation of the different components in the grid-square (millet, savannah, tiger-bush) to a single flux value. Therefore, the most suitable model has to be able to attach distinctive properties to these vegetations (resistances, available enegy etc.), but **not be too sensitive** for certain, sometimes ill-defined, **model parameters**. Consequently, a study was made of the sensitivity of the resistances employed in the various models to several important input parameters.

These sensitivity studies also served to highlight the possible **differences between savannah and tiger-bush**. A comparison was made of the magnitude of their resistances and available energy as calculated by the models. One of the aims of this comparison was to test the findings of Gash et al. (1996), saying that the variability of the evaporation observed in the HAPEX-square was predominantly caused by differences in available energy, rather than by the resistance values representing the surface. Section 8.3.3 will concentrate on testing this result. This will be accomplished by sensitivity analyses applying a simplified version of the TL-model described in Chapter 4. These sections will be confined to the possible differences in evaporation between the savannah and the tiger-bush and what the most likely causes of these differences are.

In § 8.4 all SEB-fluxes are described, which are calculated with the various SVATs and combinations of their components. All models were run with the same r_c^s-values, in order to underline the differences in the atmospheric resistances and the parameterization of soil heat flux. Furthermore, the assumption that the canopy surface resistance is a constant (SW) or a function of radiation only (CM) is superseded, since many recent studies (see references in Chapter 6) have underlined the importance of atmospheric humidity and soil moisture in conductance parameterizations.

Finally, a relatively simple model ('evapoclimatonomy' model, see Nicholson and Lare, 1990) will be applied to extend the knowledge of the energy balance on a diurnal/seasonal scale to an annual scale (§ 8.5). To accomplish this, ten years of measured (e.g u, T_a) or simulated (for example, R_n) monthly averages of model input or parameters will be used. First, relationships between readily available meteorological parameters and surface parameters (e.g. albedo) will be derived from the SEBEX data (as presented in Chapter 5). With these relationships an extrapolation to other years will be pursued, which will give insight into the possible interannual variations of the energy balance.

8.2 Pre-study of SVATs

Van den Hurk et al. (1996) compared three SVAT- models (Deardorff, 1978; Choudhury and Monteith, 1988; Viterbo and Beljaars, 1995) simulating fluxes collected at a dry sparse vineyard site in La Mancha, Spain. These models will be referred to as DD, CM and VB, respectively. The algorithms used to describe soil heat flux density, aerodynamic transfer of water and heat between the surface and the atmosphere, and crop evaporation all have a different physical basis in these models. A common feature of the models is that interaction of many processes takes place via the surface temperature. A comparison of these schemes showed a wide range of predicted values of soil heat flux density and surface evaporation.

With respect to the soil heat flux density, the parameterization of DD gave the best results. The simple resistance approach of CM underestimated the soil heat flux density by almost an order of magnitude, due to neglecting dynamic heat storage in the upper soil layer. Viterbo and Beljaars (1995) also underestimated soil heat flux density, by approximately 30%. Much of this underestimation is due to the choice of the value for the apparent heat conductivity of the skin layer.

In all tested models the surface temperature plays a key role, since it regulates important processes such as soil heat flux, sensible and latent heat flux, and in a minor sense net radiation. CM predicted high sensible heat fluxes in the original form, since surface temperatures are strongly overestimated when too little heat is transported into the soil. However, when the soil heat flux density was forced to values simulated by DD, the CM parameterization of the aerodynamic exchange within the canopy appeared to give better results of the surface temperature than the formulation used by DD. In CM, the total exchange resistance for heat between the bare soil and the reference level resembled the value included in VB, which was based on field measurements of roughness length, surface temperature and sensible heat flux. DD prescribes a value of r_a^s which is about half as large as CM, and consequently underestimated the bare soil temperature.

The crop resistance for evaporation was best described by CM, where a calibrated function of incoming radiation was used to describe r_s^c. The dependence of r_s^c on soil moisture content cannot be expected to be realistically described by either DD or VB, which assume a much smaller root zone than found in the field. Also the response of stomatal aperture to ambient humidity deficit is not fully resolved and is still a matter for discussion. Under dry and warm conditions several plant species seem to develop a specific survival mechanism, and respond differently to air humidity than the types of vegetation from which the expression of Noilhan and Planton (1989) was obtained (Monteith, in press).

The partition of radiant energy over the vegetation and the underlying substrate is solved in two different ways by CM (adopting radiant extinction) and DD (solving separate energy balances for the two surface components). The extinction parameterization was originally developed for closed canopies, and is expected to deviate significantly from real radiative interception for a vegetation stand with widely separated plants. However, drawing up separate radiation balances does not take all edge effects into account. Which of the parameterizations is to be preferred can only be supported by detailed measurements and modelling efforts, and will most likely be different for each type of vegetation.

In large scale application a land surface scheme needs to be able to describe accurately a wide range of land surface types, covering the full transition from densely vegetated to completely bare. From the current study, a general conclusion can be made that for a rather sparsely vegetated surface none of the three models compared can be considered to be the 'ideal' land surface scheme. Each of the schemes involved in this test has some superior qualities compared to the others, but also shows significant deficiencies when applied to a very sparse canopy. A combination of parts from each of the models will likely give optimal results for the surface for which this comparison was run. In line with the conclusions presented above, such a combined model would consist of a soil heat flux parameterization using the Force-Restore method, an aerodynamic exchange process simulated using the resistance formulation of CM, and a canopy resistance parameterization that realistically accounts for stomatal responses to soil moisture content and air humidity. This resulted in the so-called DCM (Dual Component Model) and the TCM (Triple Component Model), described in Chapter 4.

8.3 Preliminary analyses

8.3.1 Introduction

Several differences can be put forward when comparing the savannah and tiger-bush. First of all, the tiger-bush has a bare substrate and a higher upperstorey. Additionally, the tiger-bush is not composed of truly scattered bushes, but of elongated, clumped bush/tree structures that can be considered as an intermediate form between row crops and a random surface coverage. The implications of the effect these different canopy structures have on the drag partition has been described in Section 6.1. These properties lead to different values of z_{0m} and d and thus to variation in exchange coefficients (see Eqs. 4.8 or 4.13, for example), i.e in the aerodynamic resistances between the substrate and the canopy source height and between the latter and the reference height. Furthermore, under dry circumstances the bare soil will exhibit a higher surface resistance (r_s^s) than that of the vegetated understorey of the fallow savannah.

Another difference between both vegetations is their fractional vegetation cover, which in this case refers to the coverage by shrubs. As far as the savannah and tiger-bush surfaces monitored in the HAPEX-square were concerned, tiger-bush appeared to have a higher percentage of canopy coverage ($\approx$ 30-40 %, compared to 10-20 % for savannah). This variation will influence available energy, leading to higher values of (R_n-G) for the more densely vegetated surface as explained in Section 5.4. The higher canopy cover in combination with the higher tiger-bush vegetation strips will also lead to a higher value of LAI_c (here estimated to be 1.0). Unfortunately, there are no field data available to confirm this.

The following sections describe a step-wise investigation into the factors influencing the definitive value of evaporation. To begin with, the resistances will be compared as calculated by several parameterizations

8.3.2 Analysis of resistances

a) Difference between parameterizations and vegetations

Table 8.1. gives the general input values necessary for all further model calculations. Values were either measured (e.g. canopy height), estimated (tiger-bush *LAI*) or prescribed by the experimental set-up (e.g. reference height).

TABLE 8.1. General input variables used for all models.

Description	Symbol	Value		Units
		Savanna	Tiger-bush	
Reference height	z	4.5*	14.0*	(m)
Canopy height	h	2.5	4.0	(m)
Height of understorey	h_u	0.5		(m)
LAI of canopy	LAI_c	0.35	1.0**	(m^2 m^{-2})
LAI of understorey**	LAI_u	0.80		(m^2 m^{-2})
Ratio substrate/bush	α	0.80/0.85	0.67	(-)

* In the test runs z has been set to $2h$ in order to make savannah and tiger-bush comparable.

** This input is only used for the TL-model.

Table 8.2 lists the user-defined model parameters (n, c_d, w_c, w_h) necessary for the calculation of the aerodynamic and boundary layer resistances. Canopy roughness lengths, z_{0m}, and displacement heights, d, for SW and TL were calculated with $z_{0m} = 0.13h$ and $d = 0.66h$. For CM and DD the same formulas were applied, as given by Eq. 4.17a and 4.17b. In the final model runs, TL will be run with $n = 4.23$, because this parameter was jointly optimized during the inverse calculations of the understorey r_s^c.

For all models, substrate roughness lengths were set to 0.01 for the bare tiger-bush soil and to 0.05 for the savannah herb/grass-layer, the displacement height of the substrate, d_u, is only needed in the TL-model. It was found from $0.66*h_u$, where h was taken as 0.50 m. The TL-model also required an estimate of the roughness length of the total vegetation. The measured values given in Table 6.1. were used for the savannah ($z_{0m} = 0.25$ and $d = 1.14$) whilst for the tiger-bush $d = 1.60$ and $z_{0m} = 0.28$ were applied.

TABLE 8.2. User-defined parameters applied in the resistance calculations by the different models (See for example Fig. 8.1). An empty space means the model does not apply this parameter.

Description	Symbol (Units)	Parameter value		
		SW	CM, DD, DCM, TCM	TL
Attenuation coefficient of eddy diffusivity within the vegetation	n	2.5	2.5	2.5*
Attenuation coefficient of wind speed within the vegetation	m		2.5 (CM, DCM, TCM)	
Drag coefficient for leaves	c_d		0.2	0.2
Upper canopy leaf width	w_c		0.02	0.02
Leaf width of undergrowth	w_u		0.005 (TCM)	0.005

Fig. 8.1 shows the aerodynamic, r_a^a and r_a^s, and boundary layer resistances, r_b^c, as calculated with SW, CM, DD and TL and the input given in Tables 8.1 and 8.2. In all calculations a neutral stability was assumed and u was set to 2.5 m s^{-1}.

Regarding r_a^a, it appears that the models predict a lower (CM and DD, having the same parameterization) or similar value for the tiger-bush (TL), except SW, which predicts a higher value for the tiger-bush compared to savannah. The values of r_a^s are higher for the tiger-bush (especially the value predicted by SW) according to SW, CM, and TL. This is mainly caused by the lower value of $z_{0m,u}$. DD predicts a slighly lower value for the tiger-bush and its values of r_a^s are rather low compared to the other parameterizations, as already noted by Van den Hurk et al., 1996. This fact has led to the incorporation of the CM-aerodynamic resistance formulation in DCM and TCM. The last resistance, bush r_b^c, is consistently calculated lower for the tiger-bush, mainly as a result of larger LAI-values for the tiger-bush. The relatively small values simulated by TL are created by the fact that their parameterization incorporates bush coverage fraction, here taken as 0.15 and 0.33 for the savannah and tiger-bush, respectively.

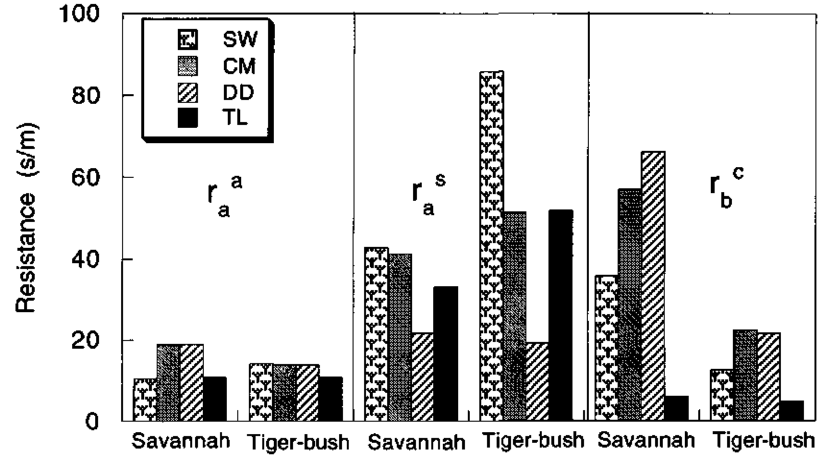

FIGURE 8.1. The different values of the aerodynamic (r_a^a and r_a^s) and boundary layer (r_b^c) resistances as calulated for savannah and tiger-bush by four model parameterizations. Values for DCM and TCM are not shown as they are equal to DD (r_a^a and r_b^c) or CM (r_a^s).

b) Influence of model parameters on resistances

This section investigates the influence of three model parameters (upperstorey *LAI*, $z_{0m,u}$ and n), that are used in all models, on the the resistances r_a^a, r_a^s and r_b^c. *LAI* was chosen because it is an important user-supplied input, which is not easy to determine and therefore may give a different outcome, depending on the method used. From the above described analysis, the parameter $z_{0m,u}$ is suspected of having a large influence on the value of r_a^s. However, the measurement arrangement was not designed to find a value for $z_{0m,u}$ and the values reported in literature vary widely (Ten Berge, 1990; Jacobs et al., 1991). Finally, n also exhibits a large range (Choudhury and Monteith, 1988; Huntingford et al., 1995) and it is not possible to determine this parameter independently.

Understanding the sensitivity of the several model resistances to the independent model parameters is important for two reasons. First, it will help understand the possible difference in evaporation predicted by the models and for the different surfaces. Secondly, it gives an indication as to which model parameters should be supplied with the largest accuracy.

Figs. 8.2 to 8.4 show the influence of *LAI*, $z_{0m,u}$ and n on r_a^a, r_a^s and r_b^c, respectively. The left-hand graphs give the results for the savannah, the right-hand graphs represent the tiger-bush results, as both vegetations have a different canopy height (and thus reference height, in this case taken as $2h$), *LAI* and roughness parameters. The x-axis has three sections: one for each model parameter. Each segment shows two values, 0.5 and 2.0, referring to 0.5 and two times the standard parameter value, respectively. Hence, the x-axis is titled 'relative parameter value'. Standard values of *LAI*, $z_{0m,u}$ and n for the two surfaces are given in Tables 8.1 and 8.2. The y-axis shows the percentage difference of the resistance under consideration. A positive value means that changing a certain parameter from its reference value increases the resistance value. In each graph the estimates by the four models are given, thus indicating the sensitivity of the resistance predicted by each SVAT.

First of all, Figs. 8.2-8.4 illustrate that different parameters are involved in the resistance estimated by the different models, as was already explained in Chapter 4. For example, *LAI* is not used in the calculation of r_a^a by the TL-model, whereas it has a considerable influence on the r_a^a-values calculated by CM and DD.

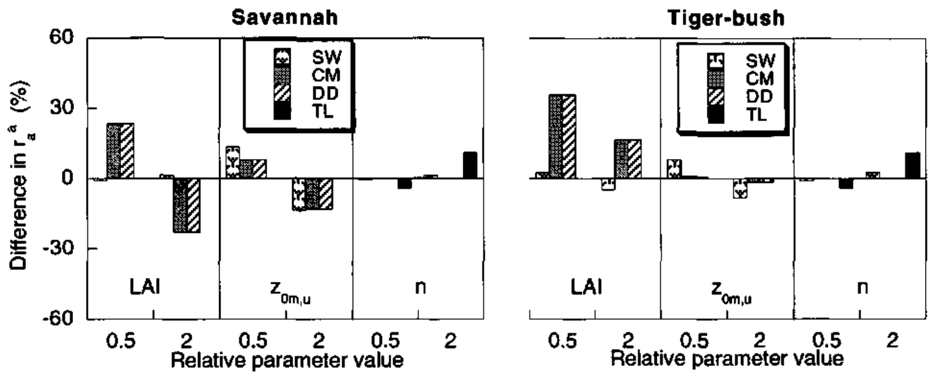

FIGURE 8.2. Sensitivity, expressed as a percentage change, of the aerodynamic resistance between the mean canopy air stream and the reference level, r_a^a, to a change in LAI, $z_{0m,u}$ and n, respectively. Standard parameter values are multiplied by 0.5 and 2.0. The left-hand part of the figure gives the results for savannah (standard parameter values: $LAI_b = 0.35$, $z_{0m,u} = 0.05$, $n = 2.5$), whereas the right-hand graph deals with the calculations made for tiger-bush (standard parameter values: $LAI = 1.0$, $z_{0m,u} = 0.01$, $n = 2.5$).

Considering r_a^a (See Fig. 8.2), it appears that *LAI* is a relatively important parameter in the CM/DD (and thus in the DCM/TCM) parameterization. This is caused by the dependence of the z_{0m} and *d*-estimate (see Eq. 4.17) on *LAI*. A two-fold variation in *LAI* changes r_a^a by around + (0.5 *LAI*) or - (2.0 *LAI*) 20 % for the savannah. In the case of tiger-bush, an alteration of *LAI* in both instances led to an **increase** in r_a^a (up to 35 %) compared to the outcome calculated with the standard value of 1.0. The influence of *LAI* on the SW-result is small and opposite for the the savannah and tiger-bush case. *LAI* exerts no influence on TL estimates of r_a^a , because of its α-approach.

The roughness length of the understorey, $z_{0m,u}$, influences the results of the SW and CM/DD parameterizations by up to about +/-10 %. For all models, and both surfaces, a decrease in $z_{0m,u}$ leads to an increase in r_a^a. The r_a^a-estimate of the SW parameterization is influenced most by $z_{0m,u}$. This is especially obvious for the tiger-bush. The CM/DD model estimates of r_a^a for tiger-bush are hardly influnced by $z_{0m,u}$, because of its small values (0.005 and 0.02).

The model parameter n, the attenuation coefficient of eddy diffusivity within the vegetation, plays a role in the SW and TL model only. A decrease in n induces a decrease in r_a^a, wheras an increase yields the opposite effect. Maximum changes of + 10 % are observed for the TL model.

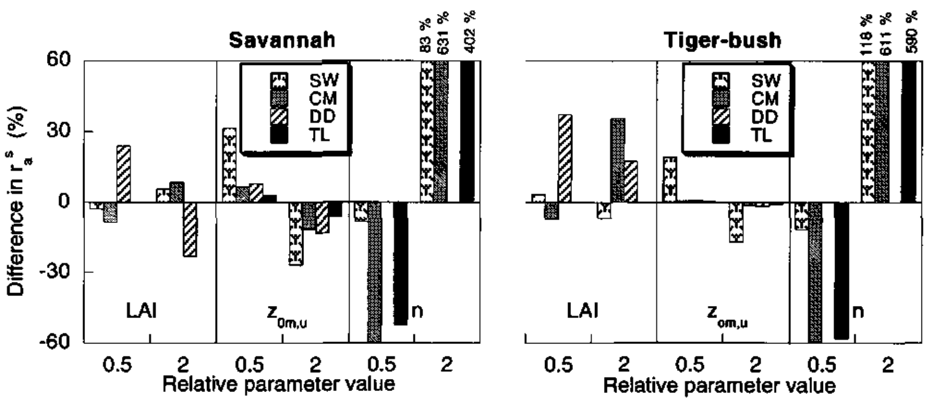

FIGURE 8.3. Sensitivity, expressed as a percentage change, of the aerodynamic resistance between the surface and the mean canopy air stream, r_a^s, to a change in LAI, $z_{0m,u}$ and n, respectively. Standard parameter values are multiplied by 0.5 and 2.0. The left-hand part of the figure gives the results for savannah (standard parameter values: LAI = 0.35, $z_{0m,u}$ = 0.05, n = 2.5), whereas the right-hand graph deals with the calculations made for tiger-bush (standard parameter values: LAI = 1.0, $z_{0m,u}$ = 0.01, n = 2.5).

Fig. 8.3 leads to the following conclusions. Again, *LAI* is employed only in the SW, CM and DD parameterizations. As shown in Chapter 4, CM and DD apply a different equation for calculation of r_a^s. Apparently, this causes the influence of a change in *LAI* to be opposite for the savannah case. This adverse effect is only found for the 0.5-case where tiger-bush is concerned. The sensitivity of r_a^s to *LAI* is similar to the one observed in Fig. 8.2.

As expected, the influence of $z_{0m,u}$ on estimates of r_a^s is larger compared to the r_a^a-estimates. The estimates by the SW-model turn out to be relatively sensitive to $z_{0m,u}$, and in this they are similar to the results in Fig. 8.2.

The last segment shows that the parameter *n* appears to be extremely important in the calculation of r_a^s especially by CM and TL. The positive bars go up to the values written on top of them, for both vegetations. In the DD-approach, r_a^s is independent of *n*, because it is parameterized as a function of windspeed, *u*, and friction velocity, $u*$ (see Eq. 4.18).

Fig. 8.4 shows that the bulk boundary layer resistance, r_b^c, is predominantly determined by *LAI*. $z_{0m,u}$ plays a very minor role in the CM and DD-parameterizations. The parameter *n* only influence the estimates of the TL-model, up to values of 30 %.

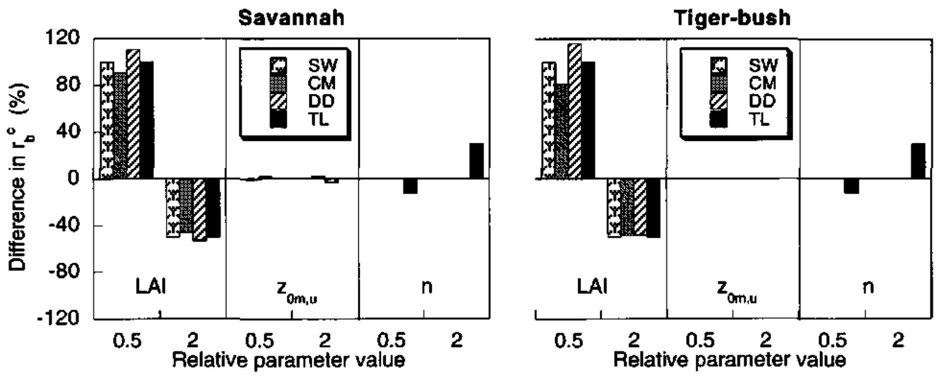

FIGURE 8.4. Sensitivity, expressed as a percentage change, of the boundary layer resistance, r_b^c, to a change in LAI, $z_{0m,u}$ and n, respectively. Standard parameter values are multiplied by 0.5 and 2.0. The left-hand part of the figure gives the results for savannah (standard parameter values: LAI = 0.35, $z_{0m,u}$ = 0.05, n = 2.5), whereas the right-hand graph deals with the calculations made for tiger-bush (standard parameter values: LAI = 1.0, $z_{0m,u}$ = 0.01, n = 2.5).

8.3.3 Possible difference in evaporation between savannah and tiger-bush

In § 8.3.2 we established typical values for the various 'above-surface' resistances found for the savannah and tiger-bush (see Fig. 8.1) and we studied the sensitivity of the resistance networks to the most important input parameters. Here, we will investigate what the influence of these different resistances will be on the final values of evaporation found for both surfaces, in combination with the disparate vegetation coverage leading to different values of (R_n-G). Several sensitivity runs have been executed with the TL-model to investigate the influence of the different surface parameters and substrate/bush ratio as observed for the savannah and tiger-bush. The graphs given hereafter summarize the theoretically possible difference in evaporation coming from the savannah and tiger-bush surfaces. For this purpose, net radiation between 8-16 GMT, calculated from the hour of day, has been used as input. This particular time span was chosen, because evaporation and evaporative fraction have been calculated for this period in Gash et al. (1996), and Moncrieff et al. (1996a), for example. Moreover, most of the exchange will take place between these times. To mimic the higher net radiation for the vegetated surface elements, $R_{n,b}$ was arbitrarily parameterized as 1.2 times R_n, whereas $R_{n,u/s}$ was only 80 % of R_n. G_b was assumed to be 10 % of $R_{n,b}$, whereas $G_{u/s}$ was 30 % of $R_{n,u/s}$. The other atmospheric input values, T_a, D and u were kept constant, and set to representative values. *LAI* was given typical values of savannah and tiger-bush.

Four comparison runs were executed as characterized by four different combinations of savannah and tiger-bush r_s^s, thus simulating the drying of the substrate, and logical values of T_a and D, in order to simulate the concurrent drying of the atmosphere. For all runs u was kept at 2.5 m/s. Reference situations were established as described by the input values given in Table 8.3. For each run the reference situation is given by the middle column of Table 8.3 and a value for α of 0.66 (i.e. simulating tiger-bush). This combination of resistances and α yields an average evaporation (8-16 GMT). So in total four reference situations were created, with tiger-bush r_s^s attaining values of 100, 2000 6000 and 10000, respectively. Savannah was given values of r_s^u of 100, 200, 300 and 2000, while during those runs α was given a value characteristic for savannah, with a corresponding change in *LAI*. Furthermore, the resistances were doubled or halved in order to assess their influence on the evaporation. This produced 25 evaporation values describing deviations from the reference per combination of r_s^s and r_s^u. For consistency reasons, all resistances were multiplied by 0.5 and 2.0.

TABLE 8.3. Resistance values used in the sensitivity analyses described in Figs. 8.5-8.8.

Type of resistance	Value (s/m)			α		T_a (°C)	D (kPa)
r_a^a	12.5	25	50	0.66	0.80		
$r_a^{s/u}$	25	50	100	0.66	0.80		
r_b^c	12.5	25	50	0.66	0.80		
r_{st}	150	300	600	0.66	0.80		
r_s^s	50	100	200	0.66		30	1.5
with r_s^u	50	100	200		0.80	30	1.5
r_s^s	1000	2000	4000	0.66		32	2.5
with r_s^u	100	200	400		0.80	32	2.5
r_s^s	3000	6000	12000	0.66		34	3.5
with r_s^u	150	300	600		0.80	34	3.5
r_s^s	5000	10000	20000	0.66		34	4.0
with r_s^u	1000	2000	4000		0.80	34	4.0

The stomatal resistances, r_{st}, given in Table 8.3 are averages of between 8-16 GMT, derived from the inversely calculated conductances (see Table 6.8) of the *Guiera* bushes and tiger-bush strips. Values of r_{st} are comparable to values given in the literature (Shuttleworth and Wallace, 1985; Lafleur and Rouse, 1990; Nichols, 1992). During the IOP, day-time averages of r_s^u ranged from 100 s/m, for days when the soil had been recently wetted and the understorey was non-stressed, until 400 at the end of the IOP when the topsoil was dry and the grasses and herbs started to senesce (see also Wallace et al., 1994). The range observed for r_s^s was much larger, as shown in Fig. 6.11, which gives values for tiger-bush r_s^s calculated from measured evaporation and the TL-model. On wet days, values as low as 100 s/m were calculated, which is very similar to the value of r_s^u during those days. On the contrary, during the dry-down r_s^s increased rapidly to values of around 5000, whereas for a completely dry top-layer values of around 10000 were assumed.

Figs. 8.5-8.8 summarize the results of the sensitivity study described above. The x-axis gives the resistance ranges listed in Table 8.3. This is not a continuous axis - it is divided into five segments, each representing one resistance. The y-axis represents the percentage difference in evaporation flux, compared to the reference (tiger-bush, middle resistance column of Table 8.3) as calculated with departing resistance and/or *LAI* plus α-values. Differences can be positive, i.e. the run with one resistance or α/*LAI* changed results in a larger L_vE, or negative. A column representing tiger-bush and savannah is shown for each resistance value (e.g. 12.5 for r_a^a). The middle part of each resistance segment only shows the savannah column, as the tiger-bush column is supposed to be the reference, and hence the difference is zero. Looking at the tiger-bush columns within a certain resistance segment, shows the influence of a changing resistance on the final flux value, while the other resistance are kept at their reference value. For example, Fig. 8.5 shows that decreasing r_a^a will lower L_vE for tiger-bush (because H increases).

The savannah columns illustrate the combined effect of α increasing (0.66 ---> 0.80) and *LAI* decreasing (1.0 ---> 0.35), as given by the savannah column at the reference resistance value, or the combined effect of resistance and α plus *LAI* changing (i.e. the speckled columns for r_a^a= 12.5 or 50 s/m). Logically, the reference savannah column will be the same for all resistance segments.

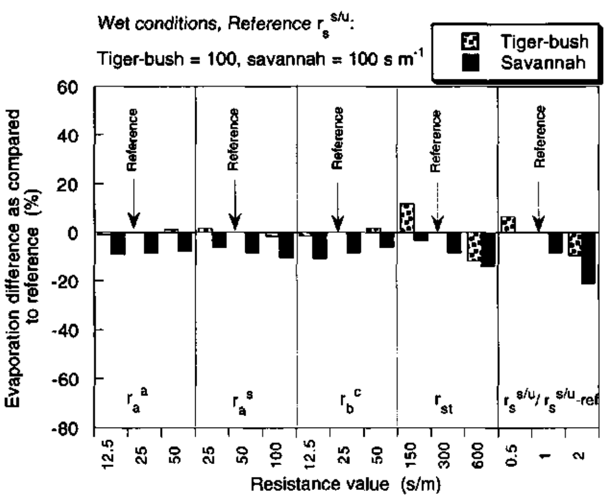

FIGURE 8.5. The influence of a change in a single resistance on tiger-bush L_vE (speckled columns) and the influence of a change in vegetation coverage, $(1-\alpha)$, plus LAI to values representative for savannah, with or without a concurrent change in resistance (black columns). This figure represents a wet understorey (r_s^s = 100, r_s^u = 100) and relatively mild atmospheric conditions (T_a = 30 °C, D = 1.5 kPa).

Fig. 8.5 illustrates that under wet conditions (i.e. during the rainy period), with $r_s^s = r_s^u$ = 100 s m^{-1}, savannah evaporation will be around 10 % less than the tiger-bush evaporation (see also Gash et al., 1996). This will mainly be caused by the larger available energy received by the tiger-bush as a result of a larger proportion of bushes. The atmospheric resistances do not influence the differences between savannah and tiger-bush very much - the largest effect is achieved by changing surface resistances. For example, if the tiger-bush r_{st} is two times lower than savannah r_{st} (which is quite well possible, see Fig. 6.13), savannah L_vE would be about 25 % lower.

FIGURE 8.6. The influence of a change in a single resistance on tiger-bush evaporation (speckled columns) and the influence of a change in vegetation coverage, (1-α), plus LAI to values representative for savannah, with or without a concurrent change in resistance (black columns). This figure represents a drying understorey (r_s^s = 2000, r_s^u = 200), and intermediate atmospheric conditions (T_a = 32 °C, D = 2.5 kPa).

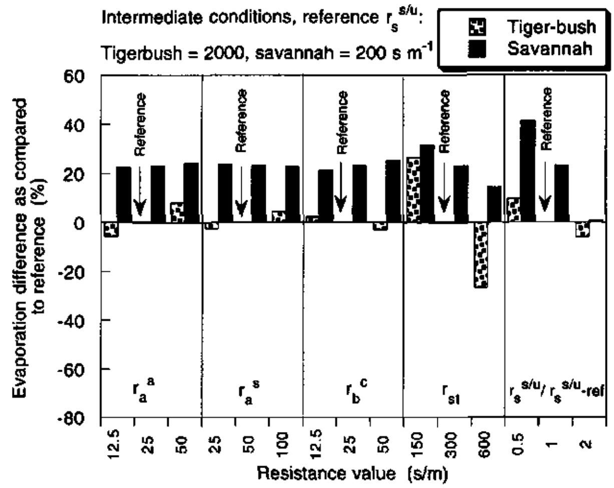

As soon as the bare soil dries up, reaching r_s^s-values of around 2000 (observed around day 270), and the savannah understorey surface resistance increases to 200 s m^{-1}, savannah evaporation appears to be largest (see Fig. 8.6). Again, the atmospheric resistances (r_a^a, r_a^s, and r_b^c) do not affect the results very much - the largest influence is observed for r_b^c. The result of a change in r_a^s or r_b^c on tiger-bush evaporation is opposite compared to Fig. 8.5. As in Fig. 8.5, largest differences are caused by changing surface resistances, especially r_s^u.

Further drying of both understoreys (r_s^s = 6000, r_s^u = 300 s m^{-1}, see Fig. 8.7) makes the differences less, but savannah evaporation is still considerably higher (about 18 %). This is the kind of situation that could be expected during the last two weeks of the IOP.

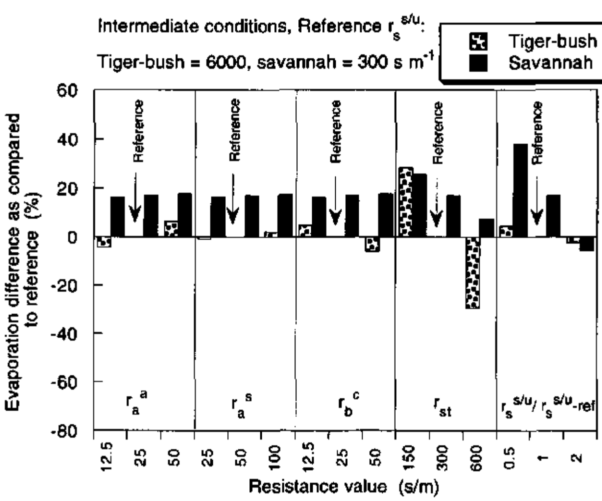

FIGURE 8.7. The influence of a change in a single resistance on tiger-bush L_vE (speckled columns) and the influence of a change in vegetation coverage, (1-α), plus LAI to values representative for savannah, with or without a concurrent change in resistance (black columns). This figure represents a drying understorey (r_s^s = 6000, r_s^u = 300) and dry atmospheric conditions (T_a = 34 °C, D = 3.5 kPa).

Finally, Fig. 8.8 shows what the possible difference in evaporation would be if the bare soil is totally dry and most of the undergrowth would be senesced. This situation would occur around one or two months after the end of the IOP (November-December). It is obvious that tiger-bush evaporation is higher, because of its higher α and hence higher available energy.

*FIGURE 8.8. The influence of a change in a single resistance on tiger-bush L_vE (speckled columns) and the influence of a change in vegetation coverage, $(1-\alpha)$, plus LAI to values representative for savannah, with or without a concurrent change in resistance (black columns). This figure represents a dry/senesced understorey (**$r_s^s = 10000$, $r_s^u = 2000$**) and dry atmospheric conditions (**$T_a = 34$ °C, $D = 4.0$ kPa**).*

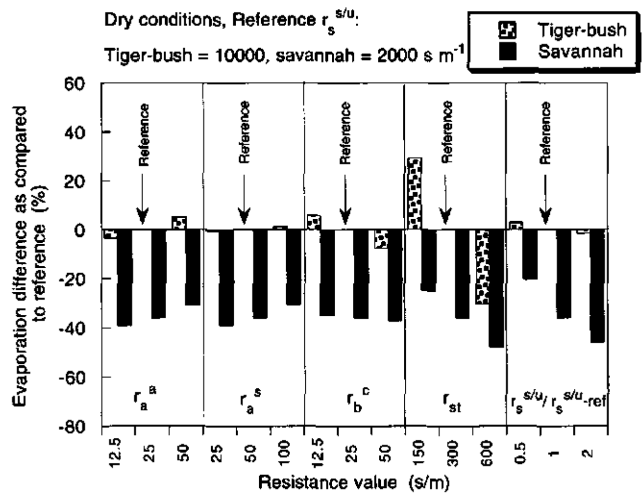

8.4 Results of original and combination models

8.4.1 General

This paragraph describes the results of the various SVATs. Not all models can be used for the calculation of the energy balance of both vegetations. TCM can only be used in the case of savannah, for example. CM, DD and DCM can be used for savannah calculations, but this requires averaging the two vegetation components (bushes and undergrowth), as the understorey evaporation is not evaluated through resistances. Both SW and TL describe the understorey evaporation through a single lumped surface resistance. Furthermore, they do not employ a prognostic soil moisture model, which makes them very suitable for calculating the evaporation of the savannah.

The models have been run with the controlling parameters set to the values given in Tables 8.1 and 8.2. Additional parameters, mainly concerned with the calculation of soil evaporation and soil heat flux, are given in Table 8.4. In all models the canopy surface resistances (i.e. r_s^c, not r_{st}, to avoid differences by dividing r_{st} by $2LAI$ or by LAI) were prescribed by the same parameterization (see Eq. 4.25- 4.26 and Table 6.8). Hence, the TL-model was taken as a reference, because it was considered to be most suitable for describing this layered vegetation. It also applies measured values of component R_n and G values. However, whereas all models were suitable for incorporating the canopy (bush) resistance, it was possible to incorporate the exact understorey values only in the SW-model, it being the predecessor of the TL-model. An average canopy resistance was calculated from the bush and the understorey resistance, while the bare soil was treated separately, in the other two-component models (CM, DD, DCM).

TABLE 8.4. Input parameters for the SVATs.

Vegetation parameters (SW,CM)		Savannah	Tiger-bush	Units
Extinction coefficient for net radiation	:	0.45	0.45	(-)
Vegetation parameters (DD, DCM, TCM)				
Canopy surface albedo	:	0.20	0.19	(-)
Canopy surface emissivity	:	0.97	0.98	(-)
Canopy surface water	:	0.00	0.00	(kg)
Maximum canopy surface water	:	0.80	0.80	(kg)
Soil parameters (CM)				
Reference depth of wet soil layer	:	0.50	0.50	(m)
Reference depth of dry soil layer	:	0.05	0.05	(m)
Depth of atmosphere-soil interface	:	0.03	0.03	(m)
Thermal conductivity of saturated soil	:	2.0	2.0	(W/ m K)
Thermal conductivity of dry soil	:	0.5	0.5	(W/ m K)
Porosity factor of soil	:	0.40	0.40	(-)
Tortuosity factor of soil	:	2.0	2.0	(-)
Soil parameters (DD, DCM, TCM)				
Soil type index	:	0	0	(-)
Soil surface albedo	:	0.25	0.25	(-)
Soil surface emissivity	:	0.91	0.95	(-)
Volumetric water content at saturation	:	0.36*	0.32**	(m^3 m^{-3})
Volumetric water content at wilting point	:	0.02	0.02	(m^3 m^{-3})
Volumetric water content at field capacity	:	0.27	0.24	(m^3 m^{-3})
Matric potential head at saturation	:	-0.12	-0.12	(m)
Saturated hydraulic conductivity	:	2.12 10^{-5}*	4.21 10^{-6}**	(m s^{-1})
Diurnal soil moisture cycle depth	:	0.10	0.10	(m)
Seasonal soil moisture cycle depth	:	2.0	2.0	(m)
Initial parameter settings				
Initial temperature of upper soil layer	:	302.9	302.9	(K)
Initial temperature of lower soil layer	:	305.3	305.7	(K)
Initial vol. water content of upper soil layer	:	0.05	0.05	(m^3 m^{-3})
Initial vol. water content of lower soil layer	:	0.11	0.11	(m^3 m^{-3})
Depth of diurnal soil moisture cycle	:	0.1	0.1	(m)
Depth of seasonal soil moisture cycle	:	2.0	2.0	(m)

* Value obtained by the Multistep Outflow method as performed the Department of Water Resources, Wageningen, The Netherlands.

** Gaze (1994), personal communication.

8.4.2 Differences between model estimates

Fig. 8.9 shows the cumulative totals of day-time R_n, G, L_vE and H as calculated with several models for the CWS tiger-bush site. Here, fluxes were calculated for 8-16 GMT and summed over day 264 (day of last rainfall at the savannah site) to 283. Cumulative totals were considered adequate to emphasize systematic trends between models and surface-types. The results of the TL-model can be considered as the actual occurring values, because the model was calibrated on the measurements and because it employs measured values of R_n ($R_{n,b}$ and $R_{n,u}$) and G (G_u and G_b). Fig. 8.9a indicates that differences between model estimates of R_n were relatively small (< 10 %). SW, CM and TL exhibit the same course as they apply measured values of R_n. However, their values of $R_{n,b}$ and $R_{n,u/s}$ will not be the same as SW and CM adopt radiation extinction, whereas TL used measured values of these variables. The DCM model has the lowest values of R_n which is mainly the result of the relatively high values of $T_{s,b}$ and $T_{s,u}$.

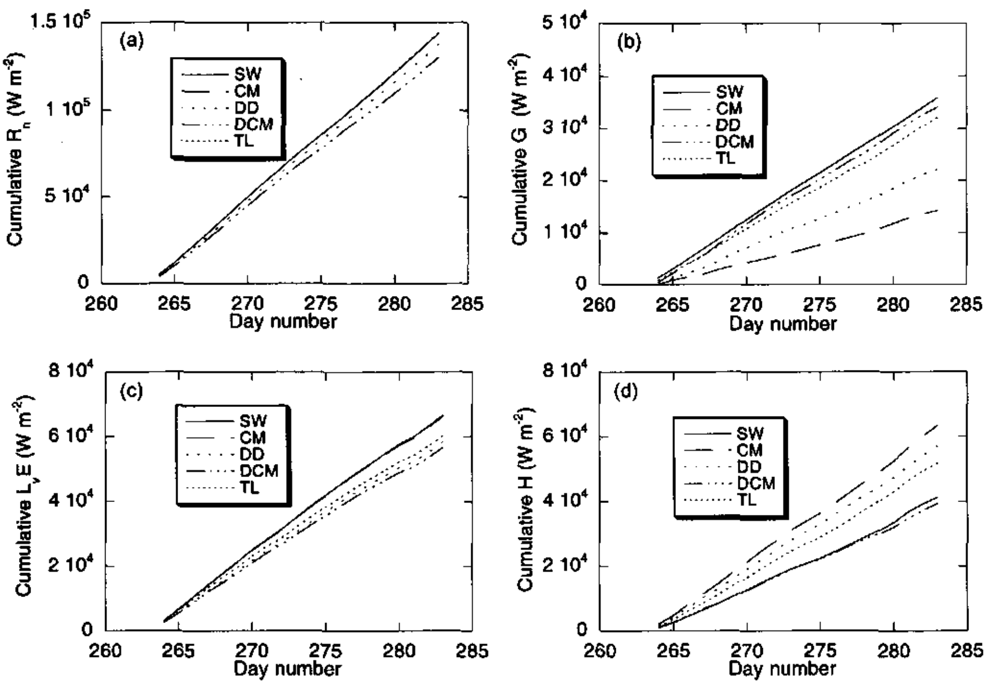

FIGURE 8.9. Cumulative totals of daily average (8-16) values of tiger-bush net radiation (a), soil heat flux (b), latent heat flux (c) and sensible heat flux (d) as calculated by the SW, CM, DD, DCM and TL model. The TL-model can be regarded to represent true R_n, G, L_vE and H.

Variation in G appears to be much larger (> 100 %) - a severe underestimation of G is obvious in the case of CM (as also found by Van den Hurk et al., 1996), while estimates obtained by DD are about 40 % lower than the observations, at the end of the IOP. SW, applying $G = 0.25\ R_n$, gives a slight overestimation, which means that the constant could probably be lowered to 0.20. Best guesses (also on a diurnal scale) were obtained by DCM, employing the Force-Restore method (see Eqs. 4.57 - 4.58).

Fig. 8.9c illustrates that, despite the large variation in G, model estimates of L_vE are quite similar (maximum differences of around 15 %). SW and CM predict an almost identical course of cumulative L_vE. The prognostic models and the TL-model (i.e. the observations) are quite close to each other. Closest resemblance was obtained by DD.

From Fig. 8.9d, which shows the cumulative values of the sensible heat flux, it can be deduced what caused the relatively small differences in estimates of L_vE. The H-flux is considerably overestimated by CM as a result of too high surface temperatures, which were predominantly caused by the small values of G. Cumulative estimates found by SW are lower than the TL-values as a result of a combination of too high G and high values of r_a^s (see Fig. 8.1). On the other hand, the comparatively low values of r_a^s as calculated by DD, caused a serious overestimation of H. However, this was mainly taken into account by the lower values of L_vE, resulting in good estimates of L_vE.

Fig. 8.10 shows a similar graph for the savannah model calculations. Difference in R_n are small, only the TCM model shows slight overestimation. The soil heat flux (Fig. 8.10b) shows much more variation, similar to the tiger-bush results. As expected, CM again leads to serious underestimations. The other G-estimates are relatively close together, although TCM appears to overestimate G by $\approx$ 30 %, which is mainly the result of a higher forcing (R_n).

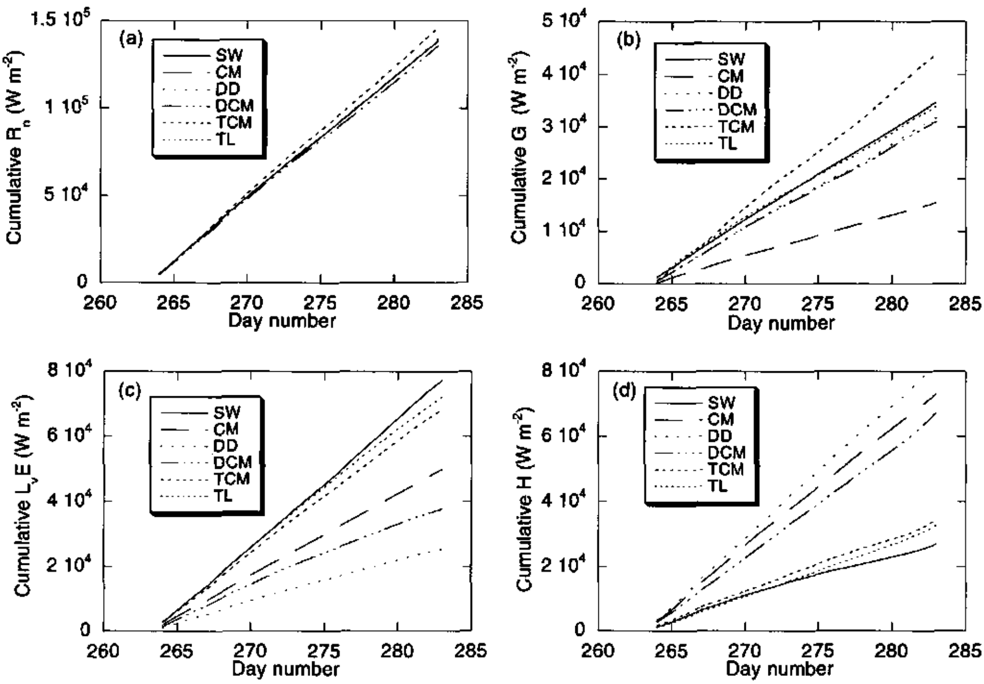

FIGURE 8.10. Cumulative totals of daily average (8-16) values of savannah net radiation (a), soil heat flux (b), latent heat flux (c) and (d) sensible heat flux as calculated by the SW, CM, DD, DCM, TCM and TL model. The TL-model can be regarded to represent true R_n, G, L_vE and H.

The evaporation results exhibit a large difference, compared to the tiger-bush (see Fig. 8.9c). Only SW and TCM are close to the line symbolizing real evaporation. Underestimation of CM is again caused by high values of H, which are the result of seriously underestimated values of G. Also, H-values for DD are too high (too low $r_a{}^s$) which, in combination with reasonable estimates of G, create miscalculated values of L_vE. DCM also found far too high values of H, which illustrates that lumping the upper- and understorey vegetations into one layer did not work satisfactorily. On the other hand, TCM resulted in L_vE and H values closely resembling the observations.

Several conclusions can be drawn from the rèsults presented above. However, they are preliminary as the models have not been tested with changed input parameters. First, net radiation appears to be calculated satisfactorily by all present model parameterizations. If measured R_n is used (SW and CM), proper values of $R_{n,u}$ and $R_{n,s}$ for these sparse canopies can be obtained by setting the extinction coefficient to a value around 0.5 (here 0.45), instead of the usually applied value of 0.7, which is valid for relatively closed canopies only. If no soil model is available, G can be sufficiently well parameterized by multiplying R_n with a certain factor (between 0.20 to 0.30). This works better than applying an extended soil model without heat storage. A Force-Restore method is indispensable for prognostic simulations (DD, DCM, TCM), but it will only yield proper results if it is used in combination with a reliable parameterization of $r_a{}^s$ (i.e. the parameterization proposed by CM). Fig 8.10 indicates that savannah, consisting of three components, cannot be described properly by a two-component model, unless the undergrowth and soil are combined to a single understorey component, which is possible in the SW and TL case. A three-component solution, treating the bushes, undergrowth and soil separately works very satisfactorily. Note that $r_c{}^s$ is given the same values in all models, which means that variation in L_vE is potentially larger if the original parameterizations of g_l were to be used.

8.4.2 Comparison between savannah and tiger-bush

In § 5.4 it has been shown that tiger-bush received about 10 % more available energy on a cumulative basis. Furthermore, Table 6.8 and Fig. 6.13 indicated that the average conductance of the tiger-bush strips was considerably higher. However, the conductance of the tigerbush soil was much lower compared to the herbaceous understorey of the savannah. It will depend on the proportional area of the upper-and understoreys, also defining the total surface resistance, in combination with the resistance network and the available energy, what the final evaporation will be. Table 8.1 showed that differences between savannah and tiger-bush will manifest itself through generally higher values of tiger-bush values of $r_a{}^s$ (lower values of $z_{0m,u}$) and lower values of $r_b{}^c$ (higher LAI_c).

Fig. 8.11 shows the cumulative values of the savannah and tiger-bush latent and sensible heat fluxes during the last three weeks of the IOP (TL-model). Around day 267, L_vE for savannah starts to deviate from the tiger-bush, which leads to the total sum being around 16 % lower in the case of tiger-bush. Gash et al. (1996) compared the evaporation from the SSS savannah and tiger-bush site and concluded that tiger-bush evaporation was slightly higher than the values recorded for savannah. However, their time series already started during the wet period when tigerbush evaporation is larger as a result of high soil evaporation (see Fig. 8.5). From this, and supported by the findings presented in Fig. 8.5 - 8.8, it can be concluded that tigerbush L_vE will be higher during the rainy period. Hereafter, the savannah will evaporate more, because of its green herb-species and grasses. This period will last approximately two to three months. However, after wilting of the undergrowth, the tiger-bush bushes will evaporate at a higher rate (higher α and g_l). There are indications (see Fig. 5.29b) that tiger-bush evaporation will go on even during the dry season.

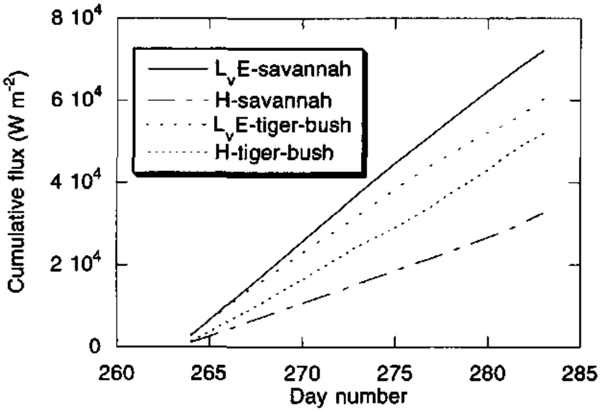

FIGURE 8.11. Cumulative amounts of evaporation and sensible heat flux as calculated by the TL-model for savannah and tiger-bush.

8.5 Interannual variations of the energy balance

8.5.1 Introduction

Several micrometeorological experiments have been conducted in the SSZ during the last decade. The area around Niamey (Niger) has been sampled particularly frequently, because of its good infrastructure and relatively calm political situation. The ECLATS experiment took place in this region in 1980 (Druilhet and Tinga, 1982), the Yantala experiment in 1984 (Pagès et al., 1988), the SEBEX experiment was conducted from 1988-1990 (Wallace et al., 1992) and the last experiment was in 1992 (HAPEX-Sahel, Goutorbe et al., 1994).

These experiments improved our understanding of the surface exchange processes in this specific semi-arid area. However, most of them were relatively short, which meant that only a brief part of the annual cycle was covered. During the Yantala experiment the dry period of what can be considered as the driest year of the last decade (1984) was sampled, whereas SEBEX provided the wettest months of the wettest year (1988). HAPEX-Sahel covered the rainy period of a relatively average year. For many scientists involved in the SSZ, such as climate-modellers (GCMs, necessary to understand the desertification process), ecologists (wildlife, species), agronomists (biomass/yield), remote sensing specialists (constants in simple functions), and soil scientists (soil erosion) it is very useful to find out to what extent the surface parameters and fluxes (especially L_vE) vary when rainfall and radiation load change.

To set-up a long-term experiment in these areas would hardly be possible from a financial, labour and technical point of view (complicated measurements). Therefore, in this thesis, information about the energy balance and surface parameters for climatologically different years was obtained by extrapolating existing knowledge to other years. The used 'calibration' data (SEBEX measurement campaign) have been presented in Chapter 5. In this paragraph we aim at extrapolating the 1989-1990 energy balance and surface parameters to other years by using readily available meteorological measurements monitored during ten years at the ICRISAT Sahelian Centre. To achieve this, the Evapoclimatonomy (Nicholson and Lare, 1990) model will be used. It is recognized that not enough data are available to verify the generated input and output. However, this exercise still provides insight into the theoretically possible variation of the energy balance fluxes. Only savannah data will be used for this exercise. Note that ICRISAT is located in the southern part of the HAPEX-grid, meaning that rainfall amounts have possibly been lower for the other super-sites. As a result of the steep rainfall gradient in the SSZ, outcomes of L_vE and related parameters will be considerably different, even though meteorological variables are quite similar, as observed during the HAPEX-Sahel campaign.

8.5.2 Evapoclimatonomy model

The applied model is the relatively simple Evapoclimatonomy submodel (Nicholson and Lare, 1990), which has been described briefly in Section 4.4. The model was run with monthly input values. It will therefore yield monthly output values, which were averaged per year to calculate annual means. The Evapoclimatonomy model requires two types of input - hydrological and radiation input.

a) Hydrological input

Rainfall, P, was directly measured at ISC. Annual mean values of runoff, N, were estimated from the runoff ratio, $C = N/P$, with $C = \tanh D$. In this last formula D is the dryness ratio that can be found from $R_n/L_v P$ (see Nicholson and Lare, 1990). The evaporativity, e^*, was set to the following values for January until December: 0.80, 0.80, 0.80, 0.70, 0.65, 0.60, 0.50, 0.50, 0.70, 0.75, 0.80, 0.80. According to Nicholson and Lare, the evaporativity is a "non-dimensional measure of the capacity of the land surface to use a portion of the monthly solar radiation to evaporate precipitation received during the same month ". These values are the same as used by Nicholson and Lare (1990) for their original model calculations. Following this same paper, values for t^*, a residence time, were set to 1.5.

b) Radiation

The seasonal course and interannual variation of R_s has already been shown in Figs. 3.5 and 3.6. The monthly and annual averages will be used for calculations with the Evapoclimatonomy model. These data have been calibrated with R_s-values as measured during the SEBEX campaign ($R_s = 1.1$ (R_s (ISC)/0.0864) + 13.753, $r^2 = 0.85$).

The albedo in the Sahel presents a strong variability both in time and space. Both variabilities are linked to the variability of the rainfall, which displays the same large time-place spectrum. (Diabaté et al., 1989). However, when comparing dry season albedos with the occurrence of dry and wet years, Courel et al. (1984) found no correlation between the decrease in albedo and increase in rainfall. This was probably caused by the fact that during the dry season hardly any vegetation is present, which masks the differences between wet and dry years.

In the Sahel, the dramatic rainfall-induced increase in vegetation cover causes a decrease in albedo as shown in Fig. 5.5. Whereas albedo decreases gradually from March onward, a sudden increase is observed after the last rains. Therefore, the parameterization of albedo was done by using a different description for the 'wetting' and the 'drying' branch. The wetting branch was described by a polynomial description with the sum of saturation deficits (daily mean in mbar), ΣD, as the independent variable. The first constant of the polynomial is determined by the average of the actual, $P(i)$ and the previous $P(i\text{-}1)$ annual rainfall. This is done because a dry year preceding a wet year will probably lead to a higher starting value than a wet year preceding a wet year. The drying branch was parameterized with ΣD only:

1) wetting branch

$$c_1 = 0.38829 - 0.000291918\ ((P(\mathrm{I})+P(\mathrm{I}-1))/2.0) \qquad (8.1a)$$
$$c_2 = 0.39329 - 0.000291918\ ((P(\mathrm{I})+P(\mathrm{I}-1))/2.0) \qquad (8.1b)$$

$$\alpha_b = c_1 + 6.1774\mathrm{E}^{-6}\ \Sigma D - 2.96\mathrm{E}^{-9}\ \Sigma D^2 + 1.2869\mathrm{E}^{-13}\ \Sigma D^3 \qquad (8.2a)$$
$$\alpha_h = c_2 - 2.4941\mathrm{E}^{-6}\ \Sigma D + 2.1391\mathrm{E}^{-9}\ \Sigma D^2 - 5.2411\mathrm{E}^{-13}\ \Sigma D^3 \qquad (8.2b)$$

2) drying branch

$$\alpha_b = 0.0030418 + 2.9664\mathrm{E}^{-5}\ \Sigma D \qquad (8.3a)$$
$$\alpha_h = -0.015724 + 3.0118\mathrm{E}^{-5}\ \Sigma D \qquad (8.3b)$$

A summed parameter rather than an instanteneous one offers the advantage of yielding smooth results. ΣD was chosen because this variable, plotted against time (day number), shows three distinct trajects. It will increase at a certain rate, which is very similar for all years, until the arrival of the first rains. After that the rate of increase in D will level off. After the last rains this rate will increase markedly again. This parameter thus indirectly indicates the start and end of the wet season. It has an advantage above ΣP, because a few days without rain would mean a stagnating albedo or even an decrease, and ΣD is also smoother. Furthermore, D is closely related to water use efficiency, CO_2 and L_vE-flux, as shown in Chapter 7, and thus to green biomass which makes it a good indicator of albedo. Correlation between the simulated and measured (SEBEX, 1989-1990) a-values was 95 %.

Fig. 8.12a shows the seasonal course of albedo for 1984 and 1988, whereas Fig. 8.12b gives the thus generated annual means. The range of these values compares well to the numbers given in the literature (see § 5.2.2).

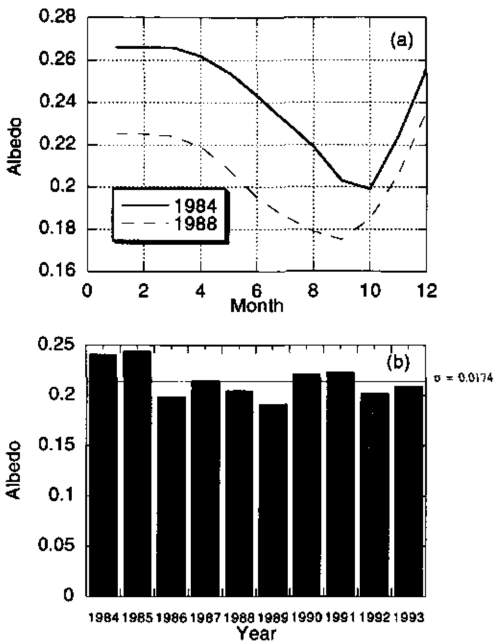

FIGURE 8.12. Simulated albedo for the SEBEX fallow savannah as parameterized from the incremental sum of vapour pressure deficit, ΣD, and current and previous annual rainfall. (a) Seasonal variation during a dry (1984) and a wet (1988) year and (b) interannual varation for 10 years.

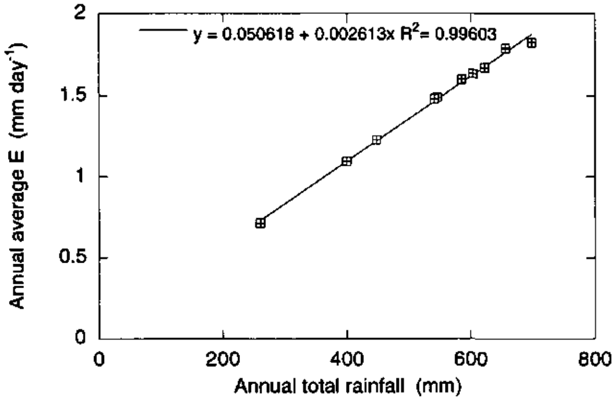

FIGURE 8.15. Annual values of daily average evaporation calculated by the Evapoclimatonomy model as a function of annual total rainfall.

Fig. 8.16 shows the seasonal course of $L_V E$ during the years 1984 and 1988. Average monthly evaporation during 1984 is clearly less and it peaks earlier. During 1988, evaporation is predicted to continue until December, because of the large amount of rainfall received during August and September.

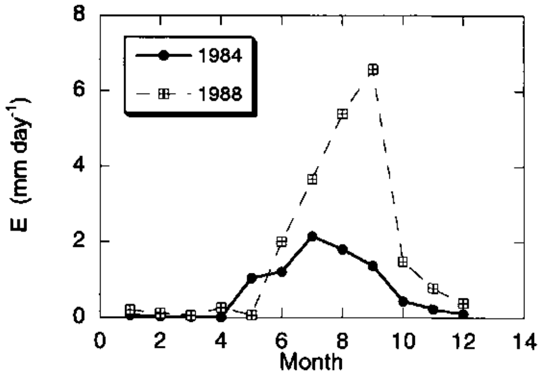

FIGURE 8.16. Monthly average values of daily E calculated by the evapoclimatonomy model for a dry (1984) and a wet year (1988).

Appendix 1 Theoretical correction of IR surface temperatures

Surface temperature as measured directly by an IRT has to be corrected for longwave incoming radiation according to the following formula

$$\sigma T_s^p = \varepsilon_s \sigma T_s^p + (1-\varepsilon_s) R_{l,\downarrow} \tag{A1.1}$$

where the symbols are as defined before. The superscript p is the power to which T_s has to be raised (customarily given a value of 4.0).

Eq. 2.2, necessary for calculation of $R_{l,\downarrow}$, holds for the entire longwave spectrum (3-50 μm). Although the majority of the radiation will have a wavelength between 8-14 μm (as a result of the atmospheric window), some longwave radiation will have values of μ smaller than 8 or larger than 14 μm. The emissivity representing a window of only 8-14 μm reads (Idso, 1981)

$$\varepsilon_{8-14\mu m} = 0.24 + 2.98 * 10^{-8} e_a^2 \exp\left(\frac{3000}{T_a}\right) \tag{A1.2}$$

where e_a is the vapour pressure of the air in mb and T_a the air temperature in K. The height at which these e_a and T_a should be evaluated is still disputable. The measurements at reference height are most obvious and available, but it can be defended that for longwave sky radiation a much higher level should be taken.

Furthermore, the power p is usually attained a value of 4.0 and σ the well-known value of $5.67.10^{-8}$. It is true that if Planck's curve is integrated over the *entire* spectrum the law of Stefan-Boltzmann is obtained, as given in Eq. 2.2, with p and σ as given above. Most instruments, however, only cover a certain μ-range, e.g. the optical window from 8-14 μm as sampled by IRTs. In those cases, involution has to be executed with a value slightly lower or higher than 4.0 and a different Stefan-Boltzmann 'constant'. For the 8-14 μm window the values are 4.49 and $1.25.10^{-9}$ for p and σ, respectively (Personal communication B. Van den Hurk, 1994). So Eq. A1.1 will read:

$$\sigma_{8-14} T_s^{p,8-14} = \varepsilon_s \sigma_{8-14} T_s^{p,8-14} + (1-\varepsilon_s) R_{8-14,\downarrow} \tag{A1.3}$$

where the last term on the RHS is obtained from Eq. 2.2 using ε_{8-14} and $T_a^{4.49}$.

Appendix 2 Methods used to estimate soil thermal properties

a) Volumetric heat capacity

In this thesis, C_h was calculated by the following formula (De Vries, 1963):

$$C_h = \sum_i C_{h,i}\phi_i \tag{A2.1}$$

where $C_{h,i}$ is the volumetric heat capacity for each soil component and φ_i is the volume fraction of component i. Organic matter and air were not taken into account because their contribution is negligible. The volumetric heat capacities for the mineral soil components, $C_{h,s}$, and water, $C_{h,l}$, are 2.0, and 4.2 MJ m^{-3} K^{-1}, respectively. With knowledge of the water and solid phase fractions, C_h for the upper soil layer can be calculated using

$$C_h = C_{h,s}\frac{{}^{b}\rho_d}{\rho_s} + C_{h,l}\theta \tag{A2.2}$$

where ρ_s is the density of the solid phase (kg m^{-3}), taken as 2650 kg m^{-3}, and ${}^{b}\rho_d$ the dry bulk density (kg m^{-3}) given in § 3.5.1.

b) Thermal diffusivity

Horton et al. (1983) evaluated six methods for determining κ. For the calculation of κ five of their methods will be applied, viz. the Amplitude equation, the Phase equation, the Arctangent equation, the Logarithmic equation and the Harmonic equation. All methods will be used to determine κ for the HAPEX-Sahel savannah experiment. For the SEBEX-experiment only the Amplitude method will be applied. A summary of these methods is given below.

b1) Method 1. The amplitude equation.

The amplitude equation is given by

$$\kappa = \frac{\omega}{2}\left[\frac{z_2 - z_1}{\ln A_1 / A_2}\right]^2 \tag{A2.3}$$

where A_1 and A_2 are the amplitudes at depths z_1 and z_2, respectively.

Determination of κ from this equation requires measurement of the maximum and minimum temperature at both depths during the period of the fundamental cycle (in our case 24 h.).

b2) Method 2. The Phase equation.

The phase equation is given by

$$\kappa = \frac{1}{2\omega}\left[\frac{z_2 - z_1}{\delta t}\right]^2 \tag{A2.4}$$

in which δt ($=t_2-t_1$) signifies the time interval between the measured occurrences of maximum soil temperature at depths z_1 and z_2.

b3) Method 3. The Arctangent equation.

With M=2 , the apparent thermal diffusivity can be calculated from

$$\kappa = \frac{\omega(z_2 - z_1)^2}{2\left\{\arctan\left[\frac{(T_1 - T_3)(T_2' - T_4') - (T_2 - T_4)(T_1' - T_3')}{(T_1 - T_3)(T_1' - T_3') + (T_2 - T_4)(T_2' - T_4')}\right]\right\}^2} \tag{A2.5}$$

where temperatures T_i and T_i' are recorded every 6 hours (subscripts *1* to *4*) at two depths, z_1 and z_2 (denoted by '), respectively.

b4) Method 4. The Logarithmic equation.

It was shown by Seemann (1979) that, in analogy to Method 3, the apparent thermal diffusivity can also be calculated from

$$\kappa = \left[\frac{0.0121(z_2 - z_1)}{\ln\left[\frac{(T_1 - T_3)^2 + (T_2 - T_4)^2}{(T_1' - T_3')^2 + (T_2' - T_4')^2}\right]}\right]^2 \tag{A2.6}$$

b5) Method 5. The Harmonic equation.

The analytical solution of Eq. 2.8 according to van Wijk (1963) is

$$T(z,t) = \overline{T} + \sum_{n=1}^{M} \{A_{0n} e^{\left(-z\sqrt{n\omega/2\kappa}\right)} \sin\left(n\omega t + \phi_{0n} - z\sqrt{n\omega/2\kappa}\right) \tag{A2.7}$$

where A_{0n} and φ_{on} are the amplitude and phase angle of the n^{th} harmonic for the upper boundary, respectively (Horton et al., 1983). The harmonic analysis of temperatures at z_1 will yield M values of A_{0n} and φ_{on} which can give an estimate of temperature at z_2 (provided the soil is homogeneous in the vertical) with the help of Eq. A2.7, if a proper value of κ is given. κ can be found by selecting a κ (through iteration) which gives the smallest sum of squared differences between the measured and estimated temperature at z_2.The sum of squares will be composed of 24 differences between measured and calculated temperature.

c) Thermal conductivity

Thermal conductivity, λ(W m^{-1} K^{-1}), was measured directly using non steady state probes (Van Loon, 1991). Furthermore, it was calculated with Eq. 2.9.

Appendix 3 Methods used to calculate soil heat flux, G

In this thesis four well known methods (Gradient, Plate, Calorimetric, and Harmonic method) have been used to calculate G. They were applied in Chapter 5 to calculate G for the HAPEX-Sahel savannah. For the HAPEX-Sahel tiger-bush and during the SEBEX-experiment the Plate method has been employed only.

a) The Temperature Gradient method

The Temperature Gradient method is a relatively simple method to calculate the soil heat flux. It uses an approximation of Fourier's law (Eq. 2.6), such that δT and δz are replaced by ΔT and Δz, respectively. Besides knowledge of λ, it requires addition of a storage term to yield **surface** soil heat flux, because the first thermometer is located below the surface.

b) Soil heat flux plates

The Plate method is based on the same theory. Here, G is measured with the so-called **heat flux meter**, which is a thin flat plate placed normal to the direction of flow. The temperature difference across the plate is measured and used to determine the heat flux from a calibration curve. Heat flux meters are simple to use, but may be inaccurate unless they are carefully constructed, calibrated and installed. The meters also interfere with water movement in both liquid and vapour phase and they may give erroneous results if they are installed above the evaporation front (see Kimball and Jackson, 1975; Mayocchi and Bristow, 1995).

Another problem of this method is the fact that the thermal conductivity of the soil encompassing the plate is not identical with that of the heat flux meter. This implies that the flow through the meter is not the same as the flow through the medium. The formula of Mogensen (1970), using the ratio of the thermal conductivity of the plate to that of the soil, ε, and a factor, ϕ, depending on the geometry of the meter, has been used to correct for this phenomenon. It can be written as

$$\phi = \frac{1}{1 - 1.7r\left(1 - \varepsilon^{-1}\right)} \tag{A3.1}$$

with $r = t / \sqrt{A}$. The parameter t denotes the thickness of the plate, whereas A stands for the area of the plate. Values of t, A and λ_{plate} were given in § 3.5.2e. To obtain the **surface** soil heat flux, the heat flux meter should be placed infinitively close to the soil surface. Unfortunately this is not feasible, due to possible errors caused by direct heating by solar radiation. For that reason, soil flux plates are usually placed at several centimetres below the surface (e.g. 3 or 5 cm), which requires an estimate of the heat storage above the plate. To accomplish this, the temperature at the depth of the plate and higher (at least at one depth very near the surface) are measured. A formula similar to Eq. A3.2 will be applied to calculate this storage.

c) The Calorimetric method

The Calorimetric or Temperature Integral method is based upon estimates of the change in heat storage during a certain time interval. This method requires frequent measurements of temperature at several depths in the soil profile. Furthermore, information on C_h at several depths is needed. The method applies the following formula, defining the change in heat content per unit time as follows.

$$\Delta G = C_h \int_{z_0}^{z_\infty} \frac{\left(T_{i,z} - T_{i+1,z}\right)\delta z}{\Delta t} \tag{A3.2}$$

where ΔG is the change in heat storage during the considered time interval and $T_{i,z}$ and $T_{i+1,z}$ are temperatures at times t_i and t_{i+1}, respectively, at several depths z.

Eq. A3.2 can be simplified by cutting off the temperature profile at a certain depth where the soil heat flux is assumed to be zero (no change in heat content during Δt). Furthermore, integration is executed over increments Δz instead of over infinitesimal differences δz. C_h will be calculated with the method described in Appendix 2.

Because temperatures were only measured at five depths (see § 3.5.2e), the obtained profiles had a rather angular character. To overcome this problem, the profiles were smoothed by applying interpolation using cubic splines (Press et al., 1986).

d) Harmonic Analysis (Exact) method.

The theory behind harmonic analysis has been shortly explained in § 2.3. For calculations of the heat flux, Eq. 2.10 was applied with M set to 12, yielding 12 values of A_n and B_n. The higher M, the better the estimate of the temperature value in time. For rather homogeneous soil on not too cloudy days a number of about 10 harmonics should be sufficient to make accurate estimates of temperature (Horton et al., 1983). With 12 harmonics, measured and calculated temperatures were the same up to the third digit.

The exact solution of the soil heat flux at any time and depth can be calculated according to Van Wijk and de Vries (1963):

$$G(z,t) = \sum_{n=1}^{M} \{A_{0n} C_h \sqrt{n\omega\kappa}\, e^{\left(-z\sqrt{n\omega/2\kappa}\right)} \sin[n\omega t + \varphi_{0n} + (\pi/4) - z\sqrt{n\omega}/2\kappa]\} \tag{A3.3}$$

yields the soil heat flux at any depth, where A_{0n} (° C) is the amplitude of the n^{th} harmonic at the upper boundary (in this case 0.02 m), being $(A_n^2 + B_n^2)^{0.5}$, ϕ_n is the phase shift of the n^{th} harmonic, C_h is the volumetric heat capacity (MJ m^{-3} K^{-1}), ω is the radial frequency (rad s^{-1}), κ is the thermal diffusivity (m^2 s^{-1}), and z denotes the depth below the upper boundary (m), which in this case is 0.02 m.

As already stated before, the heat storage above the highest temperature level should be added to the soil heat flux found at a certain depth. The exact heat storage in the upper soil layer can be acquired if measurements of temperatures at the surface were available. The surface temperatures as measured by IRTs may be used for this purpose. However, the sensor directed at the understorey will also see herbs and grasses. Furthermore, it was not installed above the soil plot, so that local variability may result in deviating values. For this reason, surface temperature will be calculated from Eq. 2.10 with z set to -0.02, thus denoting the soil surface with the temperature at 0.02 as a reference. This surface temperature will be used to perform the Calorimetric method from 0-50 cm and to calculate the heat stored in the layer from 0 to 0.075 m, which in turn can be added to the fluxes calculated with the Gradient method. As such, the Calorimetric method also required an estimate of κ. Thermal soil properties as calculated for

0.05 m depth were multiplied by 0.5 and 0.8 for z =0 and z =-0.025, respectively. For the Plate method the following procedure will be applied. The surface soil heat flux with the Exact method will be calculated taking z = -0.033, which is the average depth of the PT-100's installed above the plates. Similarly, the soil heat flux at a depth of 0.042 m will be deduced from the harmonics derived from the soil temperature at 0.033 m depth, by applying Eq. A3.3 with z = 0.009. The difference between G_0 and $G_{-0.042}$ is the storage to be added to the plates. Because the diffusivity, for which the value of the Harmonic method (see Eq. A2.7) was used, was computed for a depth around 0.05 cm, the κ-values applied for the Analytical and Plate method were, rather arbitrarily, multiplied by 0.80 to account for the lower moisture content around 0.02-0.03 m depth.

e) Summary of the used methods

A summary of the procedures is given in Table A3.1.

TABLE A3.1. The four methods applied to calculate G for the HAPEX-Sahel savannah, together with the depths of the used sensors, the method used to calculate κ and the depth at which κ, C_h and λ have been calculated. It is also indicated whether a storage term has been added to the calculations.

	Method κ	depth κ	C_h	λ	storage term
Gradient method	Harmonic	-0.075	-0.075	-0.075	
T_1=-0.05, T_2=-0.10		-0.05/-0.10	-0.05/-0.10		yes, from calorimetric method
Δz=0.05					
Analytical	Harmonic	-0.05	-0.05		no
T = -0.02					
Calorimetric			0-50*		no, T(0) from
T = 0-0.50			steps 0.025		Anal. method
Plates	Harmonic	-0.05	-0.05		yes, from Ana-
T=-0.033					lytical method

*C_h interpolated from -0.05 to -0.50 m. C_h (0) = 0.5 *C_h(-0.05), C_h(-0.025)=0.8*C_h(-0.05).

Appendix 4 Semi-empirical parameterizations for kB^{-1}

In the past decades various parameterizations have been presented in the literature for the value of kB^{-1}. It appeared that for smooth surfaces only the Prandtl number is involved, whereas for bluff-rough surfaces a combination of Prandtl and Reynolds numbers is needed. Besides single-formula parameterizations, also more extended models have been developed. They aim at calculating kB^{-1} on the basis of in-canopy (heat) source distribution. The articles of Cowan (1968), Brutsaert (1979), Kondo and Kawanaka (1986) and Massman (1987) have to be mentioned in this context.

Brutsaert (1982) summarized several possible expressions for the parameterization of the excess resistance for bluff-rough surfaces in his Table 4.2 (p. 93). For surfaces with bluff roughness elements a combination of the roughness Reynolds number

$$\mathrm{Re}^* = \frac{u_* z_o}{\nu} \tag{A4.1a}$$

and the Prandtl number

$$Pr = \nu/\kappa_\theta \tag{A4.1b}$$

has been applied, with ν the kinematic molecular viscosity (1.461 x 10^{-5} m^2 s^{-1}) and κ_θ the molecular thermal diffusivity (2.06 x 10^{-5} m^2 s^{-1}). At 20° C Pr equals 0.7 for air. In this thesis the following formula (Brutsaert, 1975b), amongst others, will be used

$$kB^{-1} = 2.46\left(u_* z_{om} / \nu\right)^{0.25} - 2 \tag{A4.2}$$

A similar relationship, and one of the first and most quoted, in this series is the equation of Owen and Thomson (1963), derived for *rough* surfaces and based on wind tunnel experiments:

$$kB^{-1} = \kappa\alpha\left(8u_* z_{om} / \nu\right)^m \mathrm{Pr}^n \tag{A4.3}$$

where α is a factor provisionally given an average value of 0.52 but depending to some extent on the shape of the roughness elements, and m and n are constants to which values of 0.45 and 0.8, respectively, were given. The values of m and n depend on the diffusivities in the sublayer; if purely molecular m = 0.5 and n = 0.67, whereas the effect of a turbulent contribution would be to decrease m and increase n. Originally h was parameterized as $30^* z_{0m}$, but Brutsaert (1982) changed this value of 30 to 8.0, which is the value used in this study.

Sheppard (1958) multiplied Re^* with Pr yielding:

$$kB^{-1} = \ln\left(\frac{ku^* z_{0m}}{\kappa_\theta}\right) \tag{A4.4}$$

Thom (1972) deduced for a bean crop (u_* in m s^{-1})

$$kB^{-1} = 1.35k(100u_*)^{1/3} \tag{A4.5}$$

Besides the rather uniform relationships based on a composite of Reynolds and Prandtl number some other parameterizations of kB^{-1} were developed. Recently, Kustas et al. (1989b) derived the following relationship

$$kB^{-1} = 0.17u(T_s - T_a) \tag{A4.6}$$

They used $(T_s - T_a)$ in order to deal with the diurnal course of kB^{-1} they observed during the day. Wind speed was involved because it is thought to decrease resistance to momentum transport, whereas it does not influence heat transport. The constant 0.17 was found for their specific experiment. It is not imaginary that each surface type requires its own constant.

Recent derivations (McNaughton and van den Hurk, 1995; Jensen and Hummelshøj, 1994) have shown that kB^{-1} probably is a function of leaf area index, LAI_c, and leaf width (w_c) instead of z_{0m}. The independence of kB^{-1} on z_{0m} was already stated by Thom (1972). McNaughton and Van den Hurk (1995) derived

$$kB^{-1} = k\left(\frac{120}{LAI_c}\sqrt{w_c u_*} - 2.5\right) \tag{A4.7}$$

This type of parameterization gives promising values for vegetation, although they are lower than expected on the basis of their roughness Reynolds number. For a bare soil, however, this formula is not useful.

According to Chamberlain (1968), mass or heat transport to and from aerodynamically *smooth* surfaces involves a kB^{-1} defined by Von Kármán in Chapter XV in Goldstein' s book (1938)

$$kB^{-1} = 5k\left[(\mathrm{Pr}-1) + \ln\{1 + 0.83(\mathrm{Pr}-1)\}\right] \tag{A4.8}$$

which implies that kB^{-1} for smooth surfaces is independent of u_*.

According to Brutsaert (1982), the value of kB^{-1} for smooth surfaces is only dependent on the Prandtl number, which also denies a dependence of B^{-1} on u_*. Nearly all values of kB^{-1} (for smooth surfaces) as given in literature can be characterized as

$$kB^{-1} = k(a\mathrm{Pr}^{2/3} - b) \tag{A4.9}$$

with a a constant between 11.6 and 13.6 and b a constant between 10.2 and 13.5. With the Prandtl number for air approximately 0.7, this means that all expressions given in Table 4.1 of Brutsaert (1982) yield negative values of B^{-1} ranging from -3.99 to -0.39. Multiplied by 0.4, values ranging from -1.6 to -0.16 appear plausible values for kB^{-1} for smooth surfaces, such as a bare soil.

Kondo (1975) gives an alternative expression for the value of kB^{-1}

$$kB^{-1} = k\lambda\left(\frac{\nu}{\kappa_\theta}\right)^{2/3} + \ln\frac{\mathrm{Re}^*(\nu/\kappa_\theta)^{1/3}}{\lambda} \tag{A4.10}$$

With $Re^* = 0.111$ and λ is 11.6 for smooth regimes, we get $kB^{-1} = -1.1$ at 20 °. Note that in Eq. A4.10 the roughness Reynolds number has been employed, in contrast with the other formulae for smooth surfaces which only apply the Prandtl number. The possible dependence of kB^{-1} on u_* (or Re_*) will be tested afterwards in § 6.2.2.

According to Brutsaert (1982) there is no commonly accepted theory available to model the transitional regime from smooth to rough flow. He advises to apply a suitable interpolation for practical purposes. Kondo (1975), for example, applies the formula of smooth flow (Eq. A4.10), but he allows the parameter λ to vary with Reynolds number (smaller λ with increasing Reynolds number, e.g. $\lambda = 3.0$ at $Re^* = 0.9$).

Appendix 5 A method to estimate soil evaporation [1]

At the field site the wind was very calm for the majority of the days (usually < 2 m s^{-1}) and it can be assumed that a free convection state develops at the soil surface. Generally, the type of convection which dominates can easily be estimated by using the following criteria (Gates, 1980)

$$\begin{array}{ll} \text{Free convection:} & Ra > 16\,Re^2 \\ \text{Forced convection:} & Ra < 0.1\,Re^2 \\ \text{Mixed convection} & 16\,Re^2 < Ra < 0.1\,Re^2 \end{array} \qquad \text{(A5.1)}$$

where Ra is the Rayleigh number defined as (e.g. Kreith and Bohn, 1986):

$$Ra = \frac{l^3 g \beta \Delta T}{\nu^2} Pr \qquad \text{(A5.2)}$$

where, l is a characteristic length scale of the free convective area, g is gravity, β is the expansion coefficient, ΔT the temperature difference between soil surface and ambient air, ν the kinematic viscosity, Pr the Prandtl number defined as $Pr = \kappa_a/\nu$, where κ_a is the thermal diffusivity and Re is the Reynolds number here defined as (Jacobs et al., 1994):

$$Re = \frac{ul}{\nu} \qquad \text{(A5.3)}$$

If these expressions are applied to the bare soil of HAPEX-Sahel savannah, for the length scale l the mean distance between the bushes can be taken, which was 6.5 m. For the tiger-bush this would be ≈ 40 m.

For the Sahelian vegetation, it appeared (see Appendix 12) that most conditions agreed with the free or mixed convection state. Then the exchange of sensible heat as well as the soil evaporation is dominated by the free convection exchange mechanism. The dimensionless heat transfer can be expressed in the Nusselt number, Nu, defined as (e.g. Kreith and Bohn, 1986)

$$Nu = \frac{H_s l}{\lambda_a \Delta T} \qquad \text{(A5.4)}$$

where λ_a is the heat conductivity of still air. For a flat and horizontal surface, and if $Ra > 10^7$, the latter expression equals (e.g. Jakob, 1950)

$$Nu = 0.14 Ra^{1/3} \qquad \text{(A5.5)}$$

1) Adapted from Jacobs & Verhoef, 1996

Finally, for the sensible heat flux at the soil surface, H_s, we find

$$H_s = \frac{0.14\lambda_a}{l} Ra^{1/3} \Delta T \tag{A5.6}$$

which means also that during the free convective state the sensible heat transport is independent of the length scale l.

In analogy to the sensible heat transport the mass transport under wet soil conditions can be estimated by using the Sherwood number, Sh, which is defined as (e.g. Kreith and Bohn, 1986)

$$Sh = \frac{E_s l}{\rho D_v (x_2 - x_1)} = Nu\left(\frac{Sc}{\mathrm{Pr}}\right)^{1/3} = 0.14 Ra^{1/3}\left(\frac{Sc}{\mathrm{Pr}}\right)^{1/3} \tag{A5.7}$$

where E_s is the mass flux of vapour per unit surface area from the soil, ρ is the air density, x is the mixing ratio, D_v is the molecular diffusivity of vapour in air and Sc is the Schmidt number. If the surface soil is wet the vapour flux equals the expression

$$E_s = \frac{\rho Sh D_v (x_2 - x_1)}{l} \tag{A5.8a}$$

or

$$E_s = \frac{\rho Nu\left(\frac{Sc}{\mathrm{Pr}}\right)^{1/3} D_v (x_2 - x_1)}{l} \tag{A5.8b}$$

which means that during the free convection period the soil vapour transport is also independent of the length scale l.

At the soil surface, the soil surface Bowen ratio, β_s, can be defined according to

$$\beta_s = \frac{H_s}{E_s} \tag{A5.9}$$

According to Massman (1992), the soil Bowen ratio can be expressed in the form

$$\beta_s = c_w \beta_e \tag{A5.10}$$

where β_e is the soil equilibrium Bowen ratio defined as, $\beta_e = \gamma/s$, in which γ is the psychometric constant (66 $Pa\ K^{-1}$) and s is the slope of the saturation vapour pressure curve evaluated at soil temperature and c_w is the so-called Soil Bowen Ratio Coefficient in the terminology used by Massman (1992). The latter coefficient equals $c_w = 1$ if the topsoil is wet and increases with decreasing moisture content of the topsoil. By combining the equation of the soil Bowen ratio (A5.10) and the soil sensible heat (Eq. A5.6), the soil latent heat flux is found:

$$L_v E_s = \frac{1}{c_w \beta_e} \frac{0.14\lambda_a}{l} Ra^{1/3} \Delta T \tag{A5.11a}$$

or combining Eq. A5.10 with Eq. A5.8a:

$$L_v E_s = \frac{1}{c_w} \frac{\rho L Sh D_v (x_2 - x_1)}{l} \tag{A5.11b}$$

where, L_v is the latent heat of vaporization. In the present study the latter expression will be used for estimating the soil evaporation.

Appendix 6 JS-relationships for leaf conductance according to HP95

Hanan and Prince (1996) fitted four JS-type relationships to their conductances measured at the HAPEX-Sahel CWS fallow savannah site. They defined the canopy average light response curve by

$$f_1 = \frac{R_p}{a_1 + R_p} \tag{A6.1}$$

where R_p (W m^{-2}) is the average PAR incident on the leaves.

The second 'stress' function described the dependence on air temperature:

$$f_2 = \left(\frac{T_a - T_L}{a_2 - T_L}\right)\left(\frac{T_U - T_a}{T_U - a_2}\right)^{\frac{T_U - a_2}{a_2 - T_L}} \tag{A6.2}$$

Here T_U and T_L are minimum and maximum air temperatures for stomatal conductance. They were assumed constant at 55 and 5 °.

The dependence on atmospheric humidity was given by the following relationship:

$$f_3 = \frac{1}{(1 + a_3 D)} \tag{A6.3}$$

where D is the vapour pressure deficit (mb).

The relationship between soil moisture status and vegetation stress was found from

$$f_4 = 1 - \frac{(\Psi_{\max} - \Psi_r)}{(\Psi_{\max} - a_4)} \tag{A6.4}$$

in which Ψ_r and Ψ_{max} are the average root-weighted soil water potential and the soil water potential at field capacity, respectively. The latter was taken at -39 cm. Ψ_r was a function of root-weighted volumetric soil moisture content, θ_r, which was parameterized as

$$\ln(-\Psi_r) = -0.4059 - 2.0556 \ln \theta_r \tag{A6.5}$$

The constants a_1, a_2, a_3 and a_4 are fitted parameters.

Finally, average leaf conductance, g_l, can be calculated with

$$g_l = g_e + g_{l,\max} f_1 f_2 f_3 f_4 \tag{A6.6}$$

or any other combination of stress functions. The term g_e is the cuticular conductance (m s^{-1}), taken to be zero.

Appendix 7 Determination of effective surface temperatures

Following the considerations in Section 2.5.1, the effective surface temperature for the savannah was found from $T_{s,t} = \alpha_i T_{s,i}$, where α_i represents the fractional areas and $T_{s,i}$ the surface temperature per surface class. In this formula, four surface classes, i, have been considered: sunlit bushes, sunlit understorey and their shaded equivalents.

From nadir view observations and detailed measurements of bush geometrics, it was found that the relative coverage areas for the bushes and understorey in the area immediately surrounding the WAUMET instrumentation masts were 0.2 and 0.8, respectively. This compares well with values found during the SEBEX campaign (Wallace et al., 1992). Around solar noon, and in fact during most of the day, $T_{s,t}$ will be composed of sunlit components only. For early morning and late afternoon the shaded components will play a large role. The formula used for estimation of $T_{s,t}$ is

$$T_{s,t} = \alpha_1 T_{s,bs} + \alpha_2 T_{s,bsh} + \alpha_3 T_{s,us} + \alpha_4 T_{s,ush} \tag{A7.1}$$

with α_1 is the surface fraction occupied by sunlit bushes, α_2 is surface fraction occupied by shaded bushes, α_3 is surface fraction occupied by the sunlit understorey and α_4 is the surface fraction occupied by the shaded understorey. Furthermore, $\Sigma\alpha_i = 1$. In these formulas, the subscript *bs* stands for sunlit bush, *bsh* for shaded bush, *us* for sunlit understorey and *ush* for shaded understorey.

Estimates of exposed and shaded surfaces were generated by the GEOREM model of Uylenhoet (1990). Bushes were depicted as paraboloids, sitting directly on the ground surface, so the model did not allow for the occurrence of shade below bushes. In the model, the 'bushes' were randomly scattered over the surface. They had various sizes as prescribed by five paraboloid size classes which were derived from detailed measurements of bush geometry and their respective coverage areas. Details of the classes are given in Table A7.1.

TABLE A7.1. Geometrical characteristics of 83 bushes sampled at the experimental site on day 232. Between brackets are the values for day 281 when an arbitrary increase of 10 % per week is applied for the height and 2.5 % for the length and the breadth of the bushes (until day 274, after which a levelling-of occurred). Bushes are represented by paraboloids as used for the program GEOREM.

Class	limits	Major axis	Minor axis	Height	n
1	0.5-1.5	1.15 (1.28)	0.96 (1.09)	1.74 (2.24)	8
2	1.5-2.5	2.05 (2.18)	1.71 (1.83)	1.77 (2.27)	21
3	2.5-3.5	2.97 (3.10)	2.55 (2.68)	2.19 (2.69)	31
4	3.5-4.5	3.91 (4.03)	3.06 (3.19)	2.37 (2.87)	15
5	4.5-5.5	4.93 (5.05)	3.81 (3.94)	2.44 (2.94)	8
Average		3.00 (3.13)	2.42 (2.55)	(2.10) (2.60)	Σn=83

Fig. A7.1 shows the model estimates of α_1 to α_4, respectively. Shaded surface area decreases very rapidly after 8 GMT, which means that during most of the day Eq. A 7.1 can be simplified to $T_{s,t} = 0.2T_{s,bs} + 0.8T_{s,us}$. Note that this formula does not account for shaded areas beneath the bushes.

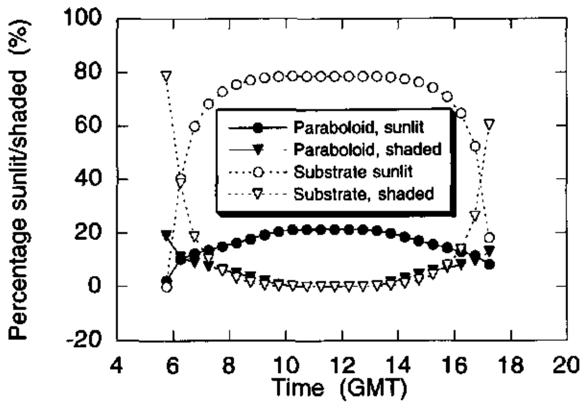

FIGURE A7.1. Directly exposed and shaded paraboloid and substrate areas expressed as a percentage of the total area.

Appendix 8 Recalibration of surface temperature as measured with Heimann IRTs

We know that the average 'true' understorey temperature lies somewhere in between the soil and the herb temperature and that the Heimann IRT was definitely overestimating because of its 0 ° view angle. Here, we assume that the Comet T_S-values as recorded for the mixture of soil, grasses and herbs, are closer to reality, because of their 45 ° view angle. Therefore, the separate manual measurements of bare soil and herbs/grass may help to find a representative understorey surface temperature by 'recalibrating' the continuous Heimann measurements with the help of the scarce Comet measurements.

The understorey temperatures, $T_{s,u}$, were described as composed of a fraction of herb temperature, $T_{s,h}$, and soil temperature, $T_{s,s}$ (the sum of the fractions equals 1) and this artificial composite temperature was compared with the measured understorey Comet surface temperatures. It was found that a linear combination of 0.581 times the herb temperatures and 0.419 times the soil temperatures gave the smallest sum of squares between directly measured and composite understorey surface temperature ($r^2 = 0.74$). Final $T_{s,u}$-values were found by $T_{s,us} = 0.61 * T_{s,\ us}$ (Heimann) + 118.4 ($r^2 = 0.90$). These values, combined with the continuously measured bush temperatures, were used to determine the composite temperature of the total savannah surface.

The surface temperatures for the *Guiera* shrubs as recorded with the Heimann IRT were also related to the Comet readings. The horizontally installed Heimann was sampling the north side of a *Guiera senegalensis* bush. Although the solar inclination was small, this temperature probably represented relatively shaded surface temperature values and was therefore considered to be too low. However, the instrument was supposed to 'look through' several bushes, thereby probably also sampling sunlit leaves. Because Heimann recordings for the shaded components were not available, their values were derived from the Comet measurements representing exposed situations. The final formulae used to calculate the surface temperature of the four subclasses are given by

$$
\begin{aligned}
T_{s,bs} &= 0.76 T_{s,b}(\text{Heimann}) + 75.0 && r^2 = 0.74 \\
T_{s,bsh} &= 0.87 T_{s,bs} + 38.7 && r^2 = 0.88 \\
T_{s,us} &= 0.61 T_{s,u}(\text{Heimann}) + 118.1 && r^2 = 0.90 \\
T_{s,ush} &= 0.60 T_{s,us} + 120.9 && r^2 = 0.78
\end{aligned}
\tag{A8.1}
$$

where all temperatures are given in degrees Kelvin. In these formulas, the subscript *bs* stands for sunlit bush, *bsh* for shaded bush, *us* for sunlit understorey and *ush* for shaded understorey.

Appendix 9 Evaluation of soil thermal diffusivity, κ

For the derivation of κ, four methods (the Amplitude, Arctangent, Logarithmic and Harmonic equation, as described in Appendix 2) have been used and compared. For the HAPEX-Sahel savannah surface κ was calculated with all four methods, after which the Harmonic method was selected for further calculations. No κ-values have been calculated for the HAPEX-Sahel tiger-bush, because of a lack of soil temperature data. For the SEBEX-campaign, κ was computed with the Amplitude method, because of its simplicity and good performance (Verhoef et al., 1996a). Thermal diffusivity was only calculated for the topsoil (at depths of 0.05 and 0.10 m), because attempts to calculate κ for deeper layers (with the Harmonic equation) yielded unrealistic values, which implies that the soil was probably not homogeneous in the vertical direction. However, for calculation of G we only need a value of κ for the upper few centimetres of soil. Fig. A9.1 gives the κ-values at a depth of 0.05 m obtained from the Amplitude, Arctangent, and Harmonic method using hourly mean values for soil temperature. The Logarithmic equation, although giving a temporal variation similar to the other methods, was much higher and is therefore not shown in these graphs. All methods give similar values, although during the dry period the Amplitude method shows somewhat lower values compared to the other two methods. The results of the Harmonic method have been selected for further calculations, because of its comparably smooth character. Another reason is the fact that κ does not increase at the end of the IOP, in contradiction to especially the Arctangent method, because this seems rather unlikely as the soil is steadily drying.

Temperature profiles were also measured underneath a more vegetated soil plot (see § 5.3.2). However, attempts to calculate κ for this location led to erratic and illogical results for all methods. This was caused by the irregular temperature profiles (caused by the vegetation) and by the fact that the actual depth at which the sensors were located deviated considerably from the intended installation depth. This discrepancy might have been the result of soil movement caused by severe flooding during several rainstorms.

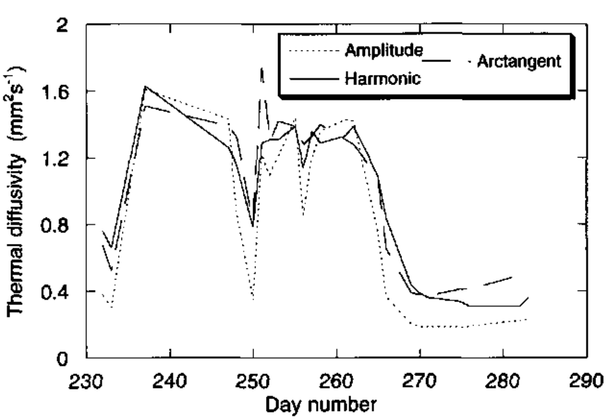

FIGURE A9.1. Course of thermal diffusivity, according to several methods, during the HAPEX-Sahel measurement campaign.

Appendix 10 Analysis of measured thermal conductivities

Fig. A10.1 shows the **measured** thermal conductivity values at several depths during the HAPEX-Sahel campaign. Fig. A10.1a shows results for the vegetated profile and Fig. A10.1b for the 'bare' (slightly vegetated) profile. In both graphs the variable course of λ during the rainy period (day 230-265) is obvious, especially for the shallow sensors (0.015 and 0.04 m) where rapid wetting and drying alternate. After the rainstorms, λ of all soil layers declines rapidly due to high evaporation rates during the drying out phase. The maximum values of λ are around 2.0 W m^{-1} K^{-1} ($\theta = \pm\, 0.15$ m^3 m^{-3}). Minimum values are approximately 0.25 W m^{-1} K^{-1} ($\theta = \pm\, 0.02$ m^3 m^{-3}). The value of 0.25 is similar to the 'dry' λ-values of the sandy soils (Ten Berge, 1990). The 'wet' λ-value of 2.0 appears to be quite high. The largest values of λ for sands recorded are about 2.30 W m^{-1} K^{-1} under wet conditions (de Vries, 1963, θ=0.21 m^3 m^{-3}; Riha et al., 1980, θ = 0.38. The high λ-values observed for the HAPEX-Sahel experiment at relatively low θ might have been caused by the presence of termites, whose activity ensured a highly conducting soil.

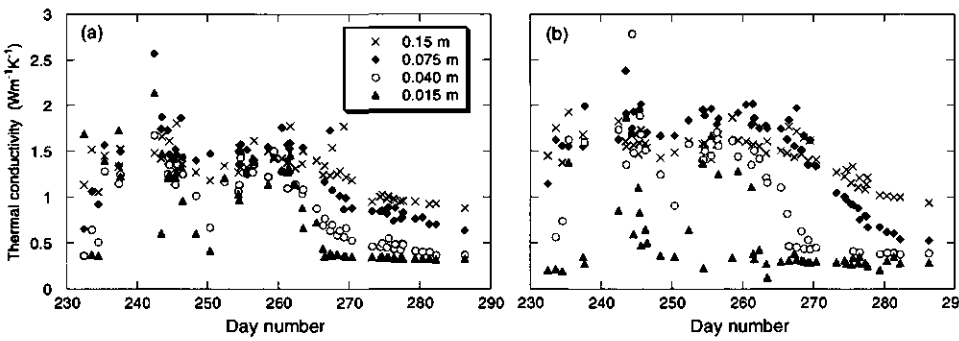

FIGURE A10.1. Measured thermal conductivity during the HAPEX-Sahel measurement campaign. (a) Vegetated soil plot and (b) bare soil plot.

The λ-values of the vegetated and the bare plot (about 5 m apart) at a depth of 0.04 m agreed well (r^2 = 0.76). At low moisture content (low λ-values) the vegetated plot yielded slightly higher λ-values, whereas for high λ-values the bare plot exhibits larger values of λ. Both aspects can probably be explained by the presence of the vegetation, which preserves moisture during dry periods, but intercepts moisture during the wet periods. This same phenomenon has been observed during EFEDA-I (Verhoef et al., 1996a). Differences between both plots are caused by soil heterogeneity (vegetation density, composition, moisture content), different depths of both sensors caused by the rough surface, and contact problems between the λ-probes and the soil. The problem of contact resistance is discussed, among others, by Nagpal and Boersma (1973) and by Van Haneghem (1981). According to Van Haneghem (1981) the contact resistance, Γ, decreases with increasing temperature and decreasing particle diameter. In an experiment using silversand, moisture content had little effect on Γ. Γ appears to be mainly determined by particle size and not by shape or stacking density. With an estimate of Γ, using data and formulae given in Van Haneghem (1981) it was found that the error in λ could lead to underestimation of around 0.10 W m^{-1} K^{-1}.

Appendix 11 Calculation of *G* according to four methods

For the savannah surface, soil heat fluxes were calculated with several methods: the Calorimetric, Gradient, Harmonic and Plate method (Tanner, 1963; Kimball and Jackson, 1975; Ten Berge, 1990) as described in Appendix 3. All methods required the installation of at least one soil thermometer (Plate method, Harmonic method) or more (two for the Gradient method and several, at least four or five, for the Calorimetric method). The Plate method used thermopile flux plates. Furthermore, all methods demanded an estimate of heat storage of the soil layer above the (upper) sensor. Besides measurements of temperature or the flux at a certain depth, an estimate of the soil thermal properties (λ, κ and C_h) was needed. The Calorimetric method required estimates of C_h, whereas for the Gradient and the Plate method values of λ and C_h (calculation of storage) were needed. For the Harmonic method all thermal properties are used. All methods haven been applied for the understorey plot. For calculation of *G* beneath the *Guiera senegalensis* bushes, only the Plate method has been used.

Fig. A11.1 shows a comparison of these four methods for sunlit soil beneath the herb layer for two days during the wet period (256-257) and during the dry period (282-283). It appeared that the Calorimetric method was always higher than the other three methods. For wet days the results from the Plates method were generally lower than those from the other methods. This was probably caused by obstruction of moisture which caused the soil area around the plate to be wetter thus leading to underestimation of the soil heat flux. During those wet days the results of the Gradient method were closest to the Calorimetric method, indicating that the high calculated λ-values were correct. During the transition period (days 269-277) the Calorimetric method was best approached by the Plate method. For the dry period the Calorimetric method was very distinct from the other methods. Difference between the other methods was smallest during those days with low θ-values (e.g. 282, three weeks after last rainfall). As expected, night-time *G*-values were lowest for the Plate method, even after heat storage correction, which might suggest a net heating of the soil even if this is not actually occurring.

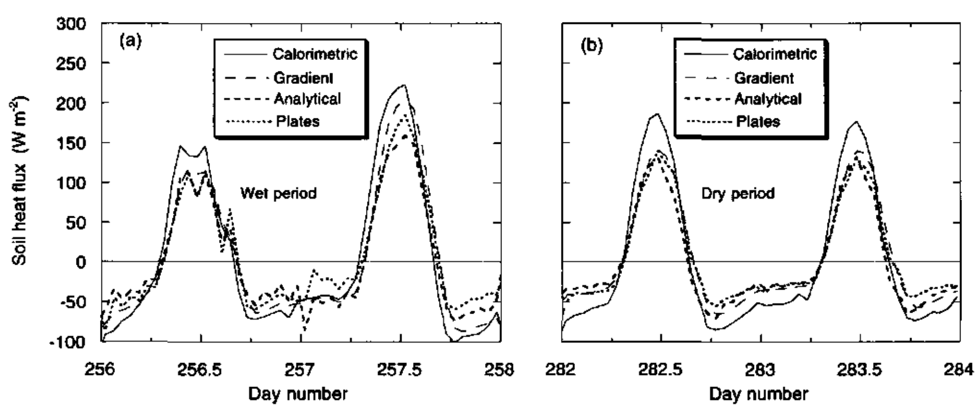

FIGURE A11.1. The understorey soil heat flux, G_u, as calculated with four methods for days during the rainy period (a), and the dry period (b) of the HAPEX-Sahel experiment.

Before it can be decided, if at all, which method performs best, it has to be established how sensitive the methods are for the required input. The specific input parameters and the depths at which they were measured (soil temperature) or calculated (C_h, κ and λ) were given in § 3.5.2. and Appendix 3.

A sensitivity test demonstrated that a decrease of 20 % in κ and C_h, caused the Analytical and Plate method to produce outputs that were roughly 30 % lower. For the Gradient and Calorimetric method this difference was only 7 %. Furthermore, taking into account the large error that can be made by assuming a sensor is located one centimetre higher or lower than the actual installation depth, it becomes clear that the Analytical and Plate method are very sensitive to the right guess of especially κ. This makes a decision about the best method very difficult. Correlation between the methods was high ($r^2 > 0.90$), which shows that the methods themselves were performing well, but their final output depended highly on the crucial estimates of κ, C_h and λ.

Therefore, it was decided that the results of the Calorimetric method were to be used for estimates of the understorey soil heat flux, G_u, because recent investigations (Horton et al. 1983, Ten Berge, 1990) showed that this method gives the most reliable estimates of G and because of its insensitivity for changes in upper soil thermal soil properties. An indirect proof for this was the fact that it ensured a considerably better closure of the energy balance (see § 5.4) than the other methods.

Appendix 12 Results of Sherwood-resistance model

For this thesis, a simple evaporation model has been developed and evaluated for the bare soil component of the HAPEX-Sahel savannah (see Jacobs and Verhoef, 1996) and tiger-bush surface. The theory of this method was given in Appendix 5. Here, the results of the method will be summarized.

For the CWS savannah, four successive days (250-253) and nights with different weather conditions at the end of the rainy period were selected to analyze. For day 251 no EC measurements were available due to heavy thunderstorms. In Fig. A12.1 the main characteristics of the weather during that period have been plotted to get a general impression. The topsoil was somewhat dried out during the first selected day. However, due to the heavy rains around midnight of day 250/251 the soil moisture increased considerably which was reflected in the significantly lower soil temperatures at day 251.

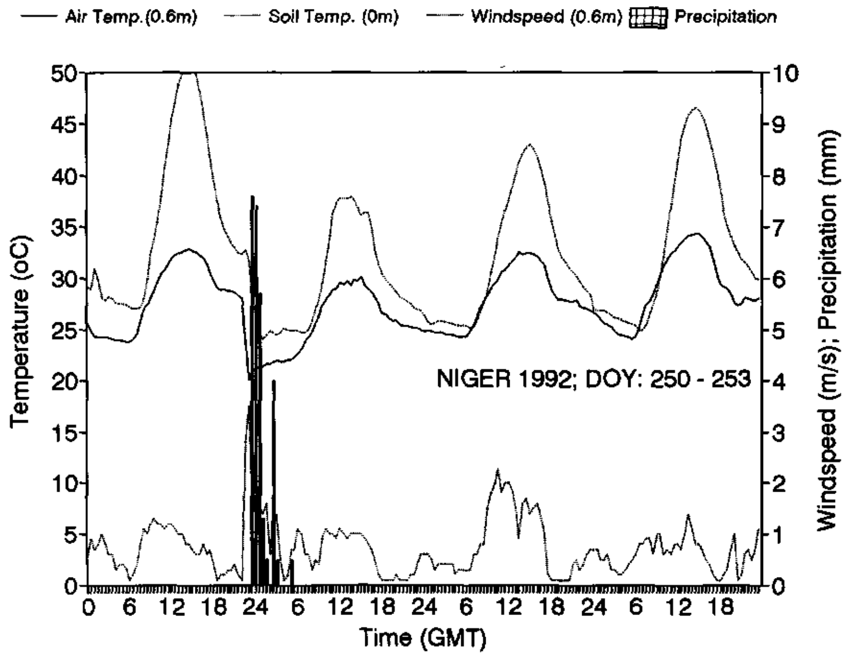

FIGURE A12.1. Air temperature (at 0.6 m height), soil temperature (at 0.0 m), windspeed (at 0.6 m) and half-hourly sums of precipitation at the HAPEX-Sahel savannah site for the days 250 to 253. Soil temperature was obtained from the Heimann IRT pointing at the understorey. Because this sensor was looking along the blades of grass, its output mainly represented bare soil (see § 5.2.4). Half-hourly precipitation values were calculated by summing 5-minute values obtained from Lebel (see Lebel et al., 1996).

To evaluate the type of convection (free or forced) during the selected period, the surface Rayleigh number (Eq. A.5.2) has been plotted versus the square of the surface Reynolds number (Eq. A5.3). It appeared that the majority of the conditions can be recognized as free or mixed convection. Only four half hour intervals of the total of 192 intervals fulfilled the forced convection criterion. These periods occurred during the thunderstorms around the midnight of day 250/251.

L_vE_t (sum sparse vegetation and soil contribution) measured by the EC-technique has been compared with L_vE_s. For a sparse vegetation, the first result must correlate well with the latent heat which originates from the soil surface. For the calculated soil latent heat flux it has been assumed that there was no restriction in soil evaporation caused by the dryness of the soil. In other words, the calculations were performed with a Soil Bowen Ratio Coefficient, $c_W = 1$ (see Eq. A5.10) . For most days the soil contribution was, as must be expected, lower than the total latent heat flux. However, the first selected day (DOY: 250) was an exception. The reason for this is, as will be explained later, that during this day the topsoil was dried out (i.e. $c_W > 1$), which reduced the maximum possible soil evaporation considerably.

From Eqs. A5.11a and A5.11b it can be seen that the soil evaporation can be estimated in two different ways; namely by using either the Sherwood number directly (Eq. A5.11b) or by using the soil Bowen ratio along with the Nusselt number (Eq. A5.11a). It is interesting to investigate whether both techniques produce the same results. Both model calculations have been plotted in which it is assumed that $c_w = 1$. It can be inferred that both ways lead practically to the same result ($r^2 = 0.94$ and 0.98 for a linear and a polynomial fit, respectively). This is an interesting result since, in general, temperature measurements (needed in Eq. A5.11a) are much easier and more reliable to be carried out than moisture measurements (needed in Eq. A5.11b). In the following and in § 5.3.3, the calculated soil evaporation results are obtained by using Eq. A5.11b only (Sherwood number technique).

It is interesting to know how well the model results agree with the measured data of the microlysimeters. In Fig. A12.2a the cumulative evaporation amounts over the selected period are compared with the measured results. In this graph a distinction is made between the sunlit and shaded microlysimeter data. During the period following the heavy rains, the calculated results agree well the measured results. Moreover, there is hardly any difference between the sunlit and the shaded lysimeter data. However, during the first day the lysimeter data deviate considerably from the calculated model results. This means that here the dryness of the topsoil must have affected the soil evaporation process.

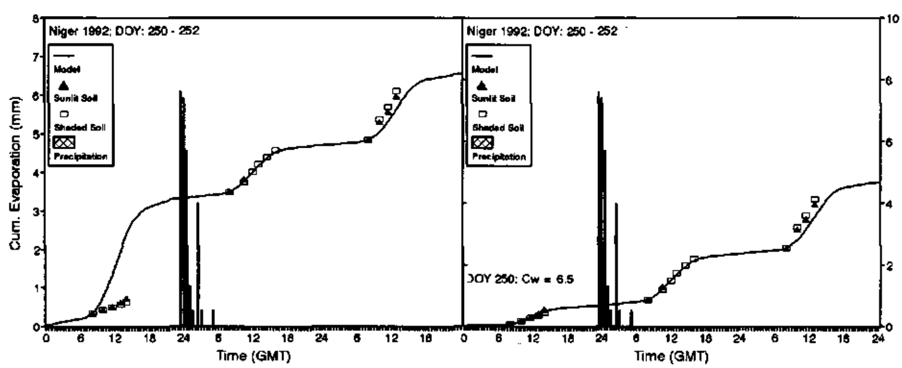

FIGURE A12.2. (a) The course of the maximum possible cumulative calculated evaporation rates ($c_W = 1$) and the measured results from the sunlit and shaded lysimeters and (b) the same but with variable c_W.

This method was also tested for the SSS tiger-bush site. In this case **diurnal** measurements of soil evaporation were provided by a small BREB set-up (see § 3.7 and Wallace & Holwill, 1996). Calculation of 'potential' ($c_w = 1$) L_vE_s yielded diurnal courses that were similar to the BREB results, although the amplitudes were much too high during most of the days, again underlining the necessity of c_w-values > 1. Values of c_w were derived by dividing calculated potential L_vE_s by measured L_vE_s. Generally, c_w varied during the day, especially during days occurring immediately after rainfall, but a clear increasing trend was observed during the IOP.

In Fig. A12.3, the Soil Bowen Ratio Coefficient, c_w, has been depicted versus the soil moisture of the topsoil. For the tiger-bush, soil moisture data from 0 - 0.08 m depth were used, whereas for the savannah θ between 0 and 0.05 m depth was used. It appeared that the maximal possible soil moisture content of the topsoil for both soils was 0.12 m^3m^{-3}. For the savannah, the Soil Bowen Ratio Coefficient was taken as the ratio between the daily lysimeter results (actual soil evaporation) and the daily calculated soil evaporation results by using Eq. A5.11b (maximal possible soil evaporation). It can be seen that at high moisture content the c_w-value is more or less constant around the numerical value $c_w = 1$. At moisture contents lower than 0.05 m^3m^{-3}, the c_w-coefficient increases rapidly at a more or less exponential rate.

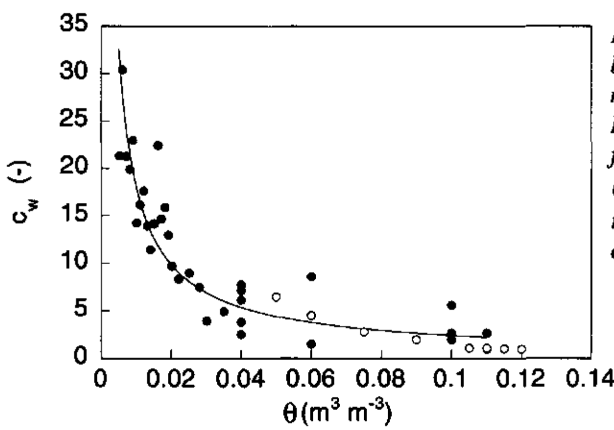

FIGURE A12.3. The relationship between SSS tiger-bush topsoil moisture content and the Soil Bowen Ratio Coefficient, c_w. The fitted line is given by $c_w=0.329\ \theta^{(-0.867)}$ ($r^2 = 0.79$). The savannah results can be fitted by $c_w=23.649\ \exp^{(-27.54\ \theta)}$.

In Fig. A12.2b, the calculated as well as measured cumulative soil evaporation results for the savannah have been plotted. The calculated evaporation figures were obtained by using a variable Soil Bowen Ratio Coefficient, c_w, dependent on the soil moisture content of the top-soil (see open circles in Fig. A12.3). Fig A12.4 shows a comparison between the measured and the calculated values of L_vE_s for the SSS tiger-bush site. Values of c_w can be found from the relationship given with Fig. A12.3.

From this result it can be concluded that the proposed technique to estimate the contribution of soil evaporation to the total evaporation can be used adequately if at the same time also soil moisture data are available and, in addition, the Soil Bowen Ratio Coefficient, c_w, is known.

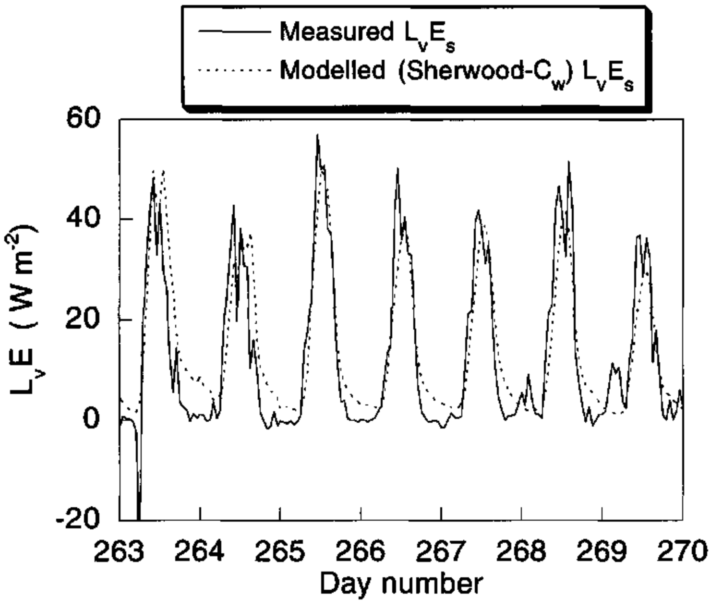

FIGURE A12.4. Directly measured (micro BREB system, see Wallace and Holwill, 1996) and calculated (Sherwood-resistance model) values of soil evaporation found for the SSS tiger-bush site.

Appendix 13 Criteria used for quality rating of experimental roughness parameters

a) Fetch

If an upwind change in roughness length occurs, the flow needs a certain distance to adapt to the new surface. The distance over this continuous, homogeneous new surface, measured along the wind path from the upwind edge to the instrument mast is called the fetch. It depends on the point of the compass. The fetch is usually determined as being 100 times the top instrument height (Brutsaert, 1982). However, the time it takes for the flow to adapt to a new surface also depends on the roughness of the vegetation (Gash, 1986). Therefore, the formula given by Wieringa (1993) is applied to find out whether a certain wind profile level still represents the local terrain roughness.

$$F \approx 2z_0\left(\frac{10z}{z_0}\left[\ln\frac{10z}{z_0}-1\right]+1\right) \tag{A13.1}$$

Here F is the minimum fetch to ensure equilibrium adaptation to the downwind roughness. To calculate this minimum fetch for the selected experiments the highest wind speed level and the experimentally determined z_{0m}-value was used. This fetch was compared to the available fetch as given for the experiments presented in Table 6.1.

b) The roughness sublayer

All (non-geometric) methods used to determine z_{0m} and d make use of the logarithmic wind profile (Eq. 2.28). Strictly taken, this one-dimensional equation is only valid for heights, z, greater than the lower boundary of the inertial sublayer. However, it can be safely applied for measurements above the upper limit of the roughness sublayer, z^*. For windspeed measurements below z^*, the wind profile will deviate largely from its exponential form due to influences of the individual canopy elements, leading to possible underestimation of d or z_{0m} and d being dependent on the location of the observation mast.

Traditionally, the depth of the roughness sublayer was calculated as a multiple of canopy height, which is a practical criterion for low-concentration surfaces (Raupach et al., 1980). A value of 2.0 has been quoted by O'Loughlin and Annambhotla (1969), whereas Garratt (1977) used a value of 4.5. Later on, the depth of the roughness layer was thought to be described more adequately by the spacing on the roughness elements, D . E.g. $z^* = 4.5D + d$ from Chen Fazu and Schwerdtfeger (1989) which follows Garratt (1980) with $z^* = 3D + d$ and $z^* = h + 1.5D$ following from Raupach's (1980)wake diffusion and inhomogeneity considerations. Another often quoted formula, although loosely defined, is $z^* = 20z_{0m} + d$ (De Bruin and Moore, 1985; Wieringa, 1993). Furthermore, z^* might be a function of stability as indicated by Chen Fazu and Schwerdtfeger (1989), which makes the above mentioned simple relationships difficult to apply.

If we want to find a practical rule for estimating z^* there are two cases to consider: one where the vegetation is close-spaced and the other where the vegetation is sparse. Here, close-spaced indicates plant spacing less than a few heights apart so the individual wakes strongly interact and quickly lose their separate identity, and sparse refers to crops where the individual wakes can be easily identified. Many crops that we would normally consider 'sparse' are close-spaced by this definition. In close-spaced crops the majority of the canopy turbulence is produced in a horizontal shear layer near the top of the canopy. In sparse crops it is produced in the wakes of the individual asperities and at the ground since significant momentum reaches the ground in such canopies. In close-spaced canopies the plant spacing (D) is not a significant size scale, so z^* can probably not be related to it. As the majority of the crops will not be sparse in the framework of the definition given above, it is doubtful whether the formulae of Chen Fazu and Schwerdtfeger (1989) and Raupach (1980) will give useful estimates of the depth of the roughness sublayer. Formulae involving spacing, D, seem to be based on the idea that wakes produce inhomogeneous flows. However, it is not only inhomogeneity, we need a deviation in the mean from behaviour of the inertial sublayer. If we see z_{0m} as being the scale at which momentum is dissipated, we can identify z_{0m} with the size scale of the eddies produced in the shear layer near the top of relatively close-spaced canopies. Eddies of this scale dominate canopy transport and momentum dissipation, and spread upwards to affect the turbulence and mean wind above. The effect of this would become negligible when the size scale for the inertial sublayer is some multiple of z_{0m}. De Bruin and Moore (1985) suggest 20 and this may be about right. While z_{0m} may not be known exactly, this is still a useful relationship because $z_{0m} = h/10$ is probably good enough for data screening (personal communication, K. McNaughton, 1994).

From the considerations given above, the formula of De Bruin and Moore (1985) will probably work best to calculate z^* for most of the crops to be presented in Table 6.1. Hence, this formula will be used for the quality rating.

Samenvatting

Deze studie behandelt het energiebudget van twee struikvegetaties voorkomende in de Sahel; een savanne en een natuurlijk open bos. De energiebalans aan het aardoppervlak is een sleutelvergelijking in meterologische studies. Deze vergelijking beschrijft hoe de totale binnenkomende energie, de netto stralingsdichtheid, wordt verdeeld over de voelbare, de latente (verdamping) en de bodemwarmtestroomdichtheid. Vanwege de verdampingscomponent is de energie balans van een (begroeid) oppervlak tevens een belangrijke schakel in wetenschappen zoals de hydrologie, de plantenfysiologie en de landbouwkunde.

Het open bos wordt lokaal 'tijgerbos' genoemd vanwege een duidelijk herkenbaar strepenpatroon lijkend op een tijgervel. De ongeveer vier meter hoge en 20 bij 40 meter grote vegetatiestroken zijn voornamelijk samengesteld uit houtige struiken (*Guiera senegalensis*) met af en toe een boom behorende tot de *Combretum* familie. De vegetatie neemt ongeveer 30 % van het oppervlak in. Tussen deze stroken bevindt zich kale grond, die ernstige slempkorstvorming vertoont. De savanne bestaat eveneens uit *Guiera Senegalensis* met een ondergroei van verschillende gras- en kruidensoorten, met daartussen kale bodem. De struiken variëren in hoogte van twee tot drie meter en bedekken maximaal 20 % van het totale oppervlak. De grassen en kruiden hebben een gemiddelde hoogte van ongeveer 50 centimeter. De savanne maakt deel uit van een gierst rotatiesysteem, waarbij de braakperiode (5 - 10 jaar) dient ter bevordering van de natuurlijke bodemvruchtbaarheid. Vanwege de geringe bedekkingsgraad kunnen de savanne en het tijgerbos geclassificeerd worden als een open vegetatie. Zij bestaan uit twee herkenbare lagen; een bovenlaag (de struiken) en een onderlaag (de gras/kruidenlaag of de kale bodem). Spaarzame vegetaties bedekken een groot deel van het (semi)-aride landoppervlak en er is nog maar weinig over bekend, in tegenstelling tot de meer gesloten vegetaties in de gematigde gebieden.

Meteorologische metingen, ter bestudering van de energiebalans, hebben plaatsgevonden tijdens de Intensieve Observatie Periode (IOP, augustus tot oktober 1992) van het HAPEX-Sahel project. HAPEX staat voor 'Hydrological and Atmospheric Pilot EXperiment' en dit experiment beoogde een beter inzicht te verkrijgen in de wisselwerking bodem-plant-atmosfeer in de semi-aride tropen. De omvang van de Sahel-zone (13° tot 17° NB) kan gedefinieerd wordt met behulp van jaarlijkse regenvalgemiddelden (200 tot 700 millimeter). De regenval valt gemiddeld in een periode van drie tot zes maanden, zodat een groot deel van het jaar volledig droog is waardoor de vegetatie sterk gereduceerd wordt. Het regenvalpatroon en andere klimaatseigenschappen (het verloop van bijvoorbeeld temperatuur en luchtvochtigheid) karakteriseren het semi-aride klimaat. De Sahel wordt de laatste twintig jaar geteisterd door een aanhoudende droogte, die zich kenmerkt door een regenval die consequent lager is dan het lange termijngemiddelde. Door de druk op de beschikbare grond vindt eveneens een landdegradatie plaats die zich vertaalt in verwoestijning en afnemende bodemvruchtbaarheid (vanwege erosie en kortere braakperiodes). De tijdens HAPEX-Sahel bewerkstelligde samenwerking tussen wetenschappers van verschillende disciplines beoogde meer duidelijkheid te verschaffen in oorzaak en gevolg van bovenbeschreven processen en hoe deze eventueel een halt kunnen worden toegeroepen.

In het HAPEX-Sahel meetgebied, tussen 2 en 3 ° OL en 13 en 14° NB, bevonden zich drie hoofdgebieden die elk verdeeld waren in een aantal subgebieden bestaande uit gierst, savanne, of tijgerbos. De metingen beschreven in dit proefschrift richtten zich voornamelijk op de meest westelijk gelegen centrale locatie (CWS). De vertikale atmosferische voelbare warmte- en waterdampstroomdichtheden zijn gemeten met de eddy covariantie methode. Met behulp van deze betrouwbare en geavanceerde methode is tevens het CO_2 transport bepaald. De CO_2 metingen hadden tot doel meer inzicht te verkrijgen in het plantenfysiologische gedrag en de watergebruiksefficientie van de savanne. Dit is van belang, daar er nog maar weinig gegevens beschikbaar zijn betreffende deze vegetaties. Met de eddy covariantie methode wordt de verticale flux van een getransporteerde grootheid (warmte, vocht of CO_2) verkregen door de fluctuaties van deze grootheid te correleren met fluctuaties in verticale windsnelheid.

De netto stralingsdichtheid vermindert met de bodemwarmtestroomdichtheid vormt de beschikbare energie die verdeeld kan worden over de voelbare warmtestroomdichtheid en de verdamping. Voor het doorgronden van de balans is het daarom van belang de twee eerstgenoemde termen nauwkeurig te bepalen. Het meten van deze grootheden bracht problemen mee die inherent zijn aan het voornaamste kenmerk van een open vegetatie: *inhomogeniteit*. Er is daarom eveneens getracht de bijdrage van de verschillende componenten (bosjes, ondergroei, bodem) aan de totale energiebalans te meten. Voor de bepaling van de verdamping van de bosjes, grassen en bodem apart, zijn hiertoe technieken zoals sapstroom metingen, porometrie en lysimetrie toegepast.

Het HAPEX-Sahel projekt beperkte zich tot een periode van half augustus tot half oktober 1992. Voor de beschrijving van de energiebalans door de seizoenen heen is gebruik gemaakt van de data van het SEBEX-experiment dat enkele jaren eerder in het zuidelijke deel van het HAPEX-Sahel vierkant had plaatsgevonden. Dit experiment werd uitgevoerd door het Institute of Hydrology (Wallingford, Engeland) gedurende de jaren 1988 tot 1990. Deze gegevens zijn verwerkt tot daggemiddelden, zodat seizoensvariaties herkenbaar werden.

De theoretisch achtergrond van deze metingen, alsmede meer informatie omtrent de meetopstelling en de toestand van vegetaties en bodem is gegeven in de Hoofdstukken 2 en 3.

In Hoofdstuk 5 zijn de vier termen van de energie balans beschreven, zowel het verloop gedurende de dag als gedurende de seizoenen. Waar mogelijk, zijn de resultaten van de savanne en het tijgerbos vergeleken evenals de bijdragen van de verschillende vegetatiecomponenten.

De netto straling werd ontleed in haar vier componenten; inkomende kortgolvige, uitgaande kortgolvige, inkomende langgolvig en uitgaande langgolvig straling. Op heldere dagen bereikte de kortgolvig inkomende straling maximale waarden van 1000 W m^{-2} (op half uur basis). De instantane waarden tijdens bewolkte dagen werden gereduceerd met 50 % of meer. Op seizoensbasis werden maximale waarden geregistreerd gedurende maart en april, wanneer de zon haar hoogste positie had bereikt en wolken vrijwel afwezig waren. Een duidelijk minimum kon worden waargenomen rond de maanden december en januari. De kortgolvige uitgaande straling wordt bepaald door de albedo; dat gedeelte van de binnenkomende kortgolvige straling dat door het oppervlak wordt gereflecteerd. Gedurende HAPEX-Sahel bleek de albedo het laagst voor de *Guiera senegalensis* struiken en de vegetatiestroken van het tijgerbos - de waarden varieerden van 0.17 tot 0.20. De onderlaag van de savanne had iets hogere waarden, tot maximaal 0.24, vanwege de aanwezigheid van kale bodem tussen de grassen en kruiden. De albedo voor de kale bodem van het tijgerbos liep op van ongeveer 0.25 voor situaties met een hoog bodemvocht gehalte tot 0.30 na uitdroging van de toplaag. Tijdens de SEBEX-campagne varieerde de daggemiddelde albedo voor savanne van 0.17 tijdens het natte seizoen to 0.25 gedurende het droge seizoen. De waarden van het tijgerbos lagen gemiddeld hoger en vertoonden minder verloop - van 0.23 tijdens het natte seizoen tot 0.27 tijdens de droge tijd. Dit wijst erop dat de vegetatiestroken van het tijgerbos waarschijnlijk het hele jaar door redelijk groen blijven.

Langolvige *inkomende* straling is een functie van de emissiviteit van de atmosfeer en de luchttemperatuur. De variatie van deze grootheid gedurende de dag was ongeveer even groot als de fluctuatie van de daggemiddelden gedurende de seizoenen (25 %, van ongeveer 350 tot 450 W m^{-2}). Verder bleek uit de SEBEX-gegevens dat er een aanzienlijke discrepantie bestond tussen berekende en gemeten waarden van atmosferische emissiviteit (die fluctueerde tussen

0.7 en 0.9), wat mogelijk aangeeft dat de alom gebruikte formules niet zonder meer bruikbaar zijn onder tropische omstandigheden. De langolvige uitgaande straling is afhankelijk van de temperatuur en de emissiviteit van het oppervlak. Overdag waren de verschillen tussen de oppervlaktecomponenten relatief groot: de oppervlaktetemperatuur van de savanne bosjes was gemiddeld ongeveer 7 ° lager dan die de onderlaag. De kale bodem bleek gemiddeld zo' n 15 ° warmer dan de bosjes. Soortgelijke verschillen tussen de oppervlakken werden gevonden voor het SEBEX-experiment. De gebiedsgemiddelde oppervlaktetemperatuur fluctueerde daar van 25 ° gedurende de wintermaanden tot 45 ° aan het begin van de natte tijd. De gemiddelde oppervlaktetemperaturen voor de savanne en het tijgerbos bleken vrijwel gelijk, omdat het grotere percentage kale (warme) bodem van het tijgerbos gecompenseerd werd door een iets groter aandeel koele struiken (33 t.o.v. 20 %). Met een oppervlakte-emissiviteit van 0.98 voor de bosjes tot 0.95 voor de ondergroei en de kale bodem, werden waarden voor langolvige uitgaande straling berekend tussen de 450 ('s nachts) en 600 (savanne onderlaag, einde IOP overdag) W m^{-2}. De variatie in daggemiddelden gedurende 1989 en 1990 was vergelijkbaar: van 425 gedurende januari t/m maart tot 550 W m^{-2} in juni en juli. Het gaat hier om gebiedsgemiddelde waarden van savanne en tijgerbos.

Alle stralingscomponenten bleken gemiddeld met 20 tot 30 % te variëren over de seizoenen, maar omdat de pieken en dalen niet rond dezelfde tijd vielen fluctueerde de netto straling met bijna 60 % (van 75 W m^{-2} rond december tot 175 W m^{-2} gedurende augustus en december). Dit uitgesproken verloop heeft gevolgen voor de beschikbare energie en dus voor de verdamping en voelbare warmtestroomdichtheden. De netto straling was over het algemeen iets groter voor het tijgerbos dan voor de savanne (gemiddeld 5 %).

De bodemwarmtestroomdichtheid wordt bepaald door de inkomende energie en door de thermische bodemeigenschappen, bestaande uit de warmtecapaciteit, het warmtegeleidingsvermogen en de diffusiviteit voor warmte. Deze eigenschappen hangen af van de samenstelling en het vochtgehalte van de bodem. Het warmtegeleidingsvermogen en de de diffusiviteit waren vrij hoog gedurende het regenseizoen. Dit werd mogelijk veroorzaakt door de hoge termietenactiviteit, die een relatief verkitte, en dus goed geleidende, bodem bewerkstelligde. Thermische diffusiviteit bereikte maximale waarden van 2 mm s^{-1} in de regentijd. Gedurende dezelfde periode was het warmtegeleidingsvermogen rond de 2 W m^{-1} K^{-1}, wat eveneens vrij hoog is. Verder bleek dat drie weken na de laatste regenval de thermische bodemeigenschappen reeds hun laagste waarden bereikt hadden (respectievelijk 0.3 mm s^{-1} en 0.25 W m^{-1} K^{-1}). Deze waarden werden namelijk ook berekend voor het droge seizoen van de SEBEX-meetcampagne. Op een (half)uurlijkse basis consumeerde de bodemwarmte-stroomdichtheid een aanzienlijk deel van de netto stralingstroomdichtheid; op sommige dagen 30 tot 40 % rond het middaguur. Op dagbasis was dit aandeel maximaal 10 tot 15 %. De bodemwarmtestroomdichtheid onder de struiken (piekwaarden rond 50 W m^{-2}) was aanzienlijk minder dan tussen de struiken (piekwaarden rond 250 W m^{-2}). Componentwaarden voor de savanne en het tijgerbos kwamen zeer goed overeen. Omdat het tijgerbos een grotere vegetatiebedekkingsgraad had, waren de gemiddelde waarden voor de bodemwarmtestroomdichtheid iets kleiner. In combinatie met de hogere netto straling bleek dat het tijgerbos ongeveer 10 % meer beschikbare energie had.

In de regentijd vertoonde de verdamping voor beide vegetaties piekwaarden (op half-uur basis) van ongeveer 450 W m^{-2} tijdens dagen vlak na regenval. Deze hoge waarden werden mede veroorzaakt door een bijdrage van de bodemverdamping. Het aandeel van de bodemverdamping was ongeveer 20 % voor de savanne, maar kon wel 50 % bedragen voor het tijgerbos.Voelbare warmte werd dan niet groter dan ongeveer 100 W m^{-2}. Na de laatste regenval nam de verdamping vrij snel af tot maximaal 300 W m^{-2}. Dit werd gedeeltelijk veroorzaakt door de gereduceerde bodemverdamping (nog maar < 5 % van de totale verdamping voor de savanne en ≈ 10 % voor het tijgerbos), maar ook vanwege het feit dat de vegetatiecomponenten langzaam begonnen uit te drogen. Het bleek dat de *Guiera senegalensis* struiken van de savanne gemiddeld 20 % (natte tijd) tot 35 % (einde van de IOP) van de verdamping voor hun rekening namen. Het aandeel van de tijgerbos vegetatiestroken in de totale verdamping varieerde van ≈ 60 % op dagen vlak na regenval tot bijna 100 % aan het einde van de IOP. In het laatste geval is de verdamping van de kale bodem dus vrijwel nihil. De bosjes in het tijgerbos hadden een ongeveer drie maal hoger bladoppervlak, wat dit verschil verklaart. De verdamping van de savanne in de overgangsperiode was gemiddeld iets hoger dan dat van het tijgerbos. Het verschil in beschikbare energie werd vooral gebruikt voor een hogere voelbare warmtestroomdichtheid voor het tijgerbos (door het hoge percentage kale, warme bodem). Dit maakte dat de Bowenverhouding (de verhouding van voelbare en latente warmtestroom-dichtheid) voor het tijgerbos in de buurt van 1.0 was, terwijl voor de savanne waarden van 0.3 werden berekend. Aan het einde van de IOP bedroeg de verdamping maximaal 250 W m^{-2} (op half-uur basis) voor de savanne en 200 W m^{-2} voor het tijgerbos. De voelbare warmtestroomdichtheid van de savanne was nog ongeveer gelijk aan de latente warmtestroomdichtheid. Echter, voor het tijgerbos was de voelbare warmtestroomdichtheid al duidelijk hoger. Dit alles leidde ertoe dat de verdamping van de savanne gedurende de laatste twee weken van de IOP hoger was dan die van het tijgerbos. Savanne verdamping varieerde van 3 tot 4 mm per dag in de natte en de overgangstijd, tot ongeveer 2 mm per dag aan het einde van de IOP. Verdamping in de natte tijd voor het tijgerbos was maximaal ongeveer 5 mm per dag. Na de laatste regenbui nam dit echter snel af tot waarden van 2 tot 3 mm per dag.

De SEBEX-gegevens boden inzicht in het gedrag van de energiebalans door de seizoenen heen. De meetcampagne werd echter gestopt in December 1989 en pas weer in mei 1990 hervat. Desalniettemin werd toch een groter vochttraject beslagen dan gedurende de IOP van HAPEX-Sahel. Daggemiddelde gemeten verdamping varieerde van 130 W m^{-2} (≈ 4 mm dag^{-1}) tot 10 W m^{-2} voor de savanne. De minimumwaarden werden halverwege november bereikt, wat laat zien dat de vegetatie (waarschijnlijk voornamelijk de ondergroei) toen al vrijwel volledig verwelkt was. De metingen aan het begin van het droge seizoen toonden aan dat de verdamping toen vrijwel nihil was. In 1989 liep de voelbare warmtestroomdichtheid op van daggemiddelden van 10 à 20 W m^{-2} tot rond de 100 W m^{-2} in December. Deze laatste waarden werden ook gemeten vlak voor het natte seizoen van 1990. In 1989 viel in de eerste week van oktober nog 22 mm regen. Desalniettemin laten de gegevens zien dat de verdamping van het tijgerbos lager was dan die van de savanne gedurende de maand october. Dit wordt waarschijnlijk veroorzaakt door het feit dat de savanne ondergroei dichter was dan gedurende HAPEX-Sahel. Aan het einde van die maand echter schieten de verdampingswaarden van de savanne onder die van tijgerbos: in minder dan een maand wordt de verdamping dan gereduceerd tot slechts 10 % van de waarden tijdens de regenperiode. De tijgerbos verdamping gaat in ieder geval door tot half december (einde campagne). Door de voelbare warmtestroomdichtheid te berekenen m.b.v. lucht en oppervlakte temperatuur kon de verdamping gedurende de wintermaanden berekend worden uit het verschil tussen netto straling en voelbare warmte. De uitkomsten wezen erop dat het tijgerbos mogelijk een groot deel van droge seizoen door verdampt, zij het op een laag niveau. De Bowenverhouding voor de savanne varieert van 0.1 gedurende de natte tijd tot rond de 10 aan het einde van 1989 en juni 1990. Voor het tijgerbos is de Bowenverhouding meestal in de buurt van de 1, behalve vlak voor de natte tijd in 1990. Dan worden ook waarden van tegen de 10 bereikt.

De bovengenoemde transporten van warmte en waterdamp kunnen worden beschreven met een 'potentiaalverschil' (bijvoorbeeld van temperatuur) en een weerstand, in analogie met de wet van Ohm. Indien een uitdrukking wordt gevonden voor deze weerstand kunnen op een relatief simpele manier de transporten in de atmosfeer worden beschreven. Modellen gebaseerd op deze weerstandsaanpak maken hier gebruik van. In Hoofdstuk 6 is het weerstandsnetwerk beschreven met de daarbij behorende belangrijkste parameters.

Allereerst zijn de ruwheidslengte en de verplaatsingshoogte behandeld. Deze spelen een rol in de zgn. aerodynamische weerstanden. Voor een bepaald gewas bestaan twee ruwheidslengten; een ruwheidslengte voor wind en voor temperatuur (of vochtigheid, CO_2, enz.). De ruwheidlengte voor wind is gedefinieerd als die hoogte boven een referentie-nivo (de verplaatsingshoogte) waarop de windsnelheid theoretisch gelijk wordt aan nul (het nivo van de impulsput) en het is een maat voor de uitwisseling van impuls. De ruwheidslengte voor temperatuur geeft respectievelijk de effektieve bronhoogte (boven de verplaatsingshoogte) voor warmte en waterdamp aan. De ruwheidslengten en verplaatsingshoogten zoals die bepaald zijn voor de savanne en het tijgerbos zijn vergeleken met waarden uit de literatuur voor soortgelijke vegetaties. De waarden bleken te kunnen worden beschreven met een wrijvingsmodel voorgesteld door Raupach (1992), waarin de ruwheidsdichtheid de enige onafhankelijk parameter is. De ruwheidsdichtheid wordt bepaald door de dimensies van de struiken. Sommige vegetatie-typen bleken niet te voldoen aan Raupach's model. In deze gevallen kon echter worden aangetoond dat er fouten in de meetopzet gemaakt waren, met name een te lage installatie van de windsensoren. De constanten benodigd in het model bleken iets andere waarden te hebben dan oorspronkelijk door Raupach voorgesteld. De in dit proefschrift bestudeerde vegetaties waren echter minder gesloten van aard. Het bleek verder dat de alom gebruikte formules waarin de ruwheidslengte en verplaatsingshoogte berekend worden via een vermenigvuldiging van de hoogte met respectievelijk 0.13 en 0.66 lang niet zo goed presteerden als het bovenbeschreven model.

De ruwheidslengte voor warmte, die meestal gelijk wordt gesteld aan die van waterdamp, is van belang wanneer we het warmtetransport of de verdamping van een oppervlak willen beschrijven met een simpele, één-lagige weerstandsformule. Deze variabele is benodigd vanwege het feit dat transport van warmte of vocht in de regel meer weerstand ondervindt dan het transport van impuls. De grootte van deze extra weerstand wordt weergegeven met behulp van de verhouding tussen de ruwheidslengten voor impuls en warmte. Is de natuurlijke logaritme van de verhouding van deze twee grootheden nul, dan is er geen extra weerstand. Hoe ruwer een oppervlak, des te groter deze extra weerstand. Voor de savanne vegetatie werd een gemiddelde waarde van ongeveer 12 gevonden. Voor een wijngaard en een kale bodem die als referentie gebruikt werden, werden waarden van respectievelijk 12 en -1 berekend. De waarden voor de begroeide oppervlakken was aanzienlijk hoger dan de vaak toegepaste waarde van 2. Dit is tevens gevonden in literatuur aangaande andere (open) gewassen, zodat geconcludeerd moest worden dat, voor betrouwbare modelvoorspellingen, deze waarde opgeschroefd moet worden naar waarden van minimaal 7. De meest betrouwbare empirische formules om de extra weerstand te beschrijven bleken de gevestigde van Sheppard (1958), Owen en Thomson (1963) en Brutsaert (1975b), die allen gebaseerd zijn op een simpele combinatie van dimensieloze getallen.

Naast de luchtweerstanden spelen vooral de oppervlakteweerstanden een grote rol bij de verdamping. Het geleidingsvermogen van de vegetatie wordt bepaald door de gemiddelde openingstoestand van de huidmondjes en het totale bladoppervlak per totaal grondoppervlak. Het gemiddelde geleidingsvermogen van de struiken in de savanne is bepaald met een porometer. Het bleek dat de huidmondjes vrij snel na zonsopgang (6 uur) opengingen, waarna het geleidingsvermogen een duidelijke piek vertoonde tussen 8 en 11 uur 's morgens. Hierna namen de waarden gestaag af zodat rond 6 uur 's avonds het nulniveau weer werd bereikt. Piekwaarden waren gemiddeld rond de 15 mm s^{-1} in de regentijd, terwijl in de drie weken na de laatste regenval de maximumwaarde gemiddeld nog maar 10 mm s^{-1} bedroeg. Ook de waarden waargenomen in de namiddag waren aanzienlijk lager. Bovendien leidde het uitdrogen van de bodem, de atmosfeer en daarmee de van vegetatie tot een vervroeging van het tijdstip waarop de piekwaarde optrad. Dit alles veroorzaakte een afname van 60 % in de gemiddelde overdag-waarden van het bladgeleidingsvermogen. Deze afname bleek vooral gerelateerd aan de afnemende luchtvochtigheid van de atmosfeer en de daarmee samenhangende afname van het bodemvochtgehalte.Twee kruidensoorten van de ondergroei vertoonden een soortgelijk patroon gedurende de dag en gedurende de IOP. De waargenomen waarden van het bladgeleidingsvermogen waren echter hoger en vertoonden meer spreiding tijdens de dag. Pogingen om het geleidingsvermogen van de struiken en de ondergroei te beschrijven met empirische functies waarin licht, luchtvochtigheid, temperatuur en bodemvocht een rol speelden lukten redelijk goed voor de Guiera struiken. Ongeveer 60 % van de variatie in de waarnemingen kon worden verklaard uit fluctuaties van bovengenoemde factoren. De grootste afhankelijkheid werd gevonden voor luchtvochtigheid. Voor de kruidensoorten werd een maximaal verklaringspercentage van 40 % gehaald en alleen door medeneming van het bodemvochtgehalte, wat aangaf dat deze variabele een grote rol speelt in het huidmondjesgedrag van de ondiep wortelende ondergroei. Een meer plantenfysiologische beschrijving van de huidmondjesgeleiding (Jacobs, 1994) leidde tot een net zo goede fit op de gegevens, maar deze parameterisatie is fysischer en is dus meer geschikt voor toepassing in bijvoorbeeld klimaatmodellen.

De waarnemingen voor het gemiddeld bladgeleidingsvermogen kunnen opgeschaald worden tot op gewas- of vegetatieniveau door vermenigvuldiging met het totale bladoppervlak. Uit deze studie bleek dat de aldus gevonden waarden, zowel voor de totale vegetatie als voor de deelcomponenten, in een één- of twee-lagig verdampingsmodel veel te grote waarden van verdamping op zouden leveren. Dit fenomeen is al vaker waargenomen en komt voornamelijk voor bij deze open vegetaties. Het wordt waarschijnlijk veroorzaakt door het feit dat de grooste bron van verdamping zich dicht bij de bodem bevindt (in het geval van de savanne), terwijl de uitwisseling van impuls aan de top van de bosjes plaatsvindt. Bovendien zijn de struiken sterk ontkoppeld van de atmosfeer, waardoor er een zeer steile gradient in luchtvochtigheid ontstaat zodat de meeetwaarden op referentienivo niet meer representatief zijn voor datgene wat er op bladnivo gebeurt. Voor alle verdere verdampingsberekeningen is daarom alleen de via inversie berekende gewasweerstand gebruikt. Dat wil zeggen: een waarde berekend uit directe waarnemingen van verdamping en omgevingsfactoren via een gewasmodel.

De oppervlakteweerstand van de bodem van het tijgerbos is eveneens via omkering van een verdampingsmodel bepaald. Het bleek dat deze weerstand zeer sterk varieerde en een duidelijke functie was van het bodemvochtgehalte. Vlak na regenval werden waarden van rond de 100 s m^{-1} berekend. Deze waarden zijn vergelijkbaar of zelfs lager dan de oppervlakteweerstanden van de vegetaties. Als de regenval echter uitblijft, neemt de weerstand zeer snel toe tot waarden van om en nabij de 8000 m s^{-1} aan het einde van de IOP. De bodemverdamping speelt dan ook voornamelijk een rol in de natte tijd en dan alleen tot ongeveer drie dagen na regenval.

Gedurende de periode na de laatste regenval (20 september tot 9 oktober), waarvoor modelberekeningen zijn uitgevoerd in Hoofdstuk 8, bleek dan de savanne een hogere (inverse) bosjesweerstand had dan het tijgerbos. De meeste gemiddelden (8-16 GMT) varieerden tussen 200 en 600 s m^{-1} voor de savanne, en 100 en 300 m s^{-1} voor het tijgerbos. De overwegende groene savanne onderlaag, daarentegen, had weerstandswaarden tussen de 100- 300 s m^{-1}, terwijl de kale bodem van het tijgerbos waarden tussen de 2000 en 8000 s m^{-1} aan de dag legde. Dit leidde tot een lagere totale weerstand van de savanne. De waarden van de andere weerstanden, in combinatie met de beschikbare energie, zal de uiteindelijk verdamping bepalen.

In hoofdstuk 7 worden de resultaten van de CO_2-flux behandeld, zoals die zijn waargenomen voor de savanne. Ter vergelijking zijn ook enkele resultaten van de andere meetlocaties gepresenteerd. Wat betreft de dagelijkse gang, vertoonde de CO_2-flux waarden variërend van +5 ('s nachts) to -10 μmol m^{-2} s^{-1} ('s morgens). Deze piekwaarden (fluxen naar het oppervlak toe worden negatief genomen) namen snel af na de laatste regenbui, zodat aan het einde van de IOP nog slechts maximale waarden van -5 μmol m^{-2} s^{-1} werden gemeten. Bovendien werd deze piek op een eerder tijdstip (tussen 8 en 10 uur) waargenomen, in vergelijking tot de regentijd (tussen 10 en 11 uur). Zodoende namen dagtotalen van de CO_2-flux met 70 % af, terwijl de afname in verdamping rond de 50 % lag. Deze aanzienlijke afname van CO_2-flux werd hoogstwaarschijnlijk veroorzaakt door de gedeeltelijke sluiting van de huidmondjes, in verband met de lage luchtvochtigheid zoals beschreven in Hoofdstuk 6. Het is echter moeilijk dit te scheiden van het effect van afnemend bodemvochtgehalte, daar beide processen verbonden zijn. Op een half-uurlijkse basis bleek de CO_2-flux een niet-lineaire functie te zijn van fotosynthetisch actieve straling. Dit wordt waarschijnlijk veroorzaakt door het open karakter van de vegetaties en de hete omstandigheden. Voor een gesloten, goed van water voorziene vegetatie zal de respons vrijwel lineair zijn. De CO_2-flux bij lichtverzadiging nam duidelijk af naarmate de luchtvochtigheid afnam. De evenredige afname van hoge (< 2 kPa) naar lage (> 4 kPa) luchtvochtigheid is vergelijkbaar voor hoge en lage bodemvochtgehaltes, wat er op duidt dat veranderend bodemvocht de respons van de vegetatie op haar atmosferische omgevingsfactoren niet beïnvloedde. Dit kan echter het gevolg zijn van het feit dat bodemvocht slechts tot 50 cm diep gemeten is. Daggemiddelden van watergebruiksefficiëntie, de verhouding tussen de hoeveelheid verdampt water en de hoeveelheid opgenomen CO_2, namen eveneens af naarmate de droge tijd vorderde. Bovendien bleek dat ook deze grootheid een duidelijk verband met luchtvochtigheid vertoonde zowel op een dagelijkse als op een seizoensschaal. Deze relatie zou eventueel gebruikt kunnen worden om CO_2-fluxen te berekenen uit beschikbare metingen van verdamping en luchtvochtigheid (mits toegepast op dezelfde vegetatie). Verder blijkt dat de globale respons op de omgevingsfactoren, zoals waargenomen voor deze ingewikkelde mengeling van struiken, grassen, kruiden en kale bodem, zeer vergelijkbaar was met het gedrag van een monocultuur.

In Hoofdstuk 8 zijn enkele voorlopige modelsimulaties uitgevoerd. Hierbij is een vergelijking gemaakt tussen een viertal reeds bestaande twee-lagen verdampingsmodellen en twee modellen die hieruit zijn afgeleid. De twee laatstgenoemde modellen zijn samengesteld uit de beste onderdelen van de oorspronkelijke modellen, naar aanleiding van een voorstudie verricht boven een wijngaard. Bovendien is in één van beide een extra laag ingebouwd zodat de drie componenten van de savanne (struiken, ondergroei en bodem) apart beschreven kunnen worden. Allereerst zijn de berekende atmosferische weerstanden onderling vergeleken. De weerstand tussen de fictieve bronhoogte voor verdamping (en warmte transport) en de referentie hoogte bleek relatief laag als gevolg van de hoge ruwheidslengte van de vegetaties. De modellen voorspelden een waarde van ten hoogste 20 m s^{-1} (uit metingen bleek dat deze waarden nog aan de hoge kant waren). Verschillen tussen de savanne en het tijgerbos waren vrij klein. De weerstand binnen de gewaslaag, dus van het oppervlak tot de bronhoogte (de ruwheidslengte plus de verplaatsingshoogte) was aanzienlijk groter en vertoonde meer variatie tussen de modellen onderling en de twee vegetaties. Deze weerstand zal met name het transport van voelbare warmte van de savanne ondergroei of de tijgerbos bodem bepalen.Van belang voor deze weerstand zijn de ruwheidslengte en verplaatsingshoogte van de onderlaag, alsmede een factor die de uitdoving van het windprofiel binnen de vegetatie beschrijft. Voorspellingen varieerden tussen de 20 en 80 s m^{-1}. Met name één model (Deardorff, 1978) berekende een erg lage waarde voor deze weerstand. Via een gevoeligheidsstudie is tevens de invloed van bepaalde modelparameters getest.

Een gevoeligheidsanalyse met een versimpelde versie van het twee lagen model gebaseerd op het werk van Dolman (1993) en Huntingford et al. (1995) liet de volgende theoretisch mogelijk verschillen tussen savanne en tijgerbos zien. Het bleek dat vooral de oppervlakteweerstanden van belang waren. Indien de oppervlakteweerstanden van de savanne en tijgerbos onderlaag gelijk zijn en bovendien laag (100 m s^{-1}, dus vlak na regenval) zal het tijgerbos altijd meer verdampen (gemiddeld ongeveer 10 %). Dit komt dan voornamelijk doordat het tijgerbos meer energie beschikbaar heeft, vanwege het feit dat de netto straling hoger en de bodemwarmtestroomdichtheid lager is. Een verandering in de andere weerstanden zal het uiteindelijke verschilpercentage beïnvloeden, maar het tijgerbos zal altijd meer verdampen gedurende de natte tijd. Echter, zodra de bodem van het tijgerbos uitdroogt en de weerstanden toenemen tot 2000 s m^{-1}, terwijl de ondergroei van de savanne slechts waarden heeft van 200 s m^{-1}, zal de savanne aanzienlijk meer verdampen (gemiddeld 20 % meer). De hogere beschikbare energie voor het tijgerbos kan de hogere oppervlakteweerstanden niet compenseren. Een toename tot 6000 en 300 s m^{-1} voor respectievelijk tijgerbos en savanne, maakt de verschillen iets kleiner, maar de verdamping van de savanne is nog steeds hoger. De twee laatstgenoemde weerstandscombinaties zullen vooral optreden in de de overgangstijd van het natte naar het droge seizoen, waarin ook de laatste drie weken van de IOP zich bevonden. Echter, als de ondergroei verwelkt, zodat de weerstand waarden aanneemt van bijvoorbeeld 2000 s m^{-1}, en de bodem van het tijgerbos een weerstand heeft van 10000 s m^{-1}, dan zal het tijgerbos tot 40 % meer verdampen. Dit wordt veroorzaakt door een combinatie van een hogere vegetatie bedekkingsgraad en bladoppervlak. Zoals al bleek uit Hoofdstuk 5, zal het tijgerbos daarom door het jaar heen genomen een hogere verdamping hebben.

In de laatste paragraaf van Hoofdstuk 8 werd een schatting gemaakt van de jaarlijkse variatie in verdamping. Hiertoe werd het zgn. 'Evapoclimatonomy' model gebruikt, dat voornamelijk invoer van regenval en straling nodig heeft. Deze invoer werd verkregen uit een tien-jarige reeks meteorologische gegevens verzameld aan het ICRISAT, daar waar het SEBEX-experiment had plaatsgevonden. Niet gemeten grootheden, zoals bijvoorbeeld de albedo of de netto straling werden afgeleid uit andere gegevens m.b.v. de informatie verkregen uit het SEBEX-experiment. Zoals te verwachten was verdamping vooral een (lineaire) functie van regenval: in het zeer droge jaar 1984 (slechts 260 mm regen) werd een gemiddelde waarde van 0.75 mm per dag berekend, de hoogste verdamping werd waargenomen in de jaren 1986 en 1988 (tussen 600 en 700 mm regenval): over het jaar gemiddeld 1.8 mm dag^{-1}. De Bowenverhouding fluctueerde van 4.5 (1984) tot 0.7 (1988).

Summary

a) Background of the study

This study deals with the surface energy balance of Sahelian shrub vegetation. The energy balance describes how the radiative energy flux reaching the earth's surface is transferred into sensible, latent and soil heat fluxes. The energy budget of a vegetated surface is a key-equation in meteorological studies and it is linked to sciences such as hydrology, plant physiology or agronomy through its evaporation component.

In order to observe the energy balance for these two Sahelian vegetation-types, measurements were carried out during the Intensive Observation period (IOP, August-October 1992) of the HAPEX-Sahel (Hydrological and Atmospheric Pilot EXperiment in the Sahel) campaign. The Sahelian zone is characterized by one distinct wet season lasting three to six months and annual rainfall ranges between 200 and 700 mm. During the past two decades, the Sahel has been plagued by declining rainfall. Understanding the reasons for this decline and the need to estimate how the climate may change in the future was the motivation for starting this major international experiment. The 100 km HAPEX square (2 to 3 ° E and 13 to 14 ° N) contained three super-sites with sub-sites in each of the principal vegetation types: millet, fallow savannah, and tiger-bush (found on the laterite plateaux). An extra millet site was established in the north-west of the square. Most of the measurements used in this thesis were collected at the Central West Super-site (CWS) by the Department of Meteorology, Wageningen Agricultural University (WAUMET).

The vegetation included a fallow savannah, being part of a millet rotation system, and a natural open forest, which is locally called tiger-bush because of its striped pattern. Both vegetation-types can be characterized as sparse canopies, having a distinct upper- and understorey. In the case of the savannah, the canopy existed of randomly scattered *Guiera senegalensis* (*G. s.*) shrubs, which were interspersed by a combination of grasses, herbs and bare soil. The portion of shrubs compared to the understorey was approximately 15-20 %. The bushes at the WAUMET site were around 2.5 m high, whereas the grass/herb-layer exhibited a maximum height of 0.50 m. The tiger-bush vegetation strips consisted mainly of 4 m high *G.s.* bushes with some occasional trees. The height of the 20-40 m wide dense vegetation strips was around 4 m, with 40-60 m wide patches of bare, crusted soil in between.

The eddy covariance technique was used to measure the atmospheric fluxes of sensible and latent heat. This method was also used to determine the CO_2 flux in order to obtain a better insight in the physiological behaviour of this particular type of vegetation and to study the water use efficiency. Furthermore, an effort was made to distinguish between the contribution of the various components (i.e. bushes, undergrowth and bare soil) to the fluxes of the surface energy balance. Here we can refer to the partitioning of net radiation and soil heat flux, which together determine the energy available. In some cases the sensible and latent heat fluxes of the component surfaces were sampled, for example by sap flow, or lysimetry. In combination with these micrometeorological measurements the status of the vegetation was gauged by employing porometry, which yielded leaf conductances of the bushes and several species in the undergrowth. The theoretical background of these various techniques is given in Chapter 2.

The data give the values of energy fluxes during the wet season and the beginning of the dry season of 1992. Information on the annual variation of the energy balance was obtained by using the results of the SEBEX-campaign (Niger, 1988-1990) which concerned the same vegetation types (although located approximately 50 km south-west of the 1992 CWS). In this case only daily averages have been used. Chapter 3 presents the necessary information

on the HAPEX-Sahel and SEBEX measurement sites and the experimental set-up, the vegetation, and the governing climatological conditions.

The gathered data are primarily meant to supply reliable data to check the model parameterizations available today and used to describe the energy balance of vegetated surfaces in semi-arid regions. These models, describing the soil-water-atmosphere transfer (SVATs) are usually referred to as sparse canopy or two-layer models and they are also employed in Global Circulation Models (GCMs) used for climate (change) prediction. The present study also briefly investigates the characteristics and shortcomings of these models when used to describe Sahelian shrub vegetation. Chapter 4 summarizes the governing equations of four of these SVATs, together with other necessary model parameterizations.

b) Surface energy balance

In Chapter 5 the four fluxes of the energy balance are discussed. Each energy flux is approached from a diurnal (HAPEX-Sahel) and a seasonal or annual point of view (SEBEX). In addition, a comparison is made between the exchange of the savannah and tiger-bush. Also, where possible, the contributions of the different surface components (shrubs, undergrowth and bare soil) are considered.

Net radiation is decomposed into its four components: shortwave incoming, shortwave outgoing, longwave incoming and longwave outgoing radiation, which are studied separately. On clear days, shortwave incoming radiation reaches maximum diurnal values of around 1000 W m^{-2}. On cloudy days during the rainy period, instantaneous values are reduced by 50 % or more. On a seasonal basis, maximum values were observed during March and April when the sun was at its highest position and there were no clouds. Values range roughly from 175 to 300 W m^{-2}. The shortwave outgoing radiation, being determined by the surface property albedo, is smallest for the vegetated components of the savannah and tiger-bush. The scattered *Guiera senegalensis* bushes and the tiger-bush vegetation strips exhibit the lowest values, ranging between 0.17 and 0.20 when the sun is at its highest position. The savannah understorey has slightly higher values of albedo (up to 0.24), as a result of the presence of bare soil between the grasses and the herbs. For wet soil conditions, tiger-bush bare soil albedos are close to the understorey values. After the last rainfall, tiger-bush bare soil albedo steadily increases up to 0.30. If the values for the vegetation components are averaged according to their fractional coverage, area-averaged values during the SEBEX campaign range between 0.17 (wet season) and 0.25 (dry season) for the savannah. Average albedo values for the tiger-bush are generally higher, but show less variation (from 0.23 to 0.27), indicating that the tiger-bush vegetation stays relatively green during the dry season.

Longwave incoming radiation is a function of atmospheric emissivity and air temperature raised to the power four, following the adapted law of Stefan-Boltzmann. Diurnal and seasonal variation varies from 350 W m^{-2} to 450 Wm^{-2}. This is large compared to temperate climates. There appears to be a considerable discrepancy between calculated and measured values of atmospheric emissivity. The latter is found from direct measurements of longwave radiation and air temperature values. This may indicate that the widely used equations to calculate sky emissivity cannot be used under these tropical conditions. Longwave outgoing radiation depends on the surface emissivity and the surface temperature. The differences in surface temperature between the various components are relatively large: the savannah understorey was an average of 7 ° warmer than the bushes during day-time, while the soil was around 15 ° warmer. Similar differences are found for the daily averages of the SEBEX experiment. Area-averages of surface temperatures vary from 25 ° during the winter months to 45 ° at the beginning of the wet period. Differences between savannah and tiger-bush are very small because the tiger-bush had a higher fractional coverage of cool bushes (33 % compared to 20 %) which counteracts the relatively high temperatures of the bare soil. With a surface emissivity of 0.98 for the bushes and of 0.95 for the bare soil and savannah understorey, diurnal values of longwave outgoing radiation vary between 450 W m^{-2} (at night) and 600 W m^{-2} (daytime, savannah understorey at the end of the IOP). The variation of daily averages through the seasons of 1989 and 1990 is comparable: from 425 during January until March to 550 W m^{-2} in June and July. These values refer to area averages of savannah and tiger-bush.

On a seasonal basis, all radiation components vary by 20 to 30 %. However, net radiation appears to fluctuate with nearly 60 % (from 75 W m^{-2} around December to 175 W m^{-2} during August and September) because the seasonal maxima and minima of the incoming and outgoing radiation terms do not occur concurrently. Net radiation for tiger-bush is on average 5 % higher than the values observed for savannah. A similar difference is found for the HAPEX-Sahel experiment. This pronounced course has implications for the available energy and hence for the values of sensible and latent heat fluxes.

Together with the net radiation, the soil heat flux determines the energy which is available for the sensible and latent heat flux. The soil heat flux is largely determined by the thermal properties comprising of bulk soil heat capacity, thermal conductivity and thermal diffusivity. It appears that wet season values of thermal conductivity and thermal diffusivity are relatively large compared to results reported in the literature. This may have been caused by termite activity, resulting in a coherent soil and thus a high conductivity. Thermal diffusivity attains peak values of around 2.0 mm^2 s^{-1} in the rainy period. At the same time, thermal conductivity is around 2.0 W m^{-1} K^{-1}, which is also quite high compared to the values given in the literature. It appeared that during the three weeks after the last rainfall, top-soil thermal properties already reached their dry-season values, which is an illustration of the high evaporation rates of this region. Dry-period values of thermal diffusivity are around 0.3 mm s^{-1}, while thermal conductivity reaches values of 0.25 W $m^{-1}K^{-1}$. Soil heat flux accounts for a large part of net radiation: around noon it consumes 30 to 40 % of net radiation. Averaged over a day, this portion is less (10-15 %). The soil heat flux below the bushes (noon values around 50 W m^{-2}) is considerably less than below the exposed soil (noon values 250 W m^{-2}). These values are very similar for the savannah and the tiger-bush. This causes the average values of tiger-bush soil heat flux to be somewhat smaller than values measured for the savannah, because of the higher fractional bush coverage of the tiger-bush. In combination with higher values of net radiation, this leads to around 10 % more available energy for the tiger-bush.

Peak (noon) values of around 450 W m^{-2} for the evaporation were observed during the rainy period for days just after rainfall. These high values were partly caused by a large contribution of soil evaporation (around 20 % for the savannah up to 50 % for the tiger-bush). During these days, sensible heat flux reached values of 100 W m^{-2} at the most. After the last rainfall event peak values of evaporation decreased to 300 W m^{-2}. This is partly caused by the reduced soil evaporation (only 5 % of the total savannah evaporation and ≈ 10 % for the tiger-bush, but also because the vegetation components had started to dry out. It appeared that the *G.s* shrubs of the savannah account for 20 to 30 % of total evaporation in the rainy period and for 35 % at the end of the IOP. The contribution of the tiger-bush vegetation strips is larger: ≈ 60 % during days just after rainfall and nearly 100 % when the soil patches are relatively dry. The leaf area of the tiger-bush vegetation strips was estimated to be around three times greater than the leaf area of the savannah, which explains the difference. After the last rainfall, savannah evaporation soon became higher than the evaporation from the tiger-bush. The higher values of available energy observed for the tiger-bush were mainly spent on a higher sensible heat flux. This resulted in a Bowen ratio (the ratio of sensible to latent heat flux) of around 1 for tiger-bush, whereas for the savannah values of close to 0.3 were attained. By the end of the IOP, maximum values of latent heat fluxes were 250 W m^{-2} for savannah and 200 W m^{-2} for tiger-bush. Average savannah evaporation ranged from 3-4 mm day^{-1} (1 W $m^{-2} \approx$ 0.03 mm) during the wet period and up to one week after the last rainfall. Its values had already decreased to 2 mm at the end of the IOP. For tiger-bush evaporation decreased from around 5 mm day^{-1} during the rainy period to 2 to 3 day^{-1} mm at the beginning of October.

With the SEBEX data insight into the seasonal course of the sensible and latent heat fluxes is obtained even though no data were available between December 1989 and May 1990. Daily averages of measured evaporation vary from about 130 W m^{-2} ($\approx$ 4 mm day^{-1}) to 10 W m^{-2} ($\approx$ 0.3 mm day^{-1}) for the savannah. Minimum values were attained around the middle of November, which shows that the vegetation (probably mainly the understorey) was already close to wilting. Evaporation at the beginning of the 1990 dry season was practically zero. The sensible heat flux during 1989 rapidly increased from around 10 to 20 W m^{-2} in October to 100 W m^{-2} in December. Pre-humid values of 1990 were also around 100 W m^{-2}. During the first week of October in 1989, both surfaces still received 22 mm rainfall. Nevertheless, the data show that the evaporation of tiger-bush (100 W m^{-2}) was less than savannah, which is unlike the observations made during HAPEX-Sahel. However, the savannah understorey of 1989 was dense compared to 1992. By the end of October, savannah evaporation fell below that of the tiger-bush ($\pm$ 50 W m^{-2}): in less than one month the evaporation of the savannah has been reduced to only 10 % of its wet season value. Tiger-bush evaporation continued until at least half December (end of eddy covariance measurements). By calculating the sensible heat flux from surface and air temperature and subtracting this from available energy, a possible course of evaporation is constructed. The results indicate that tiger-bush possibly continues to evaporate during most of the dry season, although at a low rate. The Bowen ration for the savannah varied between 0.1 during the wet season of 1989 to around 10 by the end of 1989 and June 1990. The Bowen ratio of tiger-bush was usually around 1, except in the pre-humid period of 1990 when values of about 10 were also reached.

c) The resistance network

Most SVATs include a number of resistances, which are usually defined as the ratio of a vertical difference of a scalar (e.g. specific humidity) and the flux density related to that scalar (e.g. evaporation). Chapter 6 describes the main components and parameters of the resistance network. First the roughness length and the displacement height are treated, since together they determine the aerodynamic resistance. The aerodynamic resistance is the resistance between the mean canopy source height and the reference (measurement) height and it is needed in all canopy exchange models. The roughness parameters calculated for the savannah and the tiger-bush are compared to values found in the literature for similar bush-like vegetation. Besides values previously found for savannah and tiger-bush, several row crops were selected comprising of vineyards, cotton canopies and orchards. Although savannahs usually have a scattered nature, tiger-bush can be considered to be a transition between a row crop and a randomly scattered crop, which explains the selection. It is tested whether the roughness parameters of this selected set of sparse canopies are distinctively different from the values found for relatively closed canopies. The roughness parameters of closed canopies can usually be satisfactorily described by a simple, linear relationship of height. The quality of the eleven vegetation studies is scrutinized using three criteria: fetch, homogeneity of the experimental site and the measurement height of wind speed. It appeared that all 'good' canopies are mainly dependent on their roughness density (Raupach, 1992), which is a function of the height, breadth and the spacing between the main canopy elements. In these eleven studies, displacement height varies between 35 and 80 % of canopy height, whereas ratios of roughness length and height range from 0.05 to 0.18. The lowest ratios are generally found for vegetation exhibiting the lowest roughness density, which ranged from 0.03 to 0.6. These measured values appeared to compare well with drag partition theory given by Raupach, although the best model parameters deviate from the values suggested by Raupach. The rules of thumb employing a linear function of height, which were also tested, performed worse.

Next, the roughness length for heat is discussed, a crucial parameter, which together with the roughness parameters for momentum determines the resistance for heat transfer in a single-layer bulk transfer model. This approach is used mainly in large-scale models (GCMs) and remote sensing applications. For most vegetated surfaces, its value is much smaller than the roughness length for momentum, underlining the excess resistance for heat transfer compared to momentum exchange. Usually, this excess resistance is expressed as the natural logarithm of the ratio between roughness length for momentum and heat. It was found that the still widely quoted value of 2 is far too small. This is also mentioned in recent literature on the subject. The roughness length of heat appeared to be roughly 150000 times smaller, i.e. in the order of thousands of mm, for the sparse vegetation investigated in this thesis. It was suggested that the advised value of the excess resistance be raised to 7 for sparse canopies. Furthermore, the performance of several semi-empirical equations were tested to calculate the excess resistance. Three simple and established formulae (Sheppard, 1958; Owen and Thomson, 1968; Brutsaert, 1975b), which are all based on a simple combination of Reynolds and Prandtl dimensionless numbers, performed best.

In § 6.3 the leaf and 'bottom-up' canopy conductance were studied by using porometry data and several simple conductance models. Leaf conductance of the *Guiera senegalensis* bushes showed one distinctive peak between 8 and 11 GMT, with average maximum values of around 15 mm s^{-1} during the rainy period. With increasing atmospheric demand and diminishing soil moisture content, this peak decreased to 10 mm s^{-1} for the dry period. At the same time the afternoon values were also considerably lower. At the end of the IOP, the peak occurred earlier during the day. This led to a decrease in the average daytime conductance values of around 60 %, which is mainly related to the decreased atmospheric vapour deficit and concurrent changes of the soil moisture content. Leaf conductance of two undergrowth herb species, having values which were roughly twofold the *G. s.* values, exhibit a less recognizable pattern during the day, although highest values are again observed during the morning. Two semi-empirical models (Huntingford et al., 1995; Hanan and Prince, 1996) and one mechanistic (Jacobs, 1994) leaf conductance model were fitted to the *Guiera senegalensis* and herb species data. The best fits were obtained for the bushes (around 60 % of the variation explained) which, as expected, showed a large dependence on atmospheric vapour pressure deficit. Only 40 % of the variation at most could be explained for the two herb species. In these cases, soil moisture appears to be an indispensable independent variable, which is plausible, bearing in mind the relatively shallow root zone (< 0.5 m) of the understorey species. In addition, the mechanistic approach, involving parameters with actual plant physiological meaning, does not ensure a better fit. However, this models is physically more sound and it has the ability to simulate feedback mechanisms in Planetary Boundary Models, for example. In Section 6.3.3 it is found that upscaled canopy conductances (bushes, understorey and the total savannah vegetation) do not compare very well with the so-called 'top-down' values, which are obtained from inverting a single (Penman-Monteith) or two-layer canopy model. This phenomenon has often been observed for (sparse) canopies, but in this particular case the discrepancy appears to be very large: bottom-up values being two to six times larger than top-down values. A consequence of this discrepancy is a serious overestimation of evaporation by any resistance-based canopy model if the 'bottom-up' values were to be used. A possible explanation for the large difference could be the fact that the main source of evaporation is close to the ground, instead of at the top of the vegetation, where the majority of the momentum exchange occurs. This assumption is indirectly supported by the fact that 'top-down' leaf conductances of the tiger-bush, with the main source of evaporation generally at bush level, are much closer to the 'bottom-up' values. Furthermore, the bushes seem to be highly decoupled from the atmosphere. This causes a very large gradient in vapour pressure deficit, making the reference level values used in the Penman-Monteith type equations non-representative. Therefore, the model simulations of Chapter 8 are performed with 'top-down' values only.

Tiger-bush soil surface resistance, studied in § 6.4, has been derived from inverting a two-layer model with separate values of soil and total evaporation as input. Values appear to be highly variable, ranging from 100 s m^{-1} several hours after rain, to 8000 s m^{-1} at the end of the IOP. Therefore, soil evaporation only plays a major role in the rainy period, and only until about three days after the last rainfall. Soil surface resistance values are highly correlated with soil moisture and the soil Bowen ratio coefficient discussed in Chapter 5, which offers potential for simple and reliable determination of soil surface resistances and thus soil evaporation.

During the period after the last rainfall (days 264-282), for which model calculations were performed in Chapter 8, the savannah appeared to have higher ('top-down') bush canopy resistances than the tiger-bush, most averages (8 to 16 GMT) ranging between 200 and 600 s m^{-1}, and 100 and 300 m s^{-1} respectively . However, its predominantly green understorey yielded much lower resistances (100- 300 s m^{-1}) compared to values derived for the bare soil of the tiger-bush (2000-8000). This caused the total surface resistance of the savannah to be lower. The values of the other resistances, in combination with the available energy will determine the final amount of evaporation lost from both vegetation-types.

d) CO_2 fluxes

Chapter 7 presents the results of the CO_2 fluxes observed for the CWS savannah site. Where possible, the interrelationship between the CO_2 flux, evaporation and average leaf conductance was given. To place the data in perspective, some results found at the other super-sites were also presented. Diurnal values of CO_2 flux varied between + 5 (night-time) and -10 μmol m^{-2} s^{-1} (day-time peak value, as fluxes towards the surface are negative). Peak values rapidly decline as the dry-down proceeds, leading to values of around -5 observed by the end of the IOP. These lower peaks are observed earlier in the day compared to the rainy period. Daily totals of CO_2 flux diminished by 70 % in a period of three weeks after the last rainfall, while the decrease in evapotranspiration was around 50 %. The observed decrease in atmospheric CO_2 flux during the IOP is most likely to be caused by stomatal closure in response to high vapour pressure deficit, as shown in Chapter 6. However, it is very difficult to separate this from the effect of declining soil moisture, as soil moisture was highly correlated with atmospheric humidity. Canopy photosynthesis on a half-hourly basis, appears to be a non-linear function of Q_p. This is probably caused by the sparse character of the canopy and harsh environmental conditions. For a closed, well-watered canopy the response would be almost linear (Baldocchi, 1994). F_c at light saturation (from the light response curve) clearly decreases with increasing values of D. The proportional decrease from high (< 2 kPa) to low (> 4 kPa) atmospheric humidity is similar for wet and dry soil conditions, which implies that changing soil moisture content did not influence the response of the vegetation to the controlling atmospheric parameters. However, this may be a result of the rather shallow depth over which soil moisture was measured.

Daily averages of water use efficiency decreased after the last rainfall but showed a recovery during periods of low temperature and humidity. Daily integrals and half-hourly values of water use efficiency appeared to be a strong function of vapour pressure deficit. Together with high atmospheric demand, increased soil moisture stress decreases values of CO_2 flux and water use efficiency. However, soil moisture has little effect on the empirical relationships found between environmental variables and CO_2 flux. Although the savannah consists of a complex mixture of several C_3 and C_4 species, the overall response to environmental variables shows a behaviour which is very similar to single-species crops.

e) Model calculations

In Chapter 8 several preliminary analyses and runs are performed with the SVAT models presented in Chapter 4, i.e. the model of Shuttleworth and Wallace (1985: SW), Choudhury and Monteith (1988: CM), Deardorff (1978: DD) and the two-layer model as developed by Dolman (1993) and Huntingford et al, 1995: TL). In addition to these existing, generally well established models, two new models are derived, based mainly on the material of DD (prognostic solution of the energy balance and soil heat flux) and CM (aerodynamic resistances). They were called DCM (Dual Component Model) and TCM (Triple Component model; see also Van den Berg, 1995a and b).

First, the resistances as calculated according to the various model parameterizations for the savannah and tiger-bush are compared. Aerodynamic resistances were relatively low (20 s m^{-1}, which compared to measurements appears to be quite high) as a result of the high roughness lengths of the vegetation. Largest differences among the models and the two vegetation-types are found for the in-canopy aerodynamic resistance representing the understorey. This resistance will mainly determine the flux of sensible heat from the understories and its value is governed by the roughness parameters of the understorey and an extinction coefficient for the wind profile within the vegetation. Predictions vary between 20 and 80 s m^{-1}. The DD model especially produces very low values.

A sensitivity study with a simplified version of the TL model shows some theoretically possible differences between savannah and tiger-bush. It appeared that the understorey resistances are especially important. If these resistances are the same and low (100 s m^{-1}, so just after rainfall), tiger-bush will always evaporate more (10 % on average) than the savannah, even when the other resistances are varied within their normal range. This is mainly caused by the higher available energy of tiger-bush. However, as soon as the tiger-bush soil dries and its resistance increases to 2000 s m^{-1}, while the savannah understorey exhibits values of only 200 s m^{-1}, the savannah will have a higher latent heat flux (20 % more on average). The higher available energy of the tiger-bush cannot compensate the higher resistances. An increase to 6000 and 300 s m^{-1} for tiger-bush and savannah, respectively, decreases the evaporation differences between both vegetation-types, but savannah evaporation is still higher. These two resistance combinations will mainly occur during the transition period between the wet and the dry season, which also include the last three weeks of the IOP. However, when the understorey is wilting, leading to surface resistances of e.g. 2000 s m^{-1}, the tiger-bush will evaporate up to 40 % more. This is mainly the result of the combination of a higher fraction of bush coverage and thus leaf area. As already pointed out in Chapter 4, the tiger-bush will probably have a higher evaporation throughout the year.

A comparison between the various SVATs reveals the following. When measured R_n is needed (SW and CM), proper values of $R_{n,u}$ and $R_{n,s}$ for these sparse canopies can be obtained by setting the radiation extinction coefficient to a value around 0.5 (here 0.45), instead of the usually applied value of 0.7, which is valid for relatively closed canopies only. If no soil model is available, G can be sufficiently well parameterized by multiplying R_n with a certain factor (between 0.20 to 0.30). This works better than applying an extended soil model without heat storage. A reliable parameterization of $r_a{}^s$ is indispensable for proper estimates of sensible heat flux, and thus evaporation. The savannah vegetation consisting of three components can not be described properly by a two-component model, unless the undergrowth and soil are combined to a single understorey component, which is possible in the SW and TL case. A three-component solution, treating the bushes, undergrowth and soil separately works very satisfactorily, but would be too elaborate for use in a GCM. It can be concluded that the relatively simple approach of SW, provided the upper-and understorey resistances are parameterized properly, is adequate enough to perform the surface description in a large-scale model.

In the last section of Chapter 8 an estimate is made of the interannual variation of the evaporation. Here, we employ the evapoclimatonomy model (Nicholson and Lare, 1990), which predominantly requires input of rainfall and radiation. This input was obtained from a 10-years meteorological data set that originated from the ICRISAT Sahelian Centre, where the SEBEX experiment had taken place. Values of albedo and net radiation, for example, are derived from other data through insights obtained by the variation observed during SEBEX. Annual evaporation appears to be mainly a function of rainfall: during 1984 (only 260 mm rainfall) an average daily value of 0.75 mm was calculated, whereas the highest evaporation is found for 1986 and 1988 (between 600 and 700 mm rainfall). The annual mean of the Bowen ratio fluctuates between 4.5 (1984) and 0.7 (1988).

References

Al Nakshabandi, G., and Kohnke, H.,1965. Thermal conductivity and diffusivity of soils as related to moisture tension and other physical properties. Agric. For. Meteorol., 2: 271 - 279.

Allen, S.J., Wallace, J.S., Gash, J.H.C., and Sivakumar, M.V.K, 1994. Measurements of albedo variation over natural vegetation in the Sahel. Int. J. of Clim., 14: 625-636.

Allen, S.J., 1990. Measurement and estimation of evaporation from soil under sparse barley crops in northern Syria. Agric. Forest Meteorol., 49, 291 - 309.

Allen, S.J., and Grime, V.L., 1995. Measurements of transpiration from savannah shrubs using sapflow gauges. Agric. For. Meteorol., 75: 23-41.

André, J-C., Goutorbe, J.-P. and Perier, A., 1986. HAPEX-MOBILHY: A Hydrologic Atmosphere EXperiment for the study of water budget and evaporation flux at the climatic scale, Bull. Am. Meteorol. Soc., 67: 138-144.

Arya, S.P.S., 1975. A drag partition theory for determining the large-scale roughness parameter and wind stress on the Artic pack ice. J. Geophys. Res. 80: 3447-3454.

Atzema, A.J., 1994. From the weather forecast to the prognostic moisture content of dry agricultural crops. PhD thesis, Agricultural University Wageningen, the Netherlands, 101 pp. ISBN, 90-5485-235-6.

Baker, J.M., and Van Bavel, C.H.M., 1987. Measurement of mass flow of water in the stems of herbaceous plants. Plant Cell Environ., 10: 777-782.

Baldocchi D., 1994. A comparative study of mass and energy exchange over a closed C_3 (wheat) and an open C_4 (corn) crop: II. CO_2 exchange and water use efficiency. Agric. For. Meteorol., 67: 291-321.

Baldocchi, D., Verma, S.B. and N.J. Rosenberg, 1985. Water use efficiency in a soybean field: influence of plant water stress. Agric. For. Meteorol., 34: 53-65.

Baldocchi, D.D., Luxmoore, R.J., and Hatfield, J.L., 1991. Discerning the forest from the trees: an essay on scaling canopy stomatal conductance. Agric. For. Meteorol., 54: 197-226.

Baldocchi, D.D., and Meyers, T.P., 1988. Turbulence structure in a deciduous forest. Boundary-Layer Meteorol., 43: 345-364.

Begue, A., Roujean, J.-L., Hanan, N.P., Prince, S.D., Thawley,M., Huete, A., and Tanré, D., 1995. Shortwave radiation budget in Sahelian vegetation during HAPEX-Sahel. 1. Techniques of measurement result. Agric. For. Meteorol. (in press).

Beljaars, A.C.M., and Holtslag, A.A.M., 1991. Flux parameterization over land surfaces for atmospheric models. J. Appl. Meteorol., 30: 327-341.

Bierhuizen, J.F. and Slatyer, R.O., 1965. Effects of atmospheric concentration of water vapour and CO_2 in determining transpiration photosynthesis relationships of cotton leaves. Agric. For. Meteorol., 2: 259-270.

Bhumralkar, C.M., 1975. Numerical experiments on the computation of ground surface temperature in an general circulation model. J. Appl. Meteorol., 14: 1246-1258.

Black, T.A., Gardner, W.R., and Thurtell, G.W., 1969. The prediction of evaporation, drainage and soil water storage for a bare soil. Soil Sci. Soc. Am. J., 33: 655-660.

Blackadar, A.K., 1976. Modelling the nocturnal boundary layer. In: Proceedings of the third Symposium on Atmospheric Turbulence, Diffusion and Air Quality; American Meteorological Society, Boston, U.S.A.

Blyth, E.M., 1995. Using a simple SVAT scheme to describe the effect of scale on aggregation. Boundary-Layer Meteorology 72: 267-285.

Blyth, E.M., Dolman, A.J., and Wood, N., 1993. Effective resistance to sensible- and latent-heat flux in heterogeneous terrain. Q.J.R. Meteorol. Soc. 119: 423-442.

Blyth, E.M., and Dolman, A.J., 1995. The roughness length for heat of sparse vegetation. Am. Bull. Meteorol. Soc. (accepted).

Blyth, E.M., and Harding, R.J., 1995. Application of aggregation models to surface heat flux from the Sahelian tiger bush. Agric. For. Meteorol., 72: 213-235.

Farquhar, G.D., Von Caemmerer, S., and Berry, J., 1980. A biochemical model of photosynthetic assimilation in leaves of C_3-species. Planta 149: 78-90.

Feddes, R.A., 1971. Water, heat and crop growth. PhD thesis, Wageningen, Agricultural University, The Netherlands.

Feddes, R.A., Kowalik, P.J., and Zaradny, H., 1978. Simulation of field water use and crop yield. PUDOC, Wageningen, the Netherlands.

Finnigan, J.J., and Raupach, M.R., 1987. Modern theory of transfer in plant canopies in relation to stomatal characteristics. In: E. Zeiger, G.D. Farquhar and I.R. Cowan (Eds.), Stomatal Function. Stanford University Press, Stanford, California, 385-429 pp.

Fisher, M.J., Rao, I.M., Ayarza, M.A., Lascano, C.E., Sanz, J.I., Thomas, R.J. and Vera, R.R., 1994. Carbon storage by introduced deep-rooted grasses in the South american savannas. Nature, 371: 236-238.

Friend, A.D and Cox, P.M. (1995). Modelling the effects of atmospheric CO_2 on vegetation-atmosphere interactions. Agric. Forest Meteorol., 73: 285-295.

Frère, M., and Popov, G.S., 1979. Agrometeorological crop monitoring and forecasting. Plant Production and Protection Paper 17, FAO, Rome.

Fuchs, M., and Tanner, C.B., 1966. Infrared thermometry of vegetation. Agronomy J., 58: 596-601.

Fuchs, M., and Tanner, C.B., 1967. Evaporation from a drying soil. J. Appl. Meteorol., 6: 852-857.

Garratt, J.R., 1978. Transfer characteristics for a heterogeneous surface of large aerodynamic roughness. Q.J.R. Meteorol. Soc., 104: 491-502.

Garratt, J.R., 1980. Surface influence upon vertical profiles in the atmospheric near-surface layer. Q.J.R. Meteorol. Soc., 106: 803-819.

Garratt, J.R., 1992. The atmospheric boundary layer. Cambridge atmospheric and space science series. Cambridge University Press, 316 pp.

Garratt, J.R., and Hicks, B.B., 1973. Momentum, heat and water vapour transfer to and from natural and artificial surfaces. Q.J.R. Meterol. Soc., 99: 680-687.

Gash, J.H.C., 1986. A note on estimating the effect of a limited fetch on micrometeorological evaporation measurements. Q.J.R. Meterol. Soc., 35: 409-413.

Gash, J.H.C., Wallace, J.S., Lloyd, C.R., Dolman, A.J., Sivakumar, M.V.K., and Renard, C., 1991. Measurements of evaporation from fallow Sahelian savannah at the start of the dry season. Q.J.R. Meteorol. Soc., 117: 749-760.

Gash, J.H.C., Kabat, P., Monteny, B.A., Amadou, M., Bessemoulin, P., Billing, H., Blyth, E.M., De Bruin, H.A.R., Elbers, J.A., Friborg, T., Harrison, G., Holwill, C.J., Lloyd, C.R., Lhomme, H-P., Moncrieff, J.B., Puech, D., Søgaard, H., Taupin, J.D., Tuzet, A., and Verhoef, A., 1996. The variability of evaporation during the HAPEX-Sahel Intensive Observation Period. Journal of Hydrology , special issue HAPEX-Sahel (submitted).

Gates, D. M., 1980. Biophsical ecology. Springer-Verlag, New York, 611 pp.

Gifford, R.M., 1994. The global carbon cycle: a viewpoint on the missing sink. Aust. J. Plant Physiol., 21: 1-15.

Goldstein, S., 1938. Modern developments in fluid dynamics, Oxford University Press.

Goudriaan, 1977. Crop micrometeorology: a simulation study. PUDOC, Wageningen, the Netherlands, 249 pp.

Goudriaan, J., 1982. Potential production processes. In: F.W.T. Penning de Vries and H.H. van Laar (Editors): Simulation of plant growth and crop production. Simulation Monographs. Pudoc, Wageningen, pp. 98-113.

Goudriaan, J., Van Laar, H.H., Van Keulen, H. and Louwerse, W., 1985. Photosynthesis, CO_2 and plant production. In: W. Day and R.K. Atkin (Editors), Wheat growth and modelling. NATO ASI Series, Series A, Vol 86. Plenum Press, New York, 107-122.

Goutorbe, J-P., Lebel., T., Tinga, A., Bessemoulin, P., Brouwer, J., Dolman, A.J., Engman, E.T., Gash, J.H.C., Hoepffner, M., Kabat, P., Kerr, Y.H., Monteny, B., Prince,S., Said, F., Sellers, P. and Wallace, J.S., 1994. HAPEX-Sahel: a large scale study of land atmosphere interactions in the semi-arid tropics. Annales Geophysicae 12: 53-64.

Graser, E.A., Verma, S.B., and Rosenberg, N.J., 1987. Within-canopy temperature patterns of sorghum at two row spacings. Agric. For. Meteorol., 41: 187-205.

Hall, A.E., Canell, G.H., and Lawton, H.W., 1979. Agriculture in semi-arid environments, Springer-Verlag Berlin Heidelberg New York, 340 pp.

Ham, J.M, and Heilman, J.L, 1991. Aerodynamic and surface resistances affecting energy transport in a sparse crop. Agric. For. Meteorol., 53: 267-284.

Hanan, N.P, and Prince, S.D., 1996. Stomatal conductance of West Central Supersite vegetation in HAPEX-Sahel: measurements and empirical models. Journal of Hydrology, HAPEX-Sahel special issue (submitted).

Haneghem, I.A. van, 1981. Een niet stationaire naaldmethode (warmtegeleiding, warmtecapaciteit, contactweerstand). Dissertation Dept. of Physics, Wageningen Agricultural University, 187 pp.

Hare, F.K, and Ogallo, L.A.J., 1993. Climate variations, drought and desertification. WMO Publication 653.

Hatfield, J.L., 1989. Aerodynamic properties of partial canopies, Agric. Forest Meteorol. 46 :15-22.

Hatfield, J.L., Wanjura, D.F., and Barker, G.L.,1985. Canopy temperature response to water stress under partial canopy. Trans. ASAE, 28: 1607-1611.

Heathcote, R.L., 1983. The Arid Lands: their use and abuse. Longman Inc., New york, 323 pp.

Heusinkveld, B.G., de Bruin, H.A.R., Verhoef, A., Antonysen, F., and Hillen, W.C.A.M., 1994. Procedures for reliable eddy covariance measurements of atmospheric heat and CO_2-fluxes. In: WMO, Instruments and observing methods, Report No. 57.

Hewer, F., 1993. A roughness length for temperature. Met O (APR) Turbulence and Diffusion Note No. 208, Bracknell, England, 35 pp.

Hicks, B.B., 1973. Eddy fluxes over a vineyard. Agric. Forest Meteorol. 12: 203-215.

Hipps, L.E., 1989. The infra-red emissivities of soil and Artemisia tridentata and subsequent temperature corrections in a shrub-steppe ecosysten. Remote Sens. Environ., b: 337-342.

Hodges, T. and Kanemasu, E.T., 1977. Modelling daily dry matter production of winter wheat. Agron. J., 69: 974-978.

Holtslag, A.M.M., and Beljaars, A.C.M., 1988. Surface flux parametrization schemes: developments and experiences at K.N.M.I. Scientific Report K.N.M.I. WR-NR88.06.

Horton, R., 1982. Determination and use of soil thermal properties near the surface. PhD-dissertation. New Mexico State University, Las Cruces, New Mexico, USA, 132 p.

Horton, R., Wierenga, P.J., and Nielsen, D.R., 1983. Evaluation of methods for determining the apparent thermal diffusivity of soil near the surface. Soil Sci. Soc. Am. J. 47: 25-32.

Huband, N.D.S., and Monteith, J.L. 1986, part II.

Humes, K.S., Kustas, W.P, Moran, M.S., Nichols, W.D., and Weltz, M.A., 1994 Variability of emissivity and surface temperature over a sparsely vegetated surface. Water Resour. Res. 30: 1299-1310.

Huntingford, C., Allen, S.J. and Harding, R.J., 1995. An intercomparison of single and dual-source vegetation-atmosphere transfer models applied to transpiration from Sahelian savannah. Boundary-Layer Meteorology 74: 397-418.

ICIHI, 1986. The encroaching desert: the consequences of human failure: a report for the Independent Commission on International Humanitarian Issues, Zed Books Ltd, London, 132 pp.

Idso, S.B., and R.D., Jackson, 1969. Thermal radiation from the atmosphere. J. Geophys. Res., 74: 5397-5403.

Idso, S.B., Aase, J.K., Jackson, R.D., 1975. Net radiation-soil heat flux relations as influenced by soil water content variations. Boundary-Layer Meteorology 9: 113-122.

Jacobs, A.F.G., and Van Boxel, J.H., 1988. Changes of the displacement height and roughness length of maize during a growing season. Agric. For. Meteorol., 42: 53-62.

Jacobs, A.F.G., Van Boxel, J.H., and El-Kilani, R.M.M., 1988. Nighttime free convection characteristics within a plant canopy. Boundary-Layer Meteorol., 62: 375-387.

Jacobs, A.F.G., and Verhoef, A., 1996. Soil evaporation from a sparse natural vegetation estimated from Sherwood numbers. Journal of Hydrology , HAPEX-Sahel special issue (accepted).

Jacobs, C.M.J., 1994. Direct impact of atmospheric CO_2 enrichment on regional transpiration. PhD thesis, Agricultural University Wageningen, the Netherlands, 179 pp., ISBN, 90-5485-250-X.

Jacobs, C.M.J., De Bruin, H.A.R., and Verhoef, A., 1991. The effects of surface inhomogeneities on the surface fluxes and on the development of the planetary boundary layer. Ann. Geophys., 9: 510-520.

Jacobs, C.M.J., and De Bruin, H.A.R., 1992. The sensitivity of regional transpiration to land-surface characteristics. J. of Clim., 5: 683-698.

Jacobsen, T.F., 1995. The use of carbon fluxes in climatology. PhD-thesis, Institute of Geography, Copenhagen University, Denmark.

Jacquemin, N., and Noilhan, J., 1990. Sensitivity study and validation of a land surface parameterization using a HAPEX-MOBILHY data set. Boundary-Layer Meteorology 52: 93-134.

Jakob, M., 1950. Heat transfer. John Wiley and Sons, New York, 758 pp.

Jarvis, P.G., 1976. The interpretation of the variations in leaf water potential and stomatal conductance found in canopies in the field. Phil. Trans. R. Soc. Lond., Ser. B., 273: 593-610.

Jarvis, P.G., 1986. Coupling of carbon and water interactions in forest stands. Tree Physiology, 2: 347-368.

Jarvis, P.G., and McNaughton, K.G., 1986. Stomatal control of transpiration: Scaling up from leaf to region. Advances in ecological research, 15: 1-49.

Jensen, M.E., Burman, R.D., and Allen, R.G., 1990. Evapotranspiration and irrigation water requirements. ASCE Manuals and Reports on Engineering Practice No. 70, 332 pp.

Jensen, N.O., Hummelshøj, 1994. Derivation of canopy resistance for water vapour fluxes over a spruce forest, using a new technique for the viscous sublayer resistance. Agric. For. Meteorol. (submitted).

Jones, H.G., 1983. Plants and Microclimate. Cambridge University Press. Cambridge, 323 pp.

Kabat, P., and Elbers, J.A., 1994. HAPEX-Sahel: Selected results of the Special Observation Period 1992. Contribution to the 1 st Annual Report. Contract #2 (CT90-0030). Interne Mededeling 296, Januari, 1994, SC-DLO, Wageningen, The Netherlands.

Katerji, N. and Perier, A., 1985. Determination of canopy resistance to water vapour and its various components: theoretical approach and experimental verification. Agric. For. Meteorol., 34:105-120.

Kerr, Y.H., Assad, E., Freleaud, J.P, Lagouarde, J.P., and Seguin, B., 1987. Estimation of evapotranspiration in the Sahelian zone by use of METEOSAT and NOAA AVHRR data. Adv. Space Res., 7: 161-164.

Kessler, J.J., and H. Breman, 1991. The potential of agroforestry to increase primary production in the Sahelian and Sudanian zones of West Africa. Agroforestry Systems 13: 41-62.

Kim, J. and Verma, S.B., 1990. Carbon dioxide exchange in a temperate grassland ecosystem. Boundary-Layer Meteorol. 52: 139-149.

Kim, J. and Verma, S.B., 1991. Modelling canopy stomatal conductance in a temperate grassland ecosystem. Agric. For. Meteorol., 55:149-166.

Kimball, B.A., and Jackson, R.D., 1975. Soil heat flux determination: a null-alignment method. Agric. For. Meteorol., 15:1-9.

Kimball, B.A., Mauney, J.R., Nakayama, F.S. and Idso, S.B. (1993). Effects of increasing atmospheric CO_2 on vegetation. Vegetatio 104/105: 65-75.

Kirschbaum, M.U.F., and Farquhar, G.D., 1984. Temperature dependence of whole-leaf photosynthesis in Eucalyptus pauciflora Sieb. ex Spreng. Aust. J. Plant Physiol., 11:519-538.

Klaij, M.C., and Vachaud,G., 1992. Seasonal water balance of a sandy soil in Niger cropped with pearl millet, based on profile moisture measurements. Agric. Water Manag., 21: 313-330.

Kohsiek, W., 1981. A rapid-circulation evaporation chamber for measuring bulk stomatal resistance. J. Appl. Meterol., 20: 42-52.

Kohsiek, W., De Bruin, H.A.R., and Van den Hurk, B.J.J.M., 1993. Estimation of the sensible heat flux of a semi-arid area using surface radiative temperature measurements. Boundary-Layer Meteorol., 63: 213-230.

Kondo, J., 1975. Air-sea bulk transfer coefficients in diabatic conditions. Boundary-Layer Meteorol., 9: 91-112.

Kondo, J. and Akashi, S., 1976. Numerical studies on the two-dimensional flow in horizontally homogeneous canopy layers. Boundary-layer Meteorology 10: 255-272.

Kondo J., and Kawanaka, A., 1986. Numerical study on the bulk heat transfer coefficient for a variety of vegetation types and densities. Boundary-Layer Meteorology 37: 285-296.

Kondo, J., Saigusa, N., and Sato, T., 1990. A parameterization of evaporation from bare soil surfaces. J. Clim. Appl. Meteorol., 29: 385-389.

Koorevaar, P., Menelik, G., and Dirksen, C., 1983. Elements of soil physics. Developments in Soil Science 13, Elsevier, Amsterdam, the Netherlands.

Köppen, W., 1931. Die Klimate der Erde, Berlin.

Kowal, J.M, and Kassam, A.H., 1978. Agricultural ecology of savanna, Oxford University Press, England.

Kreith, F., and Bohn, M.S., 1986. Principles of heat transfer. Harper and Row Publishers, New York, 700 pp.

Kustas, W.P., 1990. Estimates of evapotranspiration with a one- and two-dimensional model of heat transfer over partial canopy cover. J. Appl. Meteorol., 29: 704-715.

Kustas, W.P., Choudhury, B.J., Kunkel, K.E., and Gay, L.W., 1989a. Estimate of the aerodynamic roughness parameters over an incomplete canopy cover of cotton. Agric. and Forest Meteorol., 46: 91-105.

Kustas, W.P., Choudhury, B.J., Moran, M.S., Reginato, R.J., Jackson, R.D., Gay, L.W., and Weaver, H.L., 1989b. Determination of sensible heat flux over sparse canopy using thermal infrared data. Agric. For. Meteorol., 44: 197-216.

Kustas, W.P., Choudhury, Inoue, Y., Pinter, P.J., B.J., Moran, M.S., Jackson, R.D., and Reginato, R.J., 1990. Ground and aircraft infrared observations over a partially-vegetated area. Int. J. Remote sensing 11, 3: 409-427.

Kustas, W.P., and Goodrich, D.C., 1994. Preface MONSOON '90 experiment, Water Resour. Res,.30: 1211-1225.

Lafleur, P.M., and Rouse, W.R., 1990. Application of an energy combination model for evaporation from sparse canopies. Agric. For. Meteorol., 49:135-153.

Labed, J., and Stoll, M.P., 1991. Spatial variability of land surface emissivity in the thermal infra-red band: spectral signature and effective surface temperature. Remote Sens. Environ., 38: 1-17.

Lascano, R.J., Baumhardt, R.L., and Lipe, W,N., 1992. Measurement of water flow in young grapevines using the stem heat balance method. Am. J. Enol. Vitic., 43: 159-165.

Laval, K., and Picon L., 1986. Effect of a change of the surface albedo of the Sahel on climate. J. of Atm. Sci., 43: 2418-2429.

Lebel, T., Sauvageot, H., Hoepffner, M., Desbois, M., Guillot, B., and Hubert, P., 1992. Rainfall estimation in the Sahel: the EPSAT-NIGER experiment. J. Hydrol. Sci., 37: 201-215.

Lebel, T., and LeBarbé, L., 1996. Rainfall climatology of the Central Sahel during the years 1950-1990. HAPEX-Sahel special issue, Journal of Hydrology (accepted).

Lebel, T., Taupin, J.D., and LeBarbé, L., 1996. Space-time fluctuations of rainfall during HAPEX-Sahel. HAPEX-Sahel special issue, Journal of Hydrology (accepted).

Lettau, H., 1969. Note on aerodynamic roughness parameter estimation on the basis of roughness element description. J. Appl. Meterol., 8: 828-832.

Leuning, R., and King, K.M., 1992. Comparison of eddy-covariance measurements of CO_2 fluxes by open- and closed path CO_2 analyzers. Boundary-Layer Meteorol., 59: 297-311.

Levy, P.E., Moncrieff, J.B., Massheder, J.M., Scott, S., and Jarvis, P.G., 1996. CO_2 fluxes at leaf and canopy scale at the HAPEX-Sahel southern super-site. HAPEX-Sahel special issue, Journal of Hydrology (accepted).

Lhomme, J-P., 1988. A generalized combination equation derived from a multi-layer micrometeorological model. Boundary-Layer Meteorology 45: 103-115.

Lhomme, J-P., 1991. The concept of canopy resistance: historical survey and comparison of different approaches. Agric. For. Meteorol., 54: 227-240.

Lhomme, J-P., 1992. Energy balance of heterogeneous terrain: averaging the controlling parameters. Agric. For. Meteorol., 61: 11-21.

Lloyd, C.R., 1995. The effect of heterogeneous terrain on micrometerological flux measurements: a case study from HAPEX-Sahel. Agric. For. Meteorol. 73: 209-216.

Lloyd, C.R., Gash, J.H.C., Sivakumar, M.V.K., 1992. Derivation of the aerodynamic roughness parameters for a Sahelian savannah site using the eddy correlation technique. Boundary-Layer Meteorology 58: 261-271.

Lloyd, C.R., Bessemoulin, P., de Bruin, H., Cropley, F., Culf, A.D., Dolman, A.J., Elbers, J., Moncrieff, J., Monteny, B. and Verhoef, A., 1996. An intercomparison of surface flux measurements during HAPEX-Sahel. Journal of Hydrology, special issue HAPEX-Sahel (submitted).

Lof, H., 1976. Water use efficiency and competition between arid zone annuals, especially the grasses Phalaris minor and Hordeum murinum. Agricultural Research Reports, 853, Pudoc, Wageningen, the Netherlands.

Louis, J.F. 1979. A parametric model of vertical eddy fluxes in the atmosphere. Boundary-Layer Meteorology 17: 187-202.

Louis, J.F., Tiedtke, M., and Geleyn, J.F., 1981. A short history on the operational PBL - parameterization at E.C.M.W.F. In: Workshop on Boundary Layer Parameterization, 25-27 November 1981, E.C.M.W.F., Reading, U.K.

Lövenstein, H.M., Berliner, P.R., and van Keulen, H., 1991. Runoff agroforestry in arid lands. Forest Ecology and Management, 45: 59-70.

Ludlow, M.M., 1980. Adaptive significance of stomatal responses to water stress. In: N.C. Turner and P.J. Kramer (Editors), Adaptations of Plants to Water and High Temperature Stress. Wiley Interscience, New York, pp. 123-138.

Mahrt, L., and Ek, M., 1984. The influence of atmospheric stability on potential evaporation. J. Clim. Appl. Meteorol., 23: 222-234.

Malhi, Y.S., 1993. Sensible heat flux from heterogeneous surfaces. PhD-thesis University of Reading, Dept. of Meteorology, England, 261 pp.

Manabe, S., 1969. Climate and Ocean circulation I: Atmospheric circulation and hydrology of the Earth's surface. Mon. Weather Rev., 97: 739-774.

Marshall, J.K., 1971. Drag measurements in roughness arrays of varying density and distribution. Agric. For. Meteorol. 8: 269-292.

Massman, W.J., 1987. Heat transfer to and from vegetated surfaces: an analytical method for the bulk exchange coefficient. Boundary-Layer Meteorology 40: 269-281.

Massman, W.J., 1992. A surface energy balance method for partitioning evapotranspiration data into plant and soil components for a surface with partial canopy cover. Water Resources Res., 28: 1723 - 1732.

Mayocchi, C.L., and Bristow, K.L., 1995. Soil surface heat flux : some general questions and comments on measurements. Agric. For. Meteorol. 75: 43-50.

McMillen, R.T., 1983. Eddy correlation calculations done in real-time. Seventh Conf. Fire and Forest Meteorology, Ft. Collins, Co., April 25-28.

McNaughton, K.G., 1994. Effective stomatal and boundary-layer resistances of heterogeneous surfaces. Plant, Cell and Environment, 17: 1061-1068.

McNaughton, K.G., and Black, T.A., 1973. A study of evapotranspiration from a Douglas-fir forest using the energy balance approach. Water Resour. Res., 9: 1579-1590.

McNaughton, K.G, and Van den Hurk, B.J.J.M, 1995. A 'Lagrangian' revision of the resistors in the two-layer model for calculating the energy budget of a plant canopy. Boundary-Layer Meteorol., 74: 261-288.

Medina, E., 1986. Forests, savannas and montane tropical environments. In: Baker, N.R., and S.P. Long (Editors), Photosynthesis in contrasting environments. Topics in photosynthesis-Volume 7. Elsevier, Amsterdam, pp. 139-171.

Meigs, P., 1953. World distribution of arid and semi-arid homoclimates, In: UNESCO, Arid Zone Res.. Series No. 1, Arid Zone Hydrology :203-209.

Meinzer, F.C., 1982. The effect of vapour pressure on stomatal control of gas exchange in Douglas Fir (Pseudotsuga menziesii) saplings. Oecologia, 54: 236-242.

Menenti, M., 1984. Physical aspects and determination of evaporation in deserts applying remote sensing techniques. PhD-thesis. Instituut voor Cultuurtechniek en Waterhuishouding, Wageningen, 202 pp.

Meyers, T.P., and Paw U, K.T., 1987. Modelling the plant canopy micrometeorology with higher-order closure principles. Agric. For. Meterol., 7: 401-410.

Mogensen, V.O., 1970. The calibration factor of heat flux meters in relation to the thermal conductivity of the surrounding medium. Agric. For. Meterol., 41: 143-163.

Moncrieff, J.B., Monteny, B, Verhoef, A., Friborg, T., Elbers, J.H., Kabat, P., De Bruin, H.A.R., Søgaard, H., Jarvis, P.G. and Billing, H. , 1996a. Spatial and temporal variations in net carbon flux during HAPEX-Sahel. Journal of Hydrology , special issue HAPEX-Sahel (submitted).

Moncrieff, J.B., Massheder, J.M., De Bruin, H.A.R., Elbers, J.H., Friborg, T., Heusinkveld, B., Kabat, P., Scott, S., Søgaard, H. and Verhoef, A., 1996b. A system to measure surface fluxes of momentum, sensible heat, water vapour and carbon dioxide. Journal of Hydrology , special issue HAPEX-Sahel (submitted).

Monteith, J.L., 1965. Evaporation and the environment. Symp. Soc. Exp. Biol. 19; 205-234.

Monteith, J.L., 1972. Solar radiation and productivity in tropical ecosystems. J. Appl. Ecol., 9: 747-766.

Monteith, J.L., 1973. Principles of environmental physics; Elsevier, New York, 241 pp.

Monteith, J.L., 1981. Evaporation and surface temperature. Q.J.R. Meteorol. Soc., 107: 1-27.

Monteith, J.L., 1991. Weather and water in the Sudano-Sahelian zone. In: Soil Water Balance in the Sudano-Sahelian Zone, IAHS Publ. no. 199: 11-29.

Monteith, J.L., and Unsworth, M.H., 1990. Principles of environmental physics (2^{nd} edition. Arnold, London, 291 pp.

Monteny, B.A., 1993. HAPEX Sahel 1992, Campagne de mesures, supersite Central Est, 1^e partie: Synthèse sur les participations. 2^e partie: Résultats partiels et préliminaires. ORSTOM, Montpellier.

Monteny, B.A., Lhomme, J-P., Chehbouni, A., Troufleau, D., Amadou, M., Sicot, M., Galle, S., Said, F., Verhoef, A., and Lloyd, C.R., 1996. The role of the Sahelian biosphere in the water and CO2 cycle during the HAPEX-Sahel experiment. Journal of Hydrology , special issue HAPEX-Sahel (accepted).

Moore, C.J., 1986. Frequency response corrections for eddy correlation systems. Boundary-Layer Meteorol., 37: 17-35.

Morison, J.I.L., 1987. Intercellular CO_2 concentration and stomatal response to CO_2. In: E. Zeiger, G.D. Farquhar and I.R. Cowan (Eds.), Stomatal Function. Stanford University Press, Stanford, California, 229-251 pp.

Moran, M.S., Kustas, W.P., Vidal, A., Stannard, D.I., Blanford, J.H., and Nichols, W.D., 1994. Use of ground-based remotely sensed data for surface energy balance evaluation of a semiarid rangeland. Water Resour. Res. 30: 1339-1349.

Morison, J.I.L., and Gifford, R.M., 1983. Stomatal sensitivity to carbon dioxide and humidity: a comparison of two C_3 and two C_4 grass species. Plant Physiology, 71: 789-796.

Nagpal, N.K. and Boersma, L., 1973. Air entrapment as a possible error in the use of a cylindrical heat probe. Soil Sci. Soc. Am. J. 37:828-832.

Nichols, W.D., 1992. Energy budgets and resistances to energy transport in sparsely vegetated rangeland. Agric. For. Meteorol., 60:221-247.

Nicholson, S.E., 1981. Rainfall and atmospheric circulation during drought periods and wetter years in West Africa. Mon. Wea. Rev., 109: 2191-2208.

Nicholson, S.E., 1989. Long-term changes in African rainfall. Weather, 44: 46-55.

Nicholson, S.E., and Lare, A.R., 1990. A climatonomic description of the surface energy balance in the Central Sahel. Part II: The evapoclimatonomy submodel. J. Appl. Meteor., 29: 138-146.

Nicholson, S.E., and Palao, I.M., 1993. A re-evaluation of rainfall variability in the Sahel. Part I. Characteristics of rainfall fluctuations. Int. J. of Climatology 13, 371-389.

Noilhan, J., and Planton, S., 1989. A simple parametrization of land surface processes for meteorological models. Mon. Wea. Rev. 117: 536-549.

Norman, J.J., 1979. Modelling the complete crop canopy. In: B. Barfield and J. Gerber (Editors), Modificication of the areal environment of crops. Am. Soc. Agric. Eng., St. Joseph, MI, pp. 249-277.

Norman, J.M., 1993. Scaling Processes between leaf and canopy levels. In: J.R. Ehleringer and C.B. Field, Scaling physiological processes, leaf to globe. Academic Press, Inc.

Novak, M.D., 1990. Micrometeorological changes associated with vegetation removal and influencing desert formation. Theor. Appl. Climatol., 42, 19-25.

Oliver, H.R. and Sene, K.J., 1992. Energy and water balances of developing vines. Agric. For. Meteorol., 61: 167-185.

Oguntoyinbo, J.S., 1970. Reflection coefficient of natural vegetation, crops and urban surfaces in Nigeria. Q.J.R. Soc. Meteorol., 96: 430-441.

O'Loughlin, E.M., 1965. Resistance to flow over boundaries with small roughness concentrations. Ph. D. Dissertation, University of Iowa.

O' Loughlin, E.M., and V.S.S. Anambhotla (1969): Flow phenomena near rough boundaries. Journal Hydraulic Research 7, 231-250.

Overdieck, D. and Strain, B.R., 1981. Effects of atmospheric humidity on net photosynthesis, transpiration and stomatal resistance of Hydrocotyle umbellata L. and Hydrocotyle bonariensis Lam. Int. J. Biometeorol., 25: 29-38.

Owen P.R. and Thomson, W.R., 1963. Heat transfer accross rough surfaces. J. Fluid Mech., 15: 321-334.

Pagès, J-P., Frangi,J-P, Durand, P., Estournel, C., and Druilhet, A., 1988. Étude de la couche limite de surface Sahelienne - Experience Yantala. Boundary-Layer Meteorology, 43: 183-203.

Paltridge, G.W., and Platt, C.M.R., 1976. Radiative processes in meteorology and climatology. Elsevier, Amsterdam, 318 pp.

Paulson, C.A., 1970. The mathematical representation of wind speed and temperature in the unstable atmospheric surface layer. J. Appl. Meteorol., 9: 857-861.

Paw U, K.T., and Meyers, T.P., 1989. Investigations with a higher-order canopy turbulence model into mean source-sink levels and bulk canopy resistances. Agric. For. Meteorol., 47: 259-271.

Payne, W.A., Wendt, C.W., and Lascano, R.J., 1990. Root zone water balances of three low-input millet fields in Niger, West Africa. Agronomy Journal, 82: 813-819.

Pearcy, R.W. and Ehleringer, 1984. Comparative ecophysiology of C_3 and C_4 plants. Plant Cell environ., 7: 1-13.

Penck, A., 1894. Morphologie der Erdoberfläche, Stuttgart.

Penman, H.L., 1948. Natural evaporation from open water, bare soil and grass. Proc. R. Soc. London, Ser. A, 193: 120-145.

Penman, H.L., and Long, I.F., 1960. Weather in wheat: an essay in micrometeorology. Q.J.R. Meteorol. Soc., 86: 16-50.

Penning de Vries, F.W.T., Van Laar, 1982. Simulation of plant growth and crop production. Simulation Monographs. Pudoc, Wageningen, 308 pp.

Penning de Vries, F.W.T., Jansen, D.M., Ten Berge, H.F.M., and Bakema, A., 1989. Simulation of ecophysical processes of growth in several annual crops. Simulation Monographs 29. Pudoc, Wageningen, 271 pp.

Perrier, A., 1982. Land surface processes: Vegetation, in Land Surface Processes in Atmospheric Circulation models, edited by P.S. Eagleson, Cambridge University Press, New York, pp. 395-448.

Pinker, R.T., 1990. Satellites and our understanding of the surface energy balance. Paleogr. Paleoclimatol. Paleoecol., 82: 321-342.

Press, W.H., Flannery, B.P., Teukolsky, S.A., and Vetterling, W.T., 1986. Numerical Recipes, the art of scientific computing. Cambridge University Press, 818 p.

Prince, S.D., Kerr, Y.H., Goutorbe, J.P., Lebel, T., Tinga, A., Brouwer, J., Dolman, A.J., Engman, E.M., Kabat, P., Monteny, B., Saïd, F., Sellers, P., Wallace, J., 1994. The Hydrology-Atmosphere Pilot Experiment. Remote Sensing of Environment (in press).

Price, D.T. & T.A. Black, 1990. Effects of short-term variation in weather on diurnal canopy CO_2 flux and evapotranspiration of a juvenile Douglas fir stand. Agric. For. Meteorol., 50: 139-158.

Priestley, C.H.B., 1955. Free and forced convection in the atmosphere near the ground. Q.J.R. Meteorol. Soc. 81: 139-143.

Priestley, C.H.B., and Taylor, R.J., 1972. On the assessment of surface heat flux and evaporation using large-scale parameters. Mon. Wea. Rev., 100: 81-92.

Randall, J.M., 1969. Wind profiles in an orchard plantation. Agric. For. Meteorol., 6: 439-452.

Raupach, M.R., 1987. A Lagrangian analysis of scalar transfer in vegetation canopies. Q.J.R. Meteorol. Soc.113: 107-120.

Raupach, M.R., 1989. A practical Lagrangian method for relating scalar concentrations to source distributions in vegetation canopies. Q.J.R. Meteorol. Soc.115: 609-632.

Raupach, M.R., 1991. Vegetation-atmosphere interaction in homogeneous and heterogeneous terrain: some implications of mixed-layer dynamics. Vegetatio 91: 105-120.

Raupach, M.R., 1992. Drag and drag partition on rough surfaces. Boundary-Layer Meteorology 60: 375-395.

Raupach, M.R., 1995. Vegetation-atmosphere interaction and surface conductance at leaf, canopy and regional scales. Agric. For. Meteorol. 73: 151-179.

Raupach, M.R., Thom, A.S., and Edwards, I., 1980. A wind tunnel study of turbulent flow close to regularly arrayed rough surfaces. Boundary-Layer Meteorology 18: 373-397.

Raupach, M.R., Finnigan, J.J. and Brunet, Y., 1989. Coherent eddies in vegetation canopies. Proc. Fourth Australasian Conf. on Heat and Mass Transfer, Christchurch, New Zealand, 9-12 May, 1989, pp. 75-90.

Rawson, H.M., Begg, J.E., and Woodward, R.G., 1977. The effect of atmospheric humidity on photosynthesis, transpiration and water use efficiency of leaves of several plant species. Planta 134: 5-10.

Richardson, L.F., 1920. The supply of energy from and to atmospheric eddies. Proc. R. Soc. London, Ser. A., 97: 354-373.

Rider, N.E., and Robinson, 1951. A study of the transfer of heat and water vapour above a surface of short grass. Q.J.R. Meteorol. Soc., 77: 375-401.

Riha, S.J., McInnes, K.J., Clids, S.W. and Campbell, G.S., 1980. A finite element calculation for determining thermal conductivity. Soil Sci. Soc. Am. J. 44: 1323-1325.

Riou, C., Pieri, P., and Valancogne, C., 1987. Variation de la vitesse du vent à l' intérieur et au-dessus d'une vigne. Agric. For. Meteorol. 39: 143-154.

Ritchie, J.T., 1992. Model for predicting evaporation from a row crop with incomplete cover. Water Resour. Res., 8: 1204-1213.

Roberts, J., Cabral, O.M.R. and L.F. de Aguiar, 1990. Stomatal and boundary-layer conductances in an Amazonian Terra Firme rain forest. J. Appl. Ecol. 27: 336-353.

Rochette, P., Desjardins, R.L., and Pattey, E., 1991a. Spatial and temporal variability of soil respiration in agricultural fields. Can. J. Soil. Sci., 71: 189-196.

Rochette, P., Pattey, E, Desjardins, R.L., Dwyer, L.M. Stewart, D.W. and Dubé, P.A., 1991b. Estimation of maize (Zea mays L.) canopy conductance by scaling up leaf stomatal conductance. Agric. For. Meteorol., 54:241-261.

Ross, J., 1975. Radiative transfer in plant communities. In: J.L. Monteith (Editor), Vegetation and the atmosphere, Vol. 1, Academic Press, San Diego, USA, pp. 13-55.

Rowe, C.M., 1993. Global land-surface albedo modelling. Int. J. of Clim., 13: 473-495.

Sakuritani, T., 1981. A heat balance method for measuring water flux in the stem of intact plants. J. Agric. Meteorol., 37: 9-17.

Sandholt, I., and Steen Andersen, H., 1993. Derivation of actual evapotranspiration in the Senegalese Sahel, using NOAA-AVHRR data during the 1987 growing season. Remote sens. environ. 46: 164-172.

Schlichting, 1936. Experimentelle untersuchungen zum rauhigketsproblem. Ing.- Arch. 7: 1-34; NACA Tech. Mem. 823.

Schulze, E.-D., and Hall, A.E., 1982. Stomatal responses, water loss and CO_2 assimilation rates of plants in contrasting environments. In: O.L. Lange, P.S. Nobel, C.B. Osmond and H. Ziegler (Editors), Encyclopedia of Plant Physiology, New Series, Vol. 12B, Physiological Plant Ecology II. Springer Verlag, Berlin, pp. 181-230.

Schulze, E.-D., Turner, N.C., Gollan, T. and Shackel, K.A., 1987. Stomatal responses to air humidity and to soil drought. In: E. Zeiger, G.D. Farquhar and I.R. Cowan (Eds.), Stomatal Function. Stanford University Press, Stanford, California, 311-321.

Seemann, J., 1979. Measuring technology. p. 40-45. In: J Seemann et al. (Editors) Agrometeorology. Springer-Verlag, Berlin.

Seginer, I., 1974. Aerodynamic roughness of vegetated surfaces. Boundary-layer Meteorology 5 : 383-393.

Sellers, P.J., Mintz, Y., Sud, Y.C., and Dalcher, A., 1986. A simple biosphere model for use within general circulation models. J. Atmos. Sci., 43: 505-531.

Sellers, P.J., Hall, F.G., Asrar, G., Strebel, D.E, and Murphy, R.E., 1988. The first ISLSCP field experiment (FIFE), Bull. Am. Meteorol. Soc., 69: 22-27.

Sellers, P.J., Shuttleworth, W.J. and Dorman, J.L., 1989. Calibrating the simple biosphere model for Amazonian tropical forest using field and remote sensing data. Part I: Average calibration with field data. J. Appl. Met. 28: 727-759.

Sellers, W.D., 1965. Physical climatology. University of Chicago Press.

Sene, K.J., 1994. Parameterisations for energy transfers from a sparse vine crop. Agric. For. Meteorol., 71:1-18.

Shantz, H.L., 1956. History and problems of arid lands development. In: G.F. White (Editor). The future of arid lands. Amer. Assoc. Adv. Sci. Pub. No. 43, Washington, USA.

Shaw, R.H., and Perreira, A.R., 1982. aerodynamic roughness of a plant canopy: a numerical experiment. Agric. For. Meteorol. 26: 51-65.

Sheppard, P.A., 1958. Transfer across the Earth's surface and through the air above. Q.J.R. Met. Soc. 84: 205-224.

Shukla, J., and Mintz, Y., 1982. Influence of land-surface evapotranspiration on the earth's climate. Science, 215, 1498-1501.

Shuttleworth, W.J., 1976. Experimental evidence for the failure of the Penman-Monteith equation in partially wet conditions. Boundary-Layer Meteorol., 10: 91-94.

Shuttleworth, W.J., 1988. Macrohydrology - The new challenge for process hydrology. Journal of Hydrology 100: 31-56.

Shuttleworth, W.J., 1991. Evaporation models in hydrology. In: Schmugge, T.J. and André, J. (editors), Land Surface Evaporation. Springer, New York, pp. 93-120.

Shuttleworth, W.J., Gash, J.H.C., Lloyd, C.R., Moore, C.J., Roberts, J., Marques Filho, A.O., Fisch, G., Silva Filho, V.P., Goés Ribeiro, M.N., Molion, L.C. B., Sá, L.D.A., Nobre, J.C.A., Cabral, O.M.R., Patel, S.R. and Moraes, J.C., 1984. Eddy correlation measurements of energy partition for Amazonian forest. Q.J.R. Met. Soc. 110: 1143-1162.

Shuttleworth, J.W. and Wallace, J.S., 1985. Evaporation from sparse crops-an energy combination theory. Q.J.R. Meteorol. Soc., 111:839-855.

Shuttleworth, J.W., Gash, J.H.C., Lloyd, C.R., McNeill, D.D., Moore, C.J., and Wallace, J.S., 1988. An integrated micrometerological system for evaporation measurement. Agric. For. Meteorol., 43: 295-317.

Sivakumar, M.V.K, 1989. Agroclimatic aspects of rainfed agriculture in the Sudano-Sahelian zone. In: Soil, crop and water management systems for rainfed agriculture in the Sudano-Sahelian zone (Proc. international workshop, January 1987, ICRISAT Sahelian Center, Miamey (Niger), 17-38. ICRISAT, Patancheru, AP 502234, India.

Sivakumar, M.V.K, and Wallace, J.S., 1991. Soil water balance in the Sudano-Sahelian zone: need, relevance and objectives of the workshop. IAHS Publ., 199: 3-10.

Sivakumar, M.V.K., Maidoukia, A., and Stern, R.D., 1993. Agroclimatology of West Africa: Niger. Second Edition. Information Bulletin No. 5., International Crops Research Institute for the Semi-Arid Tropics, Patancheru, A.P. 502 324, India, 116 pp.

Smith, R.C.G., and Barrs, H.D., 1988. Inferring stomatal resistance of sparse crops from infrared measurements of foliage temperature. Agric. For. Meteorol., 42: 183-198.

Søgaard, H., and Lagouarde, J-P., 1994. *On estimation of evapotranspiration from surfaces with different* aerodynamic roughness within the Sahelian environment. Agric. For. Meteorol. (submitted).

Soet, M., Droogers, P., Jaarsma, M.N., Kim, C.P, Monincx, J.F. and Stricker, J.N.M., 1995. HAPEX-Sahel: Basic description of methods and datasets, rapport 43, Vakgroep Waterhuishouding, Wageningen, the Netherlands, 50 p.

Sparrow, E.M., and Cess, R.D., 1978. Radiation heat transfer. Hemisphere Publishing Corporation, London, 366 p.

Stannard, D.I., 1993. Comparison of Penman-Monteith, Shuttleworth-Wallace, and modified Priestley-Taylor evapotranspiration models for wildland vegetation in semiarid rangeland. Water Resour. Res. 29: 1379-1392.

Stannard, D.I., Blanford, J.H., Kustas, W.P., Nichols, W.D., Amer, S.A., Schmugge, T.J., and Weltz, M.A., 1994. Interpretation of surface flux measurements in heterogeneous terrain during the Monsoon '90 experiment. Water Resour. Res. 30: 1227-1239.

Steinberg, S.L., Van Bavel, C.H.M., and McFarland, M.J., 1989. A gauge to measure mass flow rate of sap in stems and trunks of woody plants. J. Am. Soc. Hortic. Sci., 114: 466-472.

Stewart, J.I., 1988. Response farming in rainfed agriculture. Wharf Foundation Press, Davis, California, 103 pp.

Stewart, J.S, 1988. Modelling surface conductance of pine forest. Agric. For. Meteorol. 43: 19-35.

Stewart, J.S., and Thom, A.S., 1973. Energy budgets in pine forest. Q.J.R. Meteorol. Soc. 99: 154-170.

Stewart, J.B., Kustas, W.P., Humes, K.S., Nichols, W.D., Moran, M.S., De Bruin, H.A.R., 1994. Sensible heat flux-radiometric surface temperature relationship for eight semi-arid areas. J. Appl. Meteorol. 33, 9:1110: 1117.

Stroosnijder, L., 1991. Verdrinken en verdrogen. Inaugurele rede Landbouw Universiteit Wageningen, 2 mei 1991, 40 pp.

Stroosnijder, L. and van Heemst, H.D.J, 1982. La meteorologie du Sahel et du terrain de l'étude. In: La productivité des paturages Saheliens, F.W.T. Penning de Vries et M.A. Djitèye (Editors), Pudoc, Wageningen.

Stull, R.B., 1988. An introduction to boundary layer meteorology. Atmospheric sciences library. Kluwer Academic Publishers, 666 p.

Sud, Y.C., and Smith, W.E., 1985. The influence of surface roughness of deserts on the July circulation (A numerical study). Boundary-Layer Meteorology, 33: 15-49.

Sverdrup, H.U., 1937. On the evaporation from the oceans. Journal of Marine Research 8: 3-14.

Swinbank, W.C., 1963. Longwave radiation from clear skies. Q.J.R. Meteorol. Soc. 89: 339-348.

Szeicz, G., and Long, I.F., 1969. Surface resistance of crop canopies. Water Resour. Res., 5: 622-633.

Tanner, C.B., 1963. Basic instrumentation and measurements for plant environment and micrometeorolgy. Univ. Wisc., Madison, Soil Bull., 6.

Tanner, C.B., and Sinclair, T.R., 1983. Efficient water use in crop production: research or re-search? In: H. Taylor, W. Jordan and J. Sinclair (Editors), Limitations of Efficient Water Use in Crop Production. Madison, WI, pp. 1-27.

Ten Berge, H.F.M., 1986. Heat and water transfer at the bare soil surface: aspects affecting thermal imagere. PhD thesis, Dept. of Soil Science and Plant Nutrition, Wageningen, the Netherlands.

Ten Berge, H.F.M, 1990. Heat and water transfer in bare topsoil and the lower atmosphere. Simulation Monographs 33. Pudoc Wageningen, the Netherlands, 207 p.

Tenhuenen, J.D., Pearcy, R.W. and O.L. Lange, 1987. Diurnal variations in leaf conductance and gas exchange in natural environments. In: E. Zeiger, G.D. Farquhar and I.R. Cowan (Eds.), Stomatal Function. Stanford University Press, Stanford, California, pp. 323-351.

Tennekes, H., 1973. The logarithmic wind profile. J. Atm. Sci., 30: 234-238.

Thom, A.S., 1972. Momentum, mass and heat exchange of vegetation. Q.J.R. Meteorol. Soc., 98: 124-134.

Thornthwaite, C.W., 1948. An approach towards a rational classification of climate. Geog. Rev., 38: 55-94.

Tolman, M., 1989. Waterhuishouding van houtachtige gewassen in het semi-aride gebied van West Afrika. Scriptie, Plantenoecologie, R.U. Groningen, the Netherlands, 28 pp.

Troen, I.B., and Mahrt, L., 1984. A simple model of the atmospheric boundary layer; sensitivity to surface evaporation. Boundary-Layer Meteorol., 37: 129-148.

Tucker, C.J., Newcomb, W.W., Los, S.O., and Prince, S.D., 1991. Mean and inter-year variation of growing-season normalized difference vegetation index for the Sahel 1981-1989. Int. J. Remote sensing, 12: 1133-1135.

Uijlenhoet, R., 1990. An investigation towards the development of a geometrical reflection model for land surfaces. Msc-thesis, Wageningen Agricultural University, the Netherlands, 69 pp.

Van Bavel, M.G. and Van Bavel, C.H.M., 1990. Dynagage Installation and Operation Manual. Dynamax Inc., Houston, TX, 80 pp.

Van de Griend, A.A., Owe, M., Vugts, H.F., and Prince, S.D., 1989. Water and energy balance modelling in Botswana. Bull. Amer. Meteorol. Soc., 70, 11: 1404-1411.

Van de Griend, A.A., Owe, M., Groen, M., and Stoll, M.P., 1991. Measurement and spatial variation of thermal infrared surface emissivity in a savanna environment. Water Resour. Res.27, 3: 371-379.

Van de Griend, A.A., and Owe, M., 1993. On the relationship between thermal emissivity and the normalized difference vegetation index for natural surfaces. Int. J. Remote Sensing, 14: 1119-1131.

Van de Griend, and Owe, A.A., 1994. Bare soil surface resistance to evaporation by vapor diffusion under semiarid conditions. Water Resour. Res. 30, 2: 181-188.

Van den Berg, A.R., 1995a. Description and manual of the CALCFLUX program. Dept. of Meteorology, WAU, Wageningen, the Netherlands

Van den Berg, A.R., 1995b. Description and manual of DCM and TCM. Dept. of Meteorology, WAU, Wageningen, the Netherlands

Van den Hurk, B.J.J.M., 1995. Sparse canopy parameterization for meteorological models. PhD-thesis, Dept. of Meteorology, WAU, Wageningen, the Netherlands.

Van den Hurk, B.J.J.M, Verhoef, A., Van den Berg, A.R., and De Bruin, H.A.R., 1996. An intercomparison of three vegetation/soil models for a sparse vineyard canopy. Q.J.R. Meteorol. Soc. (accepted).

Van den Hurk, B.J.J.M, and McNaughton, K.G., 1995. Implementation of near-field dispersion in a simple two-layer surface resistance model. Journal of Hydrology 166: 293: 311.

Van Loon, W.K.P, 1991. Heat and mass transfer in frozen porous media. PhD-thesis. Agricultural University, Wageningen, The Netherlands, 204 pp.

Van Wijk, W.R., 1963. Physics of plant environment. North Holland Publishers. Amsterdam, 382 p.

Van Wijk, W.R., and De Vries, D.A., 1963. Periodic temperature variations in a homogeneous soil. In: W.R. Van Wijk (editor), Physics of plant environment. North Holland Publishers. Amsterdam, pp. 103-143.

Veenendaal, E.M., 1991. Adaptive strategies of grasses in a semi-arid savanna in Botswana. PhD-thesis, Free Universtity Amsterdam, the Netherlands.

Verhoef, A., and R.A. Feddes, 1991. Preliminary review of revised FAO radiation and temperature methods. Rapport 16, Department of water conservation, Agricultural University, Wageningen, The Netherlands, 116 pp.

Verhoef, A., Van den Hurk, B.J.J.M, Jacobs, A.F.M, and Heusinkveld, B.G., 1996a. Thermal soil properties for vineyard (EFEDA-I) and savanna (HAPEX-Sahel) sites. Agric. For. Meterol. (accepted).

Verhoef, A., Allen, S.J., De Bruin, H.A.R., Jacobs, C.J.M. and Heusinkveld, B.G., 1996b. Fluxes of water vapour and carbon dioxide from a Sahelian savannah. Agric. For. Meterol. (accepted).

Verma, S.B., and Barfield, B.J., 1979. Aerial and crop resistances affecting energy transport. In: B.J. Barfield and J.F. Gerber (Editors.), Modification of the aerial environment of crops; Am. Soc. Agric. Eng., St. Joseph, MI, pp. 230-248.

Vetaas, O.R., 1992. Micro-site effects of trees and shrubs in dry savannas. J. Vegetat. Sci., 3: 337-344.

Viterbo, P., and Beljaars, A.C.M., 1994. An improved land surface parameterization scheme in the ECMWF model and its validation. Technical report TR 75, ECMWF, Reading, 52 pp. (Also accepted for publication by J. Climate).

Von Maydell, H.-J., 1990. Trees and shrubs of the Sahel: their characteristics and uses. Margraf, Weikersheim, Germany.

Vos, J. and Groenewold, J. 1989. Characteristics of photosynthesis and conductance of potato canopies and the effect of cultivar and transient drought. Field Crops Research, 20: 237-250.

Vugts, H.F., 1993. The need for micrometeorological research on the response of the energy balance of vegetated surfaces to CO_2 enrichment. Vegetatio 104/105: 321-328.

Waggoner, P.E., and Reifsnyder, W.E., 1968. Simulation of the temperature, humidity and evaporation profiles in a leaf canopy. J. Appl. Meteorol., 7: 400-409.

Wallace, J.S., 1995. Calculating evaporation: resistance to factors. Agric. For. Meteorol., 73: 353-366.

Wallace, J.S., Allen, S.J., Culf, A.D., Dolman, A.J., Gash, J.H.C., Holwill, C.J., Lloyd, C.R., Stewart, J.B., and Wright, I.R., 1992. SEBEX: The Sahelian energy balance experiment. Final report on ODA Project T06050C1, ODA-report 92/9.

Wallace, J.S., Roberts, J.M., and Sivakumar, M.V.K, 1993a. The estimation of transpiration from sparse dryland millet using stomatal conductance and vegetation area indices. Agric. For. Meteorol. 63: 149-169.

Wallace, J.S., Lloyd, C.R., and Sivakumar, M.V.K., 1993b. Measurement of soil, plant and total evaporation from millet in Niger. Agric. For. Meteorol. 51: 35-49.

Wallace , J.S., Brouwer, J., Allen, S.J., Banthorpe, D., Blyth, E.M., Blyth, K., Bromley, J., Buerkert, A.C., Cantwell, M., Cooper, J.D., Cropley, F.D., Culf, A.D., Dolman, A.J., Dugdale, G., Gash, J.H.C., Gaze, S.R., Harding, R.J., Harrison, R.G., Holwill, C.J., Jarvis, P.G., Levey, P.E., Lloyd, C.R., Malhi, Y.S., Massheder, J.M., Moncrieff, K.B., Pearson, D., Settle, J.J., Sewell, I.J., Sivakumar, M.V.K., Sudlow, J.D., Taylor, C.M., and Wilson, A.K., 1994. HAPEX-Sahel southern super-site report : An overview of the HAPEX-Sahel southern super-site and the experimental programme during the intensive observation period in 1992. Institute of Hydrology, Wallingford, UK, 55 pp.

Wallace, J.S., and Holwill, 1996. Soil evaporation from tiger-bush in Niger. Journal of Hydrology, special issue HAPEX-Sahel (submitted).

Wartena, L., 1973. Checking of some formulae for the calculation of longwave radiation from clear skies. Archief für Meteorologie, Geophysik und Bioklimatologie, Serie B, 21: 335-348.

Webb, E.K., Pearman, G.I., and Leuning, R., 1980. Correction of flux measurements for density effects due to heat and water vapour transfer. Quart. J. Roy. Met. Soc., 196: 85-100.

Weiss, A., 1981. On the performance of pyrgeometers with silicon domes. J. Appl. Meteor., 20: 962-965.

Weiss, A., and Allen, L.H., 1976. Vertical and horizontal air flow above rows of a vineyard. Agric. For. Meteorol., 17: 433-452.

Wessels, W., 1993. De Nederlandse ontwikkelingssamenwerking met de Sahel. Informatie Voorlichtingsdienst Ontwikkelingssamenwerking van het ministerie van Buitenlandse Zaken 15: 1-8.

White, F., 1965. The savanna woodlands of the Zambezian and Sudanese Domains. Webbia 19: 651-681.

Whitehead, D., Okali, D.U.U, and Fasehun, F.E., 1981. Stomatal response to environmental variables in two tropical forest species during the dry season in Nigeria. J. Appl Ecol., 18: 571-587.

Wieringa, J., 1993. Representative roughness parameters for homogeneous terrain. Boundary-Layer Meteorology 63: 323-363.

Wilson, N.R., and Shaw, R.H., 1977. A higher-order closure model for canopy flow. J. Appl. Meteorol., 16: 1198-1205.

Wooding, R.A., Bradley, E.F., and Marshall, J.K., 1973. Drag due to regular arrays of roughness elements of varying geometry. Boundary-Layer Meteorol., 5: 285-308.

Wong, S.C., Cowan, I.R., and Farquhar, G.D., 1979. Stomatal conductance correlates with photosynthetic capacity. Nature: 282: 424-426.

Wright, I.R., Manzi, A.O., Da Rocha, H.R., 1995. Surface conductance of Amazonian pasture: model application and calibration for canopy climate. Agric. For. Meteorol., 75: 51-70.

Xue, Y., Liou, K-N. and Kasahara, A., 1990. Investigation of the biogeophysical feedback on the African climate using a two-dimensional model. J. Climate, 3: 337-352.

Xue, Y., and Shukla, J., 1993. The influence of land surface properties on Sahel climate. Part I: Desertification. Journal of Climate 6: 2232-2245.

Curriculum Vitae

Anne Verhoef werd op 18 september 1966 geboren in Rotterdam. Na het eindexamen ongedeeld VWO, behaald in mei 1984 aan het Emmauscollege te Rotterdam, vertrok zij naar Wageningen. Na een STOVA-cursus scheikunde werd in september 1984 aan de Landbouwuniversiteit de studie Bodemkunde begonnen, met als specialisatie bodemnatuurkunde. In de zomer van 1988 bracht zij een stage door aan het 'Instituto Nacional de Investigaciones Agrarias' in Cordoba, Spanje. In 1990 studeerde zij met lof af met de afstudeervakken bodemnatuurkunde, meteorologie en hydrologie.
Vervolgens was zij 3 maanden gedetacheerd aan de vakgroep Waterhuishouding voor het uitvoeren van een adviserend onderzoek voor de FAO. Dit onderzoek betrof het testen van diverse methoden die gebruikt worden om potentiële verdamping te berekenen. In maart 1991 kreeg zij een aanstelling als Onderzoeker in Opleiding (NWO) bij de Vakgroep Meteorologie, welke na ruim 4 jaar resulteerde in het voor u liggende proefschrift. Gedurende die 4 jaar verrichtte zij onderzoek naar de energiebalans van struikvegetaties in semi-aride gebieden. Meetgegevens voor dit onderzoek werden verzameld gedurende twee meetcampagnes; EFEDA (juni 1991, Spanje) en HAPEX-Sahel (augustus-oktober 1992, Niger). De bijdrage van de vakgroep Meteorologie aan het HAPEX-Sahel experiment werd door haar gecoördineerd. In 1994 verbleef zij enkele maanden aan het 'Institute of Hydrology', Wallingford, Engeland om de seizoensvariatie van de energiebalans van savanne en tijgerbos te bestuderen. Aan dit zelfde instituut zal zij in januari 1996 een twee-jarig post-doc onderzoek beginnen getiteld "Physiologically-based models of semi-arid vegetation dynamics for improved description of land surface/atmosphere interaction in climate models".